INVESTIGATION OF COLD EXPANSION OF SHORT EDGE MARGIN HOLES WITH PREEXISTING CRACKS IN 2024-T351 ALUMINUM ALLOY

by

Dallen Lee Andrew

A thesis submitted to the faculty of
The University of Utah
in partial fulfillment of the requirements for the degree of

Master of Science

Department of Mechanical Engineering

The University of Utah

December 2011

The University of Utah Graduate School

STATEMENT OF THESIS APPROVAL

The thesis of **Dallen Lee Andrew**

has been approved by the following supervisory committee members:

David W. Hoeppner	, Chair	**10/18/2011** Date Approved
Paul N. Clark	, Member	**10/18/2011** Date Approved
Rebecca Brannon	, Member	**10/18/2011** Date Approved

and by **Tim Ameel** , Chair of

the Department of **Mechanical Engineering**

and by Charles A. Wight, Dean of The Graduate School.

ABSTRACT

When a crack indication is found at a hole, current United States Air Force (USAF) technical data require that the hole must be oversized to a larger diameter to remove the damage. Unnecessarily oversizing a hole is undesirable from a fatigue point of view. This research has the potential benefit of not requiring the hole to be oversized and potentially could reduce the number of inspections required for aircraft.

The experiments performed in this research investigated the fatigue crack growth lives of short edge margin holes. Three configurations were used – a baseline condition consisting of non-cold-expanded holes, another baseline condition of holes that were cold-expanded, and the test condition of holes containing a crack when cold-expanded. All configurations were loaded under constant and variable-amplitude loading. The hypothesis is that the cold expansion of a hole with a preexisting crack will provide a significant increase in fatigue life compared to an identical hole that was not cold-expanded.

Additionally, the USAF analytical approach used to account for the fatigue life benefit due to cold expansion is compared to the experiment data, and may not be providing conservative predictions for the specific geometry and loading used in this experiment.

TABLE OF CONTENTS

LIST OF TABLES

ACKNOWLEDGMENTS

I would like to acknowledge and thank all the wonderful people who assisted in this work. Much gratitude goes out to Dr. Paul Clark and Dr. Mark Thomsen – they were both instrumental in the development of the experimentation plan and implementation. This research would never have happened without their help and input when advice was needed. Thanks to Dr. David Hoeppner, my committee chair, for bringing me great insight and knowledge into the world of fatigue and fracture mechanics. Thanks to Dr. Brannon for putting in extra time and effort to help me quantify and explain my writing. And thanks especially to my colleagues and unofficial mentors – Scott Carlson and Robert Pilarczyk. They were there to cheer me on when I got discouraged, and to answer all the nitty-gritty questions I wanted to ask. They took the time to explain and explain and explain, and I am very grateful for their day-to-day coaching. In particular, Robert Pilarczyk was critical in assisting with specimen procurement, equipment setup, and guidance on procedure. It should be noted that the format of this thesis was patterned after previous research performed by Carlson and Pilarczyk. This research is a follow-on to their work and was formatted similarly for consistency and readability.

My gratitude goes to Jacob Warner, my colleague and fellow student. He has assisted me in every step of this research process, and was always there to help when I needed it. Between the two of us, we were able to overcome many obstacles that were placed in the way of getting these experiments completed.

Thanks to Carl Popelar at Southwest Research Institute for specimen manufacturing and preparation, and Greg Kimoto from FTI for assisting with the cold expansion.

Thanks to my colleagues in the Aircraft Structural Integrity Program office at Hill Air Force Base, especially Chuck Nelson for using his personal time to machine several sets of step studs. I must also thank those at the Hill Air Force Base Science and Engineering Laboratory, especially Dr. David Hansen, Jeff Wandrey, and Eric Billings, for signing the agreement to let us to use their facilities, for allowing us access and training for their equipment, and for the purchase of the variable-amplitude loading software.

A special thanks goes out to my bride and my daughter. They were there for me every step of the way in this whole process, and I would not have been able to complete this without their help and patience.

1 INTRODUCTION

1.1 History of Aircraft Structural Integrity

From the beginning, structural integrity has played a key role in aircraft design. The Wright brothers in 1903 had to postpone their first powered flight due to a fatigue failure of a propeller shaft.[1] With the rising expansion of the aircraft industry, aircraft began to be pushed to their limit, and failures occurred. The failures of the deHavilland Comet – the first high altitude passenger jet – raised the importance of fatigue and structural integrity in aircraft design. In January 1954, the first of two Comet passenger airplanes crashed into the Mediterranean Sea. It was discovered that the failure occurred due to fatigue which nucleated at a corner of an opening in the fuselage.[2]

1.2 Fatigue Design Philosophies

Initially, aircraft designers did not do any additional analyses to account for time-based failure methods, such as fatigue, corrosion, wear, creep, etc. This design philosophy is called the no-life paradigm.[3] It was assumed that a large safety factor built into the design would be sufficient to prevent those types of failure mechanisms. Engineers were not required to take into account the effects of time degradation, and so they did not. Later came the development of the safe life design paradigms – stress life and strain life. These approaches did not account for the behavior of cracks in a material, and assumed that a material is an ideal homogeneous, continuous, isotropic continuum that is free of any material discontinuities. This philosophy contained no way to handle a

component with a crack, the behavior of that crack, or the introduction of any type of material discontinuity into a component.[1] This led to many aircraft failures, including the Comet accidents in 1954 and the F-111 accidents in 1969.[2, 4] The F-111 supersonic interceptor aircraft experienced multiple failures that were attributed to pre-existing material discontinuities at the time of service.[4] These accidents made evident that the safe life design philosophy was not succeeding at keeping aircraft in the air and pilots safe, and a change needed to be made.

1.3 Damage Tolerance Design Philosophy

Fatigue failures in other military aircraft prompted the United States Air Force (USAF) to implement the damage tolerance design paradigm. According to the USAF military standard (MIL STD) 1530C:

> Damage tolerance is the attribute of a structure that permits it to retain its required residual strength for a period of unrepaired usage after the structure has sustained specific levels of fatigue, corrosion, accidental, and/or discrete source damage.[5]

Damage is defined by MIL-STD-1530C as, "any crack, flaw, corrosion, disbond, delamination, and/or other feature that degrades, or has the potential to degrade, the performance of the affected component."[5] Damage tolerance philosophy assumes there are cracks or material discontinuities in a component, either inherent in the material or formed as part of manufacturing or maintenance process. Fracture mechanics is then used to analyze the behavior of those cracks. Damage tolerance design consists of critical components being inspected at calculated intervals such that cracks will be detected before they propagate to failure. This philosophy consists of three key elements – residual strength, Nondestructive Inspection (NDI), and fatigue crack growth, which are discussed in the following sections.

1.3.1 Fatigue Crack Growth

ASTM E1823 defines fatigue as "the process of progressive localized permanent structural change occurring in a material subjected to conditions that produce fluctuating stresses and strains at some point or points and that may culminate in cracks or complete fracture after a sufficient number of fluctuations."[7] Fracture mechanics can be used to analyze and predict the fatigue crack growth of components, from an initial crack size to failure. This fatigue life can be identified as the sum of four parts – the nucleation phase, small crack phase, stress dominated crack growth or long crack growth phase, and instability. All are shown in Fig. 1. The horizontal axis labeled 'Life' is measured as a function of time, i.e., seconds, cycles, flight hours, etc. Damage tolerance techniques focus on the third phase in Fig. 1 and the detection of cracks by NDI. This phase of the fatigue life can be characterized by Linear Elastic Fracture Mechanics (LEFM) and Elastic Plastic Fracture Mechanics (EPFM), where the crack growth is determined by the bulk properties of the material – geometry, stress, etc.

1.3.2 Residual Strength

Residual strength is the maximum value of the far field stress, neglecting the area of the crack, that a cracked specimen is capable of sustaining.[7] It represents the remaining capability of a part to sustain a load given the presence of a crack. So as the length of a crack increases, the residual strength of the remaining material decreases, until failure of the component. This residual strength is used to determine the critical crack size or orientation that would cause failure under a given set of loading conditions. Residual strength calculations can be performed by using LEFM.

The basis of LEFM originated from the work of Griffith and Irwin and others.[9] Griffith used a strain energy approach, while Irwin added to that work and developed an equation that quantifies the stress intensity (K) at the tip of a crack, relating the crack length (a), the far field stress (σ), and a correction factor (β) for geometry and is given in Eq. 1. Others later developed correction factors for residual stresses, loading conditions, etc.

$$K = \beta\sigma\sqrt{\pi a} \quad \textbf{(1)}$$

By calculating a stress intensity for a given material, geometry, crack size, and loading, it can be determined if failure occurs by comparing the calculated stress intensity to the critical stress intensities for the material. By using this equation, the residual strength of a component can also be calculated if the crack length, stress intensity, and any correction factors are known.

1.3.3 Nondestructive Inspection

NDI is the third element used to help monitor structural reliability. NDI methods are used to determine if fatigue cracks or other discontinuities are present in a material at the time of inspection. These inspections are used to help determine if the fatigue life is behaving as predicted by the tools of fracture mechanics, which is needed to gauge if the crack will reach the critical crack length before the next scheduled inspection. Many different methods are used to perform the inspections, including eddy current, dye penetrant, x-ray, and others.[6] Each inspection method has a minimum crack size that can be detected, with some Probability Of Detection (POD).

1.3.4 Damage Tolerance Analysis

When the NDI method has been established, residual strength profile determined, and knowledge of the fatigue crack growth obtained, these pieces are brought together in a damage tolerance analysis (DTA). The main goal of a DTA is to predict the critical crack size and number of cycles to failure for a given component and loading spectrum. From this, an initial inspection can be implemented based on the time interval it takes to reach the NDI detectable crack size from an assumed undetectable Initial Flaw Size (IFS). A recurring inspection interval also is set, allowing inspections to be done in the time between reaching the NDI detectable crack size and the critical crack size. These concepts are shown in Fig. 2 and Fig. 3.

1.3.5 Benefits of Damage Tolerance Design

The use of fracture mechanics in a damage tolerance design philosophy will help to answer the following key questions.[11]

1. What is the residual strength as a function of crack size? As a function of stress?
2. What size of crack can be tolerated at the expected service load; i.e. what is the critical crack size?
3. How long does it take for a crack to grow from a certain initial size to the critical size?
4. What size of pre-existing flaw can be permitted at the moment the structure starts its service life?
5. How often should the structure be inspected for cracks?

By gaining solutions to the questions above, then implementing those solutions into the design, production, and maintenance procedures for any given component, the three key elements of damage tolerance design – fatigue crack growth, residual strength, and NDI – will be satisfied.

1.4 Aircraft Structural Integrity Issues

While there are many fatigue critical locations and geometries of aircraft, one common aircraft fatigue location are fastener holes. One technique that has been developed to help slow fatigue crack growth at fastener holes is the cold expansion process. The cold expansion process involves pulling a tapered mandrel, fitted with a lubricated split sleeve, through the hole as shown in Fig. 4. This process plastically deforms the fastener hole and results in a residual compressive stress around the hole. This residual compressive stress slows the propagation of fatigue cracks and extends the fatigue life of the component.

Fatigue Technology Inc. (FTI) has invented a cost effective manufacturing method for the lubricated split sleeve, which has led to the widespread use of the Split Sleeve Cold Expansion™ in the aerospace industry.[12] The sleeve allows for one-sided processing and shields the hole from frictional forces generated by the high interference of the expansion mandrel. Fig. 5 shows curves representing the residual stress field relative to the distance from the hole. As is shown, the residual compressive stress field extends to approximately one diameter distance away from the hole, followed by a slight tension field.

An axial ridge, which corresponds to the position of the split in the sleeve, is left in the bore of the hole during the cold expansion process. There is also some surface upset formed at the bore/surface interface due to this process. These are both shown in Fig. 6. The ridge and surface upset are typically reamed out when final reaming the hole. As a general rule, the sleeve gap which forms the axial ridge should be located away from free edges.[12]

1.5 Cold Expansion of Holes with Existing Cracks

Much research has been performed investigating the benefits of cold expansion. For example, the research performed by Carlson[13] and Pilarczyk[10] investigated the use of experimentally derived beta corrections to predict fatigue crack growth at cold-expanded holes. Carlson's research focused on 2024-T351 aluminum while Pilarczyk's research used 7075-T651 aluminum. One topic that has significantly less research is the fatigue life of short edge margin fastener holes that have been cracked prior to the cold expansion process.

1.5.1 Current Research

Pristine fastener holes are relatively difficult to maintain in an industrial environment where thousands of fastener holes have maintenance work done on them. The purpose of this research was to characterize the fatigue crack growth life of cracked fastener holes that were then cold-expanded.

For example, when an aircraft is brought into a maintenance facility for structural inspections and regularly scheduled maintenance, certain critical fastener holes and locations are inspected for fatigue cracks and other damage. Assume a specific hole was found to contain no cracks or damage, but due to its critical location it was required to be cold-expanded to prolong the fatigue life. After the cold expansion process is completed, assume the hole is again inspected by NDI methods, and an indication of a crack or other damage at the hole was detected. Current USAF policy to this situation would be that the hole must be oversized until that there are no longer any crack or other damage indications at the hole.

The importance of this example is to show that while there may have been a crack or other discrepancy at the fastener hole originally, it went undetected by NDI methods. This was due to its size being under the detectable limit for the NDI technique, or it was simply missed. If this research shows the benefits of cold-expanding a hole with a crack are great enough, the inspected component would be safe to fly for an additional number of flight hours, if needed, without need to be oversized or have other maintenance work done. This would require less maintenance, less unnecessary oversizing of fastener holes, and less aircraft downtime. More important, however, is the concept that this research will provide a more accurate prediction of the benefits of cold expansion in a industrial environment, where hole quality and surface integrity is not as high as in a lab environment.

Additionally, there are many components – spar caps, spar webs, wing skins, etc. – on an aircraft that require a short edge margin, (e/D), where (e) is hole offset, which is the distance from the edge of the part to the center of the hole, and (D) is the diameter of the hole. A typical guide for edge margin limits in rework scenarios is to keep $e/D > 1.5$. FTI recommends keeping $e/D > 1.75$, although experimentation has shown that e/D less than or equal to 1.0 may be satisfactorily cold-expanded at the nominal applied expansion levels, but with some bulging of the edge.[12] In instances where a hole must be reworked and oversized, the e/D ratio may drop below recommend values. Therefore an $e/D = 1.2$ was chosen for this research, to observe the effects of cold-expanding a short edge margin hole and to see the effects of a precracked cold-expanded hole on typical aircraft geometry. One of the objectives of this research was to determine if the choice of edge margin would be applicable for cold expansion in a maintenance environment.

In addition, the current USAF approach to take advantage of the fatigue life benefit of cold expansion is to lower the IFS in a damage tolerance analysis to 0.005 inch. It was an objective of this research to compare that 0.005 inch IFS prediction to the experiment data and determine if the prediction was conservative with respect to the data generated in this research.

1.5.2 Previous Research

Some of the earlier work done on the cold expansion of fastener holes containing cracks was done in the 1970s. The fatigue life of fastener holes continues to be a valid concern for aircraft structural integrity today.

Horsley and Wylie (1973) investigated the fatigue loading of pre-cracked expanded fastener holes in 7178-T6 aluminum alloy load transfer joints.[14] It was found that the propagation of small radial cracks (0.03 to 0.07 inch) can be retarded by deep cold expansion (3.5% interference fit cold expansion).

Petrak and Stewart (1974) and also Toor (1976) looked at the retardation of cracks emanating from fastener holes containing fasteners.[15,16] Those results indicated that cracks on the order of 0.1 inch in length can be retarded to some degree in their growth with the cold expansion process, and in some cases it was difficult to even get the crack to start growing.

Brot and Nathan (1985), with Israel Aircraft Industries, conducted a series of experiments that focused on increasing crack growth lives of short edge margin holes, with the use of cold expansion and interference fit bushings.[17] The experiments indicated that, for short edge margin ($1.0 < e/D < 1.5$) applications with 3.0% mandrel inference,

an approximate triple increase in the fatigue crack growth life. For edge margins of e/D < 1.0, the benefit of cold expansion was negligible.

The experiments of Buxbaum and Huth (1987) had similar research and similar specimen geometry – flat plate center hole specimens, 2.36 inch x 0.19 inch with 0.245 inch diameter countersunk hole.[18] It was found that the expansion of holes containing very small cracks, less than approximately 0.02 inch, may lead to crack growth lives larger than the total fatigue life in the uncracked and not expanded condition. A limit was determined for an initial crack length that would still provide fatigue life benefit from cold expansion: "The expansion process should not be applied to crack lengths being larger than the radius of the hole, since the resulting fatigue life improvement then will be rather marginal," with the term marginal representing less than two times the fatigue life improvement.[18] Others have done similar research, with aluminum and steel components, and had similar results.[19-29]

1.6 Research Program Objectives

Listed below are the objectives for this research project.

1. Determine the baseline fatigue crack growth behavior of the aluminum alloy 2024-T351.
2. Document the effect of the short edge margin on the crack front shape.
3. Determine if the cold expansion could be used with the selected hole offset in a maintenance environment, without permanently deforming structure due to the cold expansion.
4. Compare fatigue crack growth life for the non-cold-expanded configuration, the cold-expanded configuration, and the precracked cold-expanded configuration.
5. Determine if the current USAF approach of using a 0.005 inch IFS in an AFGROW model, to account for fatigue life improvement due to cold expansion, is a conservative approach with respect to the data generated in this research.

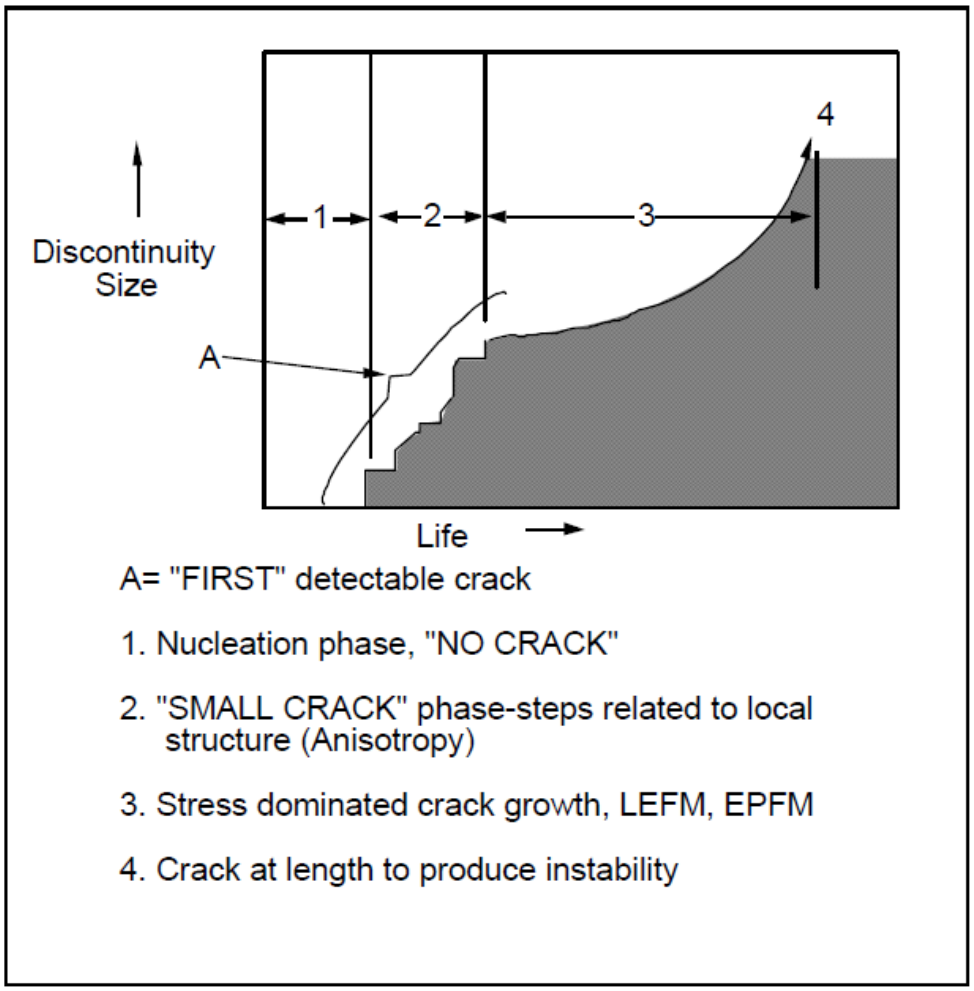

Fig. 1 Phases of life of fatigue crack growth[8]

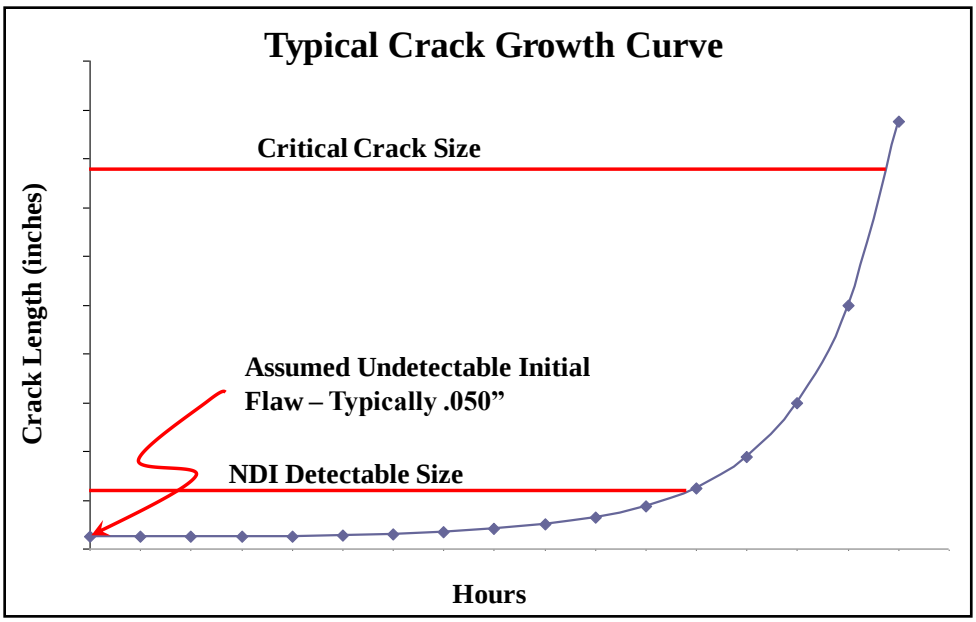

Fig. 2 Typical crack growth curve illustrating the initial flaw size, NDI detectable crack size, and the critical crack size for a damage tolerance analysis[10]

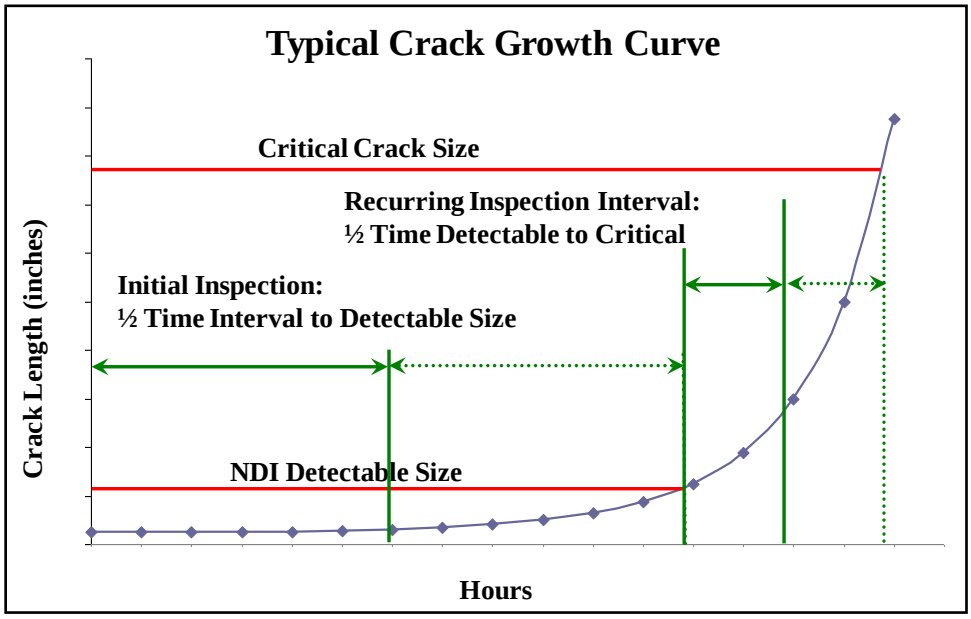

Fig. 3 Typical crack growth curve outlining the methodology used to determine the initial and recurring inspection intervals for a damage tolerance analysis[10]

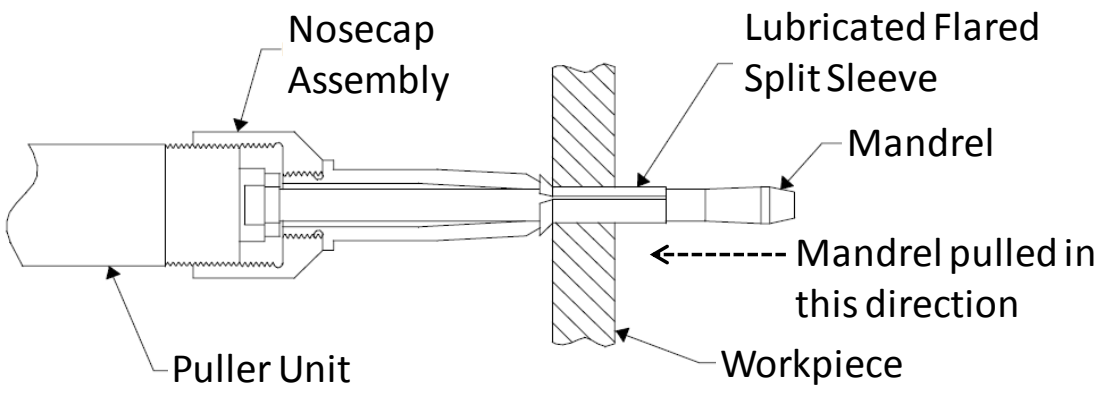

Fig. 4 Split Sleeve Cold Expansion™ process[12]

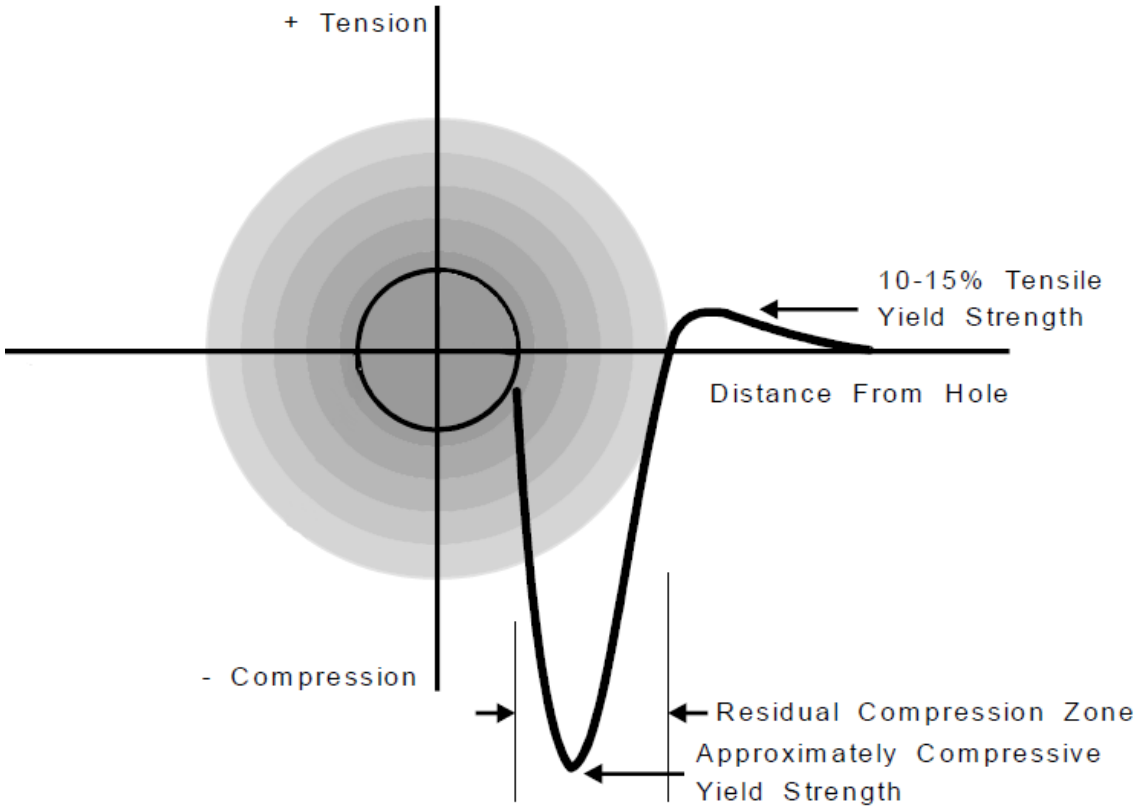

Fig. 5 Residual stress field profile relative to the diameter of the hole for a cold-expanded hole[12]

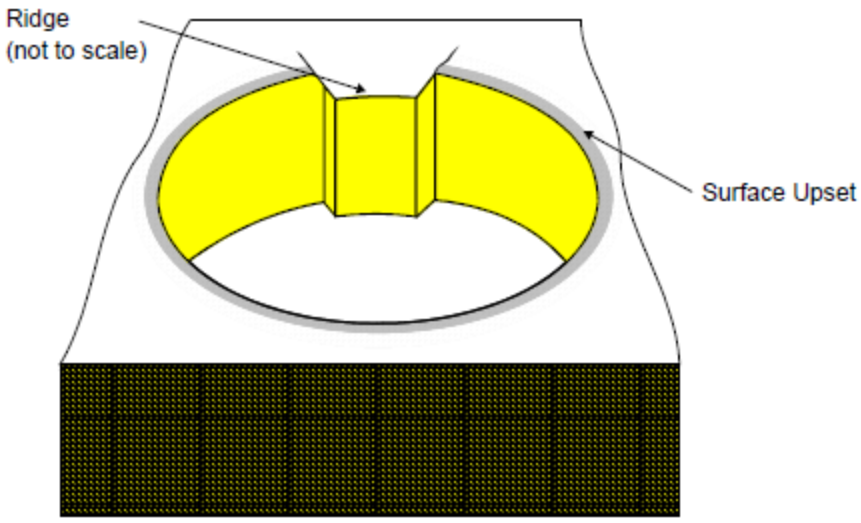

Fig. 6 Axial ridge and surface upset formed on a specimen due to the cold expansion process[12]

2 EXPERIMENT SETUP AND PROCEDURES

2.1 Fatigue Experiment Specimen Specifications

2.1.1 Specimen Material

For the fatigue experiments, 2024-T351 aluminum was chosen due to the quantity of use of it in the aerospace industry, both military and civilian. It is a high toughness, low strength aluminum alloy and is used primarily for tension dominated components. It is commonly used in fuselage structures, wing tension members, shear webs and ribs and structural areas where stiffness, fatigue performance and good strength are required.[30] Aluminum 2024-T351 is the T3 heat treatment in plate form for Al 2024.

The raw material was purchased by Southwest Research Institute (SwRI) from Kaiser Aluminum on 2 May 2011. The material certification sheet is given in Appendix A.

2.1.2 Specimen Geometry

The basic geometry for the specimens was based on the guidance given in American Society for Testing and Materials Standard Test Method for Measurement of Fatigue Crack Growth Rates – ASTM E 647[31]. The standard dimensions of the specimens were 16 inches long, 4 inches wide, and 0.25 inches thick. The specimens were middle tension with an offset hole. Two additional specimens were used to meet the requirements in ASTM E 647[31] and contained center holes. As explained previously, the hole offset (e) is the distance from the edge of the specimen to the center of the hole

and was chosen to be 0.6 inch. This value, divided by the diameter (D) of the hole, which is 0.5 inch, gives an edge margin (e/D) of 1.2. This hole offset was chosen because of the number of rework scenarios that have been performed on the A-10 Weapon System with edge margins of this or similar values. Typically, edge margins of less than e/D = 1.5 are undesirable from a fatigue point of view, as the fatigue life of the ligament is relatively short.

The process for manufacturing the specimens was completed by SwRI. This process involved several steps:

1. Cutting the specimens from the stock sheet
2. Milling to dimensional specifications
3. Drilling and reaming the hole
4. Electric Discharge Machining (EDM) a notch in the hole (if applicable)
5. Stamping the specimen identification on both ends of the specimen
6. Bonding on tabs (if applicable)
7. Polishing the surface and bore of the hole for crack propagation tracking.

The geometry and manufacturing processes for all the specimens are discussed in the following sections. It should be noted that for all specimens, the rolling direction was to be in the longitudinal (L) grain orientation, which was also the loading orientation. This was to prevent nucleation of cracks along the grain boundaries in the Long Transverse (T) orientation. The Short Transverse (ST) orientation is through the thickness, or into the page in Fig. 7. These orientations are labeled in upper right corner of the specimen in Fig. 7. Also, all specimens were required to come from the same plate and were required to come with the material certification sheet. This was done to reduce the variability of experiment data that could be introduced by using material from different plates or from material that was not certified.

2.1.2.1 ASTM E 647 Specimens

Two specimens, designated 2024-1 and 2024-2, were designed and manufactured to the geometry specifications for middle tension specimens given in ASTM E647.[31] Fig. 7 is the engineering drawing for these two specimens. These specimens were used to ensure that the material, load frame, and data collection process all conformed to the standard. The specimens had a center 0.1 inch hole, with a through thickness EDM notch of approximate length 0.010 inch on both sides of the hole.

2.1.2.2 Non-Cold-Expanded Specimens

Six specimens were used as a baseline condition and were not cold-expanded. These specimens were designated OFF-NCX2024-1 to -6. The process for the manufacturing of these six specimens is given in Fig. 8.

The hole diameter of 0.474-0.477 inch was not part of any given requirement for these six specimens, but was used to maintain continuity in the fatigue experiment process. This initial hole diameter was chosen to match the pre-cold expansion hole diameter of the cold-expanded specimens for consistency. Fig. 9 is the engineering drawing for these six specimens.

2.1.2.3 Precracked Cold-Expanded Specimens

Ten specimens were cracked prior to being cold-expanded, designated OFF-PC-CX2024-1 to -10. The process for the manufacturing of these ten specimens is given in Fig. 10. As part of this process, the pre-cold expansion hole diameter was measured, the thickness of the split sleeve and mandrel diameter were measured, and the post-cold expansion diameter was measured. These measurements were used to calculate the

applied and residual expansions for every specimen. The details of these calculations are given in Appendix B. Fig. 11 is the engineering drawing for these specimens.

2.1.2.3 Cold-Expanded Specimens

Eight specimens were cold-expanded without being precracked, OFF-CX2024-1 to -8. The process for the manufacturing of these specimens is given in Fig. 8. As part of this process, as with the precracked cold-expanded specimens, the pre-cold expansion hole diameter was measured, the thickness of the split sleeve and mandrel diameter were measured, and the post-cold expansion diameter was measured. These measurements were used to calculate the applied and residual expansions for every specimen. The details of these calculations are given in Appendix B. Fig. 13 is the engineering drawing for these specimens.

2.1.2.4 Experiment Matrix

The experiment matrix used for this research is given in Table 1. The non-cold-expanded specimens, including the ASTM E 647 specimens, are shaded to identify the specimens for which AFGROW inputs were tuned to match the experiment data.

2.2 Fatigue Experiment Equipment

All fatigue experiments took place at the 809 Maintenance Support Squadron (MXSS) Science & Engineering Laboratory at Hill Air Force Base Utah. A typical fatigue test setup, with controller and various outputs, is shown in Fig. 14. A photo of the experimental equipment setup used for this research is given in Fig. 15.

2.2.1 Fatigue Experiment Equipment Machine Specifications

2.2.1.1 Interlaken Series 3300 55 kip Fatigue Machine

The load frame that was used for this research is an Interlaken Series 3300, with a 55,000 lbf max force capability. The standard setup of this load frame was not used for these experiments, which will be discussed in the following sections. As the original manufacturer of the load frame, Interlaken, is no longer in business, all the digital electronics were manufactured by Instron.

2.2.1.2 MTS Hydraulic Wedge Grips

The standard Interlaken grips were not wide enough to provide adequate grip area for the specimens. The Interlaken grips were 2.5 inches wide, and the specimens for this experiment were 4 inches in width. The experiments performed by Carlson and Pilarczyk, both of whom had 4 inch wide specimens, had integrated the use of threaded step studs to allow the use of Model 647 MTS hydraulic wedge grips to be used with the Interlaken load frame.[10, 13] The same setup was used, and the MTS grips were attached for this research. These hydraulic grips have a 55,000 lbf capacity and are 4 inches wide. This allows the grips surfaces to contact the entire width of the specimen, which reduces the possibility of failure of the specimen at the grips.

2.2.1.3 MTS Model 685.60 Hydraulic over Hydraulic Intensifier

An MTS 685.60 Hydraulic Grip Supply, or hydraulic intensifier, was purchased in 2007 for similar[10,13] research previously discussed. This intensifier was used to increase the grip pressure on the specimens so there was no slip allowed at the grip-specimen interface. Prior to the use of the intensifier, Carlson and Pilarczyk discuss problems with

specimen slipping due to insufficient grip pressure. [10,13] When the Instron technician was calibrating the load cell, the grip pressure in the intensifier was set to 5000 psi, and the load was taken to 50 kip with no visual specimen slip, so the 5000 psi pressure was deemed adequate for the experiment.

2.2.1.4 Instron 8800 FastTrack Controller and Software

An Instron FastTrack 8800 controller was used for this research, originally with the Instron FastTrack II software. During the experiment process, new software (Instron Bluehill 2 software package), was purchased by the 809 MXSS Science & Engineering Laboratory at Hill Air Force Base to provide more capability for the lab with their fatigue machine, and to introduce the capability of variable-amplitude loading for this specific research. Two different modules were used with the Bluehill 2 software package to accomplish the experiments. Constant-amplitude loading was accomplished with the DADN, or Fatigue Crack Propagation, module and all the variable-amplitude loading was done using the Random module. Both of these modules use Labview as their source code.

2.2.1.5 Visible Crack Growth Tracking Equipment

Gaertner traveling microscopes were used to visually track the cracks, and they displayed distance travelled on a digital readout. The microscope accuracy was listed by Gaertner as ±0.00005 inch, which is well within the recommended value of 0.004 inch in ASTM E 647.[31] The microscopes were attached to the load frame by custom built fixtures that allowed easy adjustments and removal of the scopes when not needed. One scope was used to track the crack on the specimen face with the EDM notch, and another

scope was placed on the opposite side of the specimen to track the crack growth down the bore and the through thickness crack on the non-EDM face, respectively.

2.2.1.6 Fatigue Machine Calibration and Certification

The load cell and load frame were calibrated on 20 May 2011 by a certified Instron technician. The calibration is valid until 20 May 2012; therefore the experiments performed on the load frame were within the valid calibration dates. The load cell and frame were calibrated to several internal Instron standards, as well as ASTM E4 Standard Practices for Force Verification of Testing Machines.[35]

In order to reduce the amount of bending or torsion into the specimen, the line of tensile force through the load cell, grips, and actuator needs to remain concentric about the center line of these components, which are shown in Fig. 16. This concentricity was measured with a dial indicator, an instrument used to accurately measure small linear distances, with the measurement results displayed in a magnified way by means of a dial. The dial indicator was attached to a magnetic base, which was attached to the outer diameter of the upper grip. The lever was placed against the outer diameter of the lower grip, the lower grip was rotated, and the displacement was recorded from the dial. This displacement of the lever is called runout. Without having installed grips, typical fatigue load frame runout measurements between a load cell and actuator are on the order of ±0.001 inch.[33] However, with the installment of grips, the normal runout tolerance between load cell and actuator can be relaxed some. For this research, the maximum runout was measured to be 0.010 inch. This was determined to be acceptable due to the added tolerance of the installed grips in this measurement.

2.3 Specimen Preparation

2.3.1 Initial Sanding and Polishing of Specimens

All specimens were manufactured and shipped from SwRI with a mirror finish polish already on the surface and the bore of the hole. This was done to allow for easy crack propagation measurements. The process followed was to sand with 400 grit, followed by 600 grit, and then 1200 grit sand paper. That was followed by polishing with 6 micron and then 1 micron paste. All final passes during each step were performed along the longitudinal direction to prevent nucleation of cracks along the grain boundaries.

2.3.2 Cold Expansion

Cold expansion on the specimens was done according to the FTI specification 8101D STDN 16-0-N10[12] for a final hole diameter of 0.5 inch. The cold expansion process was completed at the Hill Air Force Base Wing Shop, with technical assistance and instruction from a local FTI representative.

2.3.3 Precracking

All specimens were precracked at constant-amplitude loading according to the conditions and geometry requirements given in ASTM E 647. At the end of the precracking, the desired crack length was such that the total length of the crack and the EDM would equal approximately 0.050 inch. This value was chosen because it is the USAF minimum detectable flaw size for a bolt-hole eddy current probe for 90/95 confidence, where 90/95 means that with 90% confidence that more than 95% of inspections will find a 0.050 inch crack. [36] This crack length was chosen to represent the

condition of a hole with a crack that might be missed during an actual inspection on an aircraft. The constant-amplitude specimens were precracked at the same stress as the experiment stress level. Some of the variable-amplitude specimens were precracked at approximately the Root Mean Square (RMS) average value of the spectrum file, which is a text file containing all the loads that are to be applied to the specimen. The other variable-amplitude specimens were precracked at higher loads, and will be discussed in the following section.

2.3.3.1 Load Shedding

From ASTM E 647: "The final K_{max} during precracking shall not exceed the initial K_{max} for which test data are to be obtained [where K_{max} is the maximum stress intensity]."[31] For some of the specimens that were loaded in variable-amplitude loading, load shedding or a K-decreasing process, was used as part of the precracking process. Where K is the stress intensity shown in Eq. 1. The load shedding technique allows doing some of the precracking at a higher stress level, then stepping down the stress in increments, based on the requirements from ASTM E 647.[31] The stress must be stepped down in order to have the final K_{max} from precracking not exceed the initial K_{max} for the test, as explained in ASTM E 647.[31] A visualization of this load shedding technique is shown in Fig. 17.

However, for most of the cold-expanded specimens, using the RMS average value for the precrack stress was not a high enough stress to propagate the fatigue crack through the compressive residual stress field from the cold expansion process. In these situations, precracking was accomplished using a higher stress and not using load shedding.

2.3.4 Final Reaming

After the specimens had been precracked, they all were reamed to a final hole diameter of 0.5 inch, following the process specification in the FTI specification 8101D STDN 16-0-N10[12] for a final hole diameter of 0.5 inch. This process was followed even for the non-cold-expanded specimens, to maintain consistency with all the specimens. Some of the specimens were reamed at the 809 MXSS Science and Engineering Lab at Hill Air Force Base, while some were reamed at the student machine shop in the Mechanical Engineering Department at the University of Utah. Lubricant was applied during the reaming process, and the speed was set to approximately 80-200 RPM, and the reamer was hand fed into the specimen. A standard 10 flute reamer was used to do the reaming, which meets the requirements in the FTI specification.[12] All specimens were reamed with the EDM face on the bottom, so that any chatter that occurred when the reamer entered the hole would not affect the EDM. When the reamer was all the way through the material, the machine was turned off before pulling the reamer back up to minimize any rifling or scratching of the bore.[34] A photo of the reamer and mill used is shown in Fig. 18.

2.3.5 Final Sanding and Polishing

Following the final reaming, the edges of the cold-expanded specimens were sanded with 1200 grit sand paper to reduce the discontinuities and to help prevent the formation of a crack on the edge. The edges of the hole were sanded down to remove the burrs and gouges from the reaming process. Then the surface around the hole and the bore was polished with 3 micron diamond paste, using an electric rotary tool, to allow visual tracking of the crack. The non-cold-expanded specimens were polished around the

hole in the same manner as the cold-expanded specimens. An example of the final appearance after polishing for a cold-expanded hole is shown in Fig. 19. The mirror surface finish along the crack propagation region is designated.

2.4 Specimen Experiments

All specimen experiments were done in lab air at a relatively constant controlled temperature of 71 degrees Fahrenheit, and at a relatively constant 50% relative humidity. As mentioned previously, traveling microscopes were mounted on the load frame, shown in Fig. 15. The microscope on the EDM face of the specimen was used to track the crack on that face. The microscope on the non-EDM face of the specimen was turned at an angle to track the crack propagation down the bore of the hole, and then was straightened out to track the through thickness crack. For measuring the crack propagation down the bore, the principle of similar triangles was used to determine the angle of the microscope, as is shown in Fig. 20. From this diagram, the difference between the similar triangles formed at positions one and two of the microscope can be used to create the small triangle at the bottom of Fig. 20. From this figure, the unknown angle θ of the microscope can be determined by the use of Eq. 2. Then the measured bore crack length measured value can be converted to the actual crack length according to Eq. 3 and shown in Fig. 21.

$$\sin(\theta) = \frac{\text{Measured Thickness}}{\text{Actual Thickness}} \tag{2}$$

$$\text{Actual Crack Length} = \frac{\text{Measured Crack Length}}{\sin(\theta)} \tag{3}$$

2.4.1 Constant-Amplitude Experiments

All constant-amplitude loaded specimen experiments were completed with a stress ratio, defined in Eq. 4, of 0.1 and a frequency of 20 Hz. The maximum stress was varied, with some at 10 ksi and some at 25 ksi. The input waveform for all specimens was sinusoidal.

$$\text{R} = \frac{\sigma_{min}}{\sigma_{max}} \tag{4}$$

2.4.2 Variable-Amplitude Experiments

Variable-amplitude loading, or spectrum loading, is used to represent the loading seen by an aircraft during flight. A typical loading sequence for an aircraft may include high amplitude loads from takeoff, smaller amplitude loads from loitering, and positive and negative loads from different aerial maneuvers. For this experiment, an A-10 wing spectrum was used, and a small section of this spectrum is shown in Fig. 22. The left side is a normalized load scale, limited at ±1. These values are then multiplied by a given stress. While constant-amplitude loading is defined by a mean stress and alternating stress, variable-amplitude loading is designated by a maximum spectrum stress. The maximum spectrum stress is determined, in aircraft, from operational usage from the fleet. Once determined, the scaled values in the spectrum file are multiplied by the maximum stress value. For this experiment, all the variable-amplitude loading specimen experiments were completed at the same maximum stress of 33 ksi. This stress was

chosen because it represents a common stress for fatigue critical locations on the A-10 Weapon System.

The Bluehill 2 software module, Random, which was used to do the variable-amplitude loading, had several methods for applying the load: constant frequency (as the constant-amplitude loading was done), variable frequency, or constant loading rate. The constant loading rate method was chosen for this experiment, to ensure that the peaks and valleys of the spectrum file were accurately applied to the specimen. With this method, a loading rate was chosen that was slow enough to have less than 2% error on all loads, but fast enough not to be concerned about corrosion effects from the environment on the material during the experiment. A screen shot of the Random Loading software is shown in Fig. 23.

2.4.2.1 Crack Growth Retardation

When a large stress or overload is applied, a large plastic zone is formed at the crack tip. When an overload is followed by much smaller stresses in variable-amplitude loading, this causes crack growth retardation. The crack then must grow through the plastic zone before it can begin propagating again at a higher rate. Overloads actually extend the fatigue life of components. Thus it is critical that the stress applied by the controller be accurate when applying the higher stress values of the spectrum. If the controller consistently overloads the specimen, the resulting fatigue life of the specimen will be misleading and inaccurate. The effect of crack growth retardation is shown in the crack length vs. cycles plot in Fig. 24. It should be noted that in Plot C of Fig. 24, the extended fatigue life due to overloading is small compared to Plot B. This is due to the

compressive stresses applied after the overload, which acts to undo the fatigue life extension from the overload.

2.5 Postfailure Specimen Evaluation

After ligament failure, some of the specimens were notched on the opposite side of the hole with a razor blade, and a fatigue crack was propagated from the other side of the hole until complete specimen failure. This additional crack growth life is referred to as continuing damage. It is used to augment the fatigue life of short edge margin components where ligament failure does not denote component failure. Additional fatigue life may be gained from allowing a crack to propagate from the opposite side of the hole. This is often the case in aircraft components such as spar caps, spar webs, and wing skins. For this experiment, not all the continuing damage was completed. The fracture faces from these specimens were documented by the use of a digital microscope and Scanning Electron Microscope (SEM). These images are located in Section 4.6 and Appendix G.

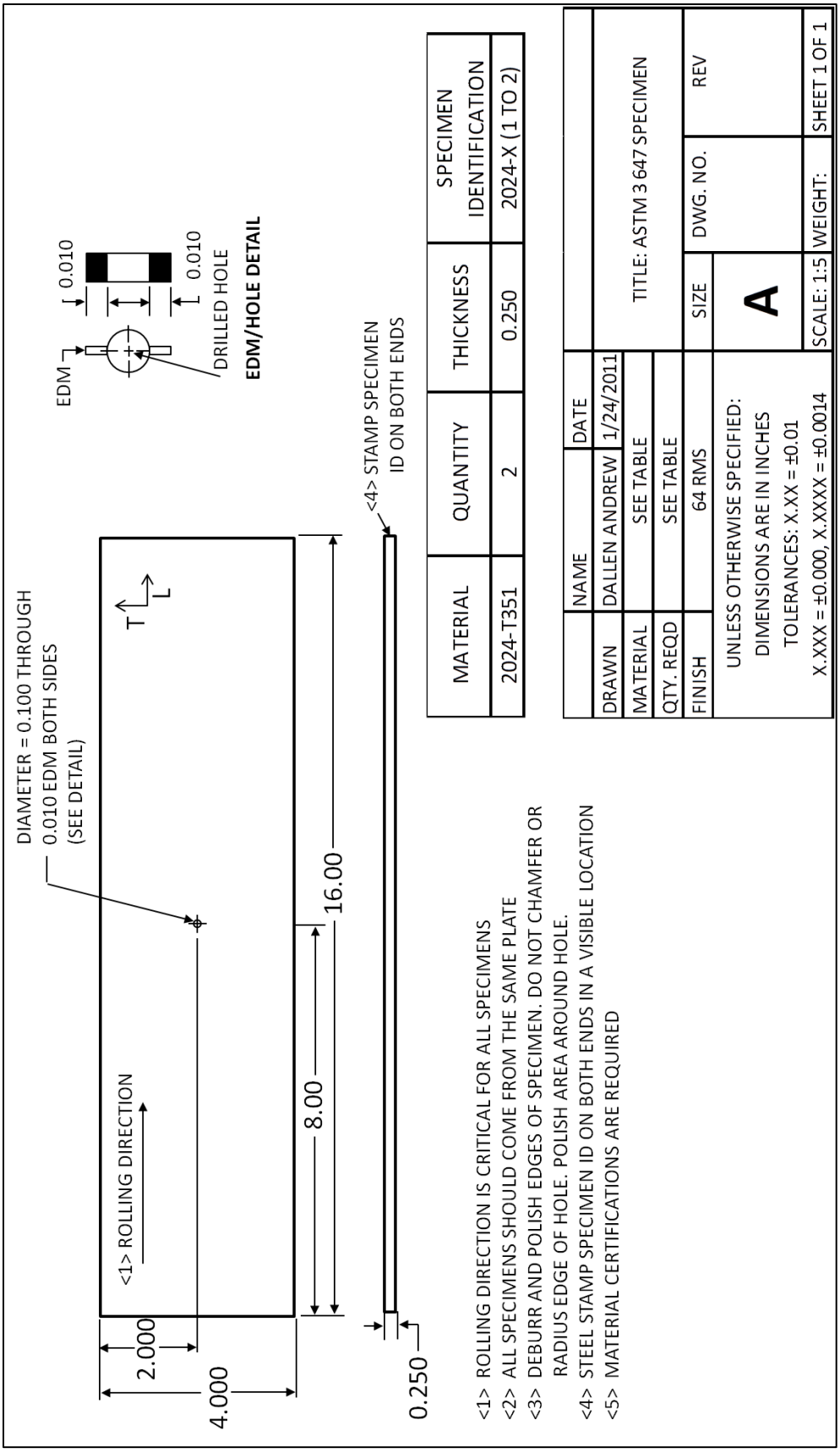

Fig. 7 Manufacturing drawing of ASTM E 647 specimens

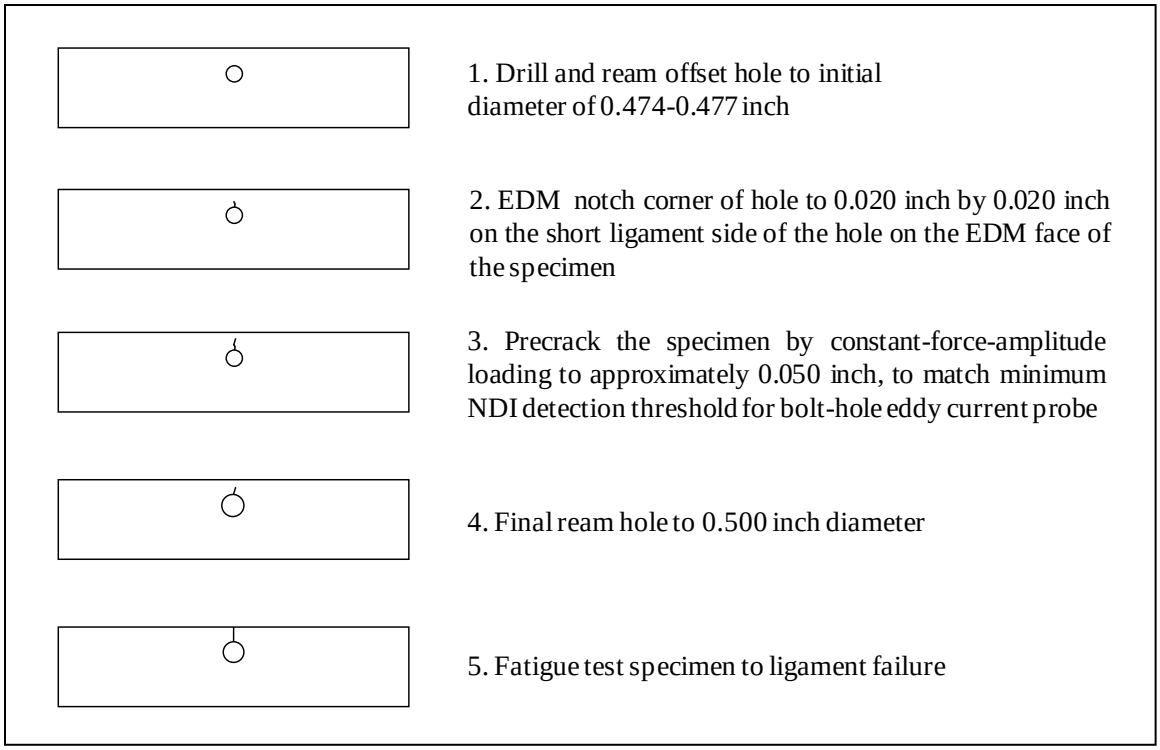

Fig. 8 Procedure for manufacturing of the six non-cold-expanded specimens

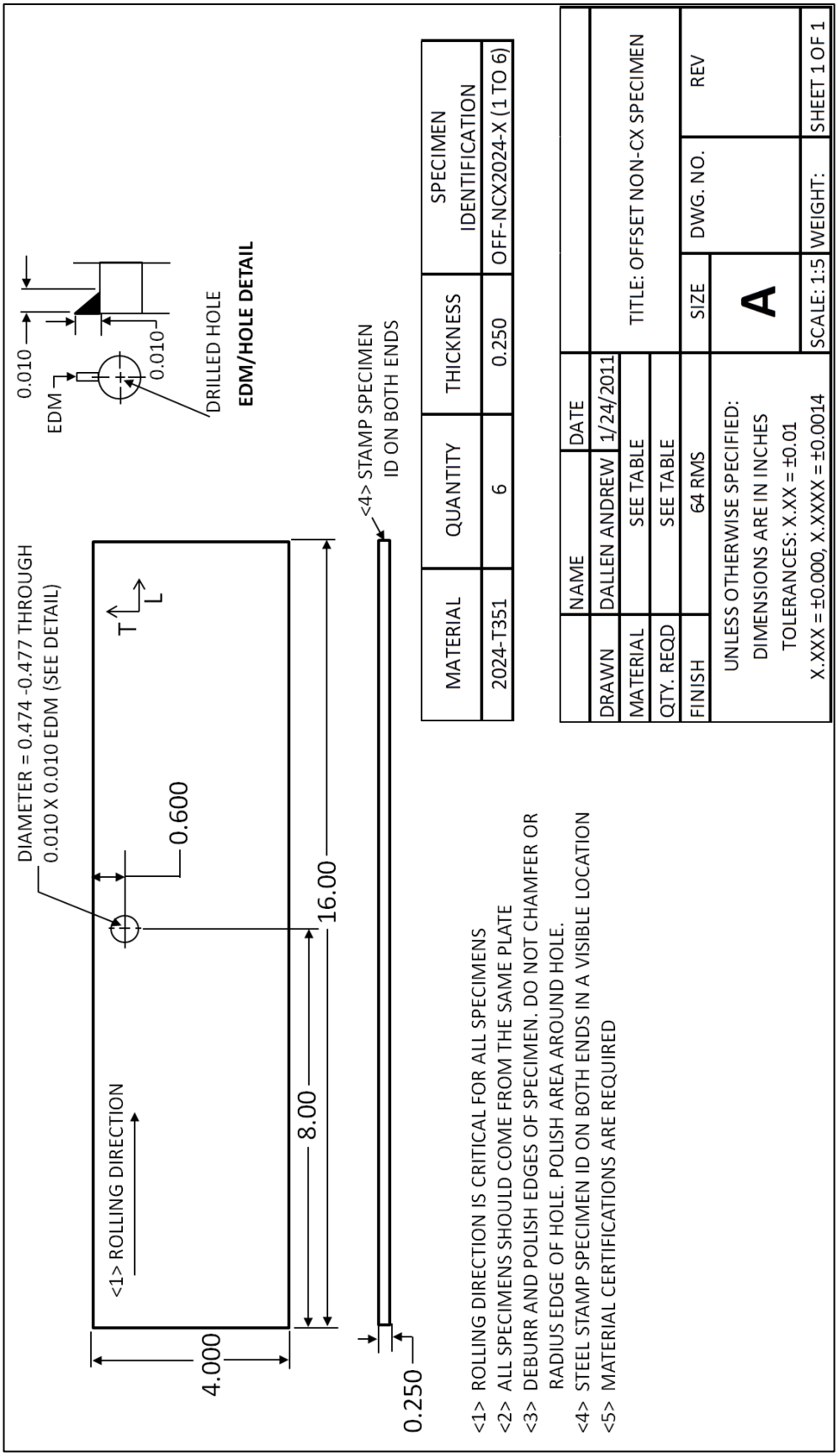

Fig. 9 Manufacturing drawing of non-cold-expanded specimens

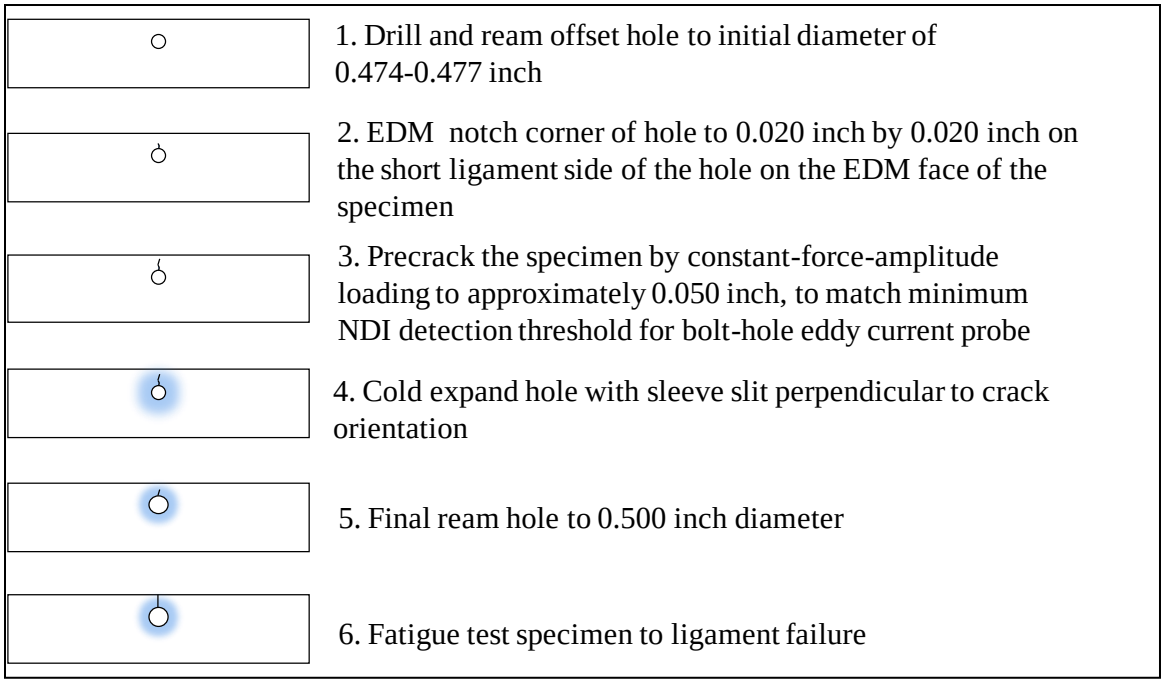

Fig. 10 Procedure for manufacturing of the ten precracked cold-expanded specimens

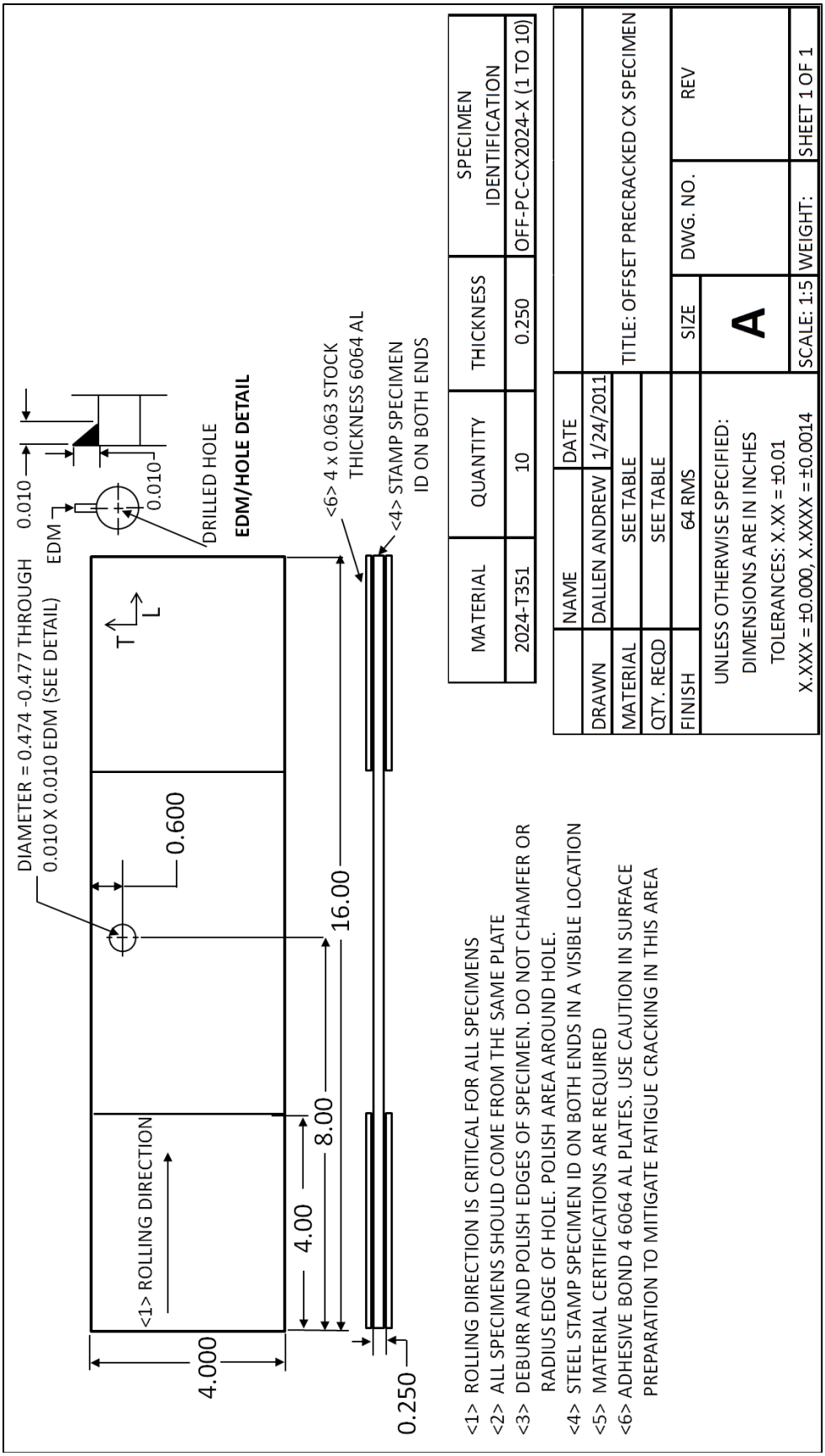

Fig. 11 Manufacturing drawing of precracked cold expanded specimens

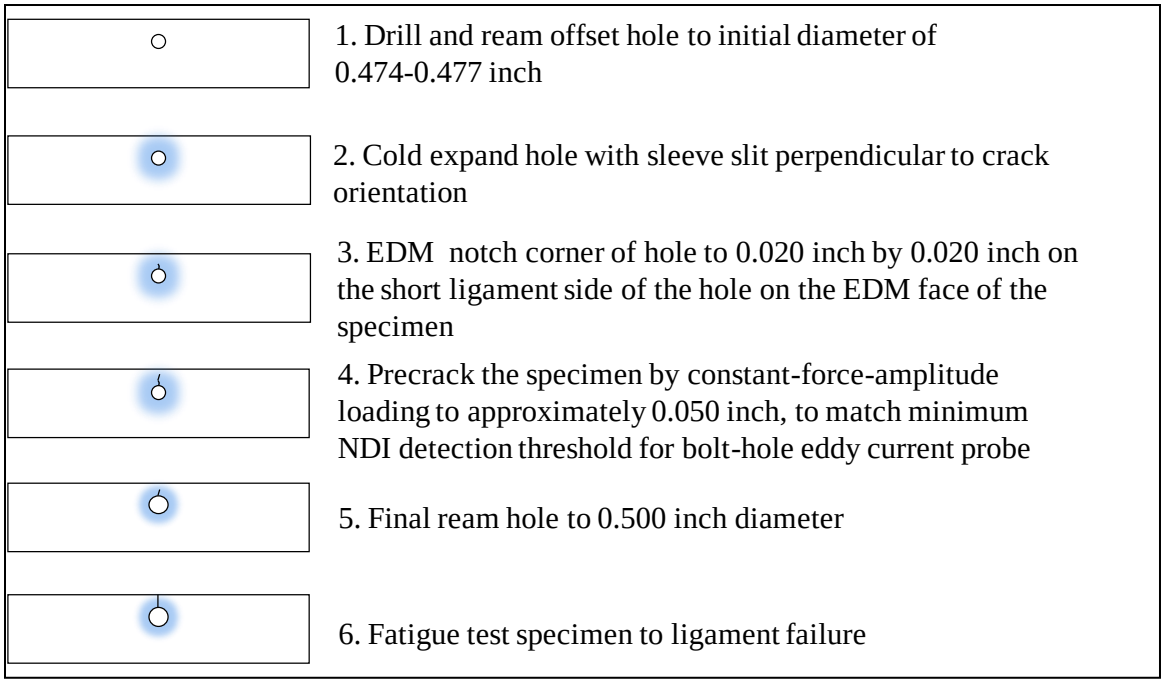

Fig. 12 Procedure for manufacturing of the eight cold-expanded specimens

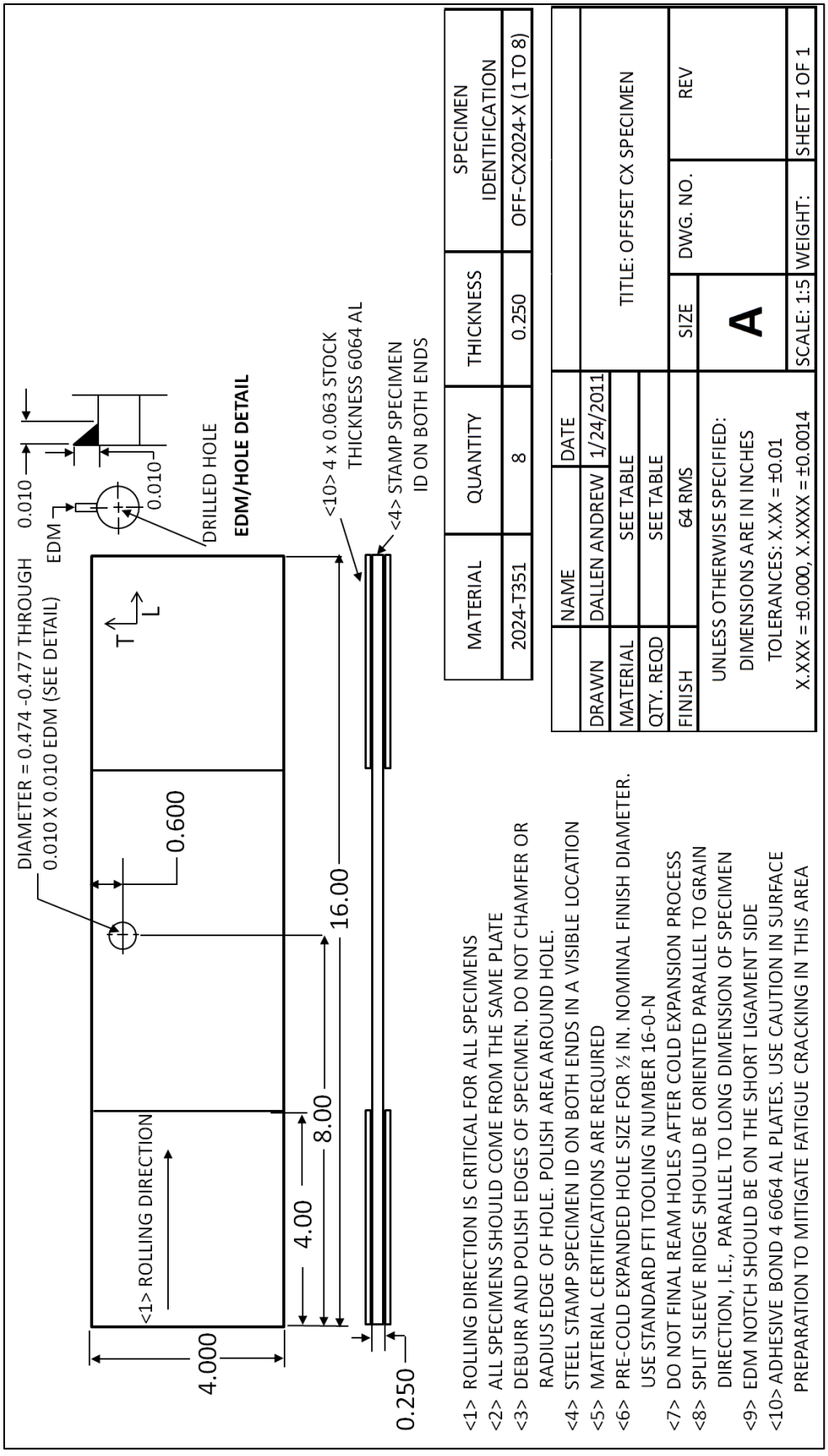

Fig. 13 Manufacturing drawing of cold expanded specimens

Table 1 Experiment matrix

Material	Thickness	Length x Width	Hole Diameter	CX/NON-CX	CA or Spectrum	Cracked Before CX	e/D	Peak Stress	Specimens
2024-T351	0.25 in.	16 in. x 4 in.	N/A	NON-CX	CA (ASTM E647)	N/A	-	11.4 ksi	2
			0.5 in.	NON-CX	CA	N/A	1.2	10 ksi	4
					Spectrum	N/A	1.2	33 ksi	2
				CX	CA	no	1.2	25 ksi	4
						yes	1.2	25 ksi	4
					CA - Markerbanding	yes	1.2	25 ksi	1
					Spectrum	yes	1.2	33 ksi	5
						no	1.2	33 ksi	4
TOTAL SPECIMENS:									26

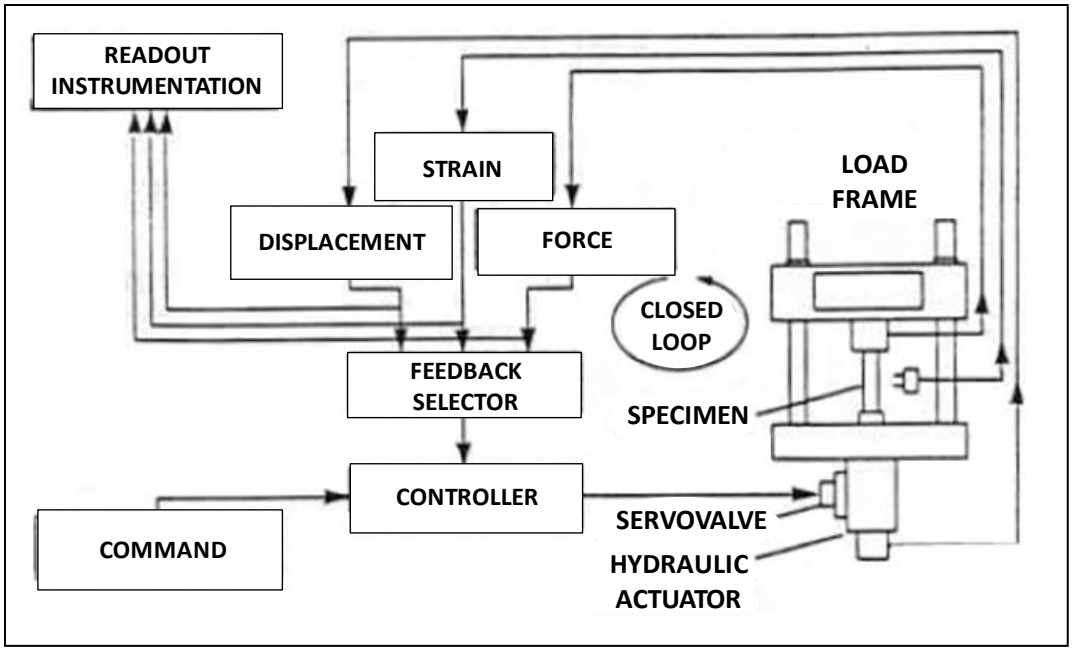

Fig. 14 Typical fatigue experiment setup[32]

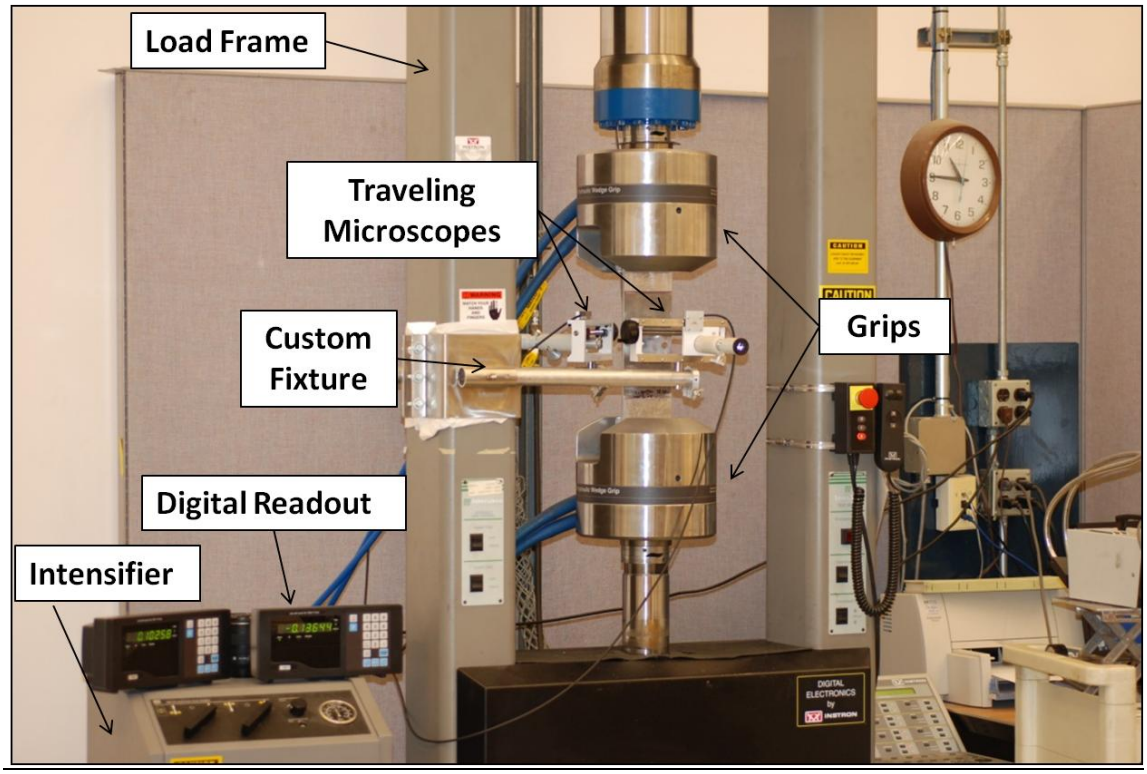

Fig. 15 Experiment setup, including load frame, MTS grips, MTS intensifier, Gaertner traveling microscopes with custom fixturing and digital readout

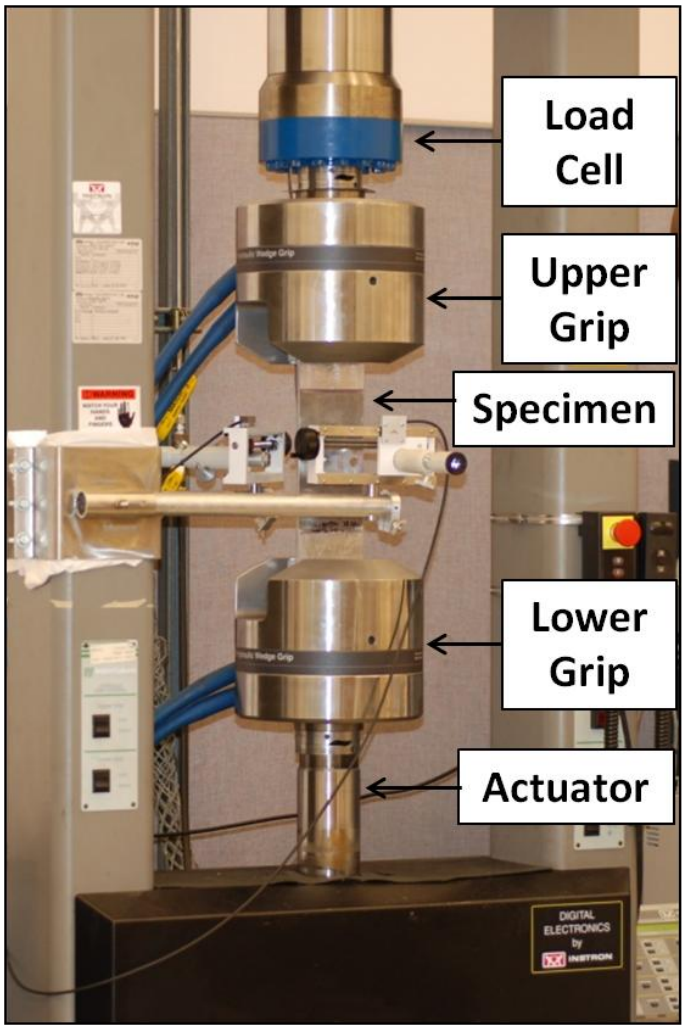

Fig. 16 Photo of load frame components

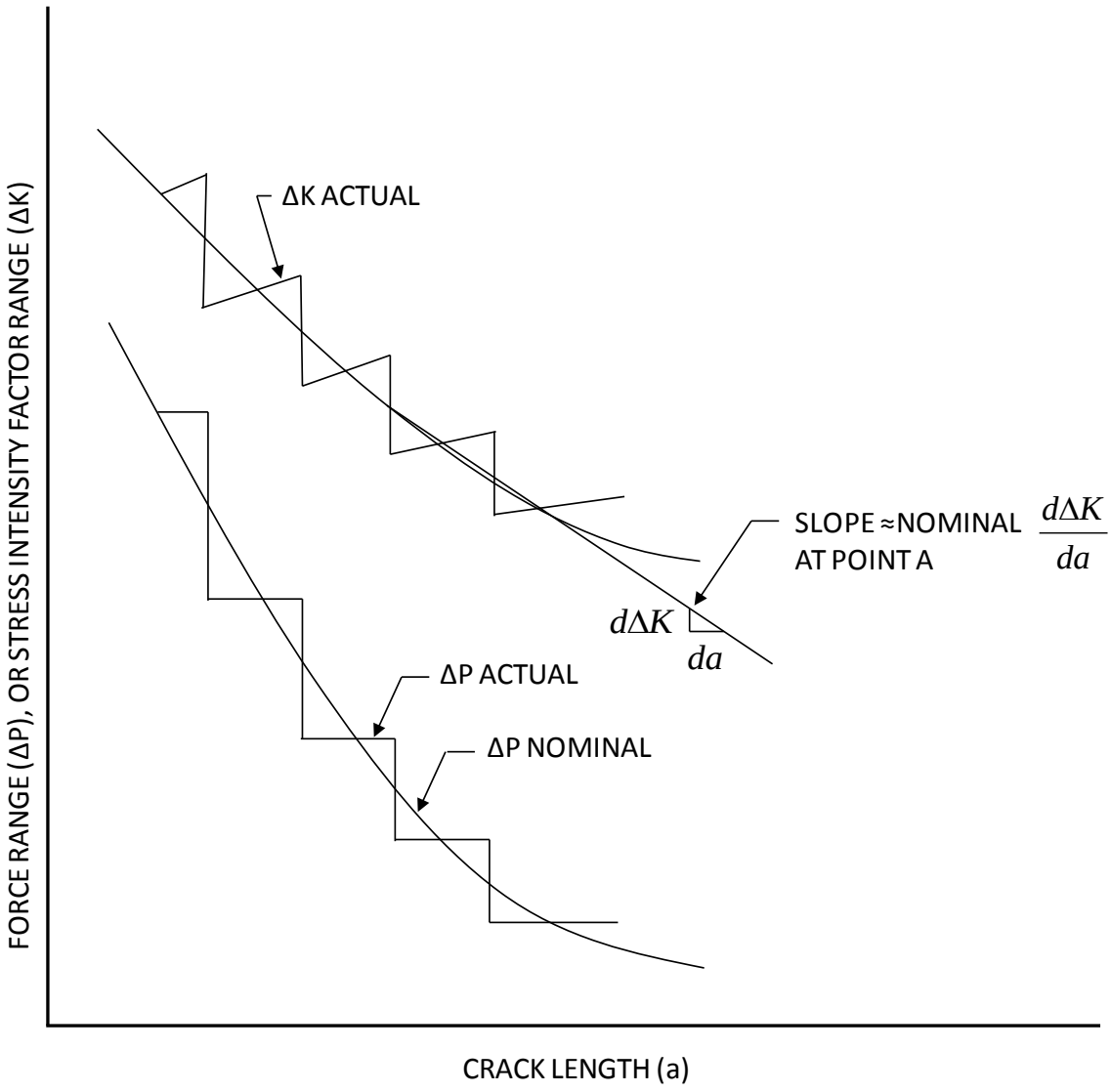

Fig. 17 Typical K decreasing process by stepped force shedding[32]

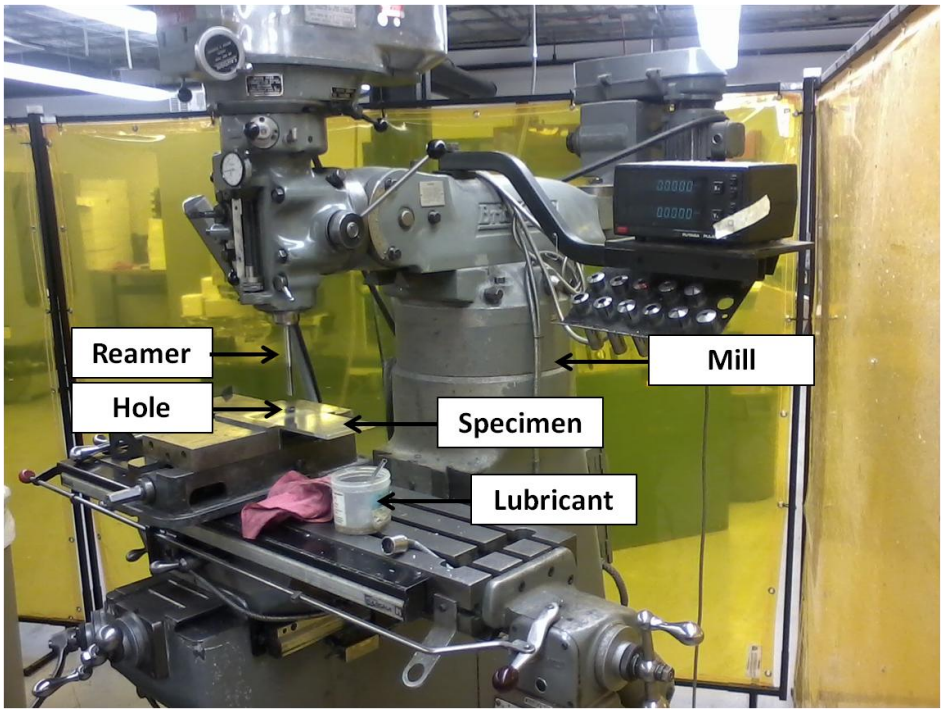

Fig. 18 Photo of mill at the University of Utah used to ream final diameter for cold-expanded specimens

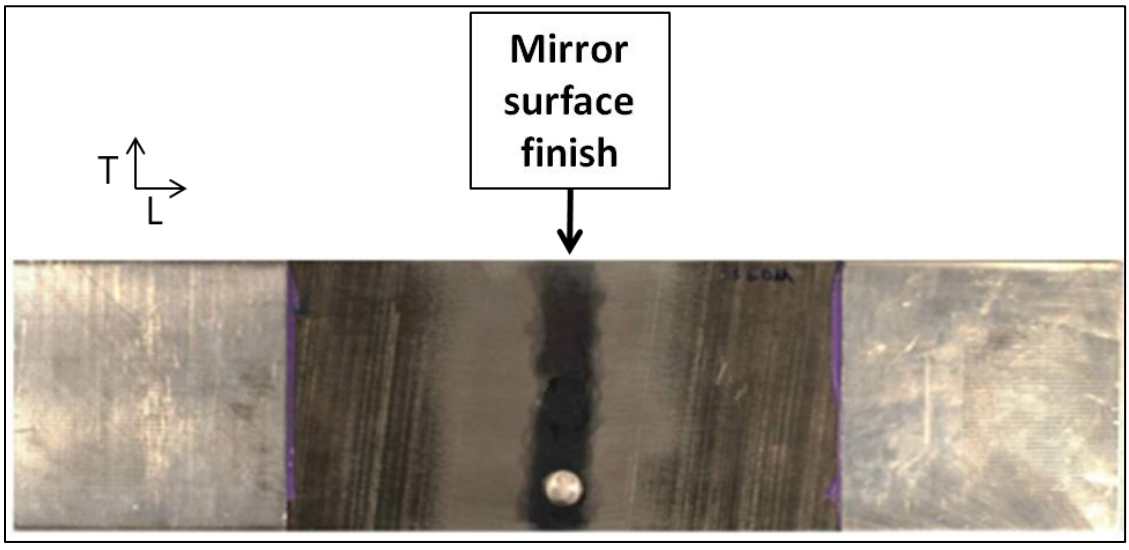

Fig. 19 Typical cold-expanded specimen after final sanding and polishing; view looking down at the EDM face, L and T orientations indicated

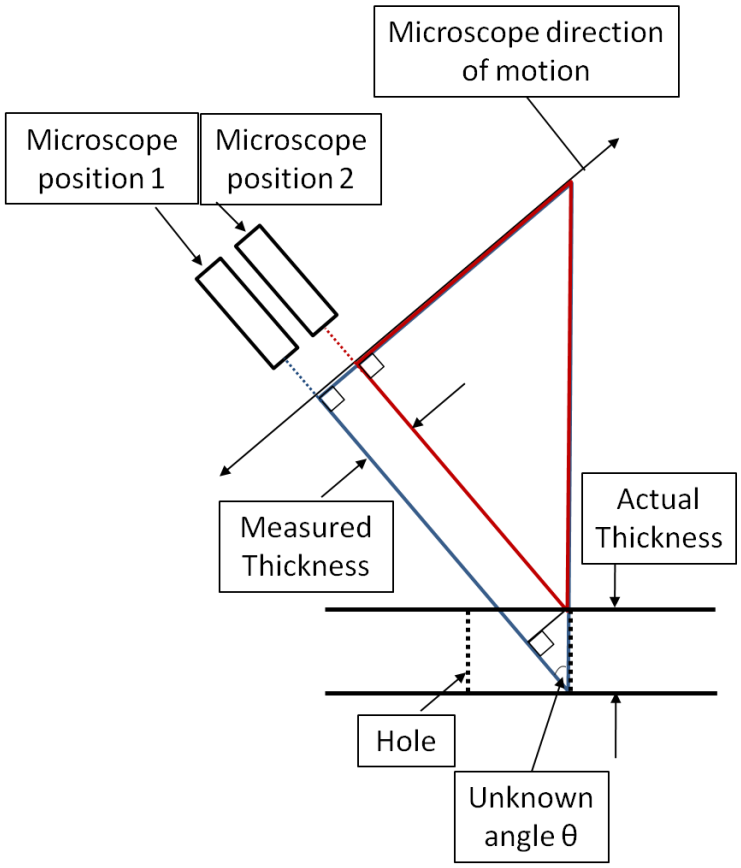

Fig. 20 Illustration showing use of using similar triangles to determine angle of microscope

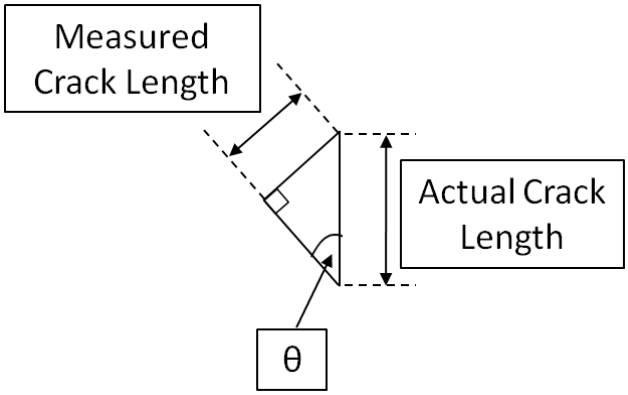

Fig. 21 Illustration showing the angle of the microscope and dimensions used to calculate the crack length down the bore of the hole

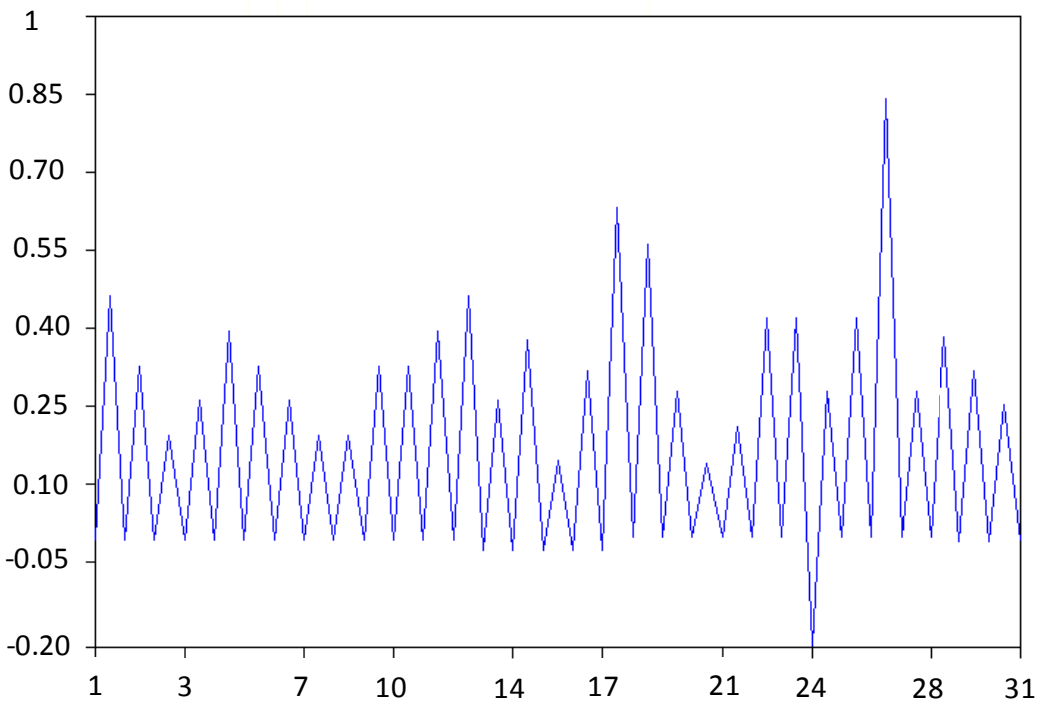

Fig. 22 Section of the A-10 aircraft wing spectrum used in the experiments

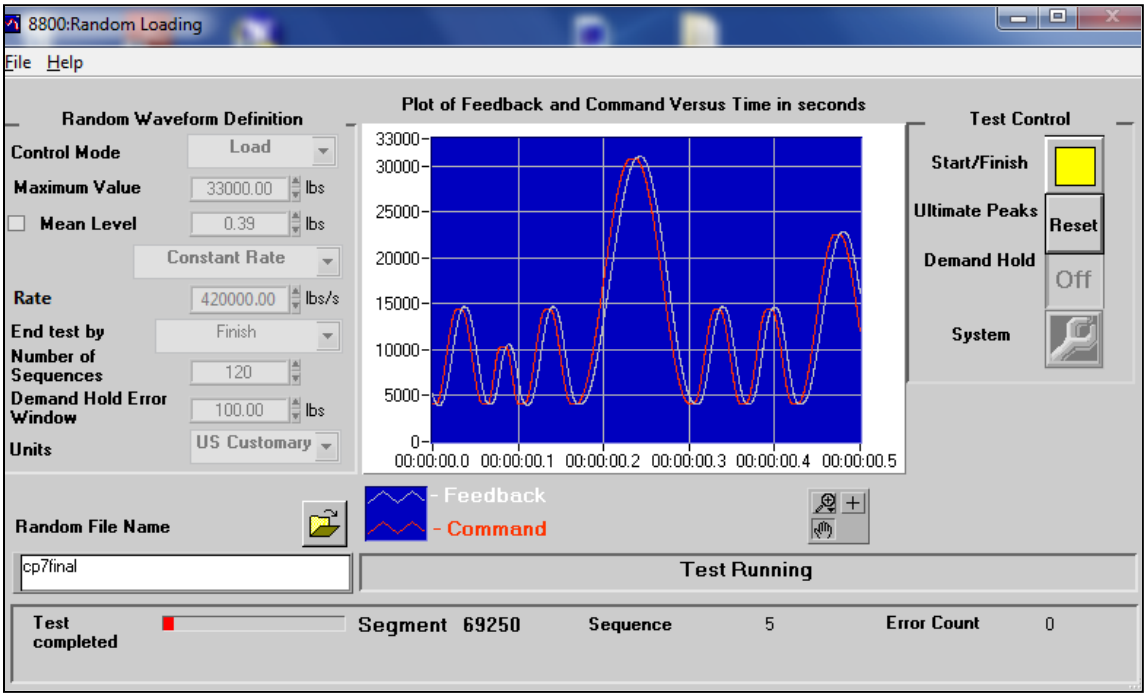

Fig. 23 Screen shot of Random Loading software module

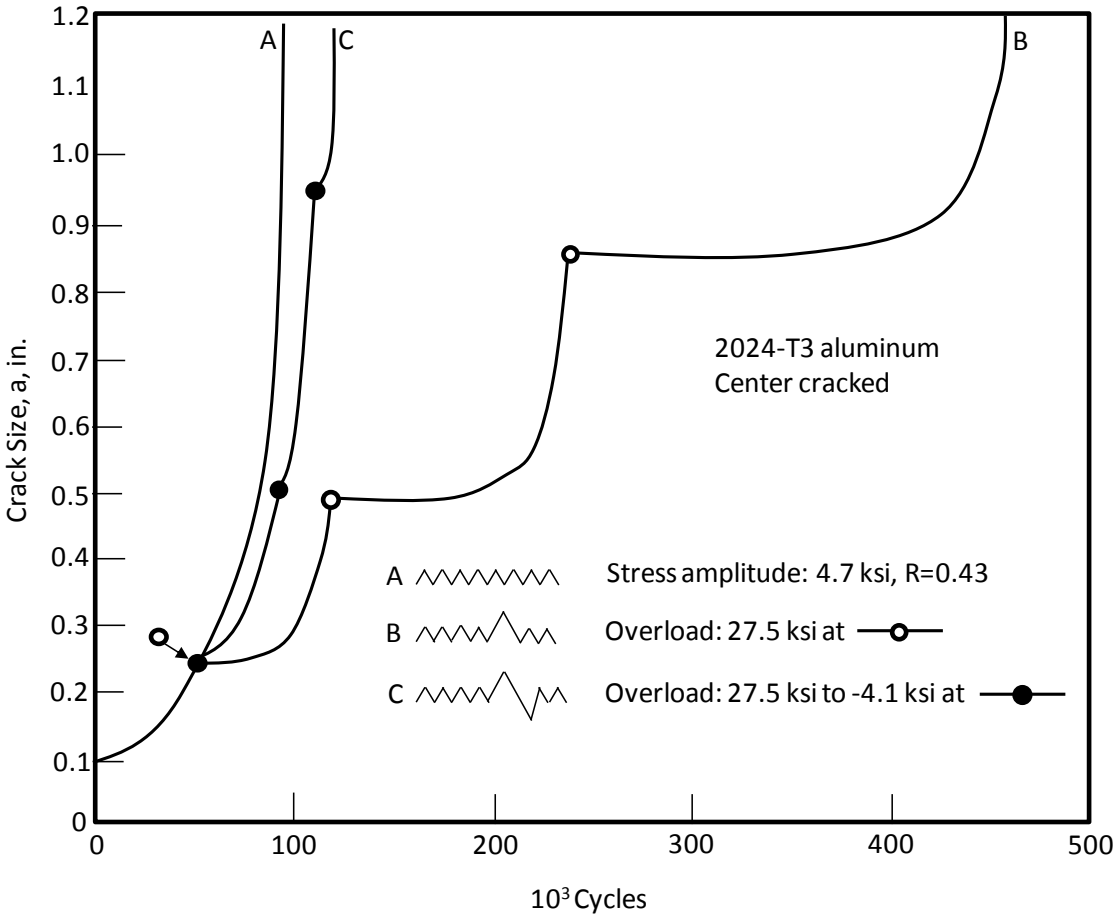

Fig. 24 Example crack length vs. cycles plot showing crack growth retardation due to positive overloads[6]

3 DATA COLLECTION AND PROCESSING

3.1 Crack Growth Rates

Crack lengths were measured on three surfaces – the EDM face, the bore of the hole, and the non-EDM face.

Using the secant method described in ASTM E 647[31], which involves calculating the slope of the straight line connecting two adjacent data points on the 'a versus N' curve, crack growth rates were calculated according to Eq. 4. Where "a" is crack length and "N" is cycles.

$$da/dN = (a_{i+1} - a_i) / (N_{i+1} - N_i) \quad \textbf{(5)}$$

The crack growth rates were calculated for the two ASTM E 647 specimens, to verify that the data collected met the requirements in the standard.

3.2 Marker Bands

As part of the work of Carlson[13] and Pilarczyk,[10] marker banding was used to document the shape of the crack front. Through this technique it was found that the cold-expanded holes exhibit a p-shaped crack front due to the cold expansion process. A photo showing the crack front from their research is shown in Fig. 25. For this research, it was desired to document the effect of the short edge margin on the crack front shape.

Marker banding is a change in the loading sequence such that a feature is created on the fracture surface which can be used to see the crack front shape. An example of the

difference between normal constant-amplitude loading and a marker banding sequence is shown in Fig. 26.

Using the same techniques employed by Carlson[13] and Pilarczyk[10], marker banding was implemented on specimen OFF-PC-CX2024-7, a precracked then cold-expanded specimen. The marker band loading information is given in Table 2.

As can be seen in Fig. 27, the p-shape crack front is still apparent in the short edge margin specimens. The specimen fractured shortly as seen in the image.

3.3 AFGROW Models

AFGROW is an fatigue crack growth prediction software tool that is used to predict the fatigue life of metallic structures. It is the current tool used by the USAF to complete DTAs for the A-10 Aircraft Structural Integrity Program (ASIP). Methodology has been put into place on guidelines and standard practices when using this tool, by Air Force Structures Bulletins, Air Force regulations, and the A-10 ASIP analysis group, and those guidelines were followed for this research.[5, 6, 36-40] The ground rules used by the A-10 ASIP group for DTAs are included in Appendix H.

3.3.1 Baseline Configurations

The data generated from the two ASTM E 647 specimens were used as a baseline to validate AFGROW model predictions. The internal through crack at a hole model was used to model the ASTM E 647 specimens. This model is shown in Fig. 28. The through crack in the model includes the two through EDM notches and the hole. This model was used because it is the most basic fracture mechanics model – a through crack in a flat plate. While it has a finite width correction it has no other additional geometry

corrections built in to it such as an offset hole correction. The only user input that affects this crack growth model, besides geometry, is the crack growth rate data discussed in the next section. These data are put into the model via a user-defined lookup table. Consequently, this AFGROW model and corresponding user-defined lookup table were validated when the fatigue life prediction corresponded to the fatigue life of the actual specimens.

3.3.1.1 Lookup File

The crack growth rate data, da/dN, collected from the two ASTM E 647 specimen fatigue tests, was used to create a da/dN vs. ΔK plot, where ΔK is the stress intensity factor range. It is calculated from Eq.5, with α calculated from Eq. 6. These equations are from the ASTM E 647 standard for middle tension specimens.[31]

AFGROW contains several options for curve fits for crack growth rate data. These include the Forman equation, NASGRO equation, Walker equation, and others. It also has the option for a user to create a tabulated lookup file that contains a manually defined set of values of da/dN and ΔK for different stress ratios. These values are used to generate curves for the crack growth rate data. This lookup file option is will be used for this research, since it provides the most accurate fit to the data. However, as the experimental data generated by this research were only for one stress ratio ($R = 0.1$) the data from the A-10 ASIP group was used for the other stress ratio ($R = 0.8$) in the lookup file. AFGROW requires two stress ratios when doing variable-amplitude loading, as it interpolates and extrapolates from this data to fit all the stress ratios that are used in the spectrum.

The original research goal was to use the A-10 ASIP derived lookup file for both stress ratios for this data. However, during the process of verifying the non-cold-expanded test data to AFGROW predictions, it was found that the tabular lookup file currently utilized by A-10 ASIP did not align well with the ASTM E 647 data generated from this research. Therefore a new curve fit to the test data was created, and a tabular lookup file made from that curve fit.

$$\Delta K = \frac{\Delta P}{T}\sqrt{\frac{\pi\alpha}{2W}\sec\frac{\pi\alpha}{2}} \quad \textbf{(6)}$$

$$\boldsymbol{\alpha = \frac{2a}{W}} \quad \textbf{(7)}$$

3.3.1.2 Constant-Amplitude Baseline

The non-cold-expanded hole specimens were used as a baseline to validate predictions from AFGROW against experiment data. Measured values from the specimens were used for width, thickness, hole diameter, hole offset, and crack sizes in the models. The AFGROW classic corner crack at a hole model was used for all predictions as seen in Fig. 29.

3.3.1.3 Variable-Amplitude Baseline

For the variable-amplitude non-cold-expanded specimens, the same type of classic AFGROW model was used. To account for the spectrum loading effects on the crack tip, a retardation model had to be selected that would give the best fit to the data. AFGROW gives several options for retardation models, including Hsu, FASTRAN, Generalized Willenborg, and Closure. The model used by A-10 ASIP is the Generalized

Willenborg model and was also the model used for this research. An excerpt from the AFGROW help file is given.[41]

> The Generalized Willenborg retardation model is one of the most commonly used retardation models in crack-growth life prediction programs. The model is based on early fracture mechanics work at Wright-Patterson AFB, OH and was named after a student who worked on the model. The model uses an 'effective' stress intensity factor based on the size of the yield zone in front of the crack tip.

The Generalized Willenborg model uses as its only input parameter, Shut-Off Overload Ratio (SOLR). This parameter was varied until the AFGROW prediction matched the final cycle count from the variable-amplitude specimen.

3.3.2 Other Configurations

AFGROW models were created for all precracked cold-expanded specimens, as well as the cold-expanded specimens. The baseline models were altered to have the specific geometry and initial crack sizes for each specimen. The corresponding crack growth predictions were used to show the increase in fatigue life due to cold expansion. The variable-amplitude specimens for the three specimen configurations were all loaded at the same stress. For these specimens, both the actual experiment data and the AFGROW prediction were compared.

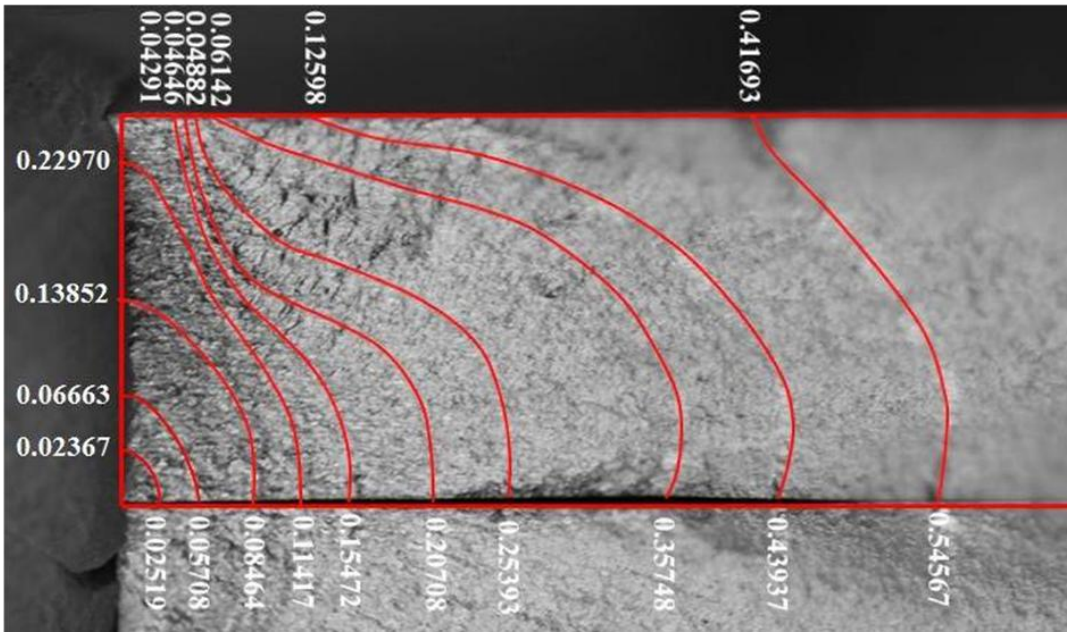

Fig. 25 Marker band specimen highlighting crack front geometry as it progressed through the specimen (dimensions are in inches)[10]

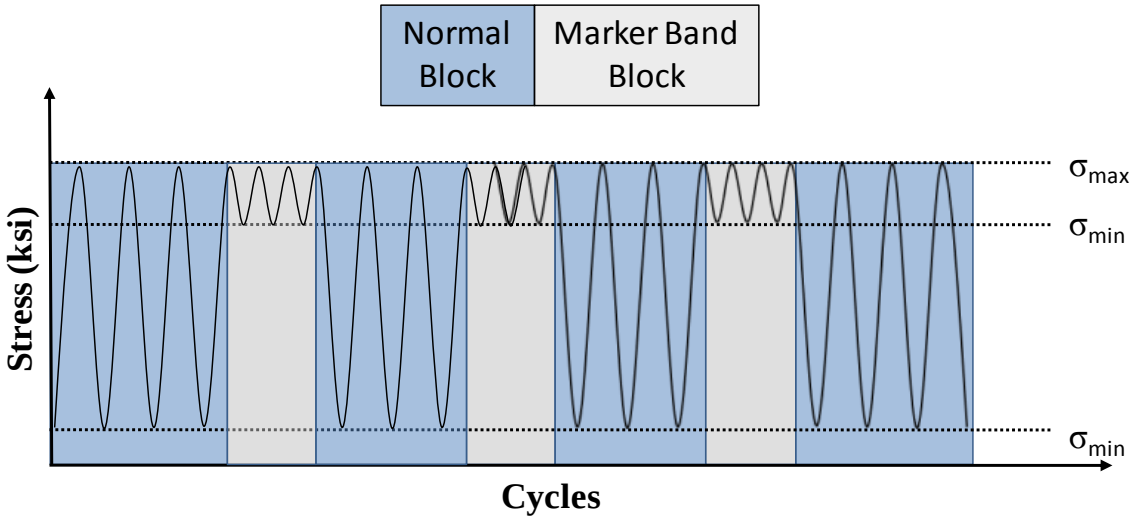

Fig. 26 Difference between normal loading and marker band loading sequence[10]

Table 2 Marker band block information

Type of block	Stress Ratio	Minimum Stress	Maximum Stress	Frequency
Normal	0.1	2.5 ksi	25 ksi	20 Hz
Marker Band	0.9	22.5 ksi	25 ksi	40 Hz

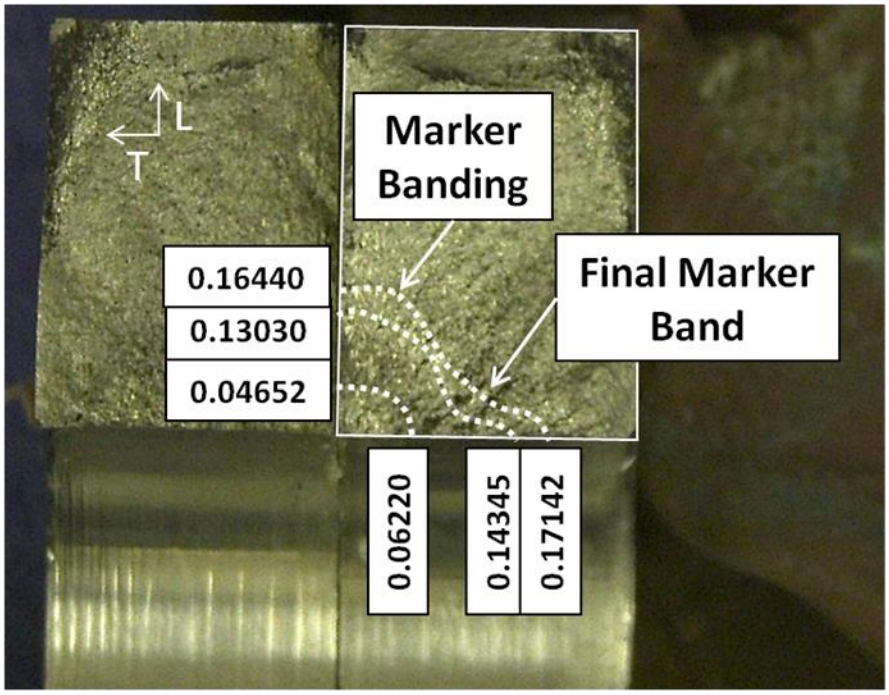

Fig. 27 OFF-PC-CX2024-7 marker band specimen showing p-shape crack front

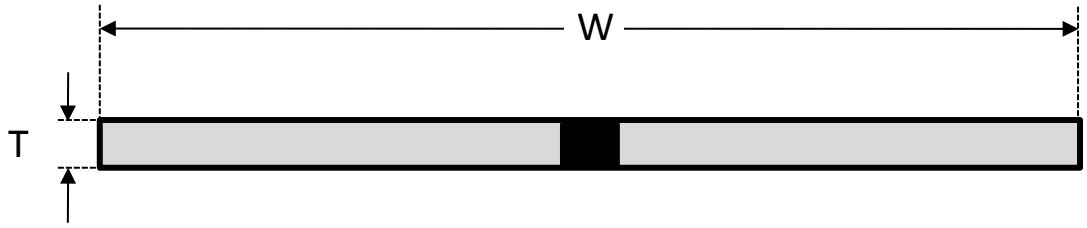

Fig. 28 Cross-sectional view of AFGROW internal through crack at a hole model used for the ASTM E 647 specimens, with through crack in center of model

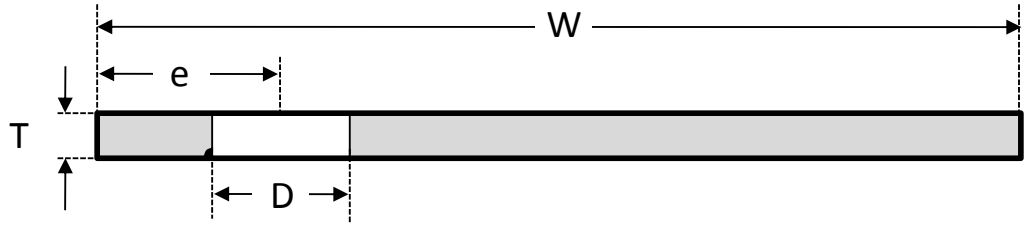

Fig. 29 AFGROW classic corner crack at a hole model used for all predictions, where D is diameter, W is width, T is thickness, and e is hole offset

4 RESULTS

4.1 Summary of Fatigue Experiments Performed

There were a total of 26 specimens used for this research. Two specimens were used in order to verify that the load frame and corresponding fatigue data were valid according to ASTM E 647. Six specimens were not cold-expanded, and were used as a baseline to compare against. Four of these specimens were loaded in constant-amplitude, and two were loaded in variable-amplitude. Eight specimens were cold-expanded without a crack in the hole, and were also a baseline condition to compare against. They represent the nominal fatigue life for a cold expansion specimen that contained no crack prior to cold expansion. Four of these specimens were constant-amplitude, and four were variable-amplitude. The test condition consisted of 10 precracked then cold-expanded specimens. Five of these were loaded in constant-amplitude, with one of those being used for marker banding. The other five were loaded in variable-amplitude. All specimens, their IDs, type, and other information are summarized in Table 3. Flight hours were calculated by Eq. 8, where moving from one load to the next load in the spectrum file was considered a cycle. The number of cycles per spectrum was determined by the number of points in the spectrum file. The number of flight hours per spectrum was determined by the A-10 ASIP DTA Ground Rules, given in Appendix H.

$$\text{Flight Hours} = \frac{\#\ \text{Cycles}}{7381\ \frac{\text{Cycles}}{\text{Spectrum}}} \cdot 240\ \frac{\text{Flight Hours}}{\text{Spectrum}} \quad \textbf{(8)}$$

4.2 Fatigue Crack Growth Data Sheets

Fatigue crack growth information sheets were created for every specimen. The naming terminology used in this research consisted of the specimen face that contained the EDM notch was called the EDM face. The opposite face was the non-EDM (NEDM) face. The short ligament side of the specimen was called side A, and the opposite called side B, as shown in Fig. 30. An example of one of these data sheets is shown in Fig. 31. As seen in Fig. 31, all cracks begin on 'EDM – A' surface. Data sheets for all specimens are attached in Appendix C.

4.3 Crack Growth Curves

Plots of crack length vs. cycles were created for all specimens and are included in Appendix C. An example of each specimen configuration is given in the following sections.

4.3.1 ASTM E 647 Specimens

The crack growth curves for the two standard middle tension M(T) specimens are shown in Fig. 32. These plots show the average crack size versus cycles from the four measured crack lengths, as is the procedure specified in ASTM E 647.[31]

4.3.2 Non-Cold-Expanded Specimens

Typical crack growth curves for the non-cold-expanded specimens are shown in Fig. 33 and Fig. 34, for constant and variable-amplitude loading, respectively. These

plots show the EDM-A, bore, and NEDM-A crack lengths. The non-cold-expanded specimens were used to create a baseline crack growth curve for holes that are not cold-expanded. They were compared to the holes that were precracked then cold-expanded, in order to show the improvement in life from cold expansion. All the non-cold-expanded specimen crack growth curves are given in Appendix D.

4.3.3 Precracked Cold-Expanded Specimens

The typical crack growth curves for the precracked cold-expanded specimens in constant-amplitude loading and variable-amplitude loading are shown in Fig. 35 and Fig. 36. The crack growth curves for all the precracked cold-expanded specimens are documented in Appendix D.

These specimens are the test configuration for this research. They represent the situation in a maintenance facility when a hole was cold-expanded when there may have been an existing crack in the hole. The plots show the EDM-A, bore, and NEDM-A crack growth curves for the specimen.

4.3.4 Cold-Expanded Specimens

Typical crack growth curves for the cold-expanded specimens are shown in Fig. 37 and Fig. 38, for constant and variable-amplitude loading. These plots show the EDM-A, bore, and NEDM-A crack lengths. The cold-expanded specimens were used to create a baseline crack growth curve for holes that were cold-expanded without a pre-existing crack in the hole. They represent the ‘nominal’ cold expansion situation. Appendix D contains all of the crack growth curves for the cold-expanded specimens.

4.4 Crack Growth Rate Curves

Crack growth rate data, da/dN, was collected from the two ASTM E 647 specimens and plotted against ΔK. These are shown in Fig. 39. Included in the figure is the test data generated by Carlson[13.] Those tests used the same material and specimen geometry for two ASTM E 647 specimens. The da/dN vs. ΔK data from Carlson and this research lie follow the same trend which shows consistency in the experiment process and validity in the data. The curve fit discussed in Section 3.3.2 is plotted with the A-10 ASIP curve fit and the NASGRO equation for comparison in Fig. 39. As can be seen from the data in Fig. 39, there is a feature referred to as a "double knee" in the data, which occurs in some crack growth rate data for aluminum. One knee occurs at approximately ΔK of 5, and the other at ΔK of about 15. The key feature about the curve fit used for this research is that it was shaped to fit the data from this specific research. It also captures the second knee, where some of the other curve fits do not. This means that the crack growth rates and stress intensities that AFGROW uses for its predictions correspond more closely with the experimental data generated in this research. Because of this, the AFGROW predicted fatigue life corresponds more closely with the crack growth data generated in this research. The crack growth rate data is attached in Appendix F.

4.5 AFGROW

4.5.1 AFGROW Predictions

An AFGROW model was created for all specimens, with the exception of the specimen used for marker banding. The models for each specimen configuration will be discussed in the following sections.

4.5.1.1 ASTM E 647 Specimens

The AFGROW prediction and ASTM E 647 specimen data are plotted for the two specimens in Fig. 40 and Fig. 41. These specimens and corresponding AFGROW predictions were used to validate the user-defined material lookup file. These plots show that the AFGROW models predict the fatigue life of the specimens to within 11.6% of the experiment fatigue life for Fig. 40, and 0.47% for Fig. 41.

4.5.1.2 Non-Cold-Expanded Specimens

4.5.1.2.1 Constant Amplitude

The comparisons between the AFGROW prediction and the crack growth experiment data for the four non-cold-expanded constant-amplitude specimens are shown in Fig. 42. For these specimens, AFGROW was used as a verification tool. For the constant-amplitude specimens, the Initial Flaw Size (IFS) used in AFGROW was varied until a consistent and accurate fatigue life prediction was generated for all non-cold-expanded specimens. For example, it was found that the best fit of the AFGROW model to the constant-amplitude experiment data was achieved when the average initial crack size from the experiment was used for the IFS for both the bore and surface crack lengths and by holding the aspect ratio (a/c) constant, where ‘a’ is the bore crack length and ‘c’ is the surface crack length. By using this approach for IFS, the average error between the predictions and experimental data for all constant-amplitude specimens was 2.9%. All other AFGROW predictions for all constant-amplitude non-cold-expanded specimens are presented in Appendix E.

4.5.1.2.2 Variable-Amplitude

The variable-amplitude non-cold-expanded specimens were used to generate the retardation parameter, SOLR, for the Generalized Willenborg retardation model. The geometry and loading were input into AFGROW, then the SOLR value was varied until the AFGROW prediction matched the crack growth experimental data. An SOLR value of 2.11 was selected for the baseline variable-amplitude loaded specimens, and was used in all other AFGROW models that used spectrum loading. The comparison between the variable-amplitude loaded specimen and the AFGROW prediction with SOLR = 2.11 is shown in Fig. 43. This prediction is within 1.2% of the experiment fatigue life, because the exact value of the SOLR is varied to adjust the life prediction to match experiment results.

4.5.1.3 Precracked Cold-Expanded Specimens

The comparisons between the AFGROW prediction and the experimental data for the precracked then cold-expanded constant-amplitude specimens and variable-amplitude specimens are shown in the plots in Fig. 44 and Fig. 45. These plots show the non-cold-expanded baseline specimen for variable-amplitude loading, as it was loaded at the same stress, as well as the AFGROW prediction for reference. The average increase in fatigue life for all the constant-amplitude specimens was found to be 3.60, and 2.27 for the variable-amplitude specimens. All AFGROW predictions for the precracked cold-expanded specimens are presented in Appendix E.

4.5.1.4 Cold-Expanded Specimens

The cold-expanded constant-amplitude AFGROW predictions for both constant and variable-amplitude loading are shown in Fig. 46 and Fig. 47. Again, these plots show the non-cold-expanded baseline specimen for variable-amplitude loading as well as the AFGROW prediction for reference. The average increase in fatigue life for the constant-amplitude specimens was found to be 6.75, and 3.26 for the variable-amplitude specimens. The AFGROW predictions for the cold-expanded specimens are included in Appendix E.

4.5.2 Lookup File

The tabular lookup file created from the da/dN versus ΔK data from the two ASTM E 647 specimens is shown in Table 4. This is for only one stress ratio, R=0.1. ΔK values for a stress ratio of R = 0.8 were taken from the A-10 ASIP analysis group for use in the variable-amplitude specimen AFGROW models. The da/dN versus ΔK data used to generate this lookup file came from this research and the research done by Carlson,[13] and is shown in Fig. 48.

4.6 Fractography

Select images were taken for fractography purposes. It should be noted, as discussed previously, that only a select number of specimens were failed on both sides of the hole. The specimens that did have continuing damage completed are the ones available for fractography. The other specimens will have continuing damage completed in the future and were not cut for that purpose.

4.6.1 Keyence Digital Microscope Images

4.6.1.1 ASTM E 647 Specimens

The fracture surfaces for the ASTM E 647 specimens were typical of a fatigue fracture. The specimens had approximately 3 inches of flat fracture surface shown in Fig. 49. These specimens were loaded at a stress of 11.4 ksi, due to this relatively low stress, the fatigue cracks propagated nearly all the way through the specimen before final fracture. Additional fracture surface images for these specimens are shown in Appendix G.

4.6.1.2 Non-Cold-Expanded Specimens

Fig. 50 contains an image of the fracture surfaces for a typical constant-amplitude loaded non-cold-expanded specimen, with the EDM faces placed together. This specimen had continuing damage conducted after the ligament failure, so there is some marking and rubbing on the fracture faces from that experiment. There were no variable-amplitude specimens that had continuing damage completed, so only the constant-amplitude specimen images are shown. The four constant-amplitude non-cold-expanded specimen fracture surfaces are shown in Appendix G.

4.6.1.3 Precracked Cold-Expanded Specimens

The fracture faces for a constant-amplitude precracked cold-expanded specimen are shown in Fig. 51, with EDM faces placed together. The ≈ 0.050 inch corner crack can easily be seen in the image, with typical flat fracture surface most of the way through the ligament. There were no precracked cold-expanded specimens that had continuing damage with variable-amplitude loading, so there are no fracture surfaces images for

those specimens. Additional fracture surfaces for the constant-amplitude precracked cold-expanded specimens are displayed in Appendix G.

4.6.1.4 Cold-Expanded Specimens

As there were no cold-expanded specimens that had continuing damage completed on them, and the specimens were not cut in order to preserve them for that valuable information, there are no fracture face images for the cold-expanded specimens.

4.6.2 SEM images

A Scanning Electron Microscope (SEM) was used to look at the fracture features for the specimen used for marker banding. The experience of learning how to use an SEM was considered a valuable tool as was looking at the microstructure of the specimens and identifying fatigue features. In Fig. 52, Fig. 53, and Fig. 54, an SEM is used to look at a location and identify fatigue striations for the marker banded specimen. This is done for another location on the marker banded specimen in Fig. 55, Fig. 56, and Fig. 57.

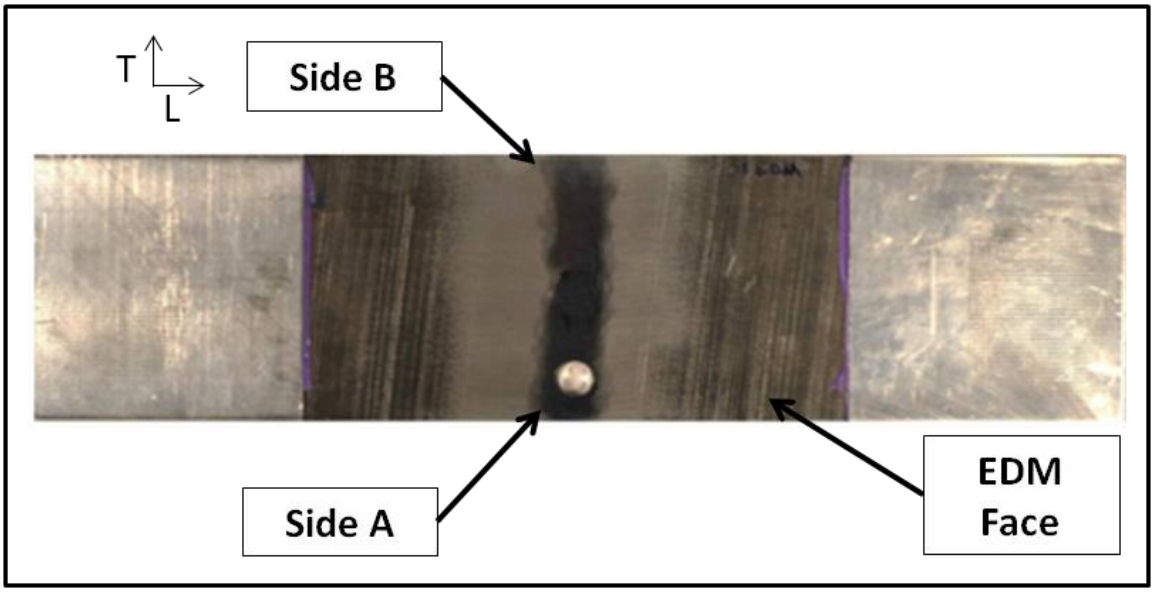

Fig. 30 Naming terminology used for all specimnes, looking at EDM face

Table 3 Summary of fatigue experiments

Specimen ID	Specimen Type	Loading Type	Test Date	Max Stress	Cycles to Ligament Failure	Flight Hours to Ligament Failure	Notes
2024-1	ASTM E 647 M(T)	Constant Amplitude	17-Jul-11	11.27	339662	NA	
2024-2	ASTM E 647 M(T)		18-Jul-11	11.25	265444	NA	
OFF-NCX2024-1	M(T) Non Cold Expanded Offset Hole	Constant Amplitude	29-Jun-11	10.00	49631	NA	
OFF-NCX2024-2			30-Jun-11	10.00	51797	NA	
OFF-NCX2024-3			30-Jun-11	10.00	61441	NA	
OFF-NCX2024-4			30-Jun-11	10.00	52051	NA	
OFF-NCX2024-5		Variable Amplitude	22-Aug-11	32.72	NA	2979	
OFF-NCX2024-6			23-Aug-11	32.79	NA	7268	Specimen Overloaded
OFF-PC-CX2024-1	M(T) Precracked Cold Expanded Offset Hole	Constant Amplitude	11-Aug-11	25.00	11168	NA	
OFF-PC-CX2024-2			11-Aug-11	25.00	14474	NA	
OFF-PC-CX2024-3			11-Aug-11	25.00	10927	NA	
OFF-PC-CX2024-4			11-Aug-11	25.00	19686	NA	
OFF-PC-CX2024-5		Variable Amplitude	18-Aug-11	32.46	NA	5374	
OFF-PC-CX2024-6			19-Aug-11	32.55	NA	7047	
OFF-PC-CX2024-7		Constant Amplitude	30-Aug-11	25.00	412936	NA	Marker Band Specimen
OFF-PC-CX2024-8		Variable Amplitude	20-Aug-11	32.55	175548	5718	
OFF-PC-CX2024-9			1-Sep-11	32.60	172250	5611	
OFF-PC-CX2024-10			6-Sep-11	32.60	255700	8329	
OFF-CX2024-1	M(T) Cold Expanded Offset Hole	Variable Amplitude	23-Sep-11	32.23	NA	6972	
OFF-CX2024-2			23-Sep-11	32.47	NA	8574	
OFF-CX2024-3		Constant Amplitude	21-Sep-11	25.00	28465	NA	
OFF-CX2024-4			8-Sep-11	25.00	18806	NA	
OFF-CX2024-5		Variable Amplitude	8-Sep-11	32.35	NA	12280	
OFF-CX2024-6			20-Sep-11	32.29	NA	14568	
OFF-CX2024-7		Constant Amplitude	8-Sep-11	25.00	61831	NA	
OFF-CX2024-8			15-Sep-11	25.00	49889	NA	

Fatigue Crack Growth Data Sheet

Specimen I.D. OFF-CX2024-4
Width: 4.0065 in. Thick: 0.2545 in. Area: 1.0197 in^2

Precrack Information
Precrack Date: 26-Aug-11 Loading Condition: Constant-amplitude R= 0.1
Frequency: 20 Hz Hole Diameter: 0.48837 in. Peak Stress: 25.0 ksi
Surface EDM Length: 0.01834 in.

Testing Information
Test Date: 8-Sep-11 Loading Condition: Constant-amplitude R= 0.1
Frequency: 20 Hz Hole Diameter: 0.50267 in.
Peak Stress: 25.0 ksi Ligament Length: 0.34906 in.
Surface EDM Length: 0.01064 in.

Total Cycles	Crack Length (inches)					Comments
	Surface of Hole				Bore	
	EDM		NEDM			
	A	B	A	B		
0						Precrack
305446	0.03398				0.03366	
0	0.03138				0.02996	Testing
2782	0.04522				0.0414	
5005	0.05614				0.05922	
5977	0.06678				0.06188	
7998	0.0768				0.07522	
9389	0.08535				0.0803	
10241	0.0934				0.08458	
11454	0.10718				0.09616	
12186	0.12186				0.10824	
14289	0.14532				0.11944	
15510	0.16602				0.1253	
16145	0.18514				0.13436	
16460	0.20562				0.14094	
16917	0.22036		0.05772			Thru Thickness
17240	0.23814		0.1014			
17527	0.34906		0.34906			
Ligament Failed						

Fig. 31 Typical crack growth data sheet

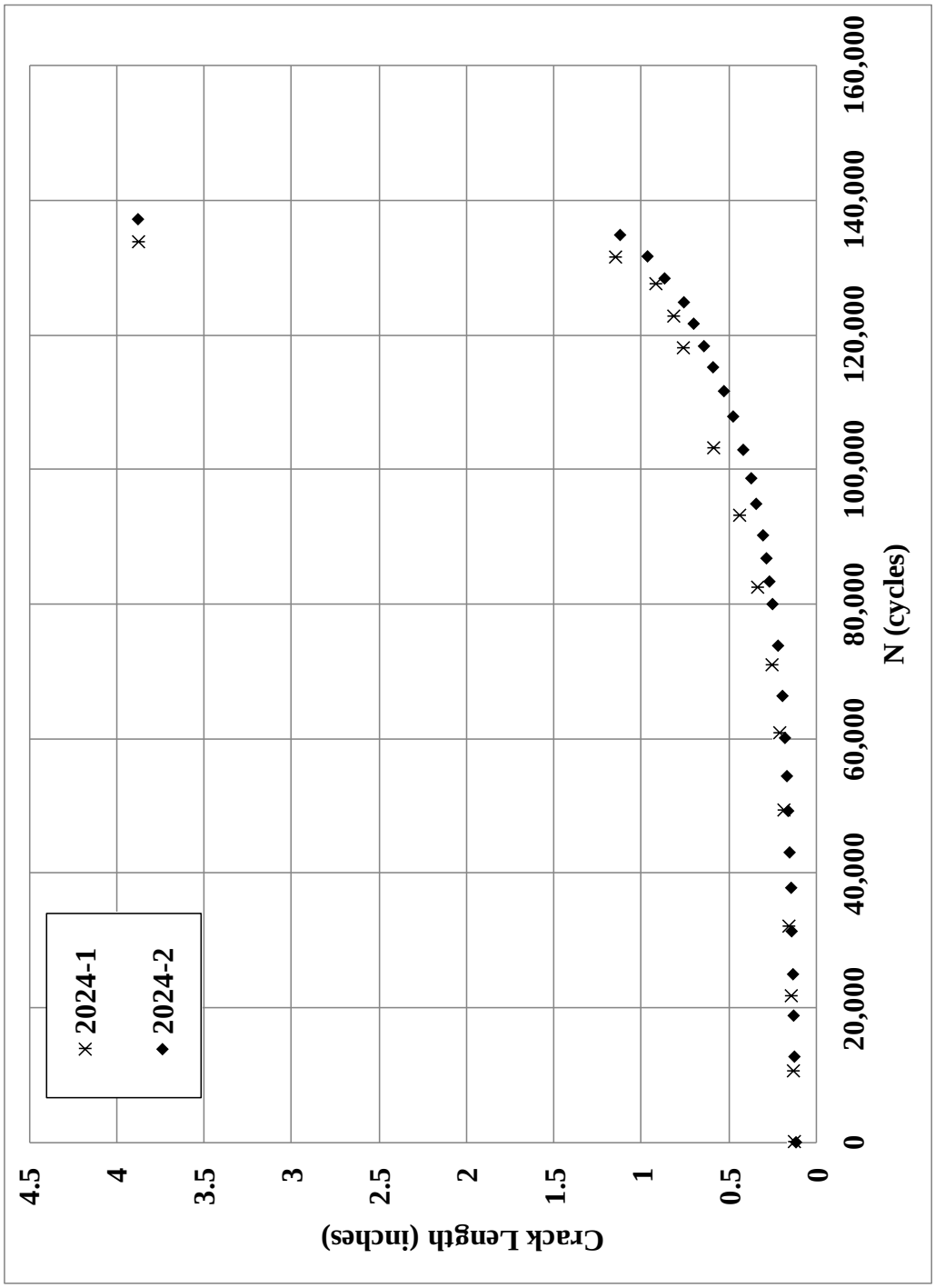

Fig. 32 ASTM E 647 specimens 2024-1 and 2024-2 crack growth curve; Constant-amplitude, R=0.1; σ_{max} = 11.4 ksi; 20 Hz, Lab Air

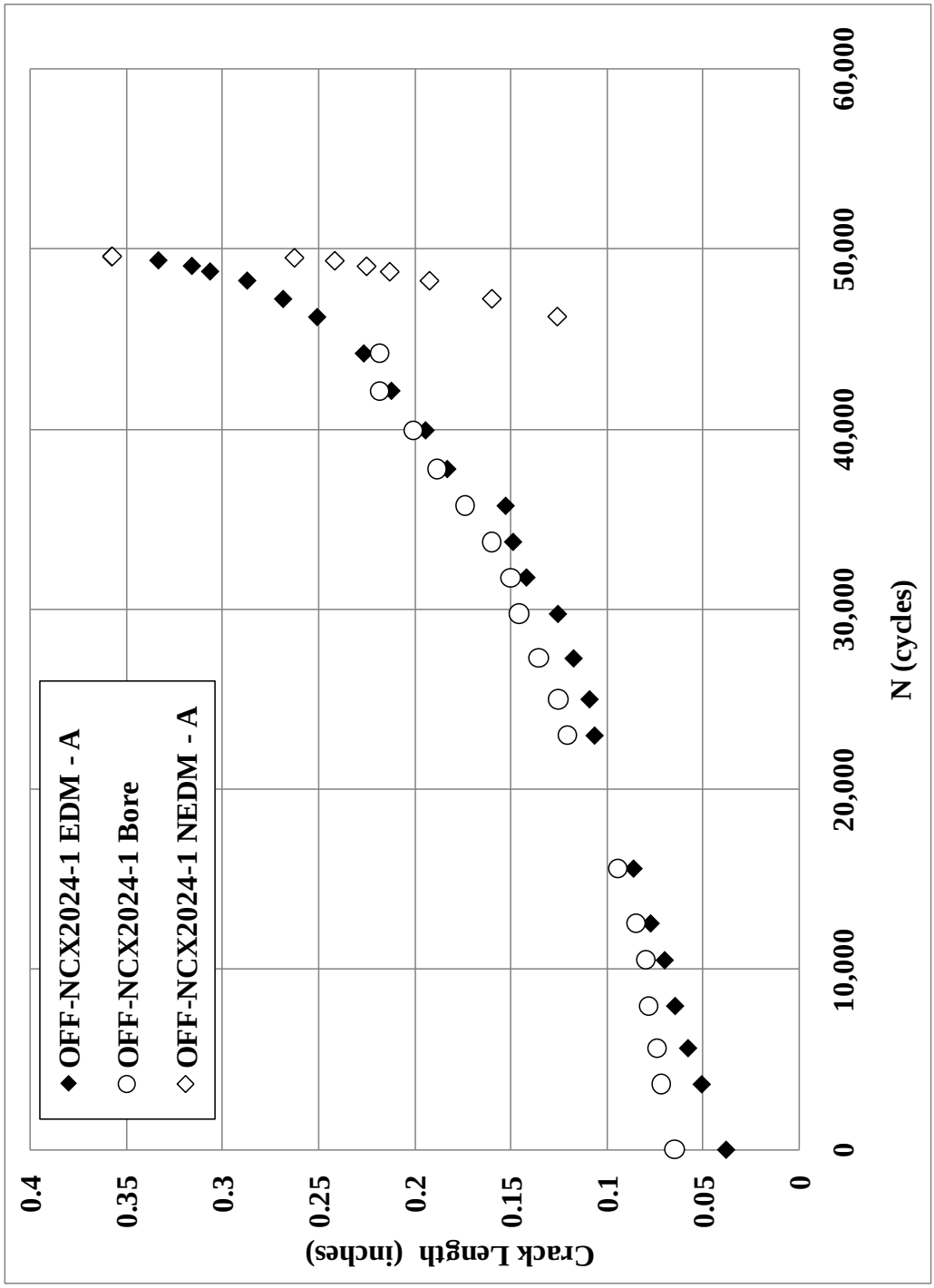

Fig. 33 Typical constant-amplitude non-cold-expanded specimen crack growth curve – OFF-NCX2024-1; Constant-amplitude, R=0.1; σ_{max} = 10 ksi; 20 Hz, Lab Air

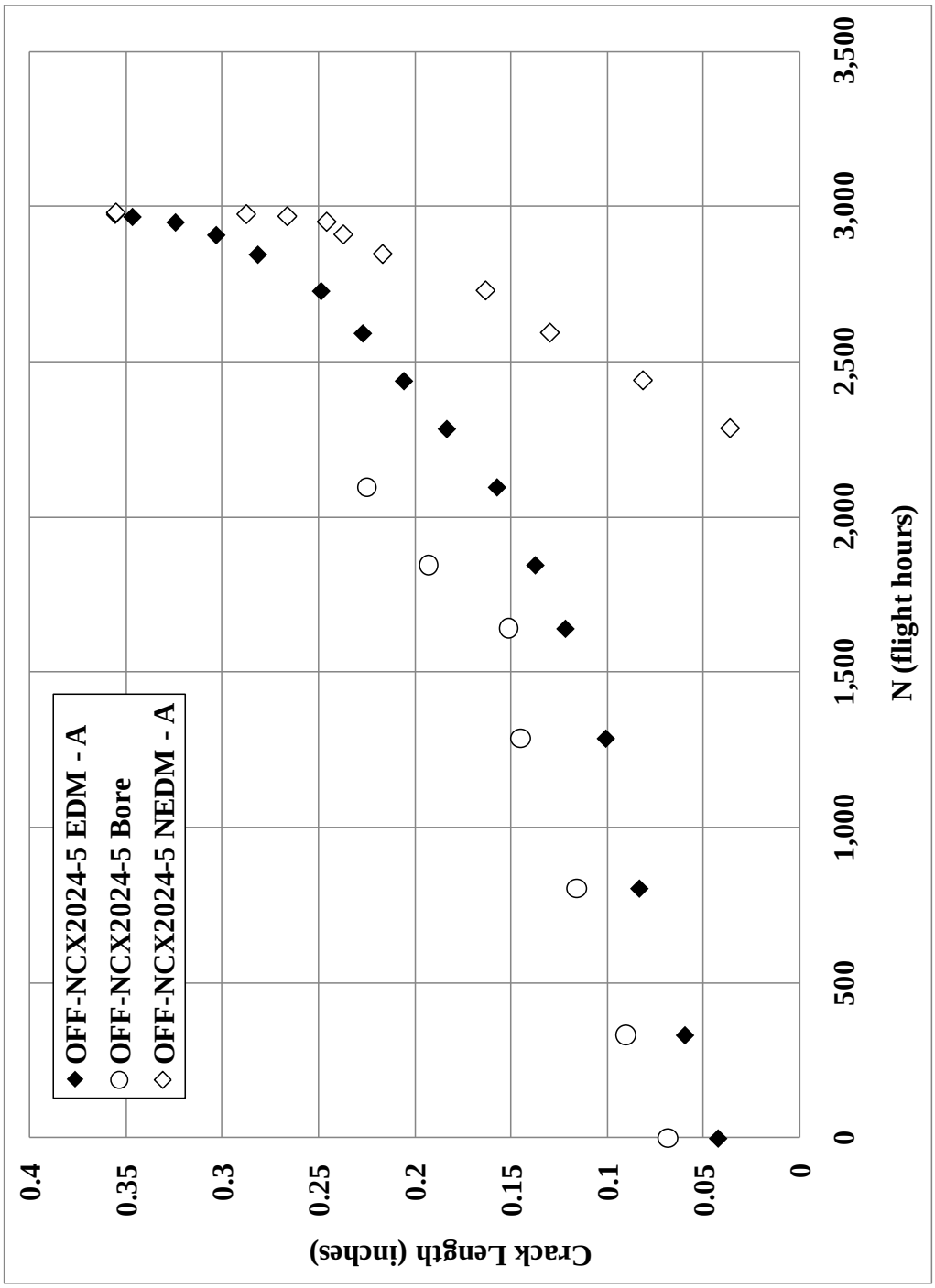

Fig. 34 Typical variable-amplitude non-cold-expanded specimen crack growth curve – OFF-NCX2024-5; A-10 wing spectrum; σ_{max} = 33 ksi; Lab Air

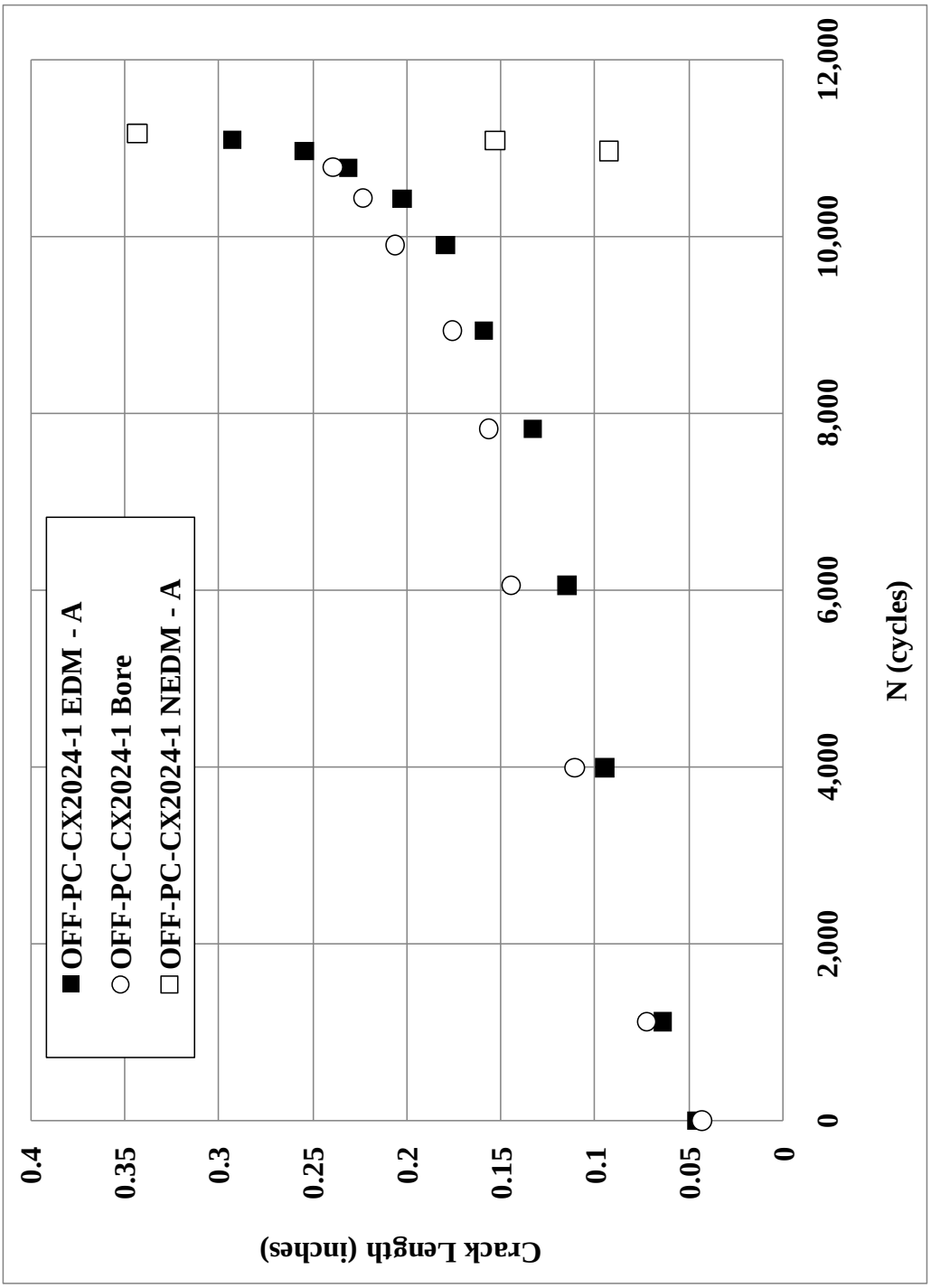

Fig. 35 Typical constant-amplitude precracked cold expanded specimen crack growth curve – specimen OFF-PC-CX2024-1; Constant-amplitude, R=0.1; σ_{max} = 25ksi; 20 Hz, Lab Air

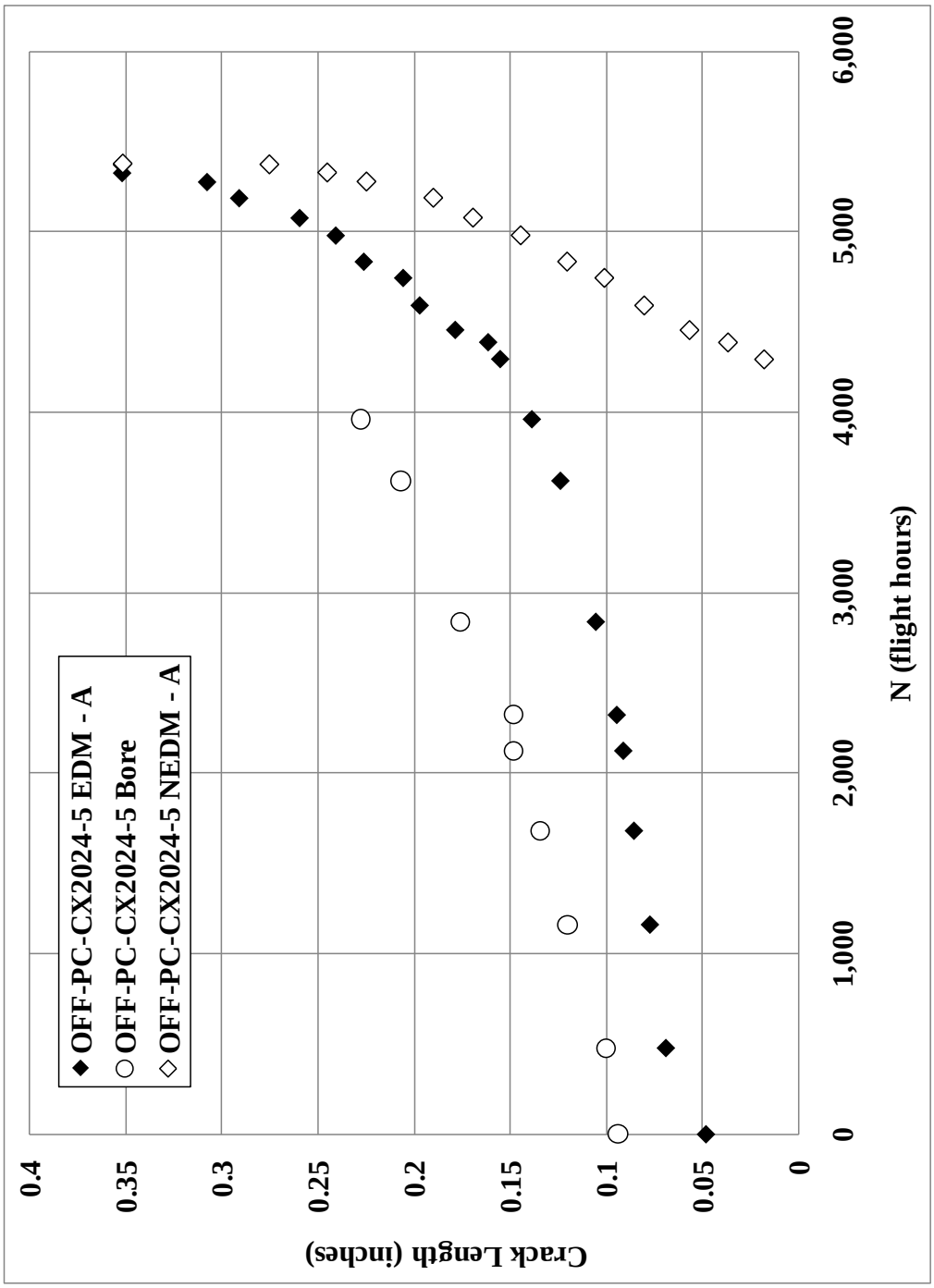

Fig. 36 Typical variable-amplitude precracked cold expanded specimen crack growth curve – OFF-PC-CX2024-5; A-10 wing spectrum; σ_{max} = 33 ksi; Lab Air

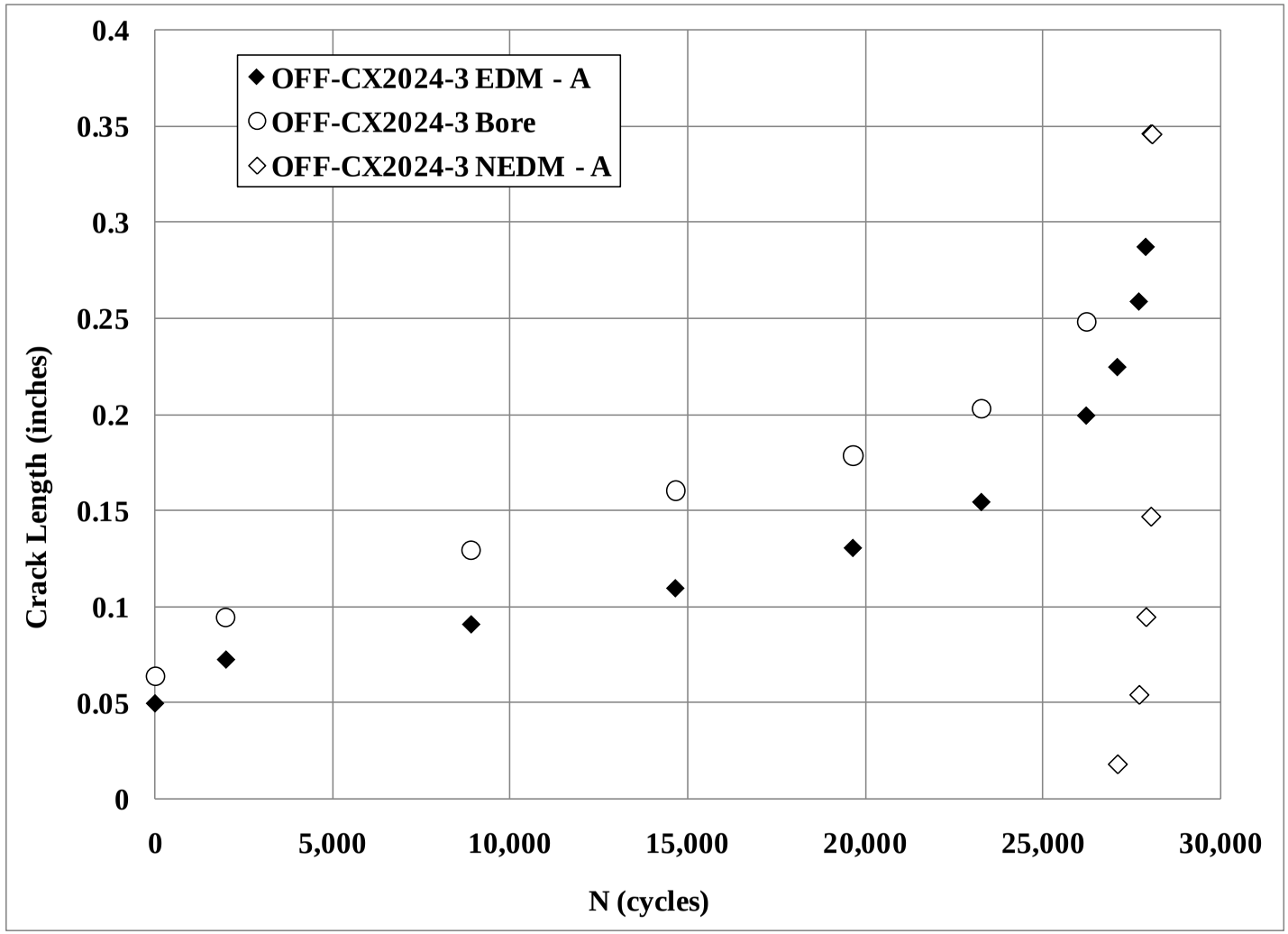

Fig. 37 Typical constant-amplitude cold expanded specimen crack growth curve – specimen OFF-CX2024-3; Constant-amplitude, R=0.1; σ_{max} = 25ksi; 20 Hz, Lab Air

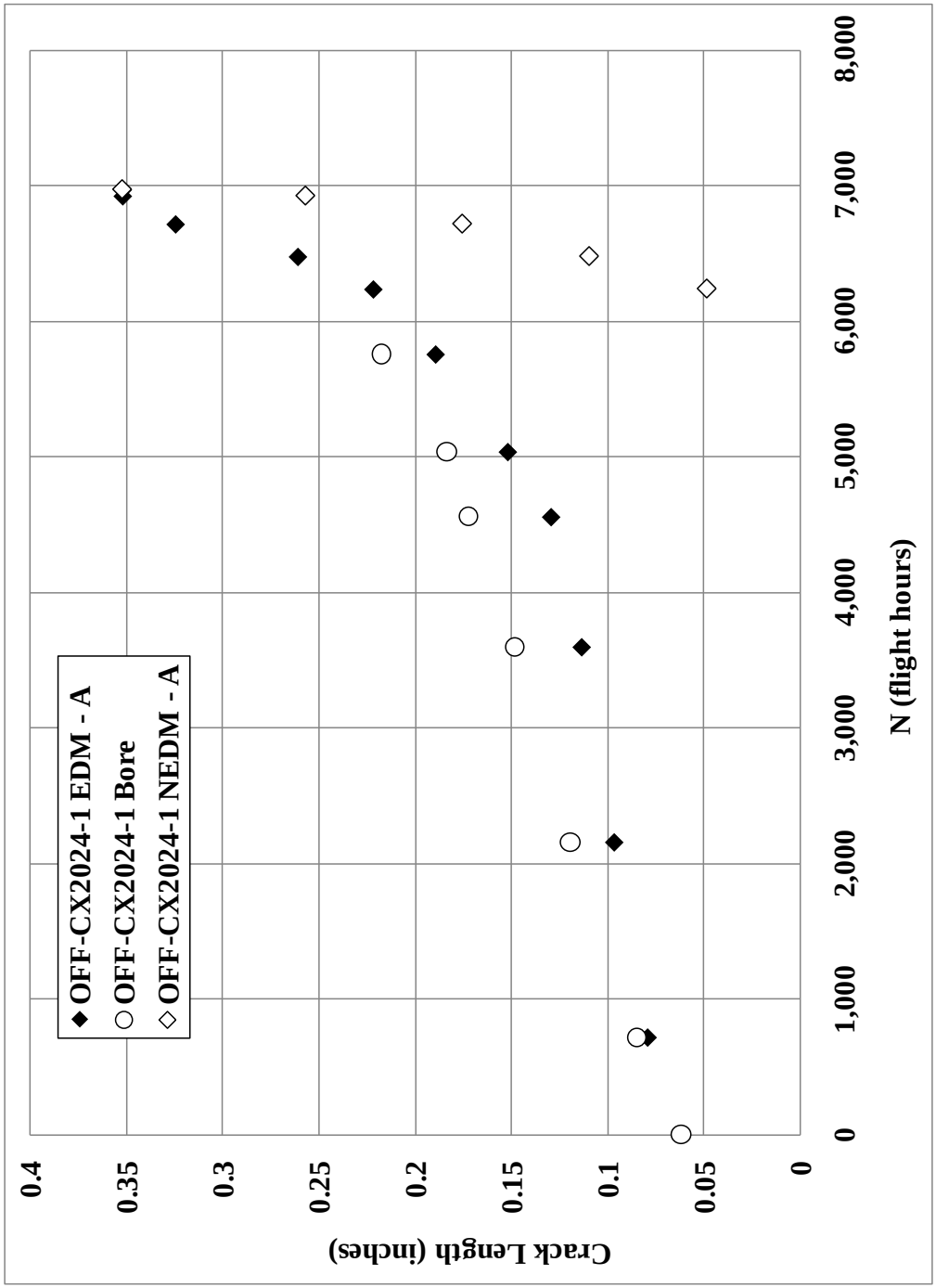

Fig. 38 Typical variable-amplitude cold expanded specimen crack growth curve – OFF-CX2024-1; A-10 wing spectrum; σ_{max} = 33 ksi; Lab Air

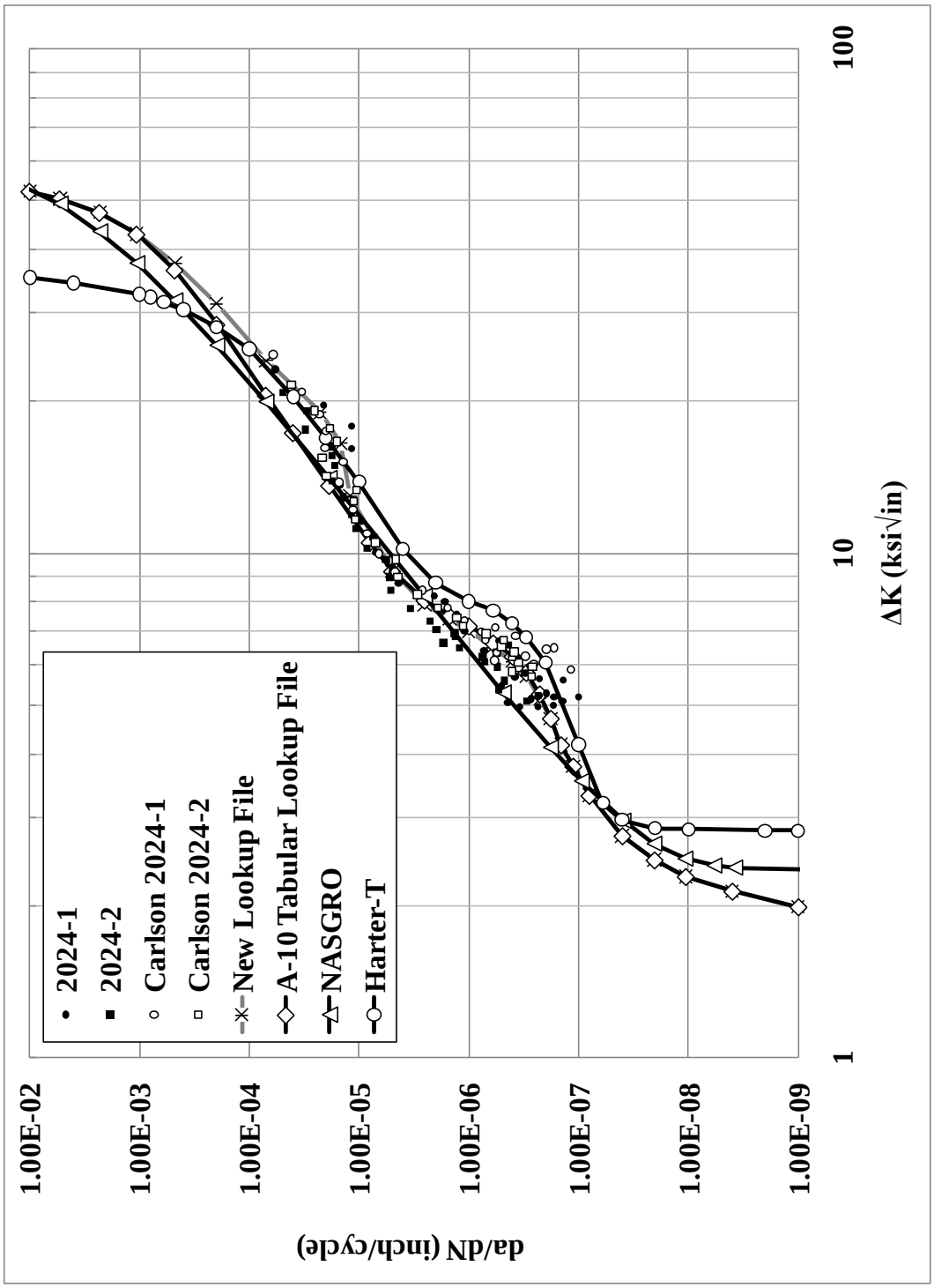

Fig. 39 da/dN vs. ΔK from ASTM E 647 specimens with several R-curve fits, R=0.1

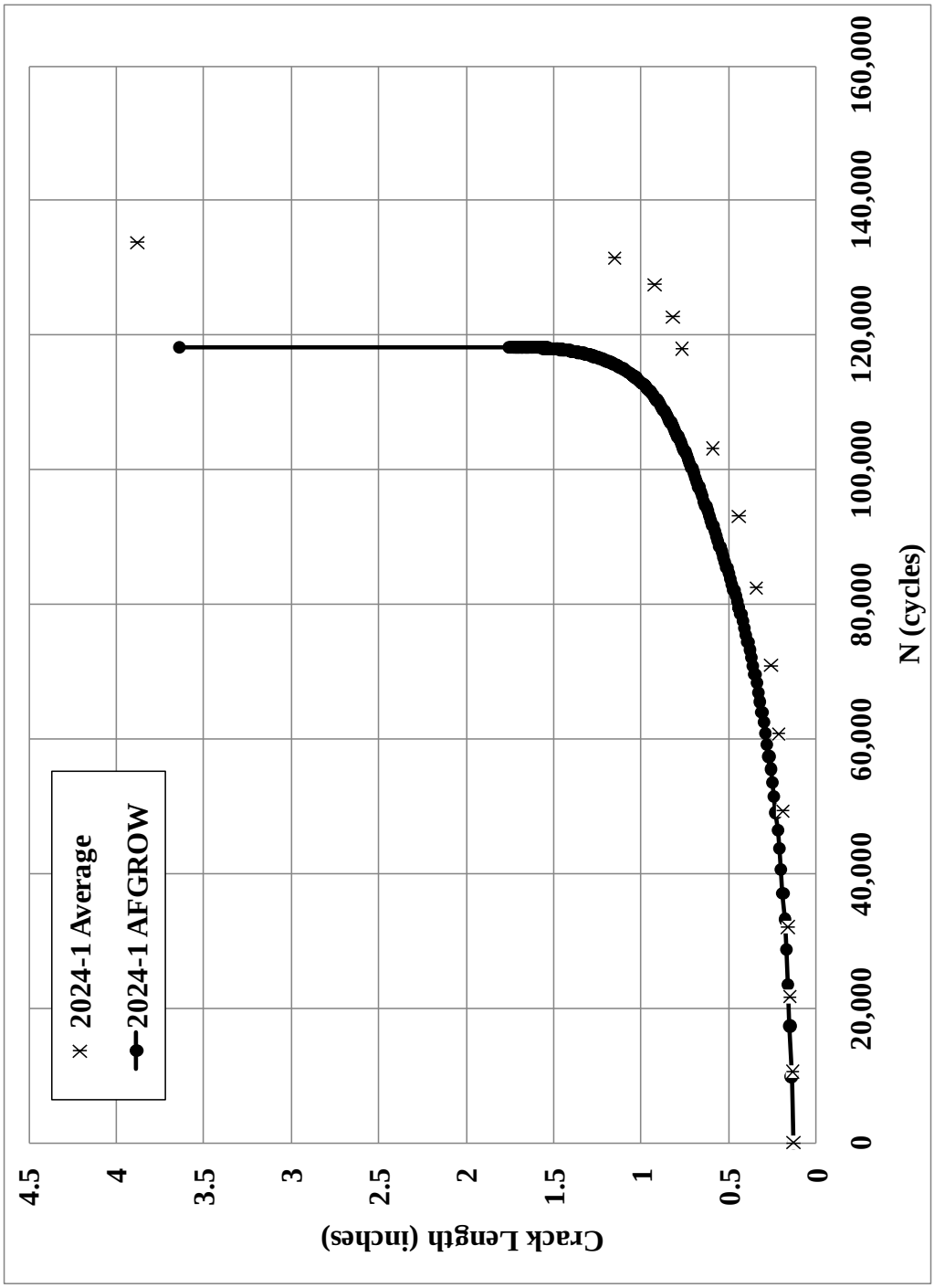

Fig. 40 AFGROW prediction plotted with test data for ASTM E 647 specimen – 2024-1; Constant-amplitude, R=0.1; σ_{max} = 11.4 ksi; 20 Hz, Lab Air

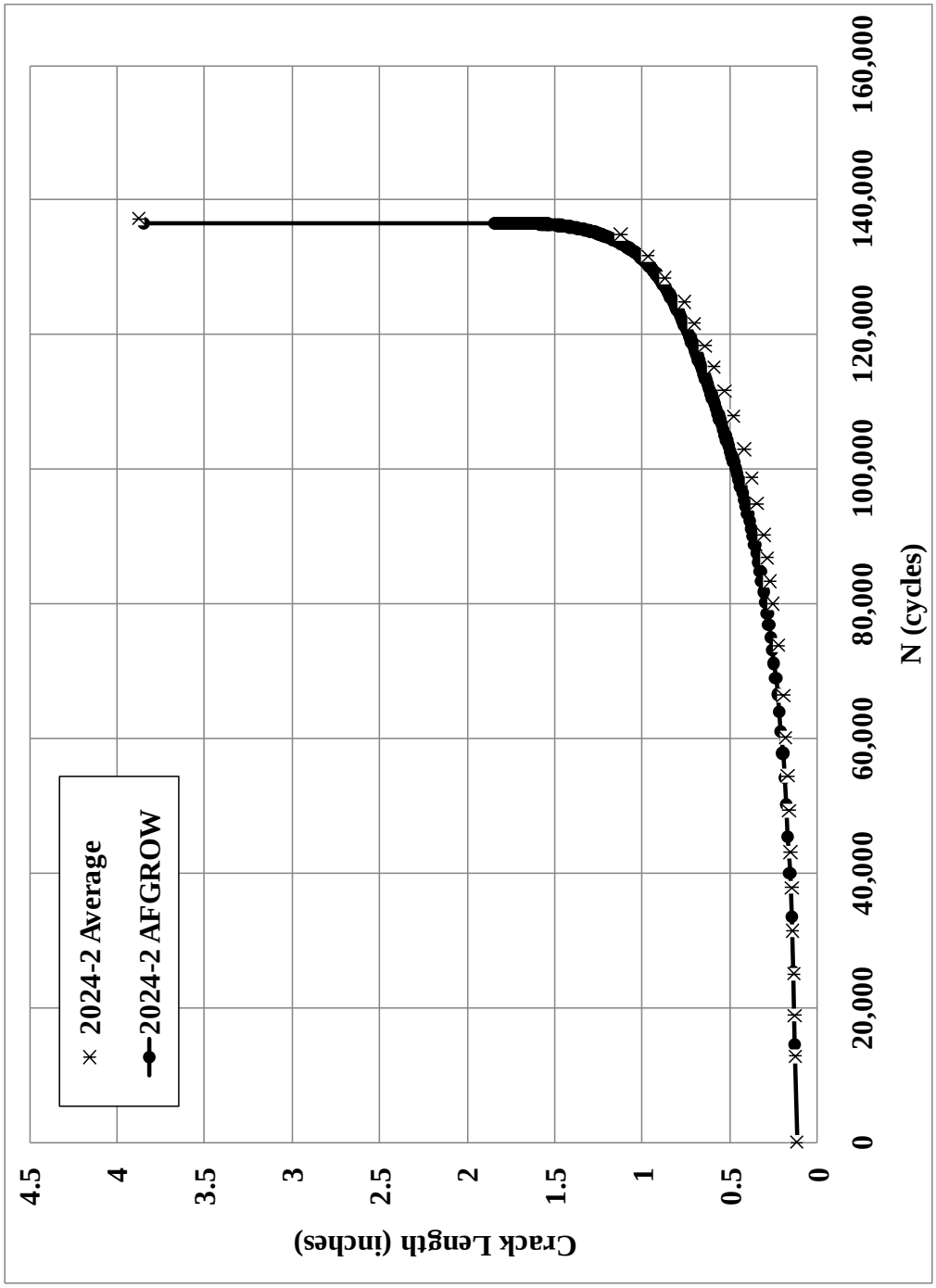

Fig. 41 AFGROW prediction plotted with test data for ASTM E 647 specimen – 2024-2; Constant-amplitude, R=0.1; σ_{max} = 11.4 ksi; 20 Hz, Lab Air

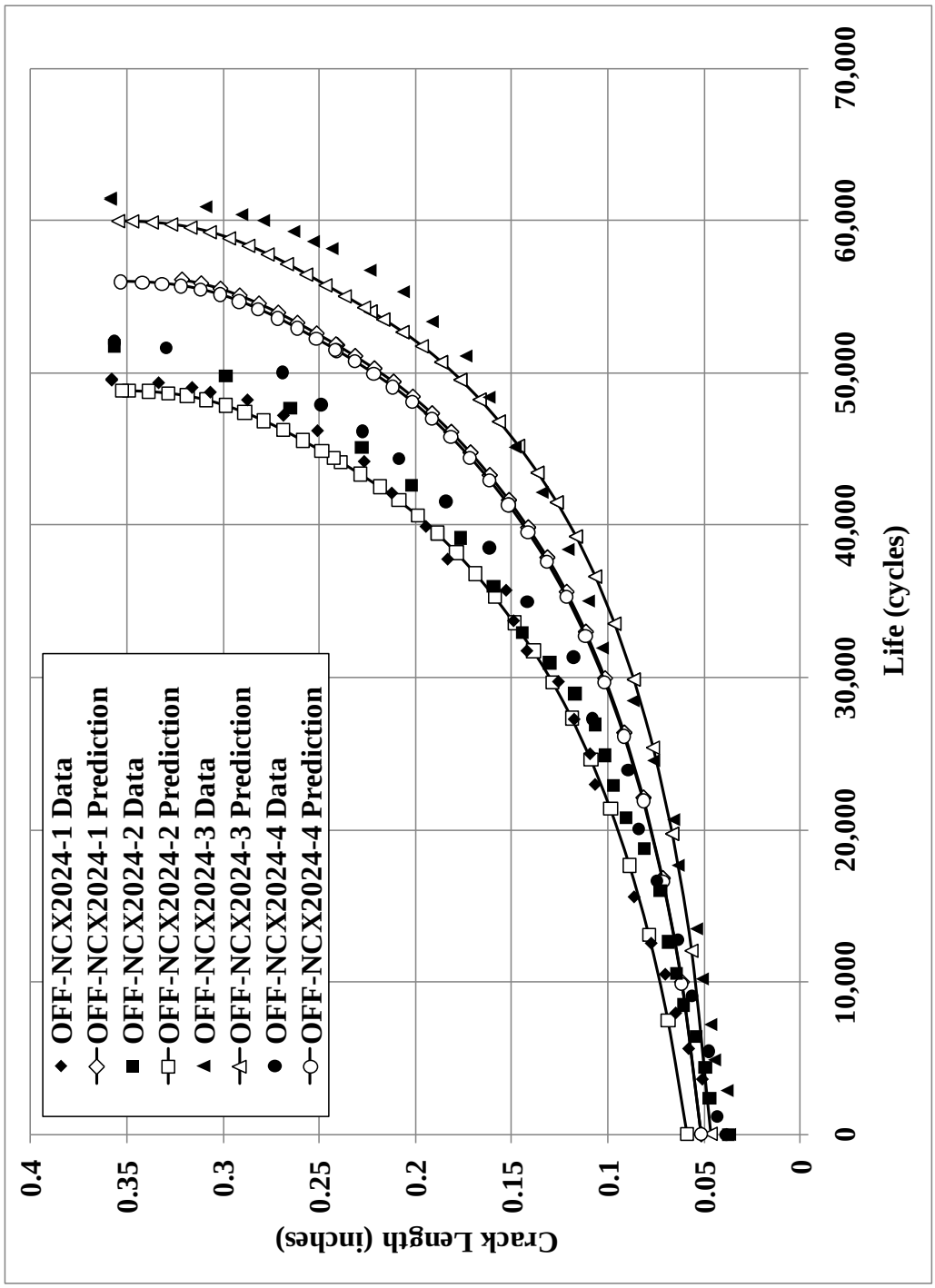

Fig. 42 Non-cold-expanded constant-amplitude specimen test data, a vs. N, plotted with corresponding AFGROW predictions – Constant-amplitude, R=0.1; σ_{max} = 25 ksi; 20 Hz, Lab Air

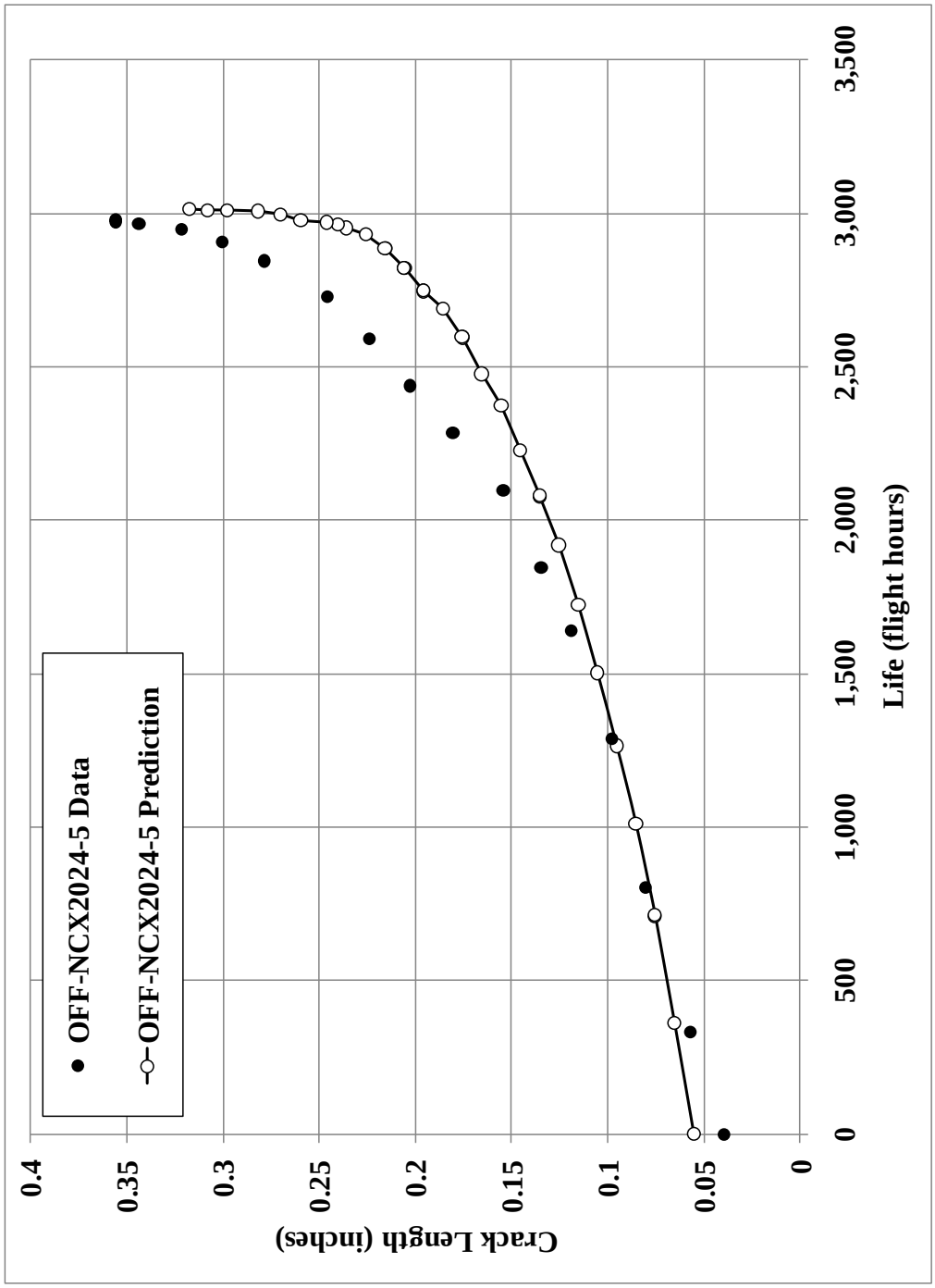

Fig. 43 Variable-amplitude non-cold-expanded specimen crack growth curve – OFF-NCX2024-5; A-10 wing spectrum; σ_{max} = 33 ksi; Lab Air

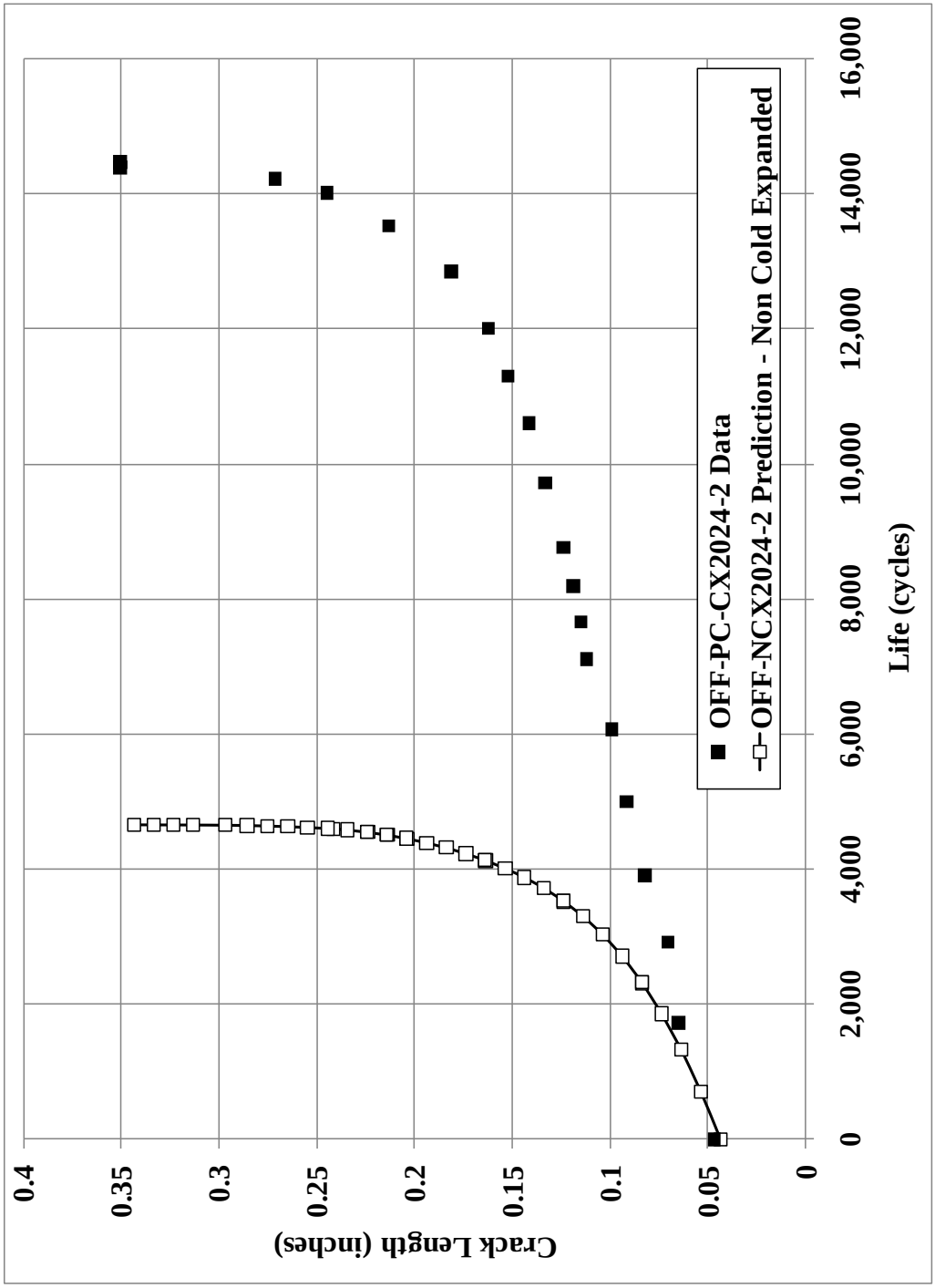

Fig. 44 Typical crack growth test data with AFGROW prediciton for a precracked cold expanded constant-amplitude specimen

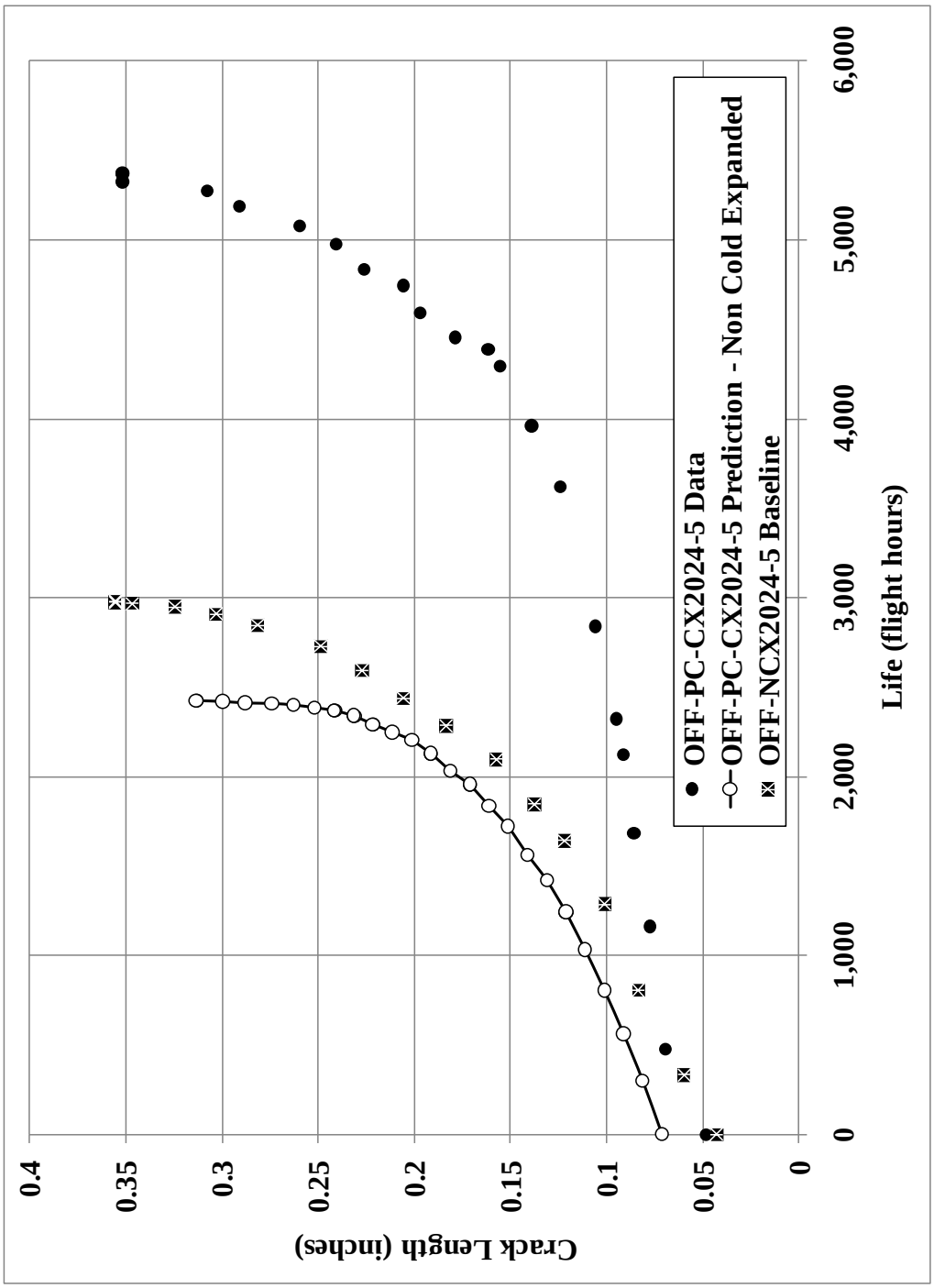

Fig. 45 Typical crack growth test data with AFGROW prediction for a precracked cold expanded variable-amplitude specimen

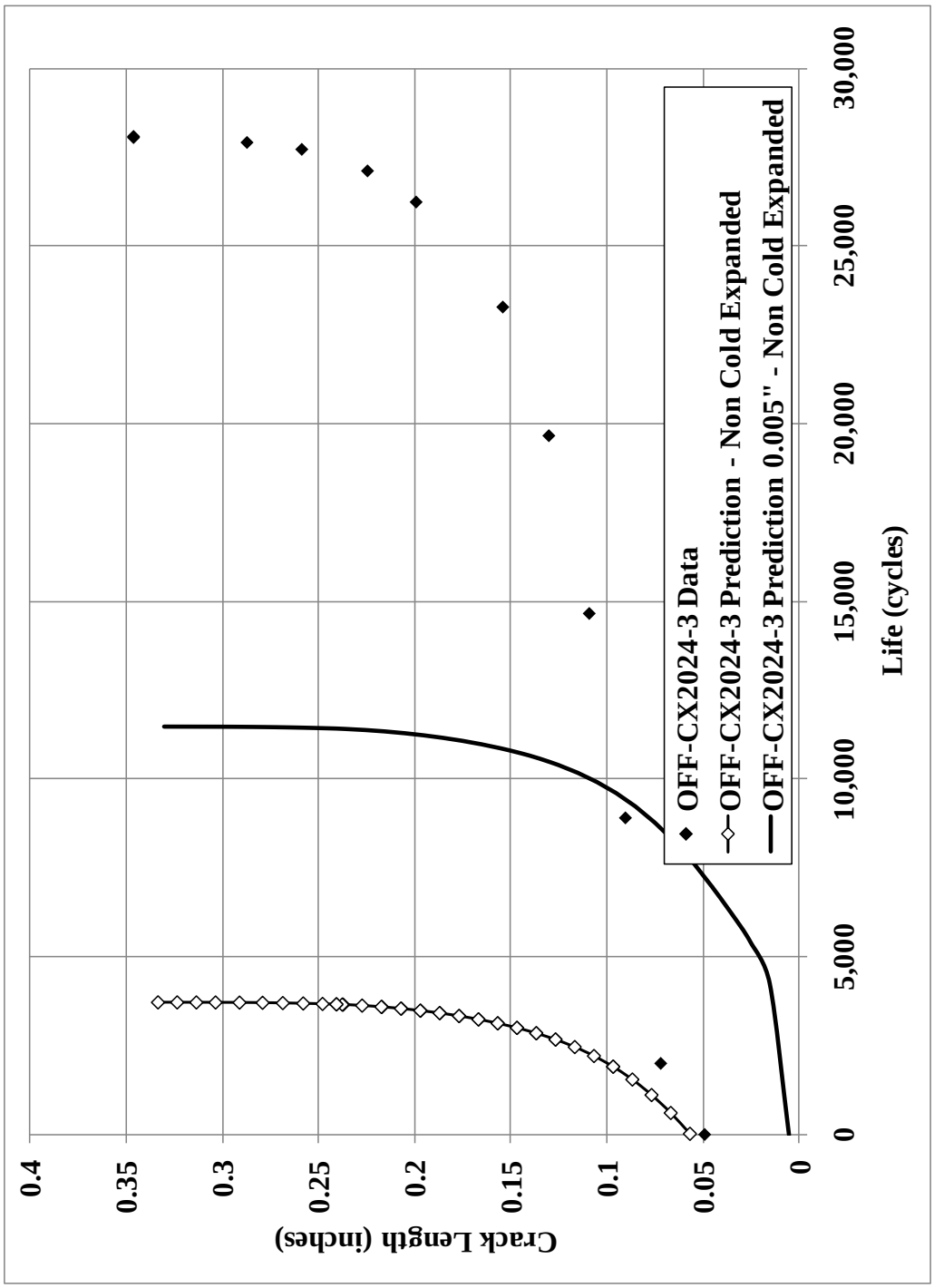

Fig. 46 Typical crack growth test data with AFGROW prediciton for a cold expanded constant-amplitude specimen

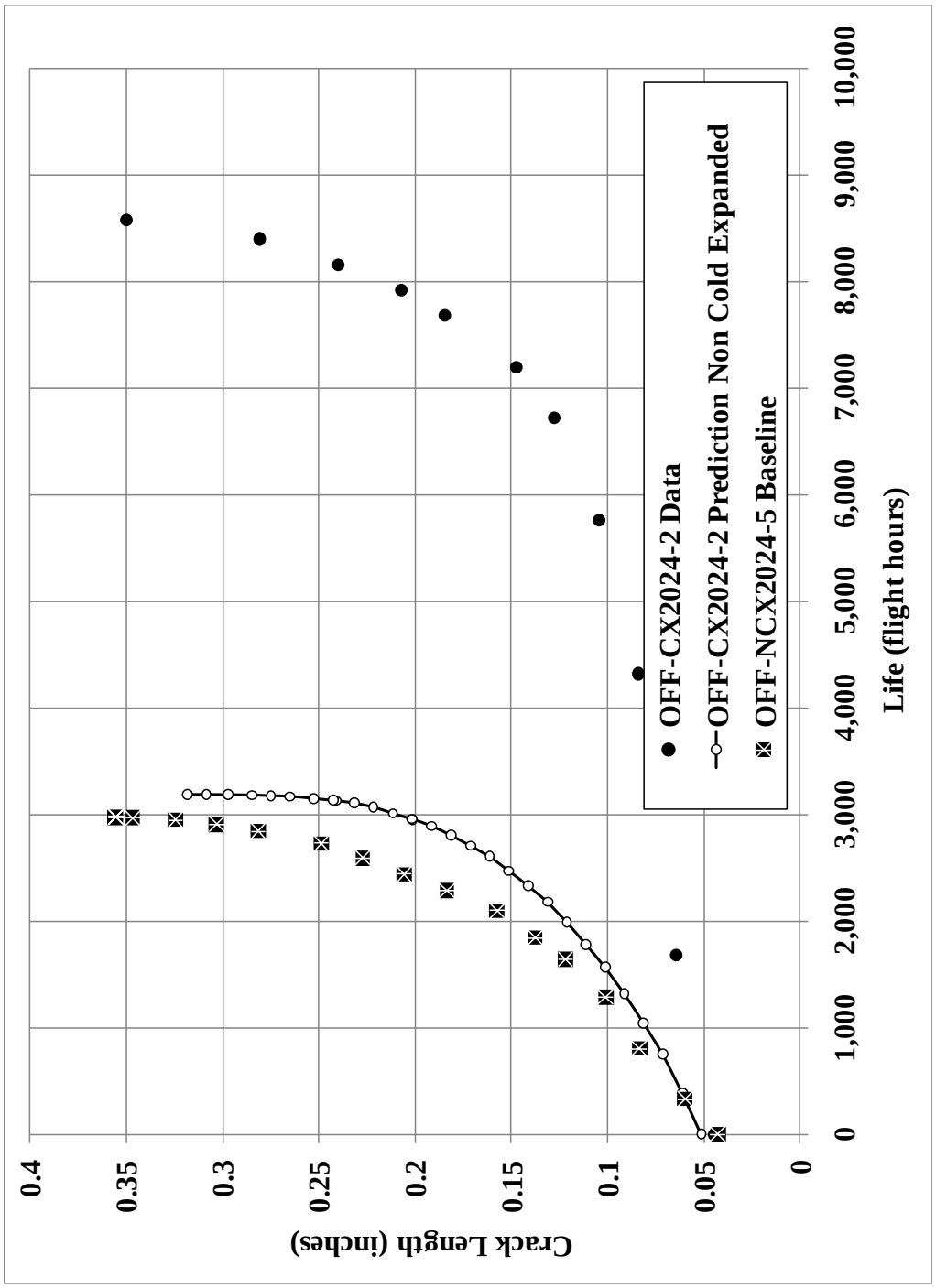

Fig. 47 Typical crack growth test data with AFGROW prediction for a cold expanded variable-amplitude specimen

Table 4 User-defined tabular lookup data generated by da/dN versus ΔK data from the ASTM E 647 specimens

LOOKUP FILE	
2024-T351 | R = 0.1	
ΔK	da/dN
1.99	1.00E-09
2.14	4.00E-09
2.29	1.06E-08
2.47	2.04E-08
2.75	4.00E-08
3.31	8.00E-08
3.78	1.12E-07
4.17	1.45E-07
4.71	1.79E-07
5.15	2.26E-07
5.70	3.00E-07
6.10	4.00E-07
6.50	6.00E-07
7.00	1.00E-06
7.40	1.50E-06
7.90	2.53E-06
9.22	5.00E-06
13.00	1.20E-05
16.50	1.47E-05
19.00	2.25E-05
24.09	7.07E-05
31.28	1.99E-04
37.57	4.78E-04
42.95	1.06E-03
47.42	2.31E-03
50.47	5.32E-03
52.24	1.00E-02

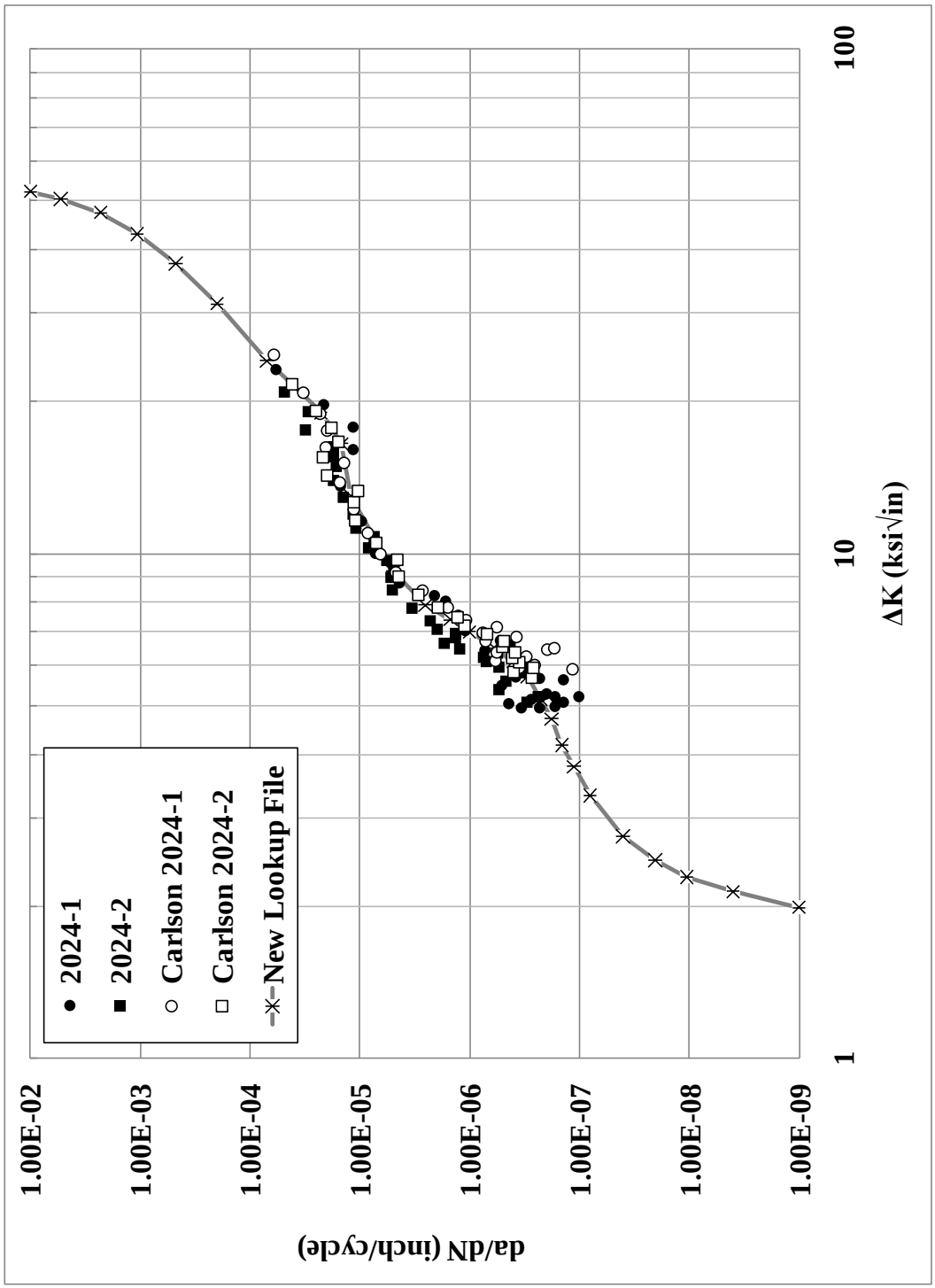

Fig. 48 da/dN versus ΔK values used to create tabular lookup file, R = 0.1

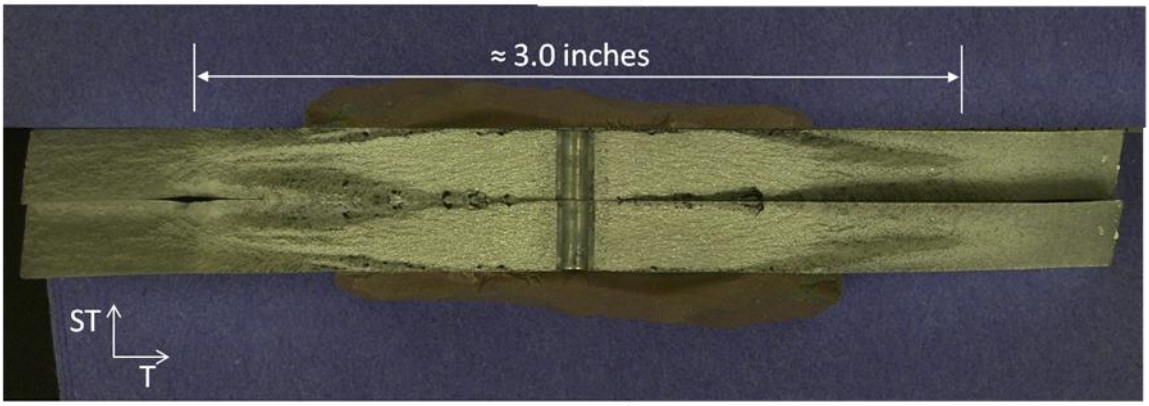

Fig. 49 ASTM E 647 specimen fracture faces (19X magnification); 2024-2, Constnat Amplitude R=0.1, σ_{max} = 11.4 ksi, 20 Hz, Lab Air

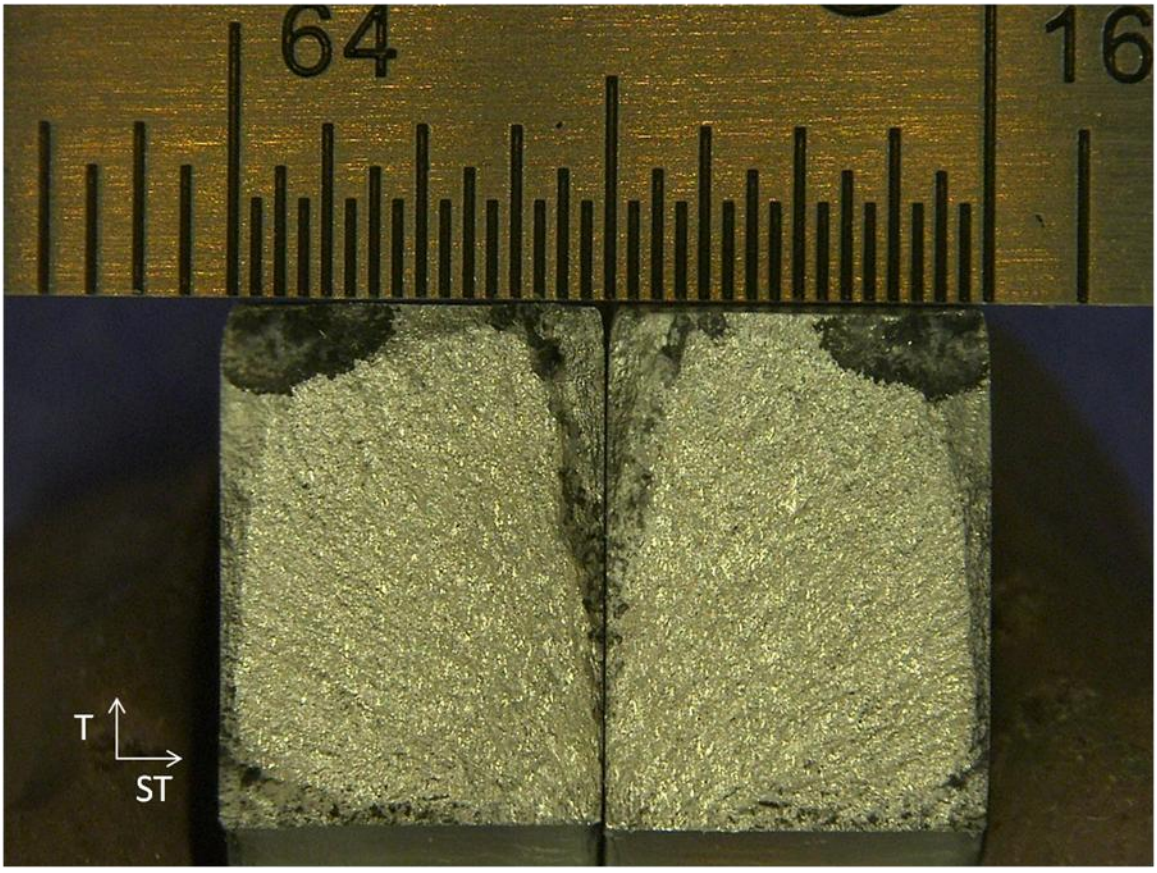

Fig. 50 Typical fracture surfaces for non-cold-expanded specimen (19X magnification); OFF-NCX2024-1, Constant-amplitude R=0.1, σ_{max} = 25 ksi, 20 Hz, Lab Air

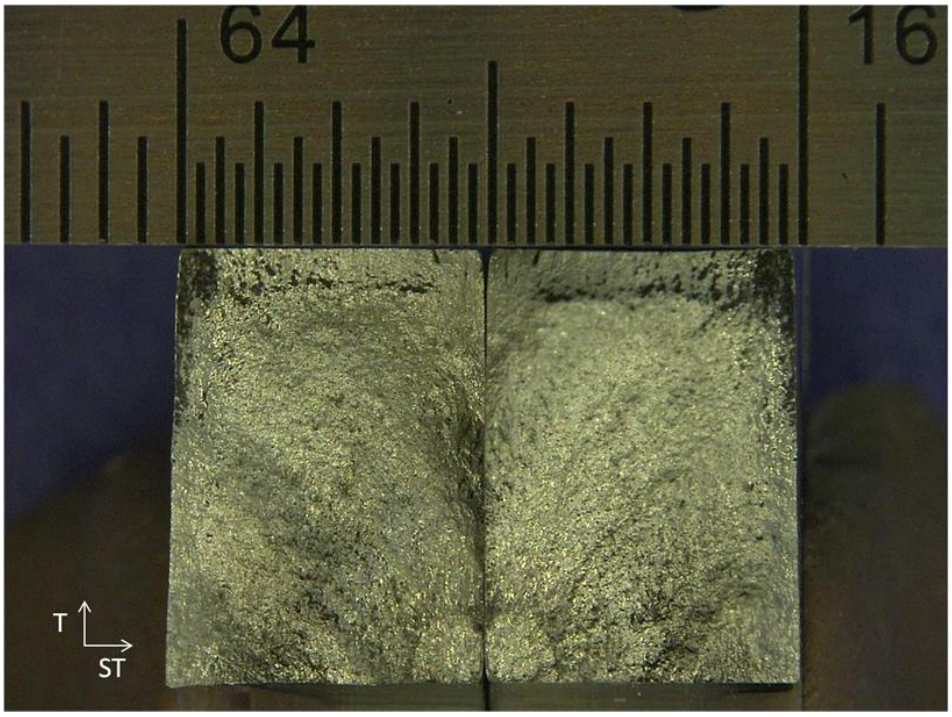

Fig. 51 Typical fracture surfaces for constant-amplitude precracked cold-expanded specimen (20X magnification); OFF-PC-CX2024-3, Constant-amplitude R=0.1, σ_{max} = 25 ksi, 20 Hz, Lab Air

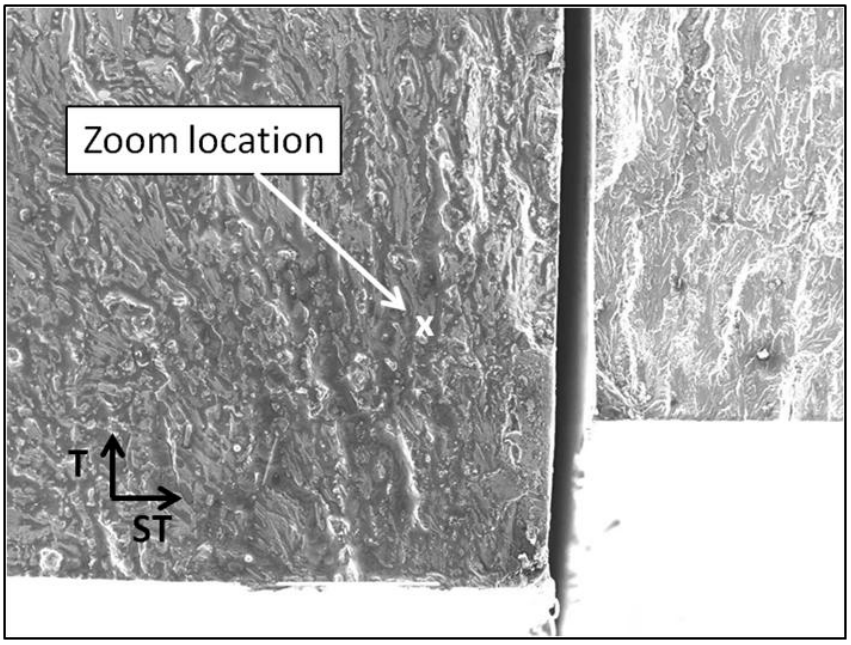

Fig. 52 SEM image (15X magnification – location 1) of precracked cold-expanded constant-amplitude specimen with marker band loading; OFF-PC-CX2024-7

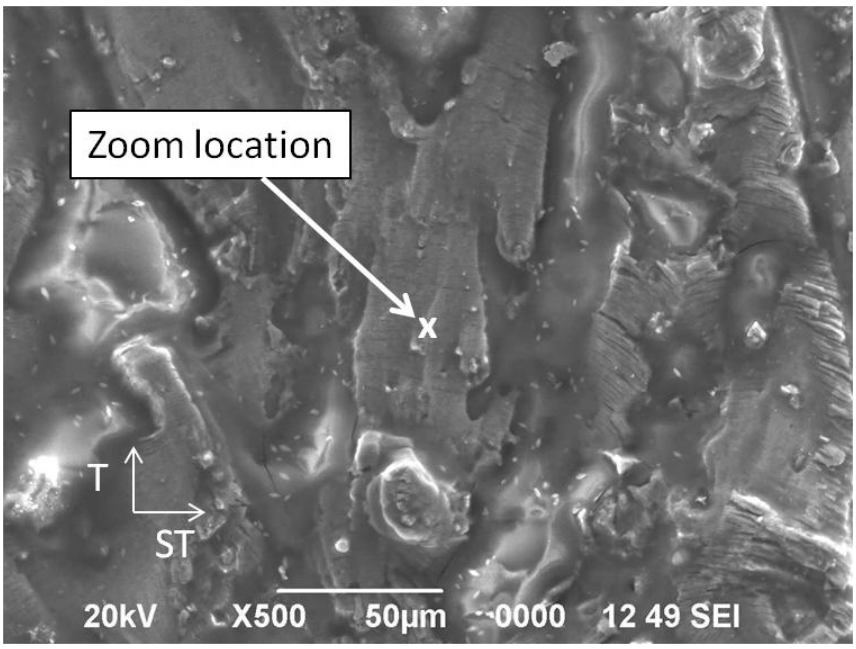

Fig. 53 Zoomed view of SEM image (500X magnification – location 1) of precracked cold-expanded constant-amplitude specimen with marker band loading; OFF-PC-CX2024-7

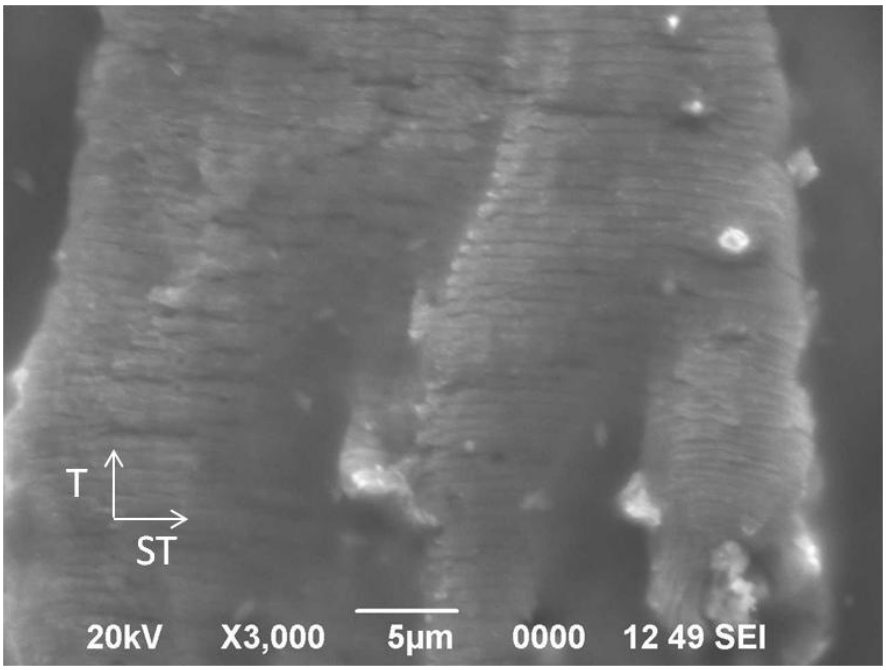

Fig. 54 Zoomed view of SEM image (3000X magnification – location 1) of precracked cold-expanded constant-amplitude specimen with marker band loading, showing fatigue striations; OFF-PC-CX2024-7

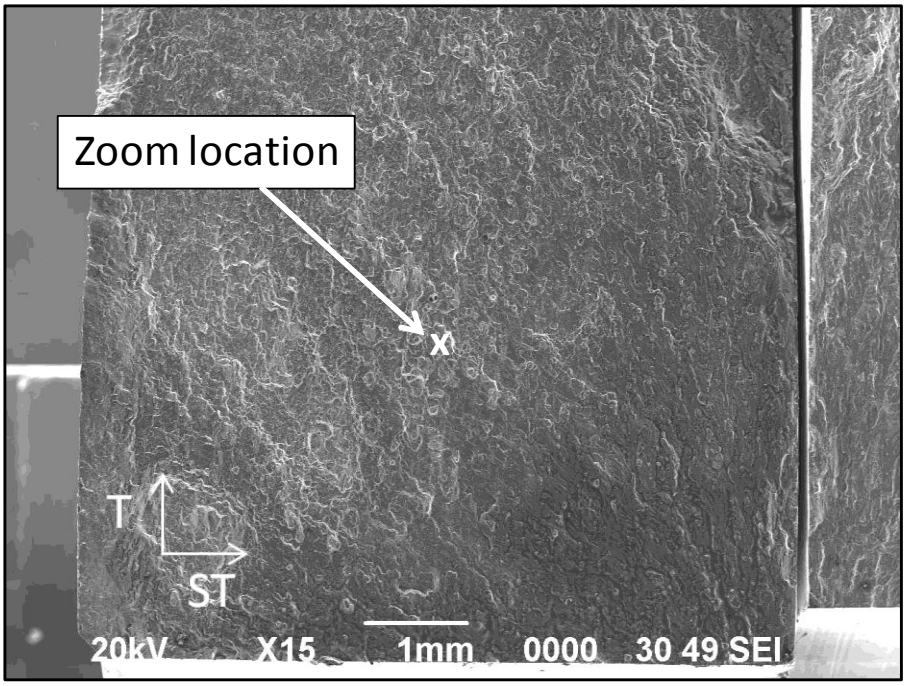

Fig. 55 SEM image (15X magnification – location 2) of precracked cold-expanded constant-amplitude specimen with marker band loading; OFF-PC-CX2024-7

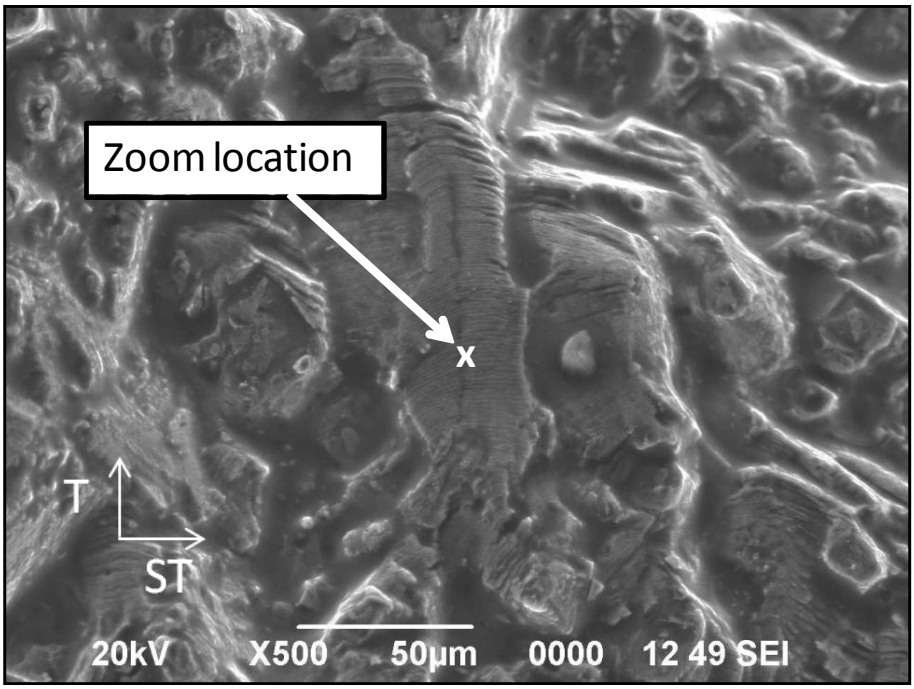

Fig. 56 SEM image (500X magnification – location 2) of precracked cold-expanded constant-amplitude specimen with marker band loading; OFF-PC-CX2024-7

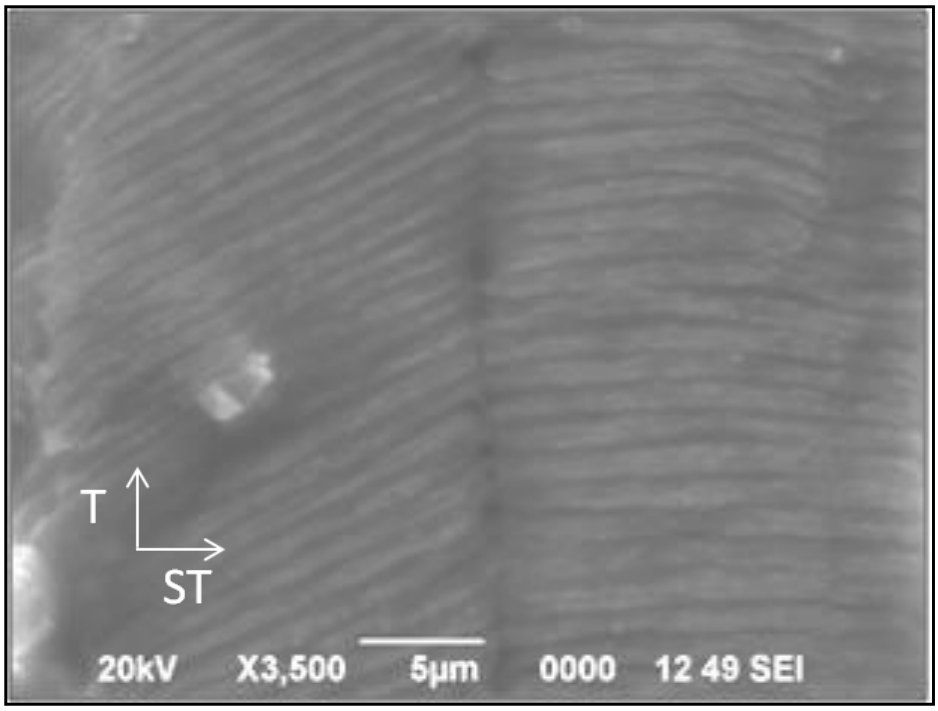

Fig. 57 SEM image (3500X magnification – location 2) of precracked cold-expanded constant-amplitude specimen with marker band loading, showing fatigue striations; OFF-PC-CX2024-7

DISCUSSION

5.1 Fatigue Crack Growth Experiment Observations

After the fatigue loading of the two ASTM E 647 specimens and plotting the corresponding fatigue crack growth data, da/dN versus ΔK, it was observed that the data correlated well with several industry standard curve fits including NASGRO and Harter-T as seen in Fig. 39. This verifies the load frame setup and experiment process.

5.2 Fatigue Life Predictions

5.2.1 ASTM E 647 Specimens

The AFGROW predictions for the two ASTM E 647 specimens are shown with the crack growth test data in Fig. 58. The average difference between the prediction and the test data for these two specimens was found to be 6.1%, which is well within reason for fatigue, as there are many factors that affect the crack growth.

5.2.2 Non-Cold-Expanded Specimens

5.2.2.1 Constant Amplitude

The AFGROW predictions for the four constant-amplitude non-cold-expanded specimens (OFF-NCX2024-1, -2, -3, -4) are shown in Fig. 59, along with the fatigue experimental data for these specimens. The average percent difference in experiment life vs. AFGROW prediction life for these four specimens is less than 3%, which is an excellent correlation for fatigue. Table 5 summarizes the percent difference in life

between the AFGROW models and experiment data. The best correlation was for specimen OFF-NCX2024-3 at -2.3% difference in fatigue life between the AFGROW model and the experiment data. The worst correlation was for specimen OFF-NCX2024-1at 12.0% difference in fatigue life between the AFGROW model and the experiment data. It should be noted that the Initial Flaw Size (IFS) varies for each specimen and each AFGROW model. As discussed in Section 4.5, it was found that a better fit of the AFGROW model to the constant-amplitude experiment data was achieved when the average initial crack size from the experiment was used for the IFS for both the bore and surface crack lengths in AFGROW, and by holding the aspect ratio (a/c) constant, where 'a' is the bore crack length and 'c' is the surface crack length.

5.2.2.2 Variable Amplitude

Only one variable-amplitude non-cold-expanded specimen (OFF-NCX2024-5) was used to verify AFGROW predictions, as the other specimen was severely overloaded which skewed the results for that specimen. The AFGROW prediction for the variable-amplitude non-cold-expanded specimen is shown in Fig. 60, along with the fatigue experiment data. The percent difference in experiment life vs. AFGROW prediction life for this specimen was found to be 1.2%. Table 5 lists the percent difference in fatigue life for this specimen. It should be noted that the reason this value is small is because the retardation parameter SOLR was varied in AFGROW until the prediction cycles to failure matched the actual experiment cycles to failure. This process was used to generate a standard SOLR value to be used with all other variable-amplitude models. The SOLR that provided the closest match to experiment data was found to be 2.11.

5.2.3 Cold-Expanded Specimens

AFGROW models were created for all cold-expanded specimens, in order to show the theoretical increase in fatigue life due to the cold expansion process with no crack in the hole prior to cold expansion. Fig. 61 and Fig. 62 show the AFGROW predictions and the corresponding experimental data for constant-amplitude and variable-amplitude specimens. Table 6 summarizes the improvement in fatigue life for these specimens due to cold expansion.

5.2.4 Precracked Cold-Expanded Specimens

AFGROW models were created for all precracked cold-expanded specimens. These models were used to generate the theoretical fatigue life for a non-cold-expanded specimen with the same geometry and initial crack sizes, to show the relative improvement in fatigue life. The predictions from these models are plotted with the experiment data in Fig. 63 and Fig. 64. The relative increase in fatigue life varied from a minimum of 1.96 times to a maximum of 6.51 times the non-cold-expanded hole fatigue life. The average increase in fatigue life was 3.60 times for constant-amplitude loading and 2.27 times for variable-amplitude loading as shown in Table 7.

5.3 Accounting For Cold-Expansion in a DTA

The current analysis approach used by the USAF in a DTA to account for fatigue life benefit of cold expansion is to lower the IFS in AFGROW to 0.005 inch. It should be noted that this approach does not relate to the physics of what the cold expansion process actual does to the material or residual stress field around the hole. It is only the approach applied by the USAF to account for cold expansion.

For this research, an additional AFGROW model was created for each specimen, but used an IFS of 0.005 inch. This was done in order to compare the results of the 0.005 inch prediction to the precracked and non-precracked cold-expanded hole experiment data. In Fig. 65 and Fig. 66, a 0.005 inch IFS AFGROW prediction is plotted against the experiment data for all specimens for constant amplitude in Fig. 65 and variable amplitude in Fig. 66. These plots show the total impact of this research – the 0.005 inch IFS prediction gives an unconservative fatigue life prediction for the specimen configuration and loading used in this research. A conservative prediction would mean that the 0.005 inch IFS fatigue life is less than any experiment data, meaning that in any situation, the 0.005 inch IFS predicted fatigue life represents the worst-case scenario and in no situation should the fatigue life be below this fatigue life. Otherwise the prediction produces a fatigue life greater than experimental data and is unconservative. This means that some components could have a shorter fatigue life than predicted by the model, and could fail before predicted and cause loss of life and/or aircraft.

As can be seen in Fig. 65, using the 0.005 inch IFS in AFGROW for the constant-amplitude loading produces an over-prediction of fatigue life for only some of the precracked cold-expanded specimens, and is conservative with respect to all the cold-expanded specimens. However, for the variable-amplitude loading specimens in Fig. 66, the AFGROW 0.005 inch IFS prediction is unconservative for all the precracked cold-expanded specimens, and unconservative for all but two of the cold-expanded specimens. In both cases, the 0.005 inch IFS prediction gives unconservative fatigue life with respect to experimental data. This is a critical point to make note of. As part of the damage tolerance design paradigm and USAF DTA guidelines, it must be assumed a crack in the

hole. The experimental data generated in this research shows that for a hole that actually did contain an approximate 0.050 inch crack, the experiment fatigue life was shorter than the AFGROW prediction generated from USAF procedures. This shows that the USAF approach of using a 0.005 inch IFS to account for the cold expansion of a hole is not conservative for this specific specimen and loading configuration and should be reviewed in light of this data.

For comparison purposes, in the experiments completed by Pilarczyk[10] and Carlson[13] the increase in fatigue life for some specimens was on the order of 50 times longer for a cold-expanded specimen versus non-cold-expanded, as seen in Fig. 67. It should be noted that these specimens were center-hole specimens, not offset hole, and were not precracked then cold-expanded. Included in the figure is the AFGROW predictions for a model with an IFS of 0.050 inch, the USAF standard IFS for non-cold-expanded models using a bolt-hole eddy current NDI technique. Also in Fig. 67 is the AFGROW prediction with an IFS of 0.005 inch, which is the USAF minimum allowable IFS used in a DTA for a cold-expanded hole. This IFS is primarily used for new structure or to account for beneficial processes such as cold expansion of holes, interference fasteners or bushings, etc.[36] Both the 0.050 inch and 0.005 inch models fall significantly short of the cold-expanded hole experimental data. As seen in Fig. 67, the benefit of using an IFS of 0.005 inch is conservative compared to actual data for the center hole specimens. However, as discussed, that was not the case for the short hole offset specimens as shown in Fig. 65 and Fig. 66. This shows the role of edge margin in the fatigue life of components. For a hole offset (e/D) of 1.2, and with a crack length of 0.050 inch in the hole during cold expansion, and the loading applied in this research, the

USAF approach of using an 0.005 inch IFS to account for the cold expansion of a hole was not conservative should not be used.

5.4 Cold Expansion Observations

The cold expansion of the fastener holes was always done so that the mandrel exit side was always on the non-EDM face of the specimen. This was done so that the greater compressive residual stress field was not on the specimen face with the EDM notch. This represents the worst case scenario, as the purpose of the EDM notch is to nucleate and propagate a fatigue crack more quickly than a non-EDM notch location, so the high residual stress field needed to be oriented away from the desired fatigue crack location. This is illustrated in Fig. 68.[10] Additionally, the applied and residual percent expansions of the hole from the cold expansion process are listed and discussed in Appendix B.

5.5 Crack Front Geometry and Behavior

As discussed by Carlson[13] and Pilarczyk,[10] the crack front behavior of a cold-expanded hole was different when compared to a non-cold-expanded hole. The crack front shape for a cold-expanded hole, shown in Fig. 68, was found to be p-shaped for some crack lengths. This seems to be related to the direction the mandrel was pulled through the specimen during the cold expansion process. The mandrel exit side of the specimen always contained a higher magnitude compressive residual stress field, as seen in Fig. 68. It was assumed that this larger residual stress field was formed due to some material sliding with the mandrel when pulled through the hole. This would cause a slightly higher residual expansion on the exit side of the specimen.

This p-shaped crack front was also found to be applicable for the precrack cold-expanded specimens, as is shown in Fig. 27. Unfortunately, only certain specimens (all constant-amplitude) were failed from both sides of the hole for continuing damage data, so only certain fracture faces were available to identify crack front shape. There was no continuing damage completed with variable-amplitude loading, which would provide banding on the fracture faces to identify crack front shape as the crack propagated.

5.6 Undesired Events/Experiment Anomalies

5.6.1 Cold Expansion Deformation

It was noted that due to the combination of cold expansion and the short edge margin, all specimens that were cold-expanded developed a slight bulge on the free edge as seen in Fig. 69 and Fig. 70. While this deformation was not desired, it was expected that there may be some edge expansion due to small edge margin. This edge margin was still selected, even though it was known this deformation may occur, in order to get a realistic idea of what edge margin is 'too small' for the cold expansion technique for this specific material and geometry. And as shown in Fig. 69 and Fig. 70, if permanent deformation of a component is not allowable, and e/D value of 1.2 is too small for cold expansion, with this material and geometry. However, if permanent deformation of a component is allowable, because it is getting repaired or replaced, and an increase in fatigue life is required, cold expansion would be acceptable.

5.6.2 Notched Section On Mill

On three of the cold-expanded specimens, after doing the final reaming as part of the cold expansion process, an indentation was found on the deformed area of the free

edge of the specimen where the cold expansion process bulged outward. After some investigation, it was found that during the reaming process, the mill that was used for the reaming of these three specimens had a missing piece in the vise. The bulge on the free edge of the specimen coincidentally was lined up on this missing section of the vise, and when the specimen was clamped down in the vise, the missing section left some indentation in the specimen. This indentation did not seem to have an effect on fatigue crack growth life, however. The vise is shown in Fig. 71, with the corresponding deformation in the specimen shown in Fig. 72. This indentation occurred on specimens OFF-CX2024-1, OFF-CX2024 -2, and OFF-CX2024-3.

5.6.3 Variable-Amplitude Maximum Spectrum Stress

When inputting the maximum load for the first variable-amplitude loaded specimen, the user put in 33 kip instead of using the cross-sectional area and calculating the specific load that would give a 33 ksi stress for each specimen. This was not part of the experiment plan. This process of using 33 kip for the maximum spectrum stress was continued for all variable-amplitude loaded specimens. However, 33 ksi was used for the maximum spectrum stress in all variable-amplitude loaded AFGROW models, as the nominal cross-sectional area is 1 inch^2 and varies minimally for each specimen.

5.6.4 Software Errors

Occasionally the Bluehill 2 software package would perform unexpected actions, and limits would get tripped and overloads and underloads were applied to the specimens. For example, while using the DADN software module, when the experiment was complete and the user clicked the ‘Finish Test’ button, the controller would zero the load,

but it would sometimes overshoot zero load and apply some compressive load to the specimen. As this occurred only when the experiment was complete and all data already gathered, it was not considered a critical point.

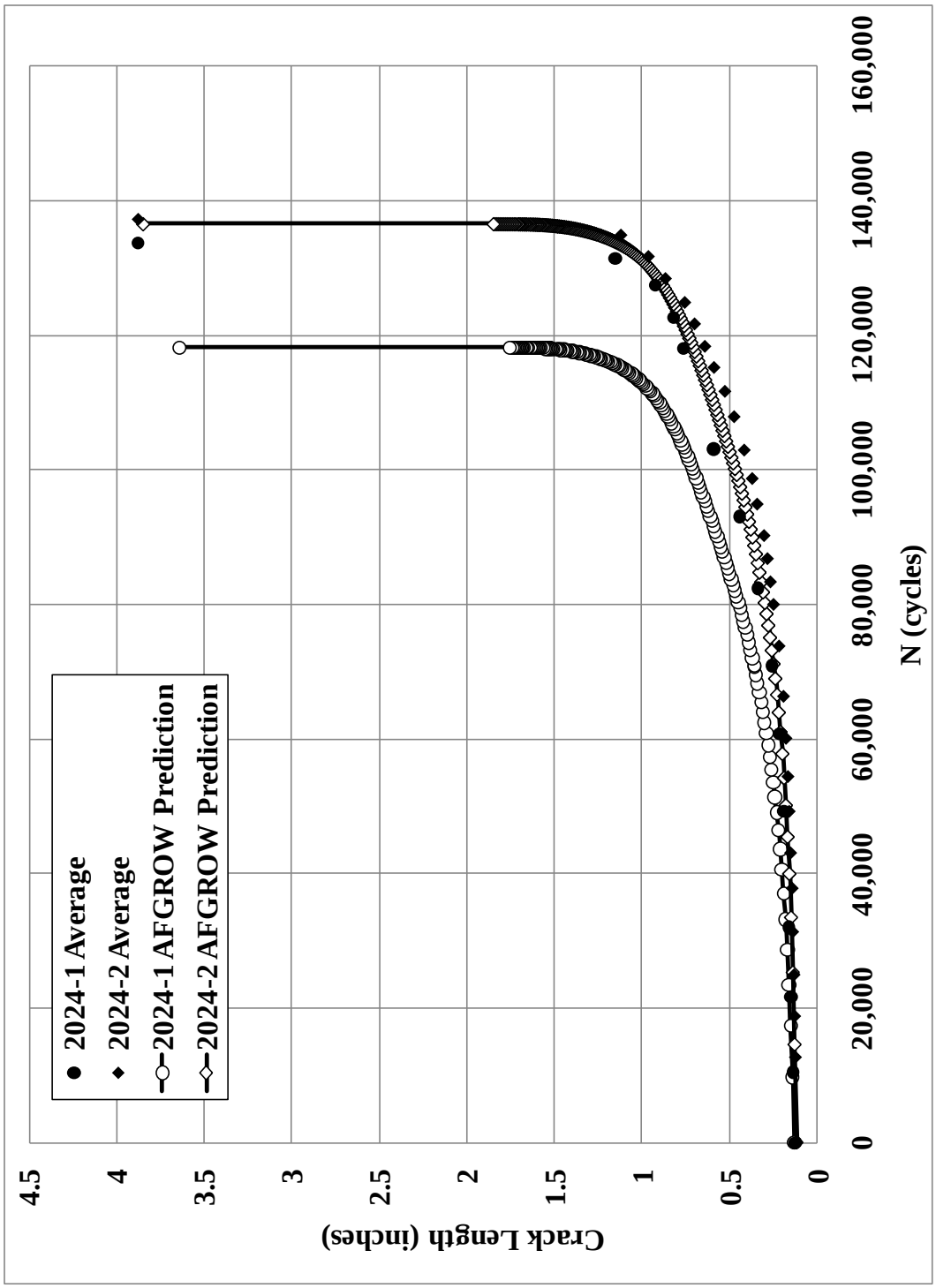

Fig. 58 Crack growth curve for ASTM E 647 specimens with AFGROW predictions

Table 5 Summary of fatigue life differences between AFGROW models and experiment data for baseline non-cold-expanded constant-amplitude loaded specimens

Specimen ID	Constant/Variable Amplitude Loading	Test Life (cycles/flight hours)	Prediction (cycles/flight hours)	% Difference in Life
OFF-NCX2024-1	Constant	49631	56415	12.0%
OFF-NCX2024-2	Constant	51797	48839	-5.7%
OFF-NCX2024-3	Constant	61441	60002	-2.3%
OFF-NCX2024-4	Constant	52051	55974	7.5%
OFF-NCX2024-5	Variable	2979	3014	1.2%
Constant Amplitude Average:				2.9%
Variable Amplitude:				1.2%

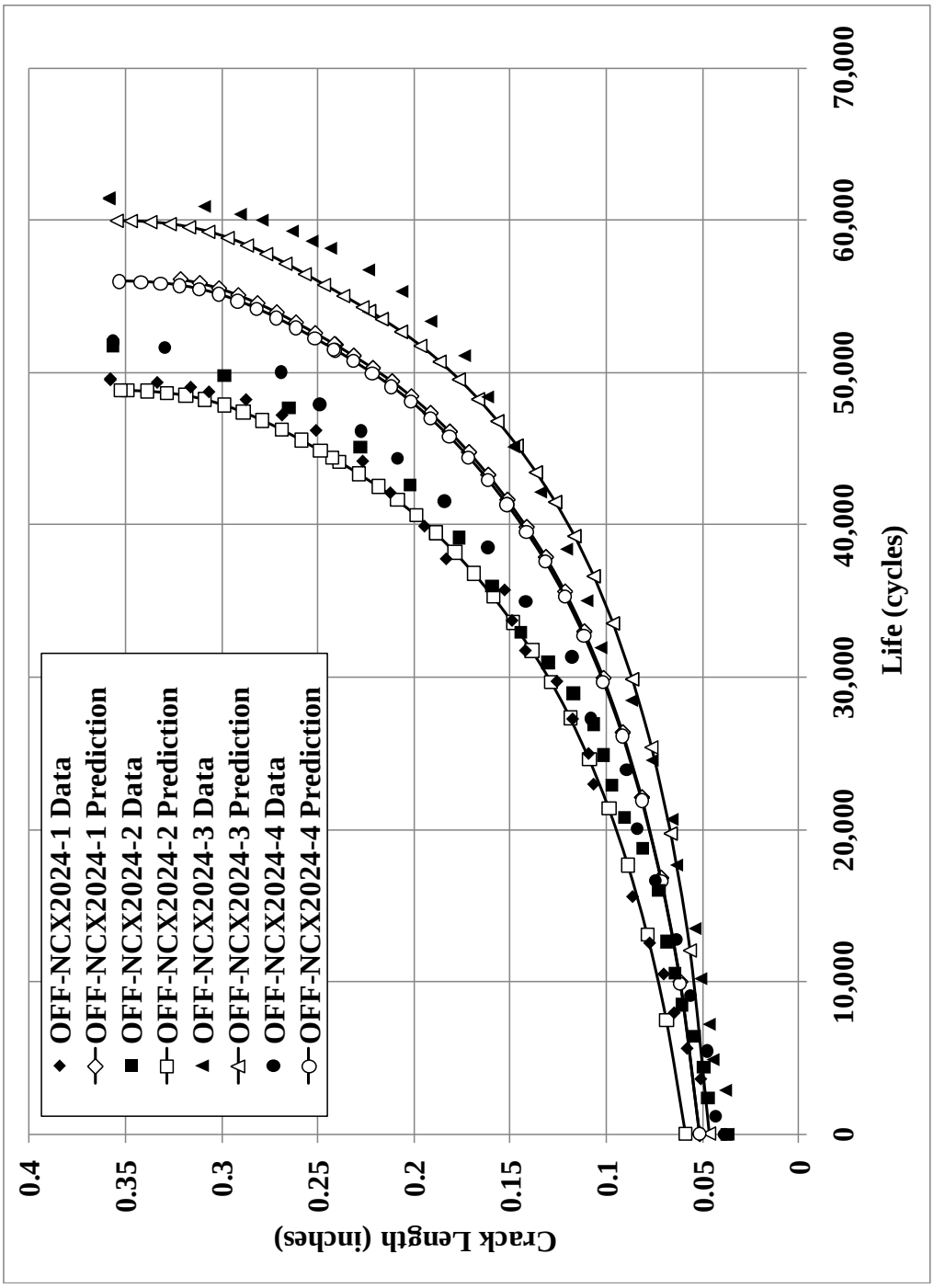

Fig. 59 AFGROW predictions and crack growth test data for four constant-amplitude non-cold-expanded specimens

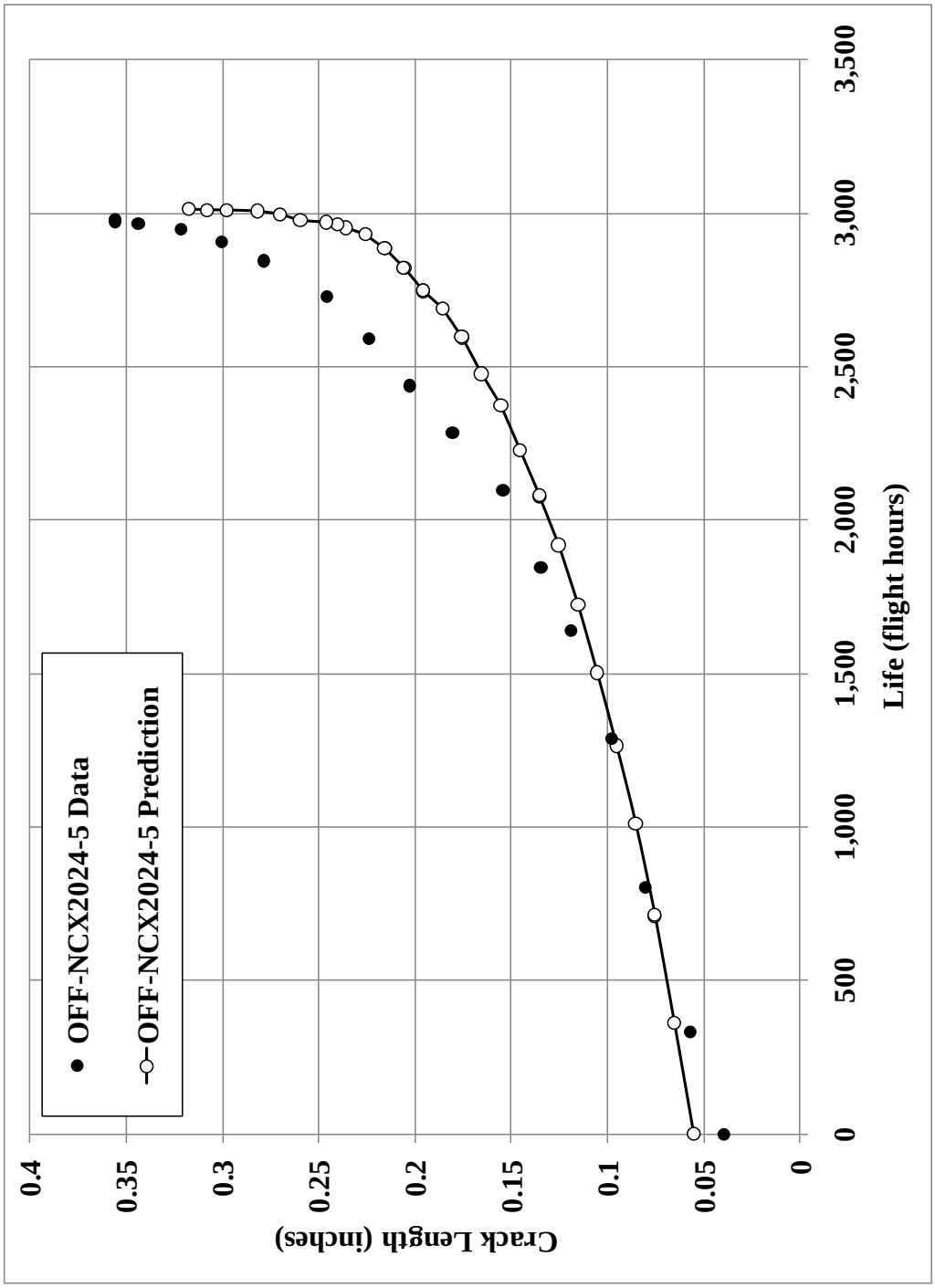

Fig. 60 Variable-amplitude non-cold-expanded specimen crack growth test data with AFGROW prediction

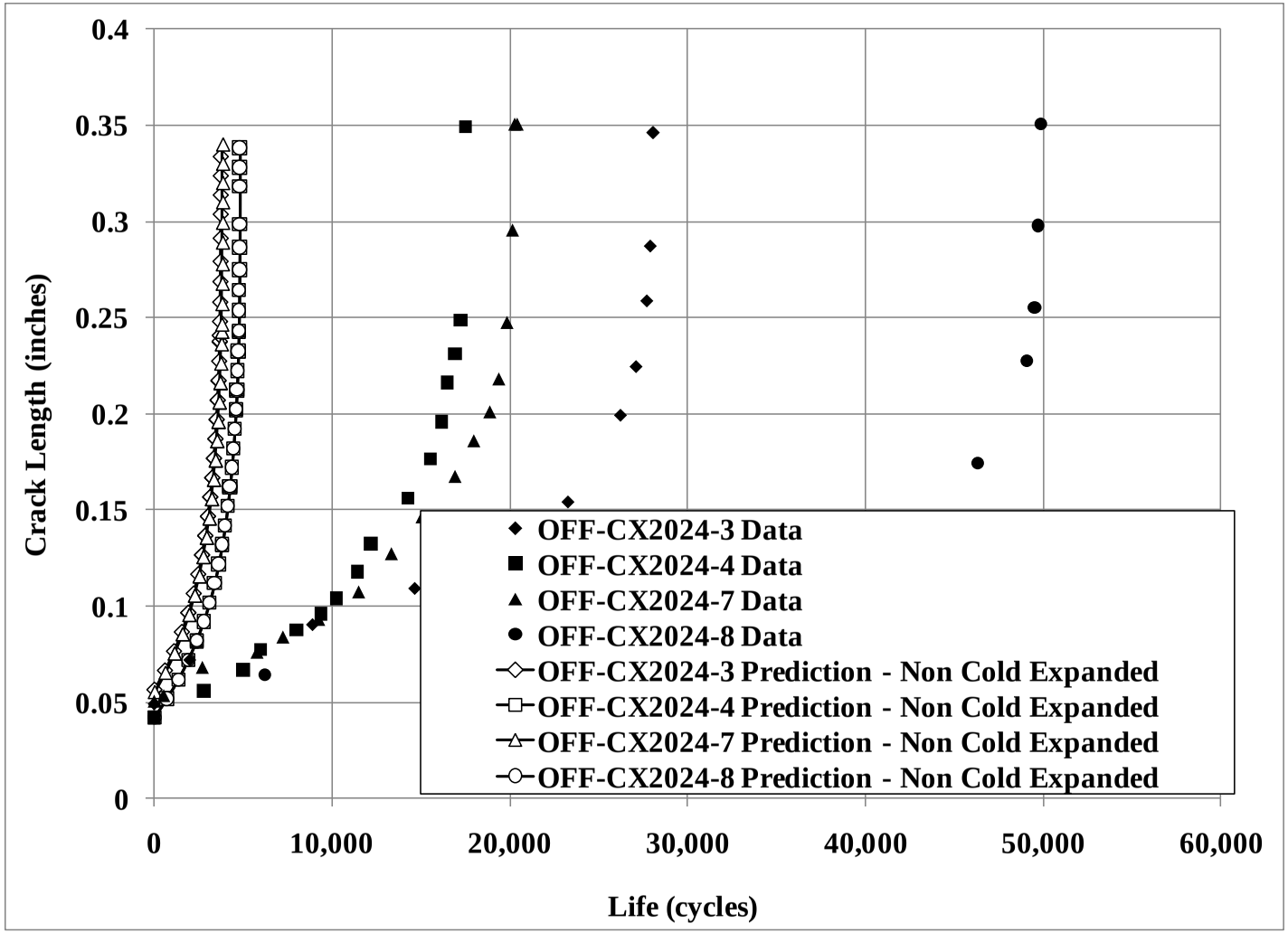

Fig. 61 Cold expanded constant-amplitude loaded specimens with AFGROW predictions for a non-cold-expanded hole not precracked condition

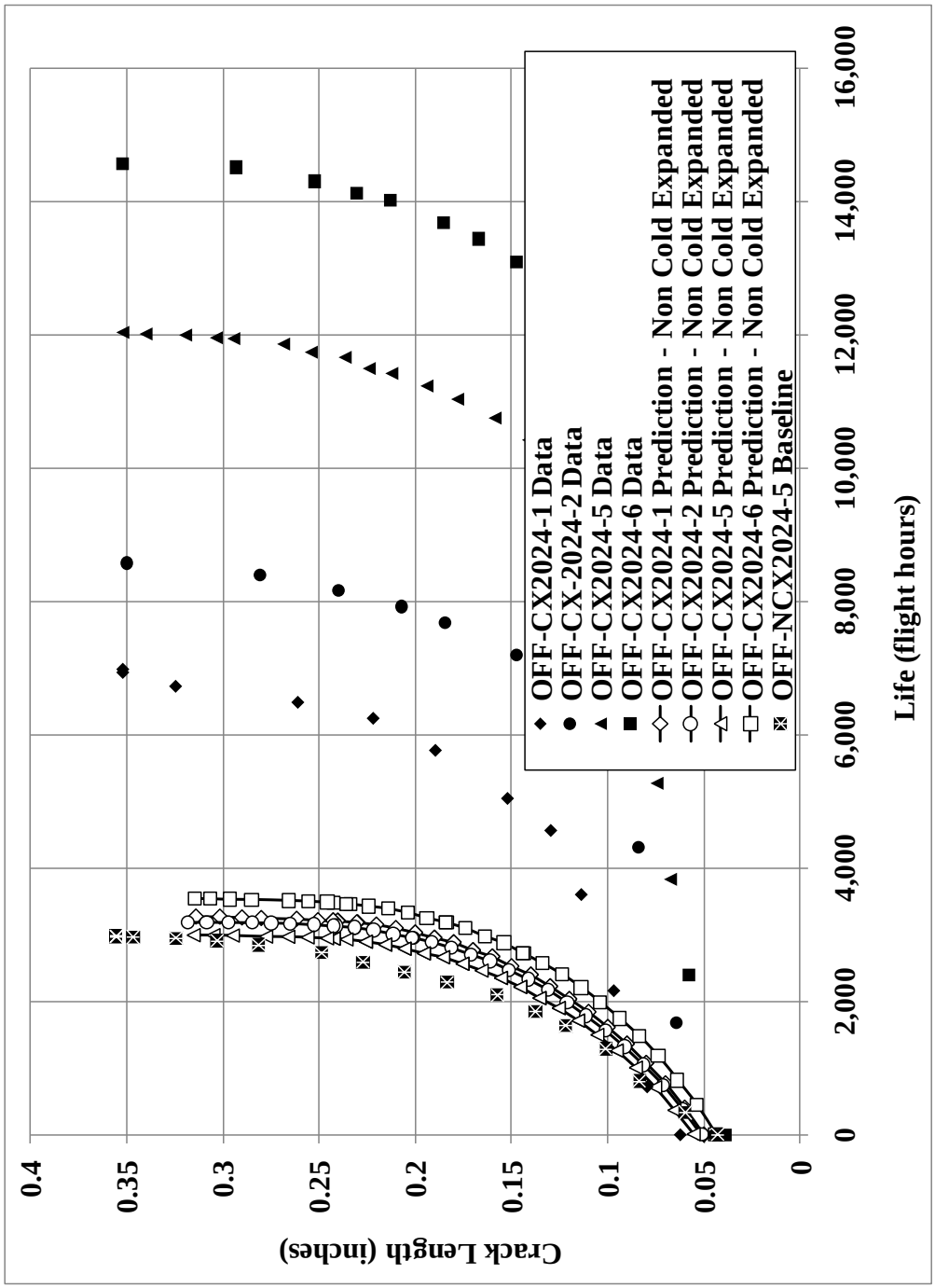

Fig. 62 AFGROW predictions and fatigue crack growth test data for variable-amplitude cold expanded not precracked specimens

Table 6 Summary of increase in fatigue life for baseline cold-expanded specimen experiment data against AFGROW model predictions

Specimen ID	Constant/Variable Amplitude Loading	Test Life (cycles/flight hours)	Prediction Life (cycles/flight hours)	X Increase in Life
OFF-CX2024-1	Variable	6972	3274	2.13
OFF-CX2024-2	Variable	8574	3187	2.69
OFF-CX2024-3	Constant	28465	3719	7.65
OFF-CX2024-4	Constant	17527	4807	3.65
OFF-CX2024-5	Variable	12280	2999	4.09
OFF-CX2024-6	Variable	14568	3541	4.11
OFF-CX2024-7	Constant	20418	3847	5.31
OFF-CX2024-8	Constant	49889	4807	10.38
Constant Amplitude Average:				6.75
Variable Amplitude Average:				3.26

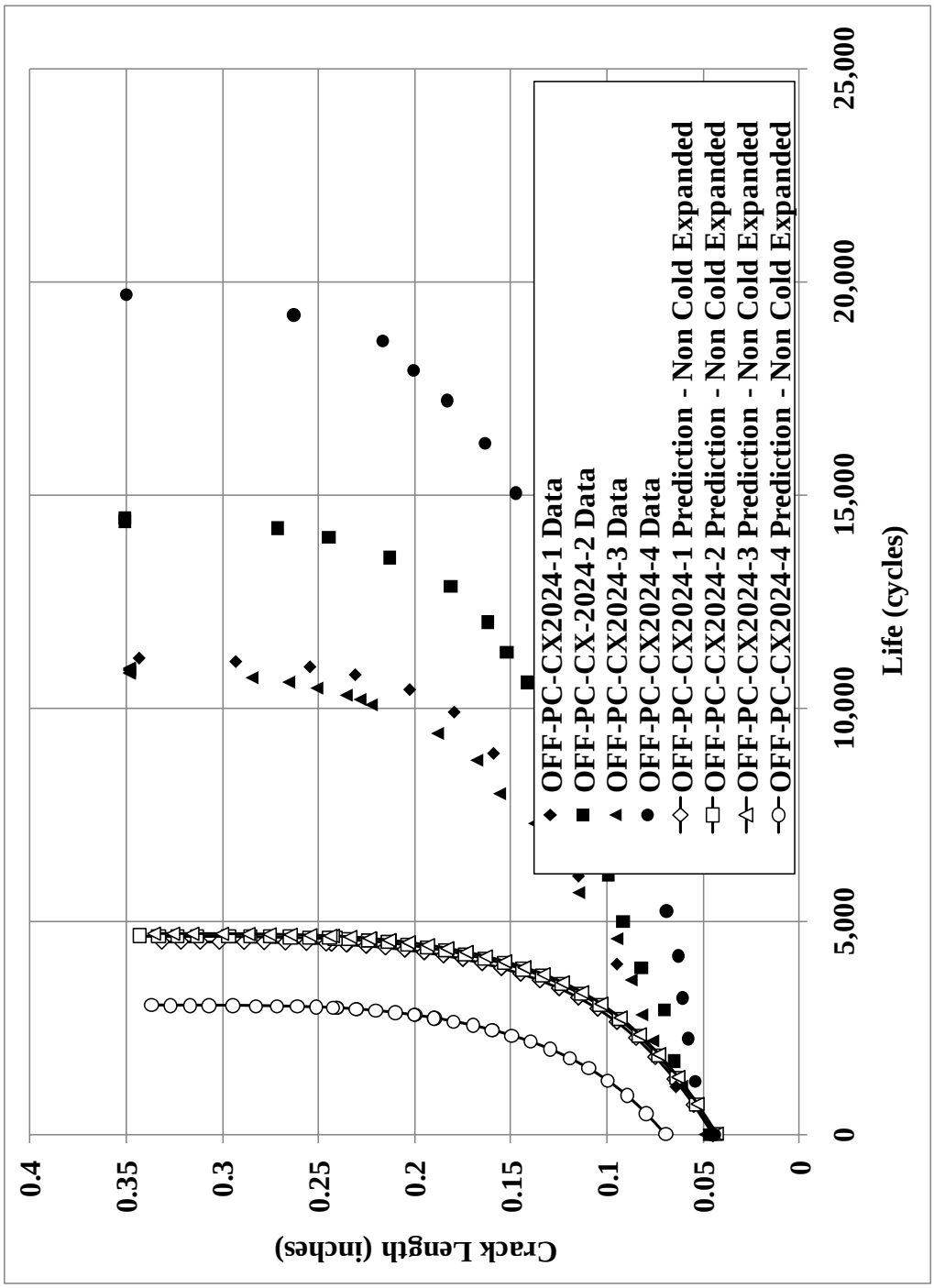

Fig. 63 Precracked cold expanded AFGROW predictions and test data for constant-amplitude loading

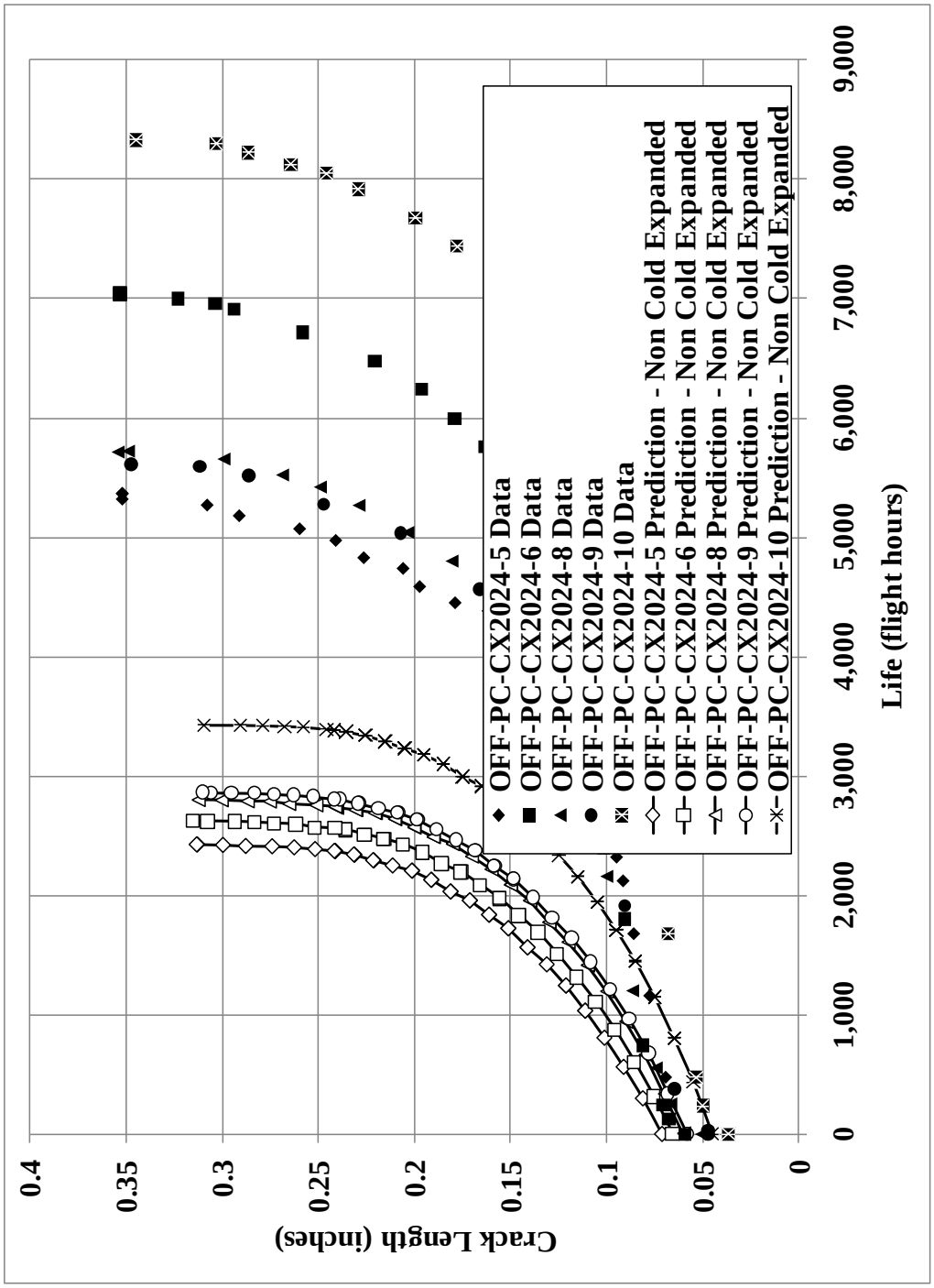

Fig. 64 a vs. N data and AFGROW predictions for the variable-amplitude loaded precracked cold expanded specimens

Table 7 Increase in fatigue life between AFGROW models and experiment data for all precracked cold-expanded specimens

Specimen ID	Constant/Variable Amplitude Loading	Test Life (cycles/flight hours)	Prediction (cycles/flight hours)	X Increase in Life
OFF-PC-CX2024-1	Constant	11168	4532	2.46
OFF-PC-CX2024-2	Constant	14474	4659	3.11
OFF-PC-CX2024-3	Constant	10927	4716	2.32
OFF-PC-CX2024-4	Constant	19686	3026	6.51
OFF-PC-CX2024-5	Variable	5374	2426	2.22
OFF-PC-CX2024-6	Variable	7047	2622	2.69
OFF-PC-CX2024-7	Used for marker banding			
OFF-PC-CX2024-8	Variable	5718	2804	2.04
OFF-PC-CX2024-9	Variable	5611	2866	1.96
OFF-PC-CX2024-10	Variable	8329	3428	2.43
Constant Amplitude Average:				3.60
Variable Amplitude Average:				2.27

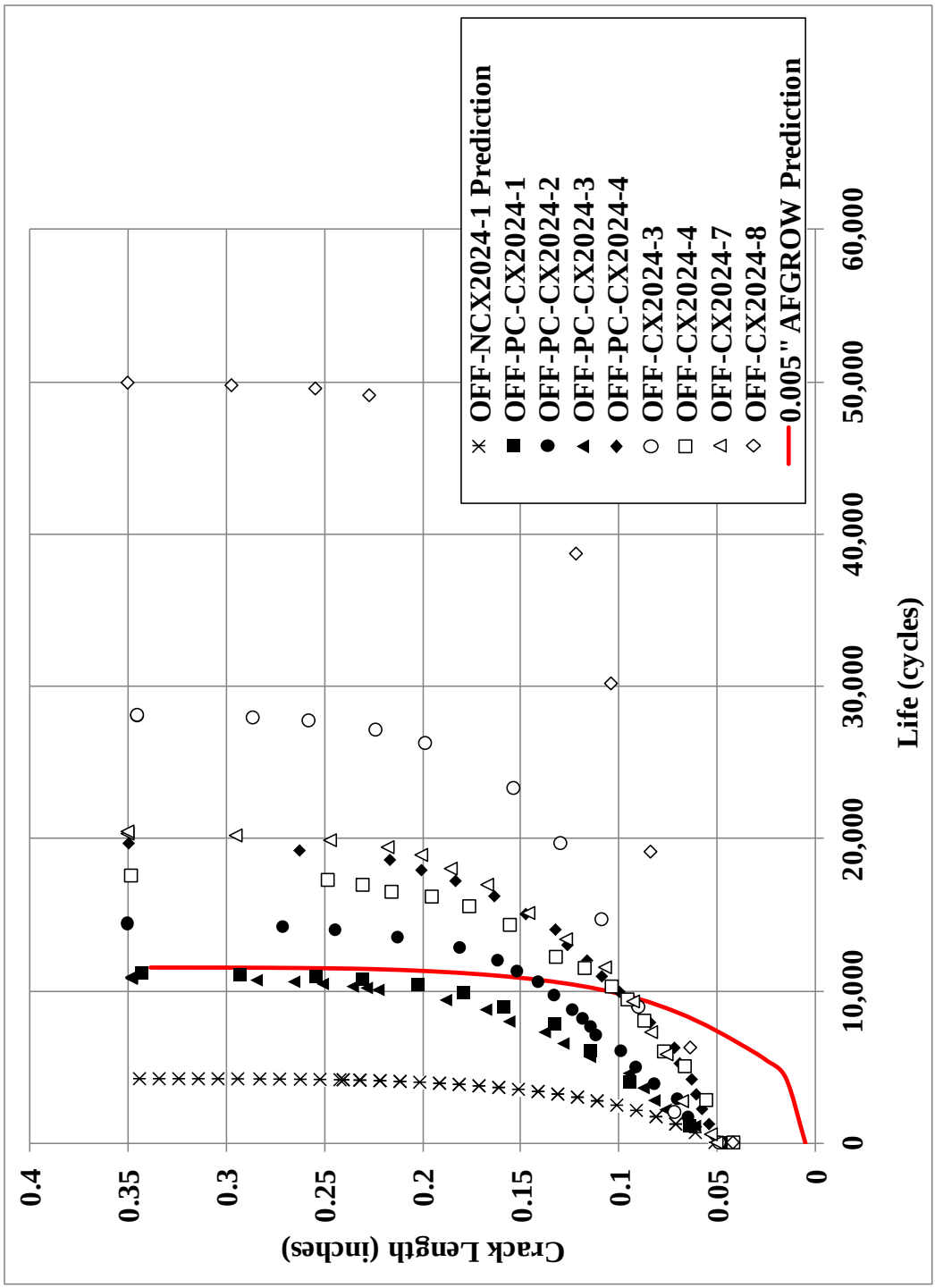

Fig. 65 Comparison of all constant-amplitude test data and 0.005 inch IFS AFGROW model

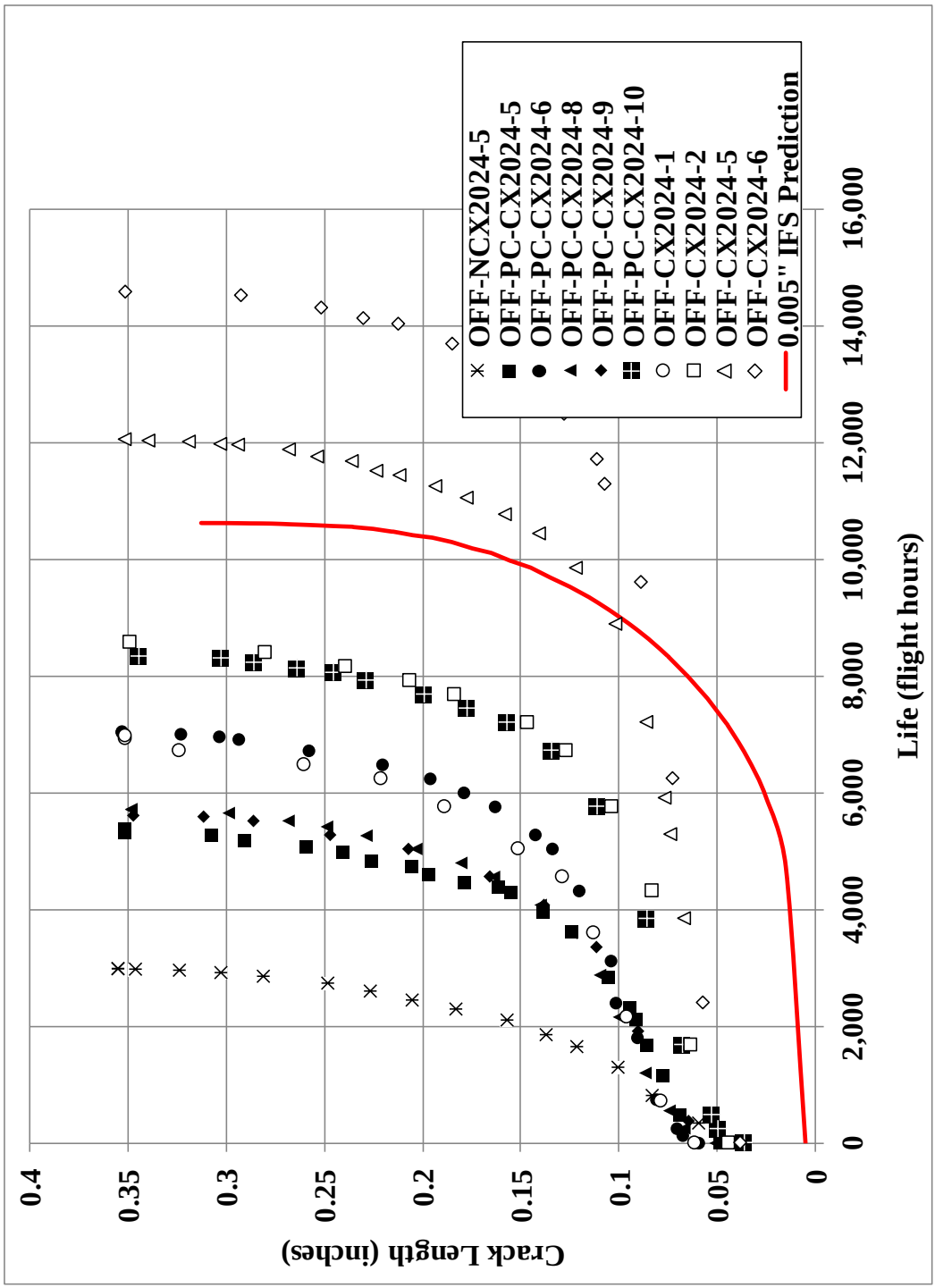

Fig. 66 Comparison of all variable-amplitude test data and 0.005 inch IFS AFGROW model

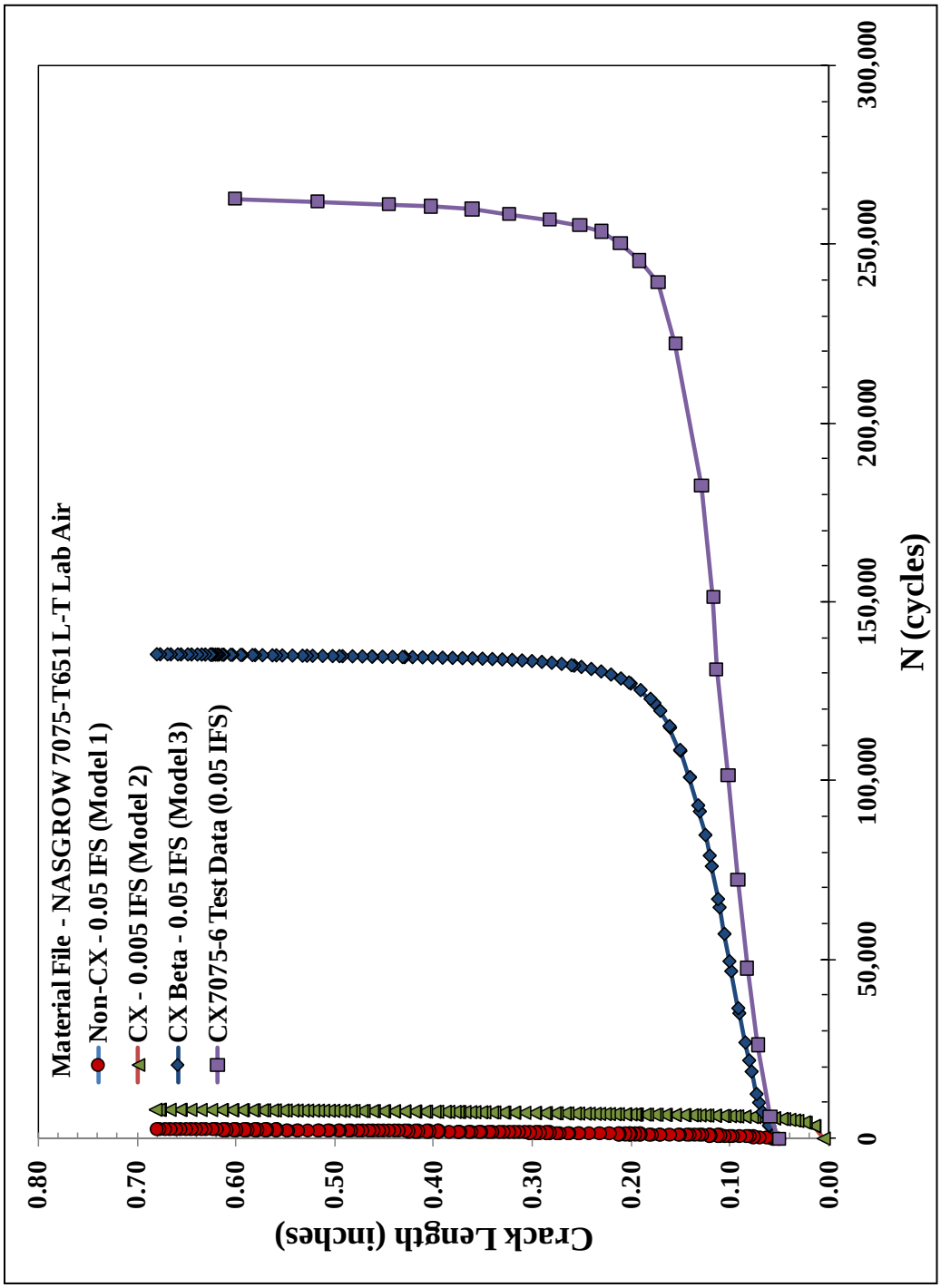

Fig. 67 Cold expansion data from the work done by Pilarczyk on constant-amplitude center hole cold-expanded specimens[10]

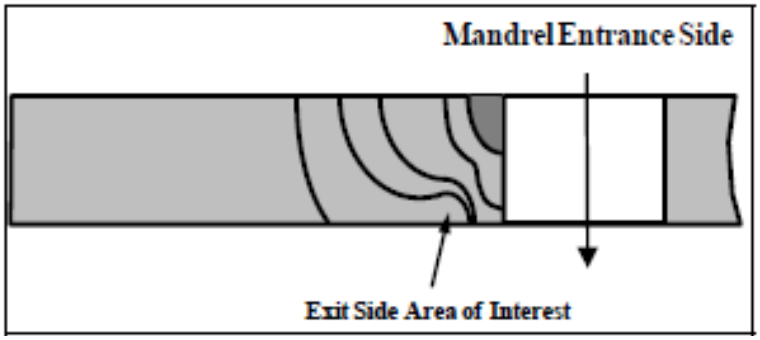

Fig. 68 Illustration of the crack front progression in a cold-expanded hole[10]

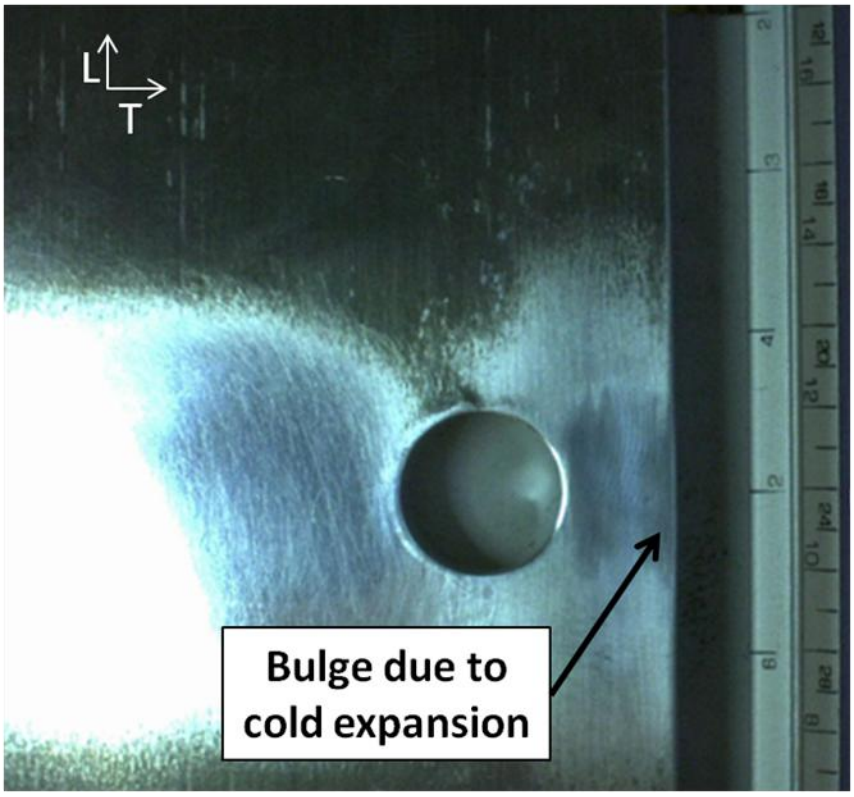

Fig. 69 Digital microscope image (5X magnification) showing the slight bulge created on the free edge of the specimen during the cold expansion process

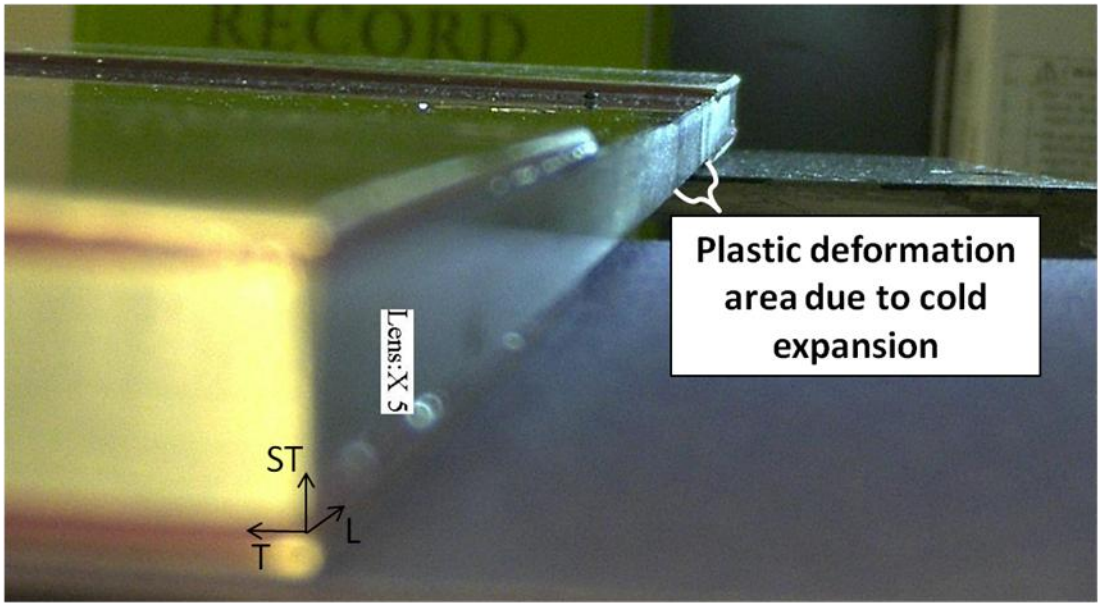

Fig. 70 Digital microscope image (5X magnification) showing the plastic deformation created during the cold expansion process

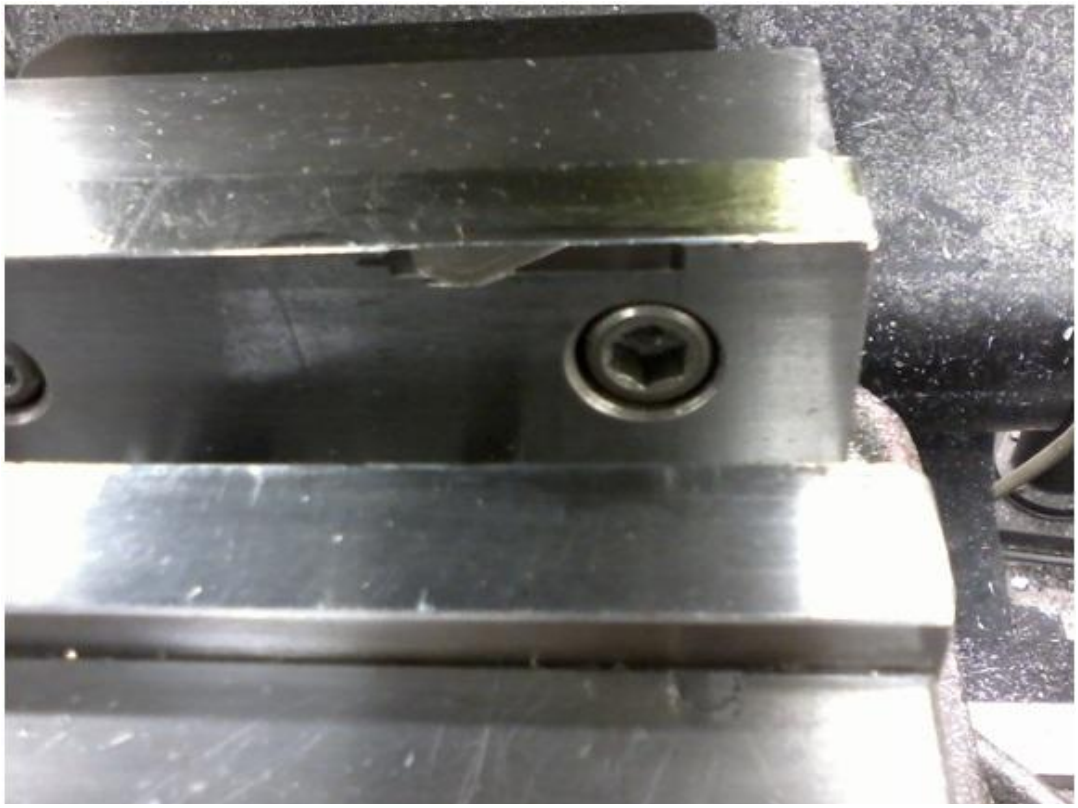

Fig. 71 Missing section in vise on the mill used for the final reaming of three of the cold-expanded specimens

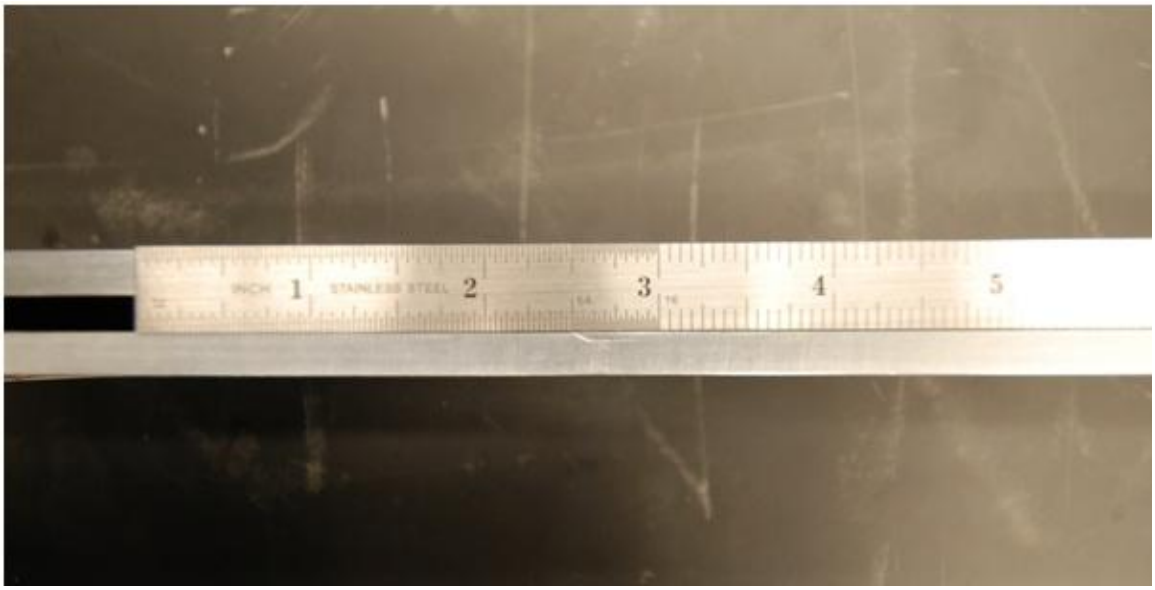

Fig. 72 Indentation in cold-expanded specimens due to vise on mill used for final reaming

6 SUMMARY

6.1 Conclusions

6.1.1 Fatigue Experiment Setup and Procedure

The data generated in this experiment met the requirements listed in ASTM E 647[31] and matched industry accepted data.

6.1.2 Fatigue Life Benefits of Precracked Cold-Expanded Holes

The relative benefit of cold-expanding a fastener hole that contains a crack is given in Table 8. For constant-amplitude loading, there was a 3.6 times improvement in fatigue life for cold-expanding a cracked hole vs. a non-cold-expanded hole, and a 6.75 times increase in fatigue life for cold-expanding a hole without a crack vs. a non-cold-expanded hole. For variable-amplitude loading, it was found that there was only a 2.27 times increase in fatigue life for the precracked then cold-expanded hole vs. a non-cold-expanded hole, and 3.26 times increase in fatigue life for a cold-expanded hole without a crack vs. a non-cold-expanded hole.

6.2 Significance

In a maintenance environment, gouges, scratches, cracks, and other damage are found in fastener holes. This damage may reduce the fatigue life benefit of processes such as cold expansion. For the experiments performed for this research, it was found that a hole containing a crack of approximately 0.050 inch and was cold-expanded, on

average reduced the fatigue life benefit of the cold expansion by approximately 50% compared to a hole that did not contain a preexisting crack.

For the specimen geometry used in this research, specifically the small edge margin, one would need to consider carefully the need for a limited improvement in fatigue life with the permanent deformation of the free edge of the specimen. The deformation of an aircraft component is typically not desired, so engineering judgment would need to be applied to decide if the fatigue life benefit would outweigh the detriment of a permanent deformation.

The major finding of the research is that the current USAF approach of lowering the IFS to 0.005 inch, for an e/D value of 1.2 with a 0.050 inch crack in the hole during cold expansion, does not produce a conservative fatigue life. The data from this research shows that this approach is not valid for this geometry and loading, and must be revised to protect the lives of USAF pilots.

6.3 Future Research and Recommendations

The following recommendations would help to further knowledge of the effect of having a crack in a hole prior to cold expansion. It would also provide guidance into procedures to account for the fatigue life benefit from cold expansion, and at what edge margins the 0.005 inch IFS AFGROW model may provide a conservative life prediction.

1. Additional Fatigue Experiments
    a. Variation of Initial Crack Length Prior to Cold Expansion
    b. Variation of Initial Discontinuity State (IDS)
    c. Variation of EDM size, Razor Notches, Corrosion Pits, Scratches, Gouges
    d. Using Different Specimen Geometry Such As Hole Offset, Hole Diameter, Thickness, Etc.
    e. Using Different Stresses for Both Constant and Variable Amplitude Loading

2. Application of Beta Corrections to account for cold expansion process for all configurations
3. Determine and validate another analytical approach to take advantage of the fatigue life benefit from cold expansion – one approach is given in (2) above.

Table 8 Increase in fatigue life due to cold expansion compared to a non-cold-expanded specimen

Type of Loading	Precracked Cold Expanded Specimens	Cold Expanded Specimens
Constant Amplitude Average	x3.6	x6.75
Variable Amplitude Average	x2.27	x3.26

APPENDIX A

MATERIAL CERTIFICATION SHEET

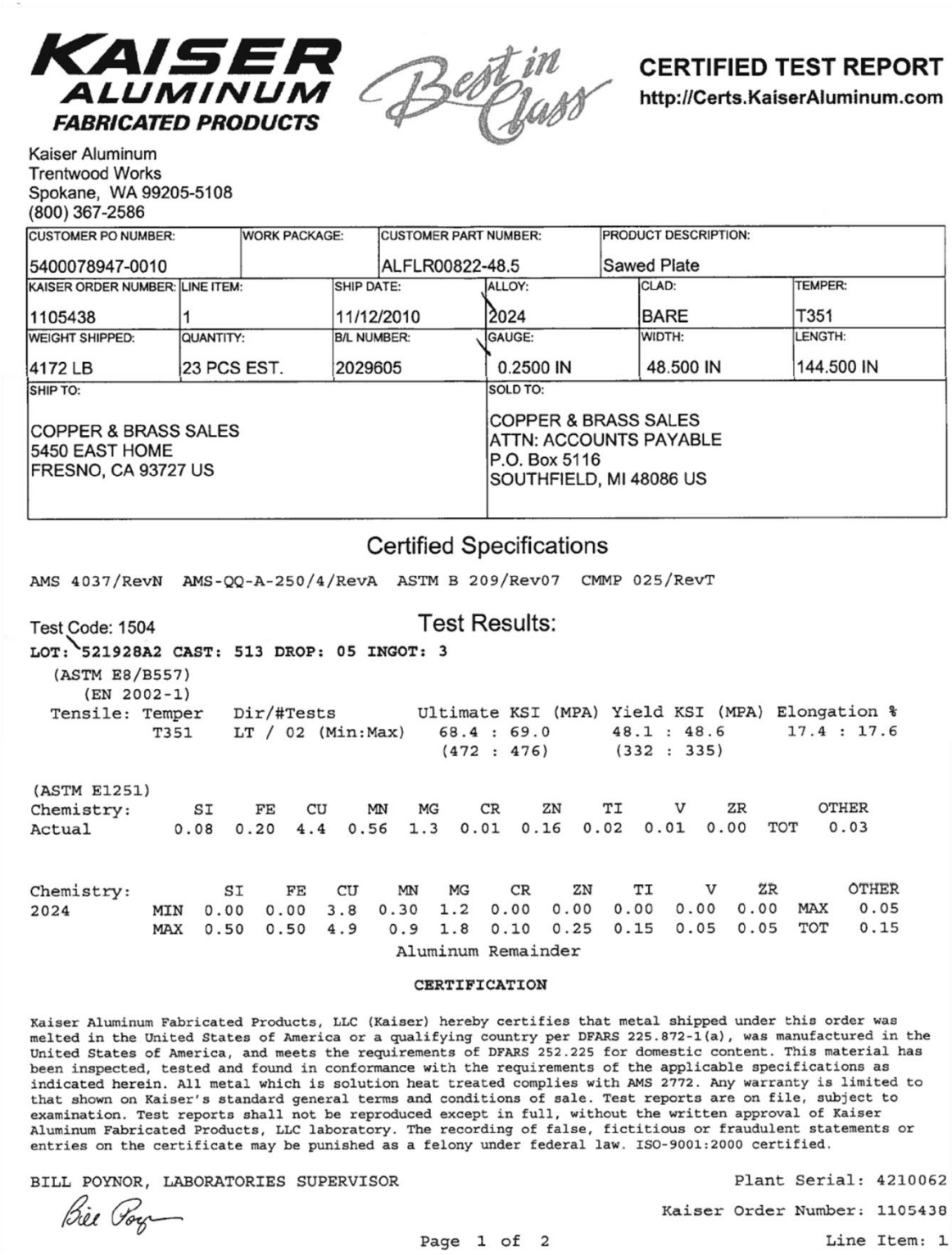

KAISER ALUMINUM
FABRICATED PRODUCTS

Best in Class

CERTIFIED TEST REPORT
http://Certs.KaiserAluminum.com

Kaiser Aluminum
Trentwood Works
Spokane, WA 99205-5108
(800) 367-2586

CUSTOMER PO NUMBER:	WORK PACKAGE:	CUSTOMER PART NUMBER:	PRODUCT DESCRIPTION:
5400078947-0010		ALFLR00822-48.5	Sawed Plate

KAISER ORDER NUMBER:	LINE ITEM:	SHIP DATE:	ALLOY:	CLAD:	TEMPER:
1105438	1	11/12/2010	2024	BARE	T351

WEIGHT SHIPPED:	QUANTITY:	B/L NUMBER:	GAUGE:	WIDTH:	LENGTH:
4172 LB	23 PCS EST.	2029605	0.2500 IN	48.500 IN	144.500 IN

SHIP TO:	SOLD TO:
COPPER & BRASS SALES 5450 EAST HOME FRESNO, CA 93727 US	COPPER & BRASS SALES ATTN: ACCOUNTS PAYABLE P.O. Box 5116 SOUTHFIELD, MI 48086 US

Certified Specifications

AMS 4037/RevN AMS-QQ-A-250/4/RevA ASTM B 209/Rev07 CMMP 025/RevT

Test Results:

Test Code: 1504

LOT: 521928A2 CAST: 513 DROP: 05 INGOT: 3

(ASTM E8/B557)
(EN 2002-1)

Tensile:	Temper	Dir/#Tests	Ultimate KSI (MPA)	Yield KSI (MPA)	Elongation %
	T351	LT / 02 (Min:Max)	68.4 : 69.0 (472 : 476)	48.1 : 48.6 (332 : 335)	17.4 : 17.6

(ASTM E1251)

Chemistry:		SI	FE	CU	MN	MG	CR	ZN	TI	V	ZR		OTHER
Actual		0.08	0.20	4.4	0.56	1.3	0.01	0.16	0.02	0.01	0.00	TOT	0.03
Chemistry:		SI	FE	CU	MN	MG	CR	ZN	TI	V	ZR		OTHER
2024	MIN	0.00	0.00	3.8	0.30	1.2	0.00	0.00	0.00	0.00	0.00	MAX	0.05
	MAX	0.50	0.50	4.9	0.9	1.8	0.10	0.25	0.15	0.05	0.05	TOT	0.15

Aluminum Remainder

CERTIFICATION

Kaiser Aluminum Fabricated Products, LLC (Kaiser) hereby certifies that metal shipped under this order was melted in the United States of America or a qualifying country per DFARS 225.872-1(a), was manufactured in the United States of America, and meets the requirements of DFARS 252.225 for domestic content. This material has been inspected, tested and found in conformance with the requirements of the applicable specifications as indicated herein. All metal which is solution heat treated complies with AMS 2772. Any warranty is limited to that shown on Kaiser's standard general terms and conditions of sale. Test reports are on file, subject to examination. Test reports shall not be reproduced except in full, without the written approval of Kaiser Aluminum Fabricated Products, LLC laboratory. The recording of false, fictitious or fraudulent statements or entries on the certificate may be punished as a felony under federal law. ISO-9001:2000 certified.

BILL POYNOR, LABORATORIES SUPERVISOR

Bill Poy

Plant Serial: 4210062
Kaiser Order Number: 1105438
Line Item: 1

Page 1 of 2

Fig. 73 Material certified test report from Kaiser Aluminum

APPENDIX B

APPLIED AND RESIDUAL EXPANSIONS

Specimen ID	Hole Diameter Before CX	Sleeve Size Before CX	Mandrel Diameter	Hole Diameter	Applied Expansion (%)	Residual Expansion (%)
OFF-CX2024-1	0.47572	0.012	0.4695	0.48865	3.74	2.72
OFF-CX2024-2	0.47570	0.012	0.4695	0.48835	3.74	2.66
OFF-CX2024-3	0.47565	0.012	0.4695	0.48907	3.75	2.82
OFF-CX2024-4	0.47562	0.012	0.4695	0.48837	3.76	2.68
OFF-CX2024-5	0.47570	0.012	0.4695	0.48872	3.74	2.74
OFF-CX2024-6	0.47575	0.012	0.4695	0.48862	3.73	2.71
OFF-CX2024-7	0.47577	0.012	0.4695	0.48857	3.73	2.69
OFF-CX2024-8	0.47572	0.012	0.4695	0.48960	3.74	2.92
OFF-PC-CX2024-1	0.47622	0.012	0.4700	0.48877	3.73	2.61
OFF-PC-CX2024-2	0.47607	0.012	0.4700	0.48912	3.77	2.69
OFF-PC-CX2024-3	0.47595	0.012	0.4700	0.48885	3.79	2.71
OFF-PC-CX2024-4	0.47632	0.012	0.4700	0.48885	3.71	2.61
OFF-PC-CX2024-5	0.47587	0.012	0.4700	0.48887	3.81	2.73
OFF-PC-CX2024-6	0.47642	0.012	0.4700	0.48885	3.69	2.56
OFF-PC-CX2024-7	0.47635	0.012	0.4700	0.48892	3.71	2.65
OFF-PC-CX2024-8	0.47565	0.012	0.4700	0.48875	3.86	2.87
OFF-PC-CX2024-9	0.47612	0.012	0.4700	0.48877	3.76	2.58
OFF-PC-CX2024-10	0.47542	0.012	0.4700	0.48887	3.91	2.79
All dimensions are in inches						

Fig. 74 Applied and residual expansions for precracked cold-expanded and cold-expanded specimens

Applied expansion (I_a) is calculated with the following formula:

$$I_a = \frac{(D + 2t - SHD)}{SHD} \times 100\%$$

Where:

D = Major Mandel Diameter
t = Sleeve Thickness
SHD = Starting Hole Diameter

Residual expansion (I_r) is calculated with the following formula:

$$I_r = \frac{(D_a - D_b)}{D_b} \times 100\%$$

Where:

D_a = Hole Diameter after Cold Expansion
D_b = Hole Diameter before Cold Expansion

APPENDIX C

FATIGUE CRACK GROWTH DATA SHEETS

2024-1 Fatigue Crack Growth Data Sheet

Width: 3.9995 in. Thick: 0.2530 in. Area: 1.0119 in^2

Experiment Information

Experiment Date: 17-Jul-11 Loading Condition: Constant-amplitude R= 0.1
Frequency: 20 Hz Hole Diameter: 0.10094 in.
Peak Stress: 11.4 ksi Ligament Length: NA in.
Surface EDM Length: 0.02034 in.

Total Cycles	Crack Length (inches)				Comments
	Surface of Hole				
	EDM		NEDM		
	A	B	A	B	
0	0.07081	0.07069	0.07025	0.07171	Testing
32377	0.07081	0.07069	0.07025	0.072076	
34445	0.07601	0.07069	0.07443	0.07559	
38449	0.07601	0.07069	0.07537	0.07745	
43495	0.07611	0.07599	0.07661	0.07771	
48511	0.07779	0.07599	0.07753	0.07851	
53534	0.07997	0.07929	0.07995	0.07943	
58661	0.07997	0.07937	0.08029	0.08189	
64545	0.08337	0.08069	0.08143	0.08243	
69875	0.08337	0.08201	0.08291	0.08319	
75020	0.08337	0.08271	0.08539	0.08483	
80218	0.08357	0.08343	0.08617	0.08521	
87017	0.08423	0.08595	0.08787	0.08647	
97037	0.08781	0.08885	0.08859	0.08719	
107114	0.09711	0.09399	0.09145	0.09029	
117279	0.09711	0.09583	0.09177	0.09379	
127584	0.09939	0.09841	0.09417	0.09595	
138158	0.10069	0.10585	0.09549	0.10199	
148460	0.10675	0.10585	0.09905	0.10507	
159668	0.11349	0.10757	0.10185	0.10637	
170666	0.11971	0.11091	0.10667	0.10777	

Continued Below

181832	**0.11995**	**0.11841**	**0.11331**	**0.11109**	
192917	**0.13429**	**0.12611**	**0.12083**	**0.11391**	
205893	**0.13801**	**0.13174**	**0.13105**	**0.11949**	
216406	**0.13937**	**0.13723**	**0.13899**	**0.12677**	
227572	**0.16333**	**0.14851**	**0.14845**	**0.13123**	
237925	**0.18715**	**0.16017**	**0.15513**	**0.14223**	
255185	**0.20695**	**0.20173**	**0.18995**	**0.16069**	
266668	**0.20713**	**0.23009**	**0.22367**	**0.19367**	
276774	**0.25655**	**0.27187**	**0.26477**	**0.23817**	
288306	**0.34971**	**0.34601**	**0.35043**	**0.31399**	
299002	**0.44355**	**0.45075**	**0.45687**	**0.42039**	
309031	**0.60947**	**0.59103**	**0.56719**	**0.59803**	
323899	**0.76685**	**0.72827**	**0.77927**	**0.78387**	
328612	**0.82993**	**0.78475**	**0.83467**	**0.82915**	
333423	**0.98797**	**0.79053**	**0.97493**	**0.93291**	
337391	**1.18945**	**1.11911**	**1.20837**	**1.09105**	
339662	**3.87822**	**3.87834**	**3.87878**	**3.87732**	
Specimen Failed					

2024- 2 Fatigue Crack Growth Data Sheet

Width: 3.9985 in. Thick: 0.2535 in. Area: 1.0136 in^2

Experiment Information

Experiment Date: 18-Jul-11 Loading Condition: Constant-amplitude R= 0.1
Frequency: 20 Hz Hole Diameter: 0.10040 in.
Peak Stress: 11.2 ksi Ligament Length: NA in.
Surface EDM Length: 0.01934 in.

Total Cycles	Crack Length (inches)				Comments
	Surface of Hole				
	EDM		NEDM		
	A	B	A	B	
0	0.06954	0.07156	0.07074	0.072	Testing
29214	0.06954	0.07156	0.07634	0.07694	
34252	0.06954	0.0763	0.07634	0.07904	
48725	0.07776	0.08292	0.07864	0.08104	
63741	0.08264	0.09144	0.08066	0.0835	
78904	0.08584	0.0982	0.08104	0.08742	
94156	0.0925	0.10396	0.09482	0.09388	
109197	0.1009	0.10868	0.10368	0.10036	
125280	0.10722	0.11232	0.1112	0.10282	
140572	0.11224	0.11968	0.12286	0.11242	
153304	0.1174	0.12656	0.13406	0.1254	
159403	0.12296	0.12678	0.13494	0.13694	
165556	0.12612	0.12976	0.1411	0.13844	
171937	0.13396	0.13766	0.15132	0.1436	
178403	0.13408	0.14026	0.15876	0.14458	
183660	0.1385	0.14702	0.16518	0.16282	
189832	0.1488	0.15136	0.1731	0.17332	
195005	0.14924	0.1582	0.18698	0.18012	
200679	0.15894	0.16906	0.1971	0.19448	
206926	0.1725	0.18198	0.21034	0.2113	
214395	0.19922	0.1986	0.23918	0.24024	

Continued Below

220580	**0.23736**	**0.23108**	**0.26422**	**0.27158**	
223933	**0.25404**	**0.2469**	**0.27772**	**0.2959**	
227382	**0.27516**	**0.2702**	**0.28926**	**0.3082**	
230806	**0.29654**	**0.28994**	**0.31146**	**0.32274**	
235481	**0.33448**	**0.33954**	**0.35152**	**0.35224**	
239282	**0.36114**	**0.3669**	**0.38492**	**0.37736**	
243510	**0.38474**	**0.41496**	**0.43502**	**0.43864**	
248469	**0.45812**	**0.45746**	**0.48056**	**0.50774**	
252237	**0.50696**	**0.53096**	**0.52586**	**0.55066**	
255787	**0.58754**	**0.59294**	**0.57074**	**0.61206**	
258925	**0.63856**	**0.63492**	**0.62136**	**0.67688**	
262260	**0.67734**	**0.67428**	**0.70054**	**0.75462**	
265444	**0.72668**	**0.71916**	**0.75492**	**0.82968**	
268994	**0.84146**	**0.90338**	**0.8271**	**0.89978**	
272272	**0.91728**	**1.0229**	**0.90172**	**1.0194**	
275452	**1.02942**	**1.19266**	**1.06354**	**1.20262**	
277796	**3.87876**	**3.87674**	**3.87756**	**3.8763**	
Specimen Failure					

OFF-NCX2024-1 Fatigue Crack Growth Data Sheet

Width: 3.9870 in. Thick: 0.2535 in. Area: 1.0107 in^2

Precrack Information

Precrack Date: 22-Jun-11 Loading Condition: Constant-amplitude R= 0.1
Frequency: 20 Hz Hole Diameter: 0.47615 in. Peak Stress: 9.9 ksi
Surface EDM Length: 0.01284 in.

Experiment Information

Experiment Date: 29-Jun-11 Loading Condition: Constant-amplitude R= 0.1
Frequency: 20 Hz Hole Diameter: 0.50087 in.
Peak Stress: 10.0 ksi Ligament Length: 0.35766 in.
Surface EDM Length: EDM removed during final reaming

Total Cycles	Crack Length (inches)					Comments
	Surface of Hole				Bore	
	EDM		NEDM			
	A	B	A	B		
0						Precrack
150903	0.0379				0.0313	
0	0.0381				0.0647	Testing
3633	0.0508				0.0715	
5640	0.0579				0.0738	
7981	0.0646				0.0783	
10524	0.0701				0.0796	
12565	0.0774				0.0846	
15609	0.0863				0.0941	
22994	0.1065				0.1203	
25008	0.1091				0.1251	
27280	0.1174				0.1354	
29749	0.1256				0.1456	
31773	0.1420				0.1499	
33748	0.1489				0.1600	
35752	0.1528				0.1737	
37794	0.1831				0.1885	

Continued Below

39942	**0.1944**				**0.2007**	
42136	**0.2122**				**0.2181**	
44213	**0.2265**				**0.2181**	
46233	**0.2507**		**0.1258**			**Thru Thickness**
47237	**0.2685**		**0.1599**			
48256	**0.2871**		**0.1924**			
48764	**0.3064**		**0.2131**			
49072	**0.3159**		**0.2252**			
49383	**0.3333**		**0.2417**			
49551	**0.3577**		**0.2627**			
49631	**0.3577**		**0.3577**			
Ligament Failed						

OFF-NCX2024-2 Fatigue Crack Growth Data Sheet

Width: 3.9830 in. Thick: 0.2550 in. Area: 1.0157 in^2

Precrack Information

Precrack Date: 22-Jun-11 Loading Condition: Constant-amplitude R= 0.1
Frequency: 20 Hz Hole Diameter: 0.47617 in. Peak Stress: 9.9 ksi
Surface EDM Length: 0.01166 in.

Experiment Information

Experiment Date: 30-Jun-11 Loading Condition: Constant-amplitude R= 0.1
Frequency: 20 Hz Hole Diameter: 0.50075 in.
Peak Stress: 10.0 ksi Ligament Length: 0.35640 in.
Surface EDM Length: EDM removed during final reaming

Total Cycles	Crack Length (inches)					Comments
	Surface of Hole				Bore	
	EDM		NEDM			
	A	B	A	B		
0						Precrack
185243	0.04998				0.05810	
0	0.03714				0.08021	Testing
2402	0.04704				0.08337	
4416	0.04918				0.08557	
6432	0.05384				0.08882	
8516	0.06042				0.09288	
10581	0.06432				0.09833	
12654	0.06860				0.10626	
15984	0.07270				0.11206	
18762	0.08114				0.11639	
20768	0.09040				0.12166	
22900	0.09700				0.12584	
24893	0.10152				0.13421	
26915	0.10664				0.13473	
28949	0.11712				0.14205	
30957	0.13030				0.14784	
32966	0.14444				0.15543	
35983	0.15938				0.16506	

Continued Below

39180	**0.17638**				**0.19397**	
42594	**0.20188**				**0.21442**	
45098	**0.22798**				**0.22427**	
47660	**0.26516**				**0.22427**	
49809	**0.29872**		**0.06886**			**Thru Thickness**
51797	**0.35640**		**0.35640**			
Ligament Failed						

OFF-NCX2024-3 Fatigue Crack Growth Data Sheet

Width: 3.9840 in. Thick: 0.2530 in. Area: 1.0080 in^2

Precrack Information

Precrack Date: 22-Jun-11 Loading Condition: Constant-amplitude R= 0.1
Frequency: 20 Hz Hole Diameter: 0.47632 in. Peak Stress: 9.9 ksi
Surface EDM Length: 0.01288 in.

Experiment Information

Experiment Date: 30-Jun-11 Loading Condition: Constant-amplitude R= 0.1
Frequency: 20 Hz Hole Diameter: 0.50090 in.
Peak Stress: 10.0 ksi Ligament Length: 0.35844 in.
Surface EDM Length: EDM removed during final reaming

Total Cycles	Crack Length (inches)					Comments
	Surface of Hole				Bore	
	EDM		NEDM			
	A	B	A	B		
0						Precrack
198402	0.05208				0.05529	
0	0.03654				0.05669	Testing
2884	0.03784				0.05930	
4894	0.04436				0.05963	
7215	0.04632				0.06012	
10206	0.05070				0.06641	
13494	0.05370				0.06707	
17659	0.06328				0.07455	
20656	0.06562				0.08137	
24533	0.07600				0.08703	
28459	0.08672				0.09682	
31915	0.10268				0.10828	
35001	0.10992				0.11546	
38382	0.12050				0.12568	
42129	0.13400				0.14182	
45091	0.14800				0.15654	

Continued Below

48369	**0.16158**				**0.18165**	
51076	**0.17358**				**0.19858**	
53331	**0.19110**				**0.21913**	
55290	**0.20612**				**0.24160**	**Thru Thickness**
56701	**0.22344**		**0.07238**			
58121	**0.24320**		**0.13794**			
58590	**0.25288**		**0.15326**			
59248	**0.26310**		**0.17520**			
59966	**0.27880**		**0.20626**			
60353	**0.29012**		**0.21748**			
60866	**0.3088**		**0.24112**			
61352	**0.35844**		**0.28216**			
61441	**0.35844**		**0.35844**			
Ligament Failure						

OFF-NCX2024-4 Fatigue Crack Growth Data Sheet

Width: 3.9850 in. Thick: 0.2535 in. Area: 1.0102 in^2

Precrack Information

Precrack Date: 22-Jun-11 Loading Condition: Constant-amplitude R= 0.1
Frequency: 20 Hz Hole Diameter: 0.47657 in. Peak Stress: 9.9 ksi
Surface EDM Length: 0.01086 in.

Experiment Information

Experiment Date: 30-Jun-11 Loading Condition: Constant-amplitude R= 0.1
Frequency: 20 Hz Hole Diameter: 0.50080 in.
Peak Stress: 10.0 ksi Ligament Length: 0.35634 in.
Surface EDM Length: EDM removed during final reaming

Total Cycles	Crack Length (inches)					Comments
	Surface of Hole				Bore	
	EDM		NEDM			
	A	B	A	B		
0						Precrack
150762	0.05076				0.06425	
0	0.03842				0.06474	Testing
1166	0.04321				0.06517	
5476	0.04752				0.07594	
9123	0.05618				0.07697	
12786	0.06362				0.08815	
16661	0.07442				0.10259	
20042	0.08404				0.10917	
23897	0.08938				0.12405	
27298	0.10796				0.13066	
31350	0.11782				0.13754	
34962	0.14192				0.16427	
38515	0.16144				0.19398	
41571	0.18424				0.20943	
44350	0.20840				0.23055	
46161	0.22766				0.24451	Thru Thickness

Continued Below

47914	**0.24902**		**0.06896**			
50024	**0.26898**		**0.16766**			
51658	**0.32950**		**0.23152**			
51951	**0.35634**		**0.26164**			
52051	**0.35634**		**0.35634**			
Ligament Failure						

OFF-NCX2024-5 Fatigue Crack Growth Data Sheet

Width: 3.9860 in. Thick: 0.2530 in. Area: 1.0085 in^2

Precrack Information

Precrack Date: 22-Jun-11 Loading Condition: Constant-amplitude R= 0.1
Frequency: 20 Hz Hole Diameter: 0.47645 in. Peak Stress: 9.9 ksi
Surface EDM Length: 0.01052 in.

Experiment Information

Experiment Date: 22-Aug-11 Loading Condition: Variable-amplitude
Loading Rate: 180000 lbs/s Hole Diameter: 0.50140 in.
Peak Stress: 32.7 ksi Ligament Length: 0.35568 in.
Surface EDM Length: 0.00298 in.

Total Flight Hours	Crack Length (inches)					Comments
	Surface of Hole				Bore	
	EDM		NEDM			
	A	B	A	B		
0						Precrack (cylces)
178433	0.04986				0.05858	
0	0.04250				0.06820	Testing (flight hours)
332	0.05972				0.09014	
805	0.08342				0.11565	
1288	0.10082				0.14480	
1641	0.12182				0.15101	
1846	0.13746				0.19247	
2096	0.15736				0.22506	
2284	0.18344		0.03604			Through Thickness
2439	0.20574		0.08138			
2592	0.22708		0.12982			
2728	0.24876		0.16328			
2846	0.28160		0.21686			
2909	0.30322		0.23732			
2950	0.32438		0.24602			
2967	0.34678		0.26650			
2974	0.35568		0.28782			
2979	0.35568		0.35568			
Ligament Failure						

OFF-NCX2024- 6 Fatigue Crack Growth Data Sheet

Width: 3.9860 in. Thick: 0.2525 in. Area: 1.0065 in^2

Precrack Information

Precrack Date: 22-Jun-11 Loading Condition: Constant-amplitude R= 0.1
Frequency: 20 Hz Hole Diameter: 0.47682 in. Peak Stress: 9.9 ksi
Surface EDM Length: 0.01170 in.

Experiment Information

Experiment Date: 23-Aug-11 Loading Condition: Variable-amplitude
Loading Rate: 380000 lbs/s Hole Diameter: 0.50130 in.
Peak Stress: 32.8 ksi Ligament Length: 0.34536 in.
Surface EDM Length: 0.00382 in.

Specimen overloaded and data invalid.

OFF-PC-CX2024-1 Fatigue Crack Growth Data Sheet

Width: 4.0010 in. Thick: 0.2560 in. Area: 1.0243 in^2

Precrack Information

Precrack Date: 8-Aug-11 Loading Condition: Constant-amplitude R= 0.1
Frequency: 20 Hz Hole Diameter: 0.47577 in. Peak Stress: 20.0 ksi
Surface EDM Length: 0.01402 in.

Experiment Information

Experiment Date: 11-Aug-11 Loading Condition: Constant-amplitude R= 0.1
Frequency: 20 Hz Hole Diameter: 0.50305 in.
Peak Stress: 25.0 ksi Ligament Length: 0.34324 in.
Surface EDM Length: 0.00654 in.

Total Cycles	Crack Length (inches)					Comments
	Surface of Hole				Bore	
	EDM		NEDM			
	A	B	A	B		
0						Precrack
14055	0.05142				0.05060	
0	0.04604				0.04308	Testing
1119	0.06392				0.07228	
3994	0.09466				0.11071	
6057	0.11468				0.14446	
7826	0.13278				0.15614	
8935	0.15886				0.17550	
9903	0.17934				0.20638	
10430	0.20248				0.22344	
10778	0.23082				0.23923	
10964	0.25436		0.09252			Through Thickness
11088	0.29296		0.15312			
11168	0.34324		0.34324			
Ligament Failure						

OFF-PC-CX2024- 2 Fatigue Crack Growth Data Sheet

Width: 4.0010 in. Thick: 0.2540 in. Area: 1.0163 in^2

Precrack Information

Precrack Date: 8-Aug-11 Loading Condition: Constant-amplitude R= 0.1
Frequency: 20 Hz Hole Diameter: 0.47615 in. Peak Stress: 20.0 ksi
Surface EDM Length: 0.01372 in.

Experiment Information

Experiment Date: 11-Aug-11 Loading Condition: Constant-amplitude R= 0.1
Frequency: 20 Hz Hole Diameter: 0.50275 in.
Peak Stress: 25.0 ksi Ligament Length: 0.35058 in.
Surface EDM Length: 0.01102 in.

Total Cycles	Crack Length (inches)					Comments
	Surface of Hole				Bore	
	EDM		NEDM			
	A	B	A	B		
0						Precrack
13309	0.05020				0.05017	
0	0.04668				0.04025	Testing
1721	0.06482				0.05341	
2916	0.07030				0.07326	
3905	0.08210				0.08697	
5002	0.09146				0.09048	
6068	0.09908				0.09689	
7107	0.11182				0.10570	
7657	0.11450				0.11139	
8193	0.11860				0.11548	
8767	0.12380				0.11890	
9726	0.13314				0.11901	
10603	0.14126				0.13845	
11301	0.15202				0.14592	
12014	0.16190				0.15016	
12850	0.18122				0.16275	

Continued Below

13530	**0.21290**				**0.17465**	
14013	**0.24470**				**0.19275**	
14220	**0.27142**				**0.20505**	
14386	**0.35058**				**0.21345**	
14474	**0.35058**		**0.35058**			
Ligament Failed						

OFF-PC-CX2024-3 Fatigue Crack Growth Data Sheet

Width: 4.0040 in. Thick: 0.2550 in. Area: 1.0210 in^2

Precrack Information

Precrack Date: 8-Aug-11 Loading Condition: Constant-amplitude R= 0.1
Frequency: 20 Hz Hole Diameter: 0.47585 in. Peak Stress: 20.0 ksi
Surface EDM Length: 0.01492 in.

Experiment Information

Experiment Date: 11-Aug-11 Loading Condition: Constant-amplitude R= 0.1
Frequency: 20 Hz Hole Diameter: 0.50192 in.
Peak Stress: 25.0 ksi Ligament Length: 0.34846 in.
Surface EDM Length: 0.01158 in.

Total Cycles	Crack Length (inches)					Comments
	Surface of Hole				Bore	
	EDM		NEDM			
	A	B	A	B		
0						Precrack
16035	0.05300				0.05383	
0	0.04922				0.03634	Testing
1130	0.06130				0.06051	
2193	0.07628				0.06318	
2803	0.08200				0.08410	
3618	0.08753				0.09700	
4584	0.09494				0.10078	
5664	0.11482				0.11940	
6541	0.12836				0.12570	
7285	0.13784				0.12578	
7982	0.15596				0.13341	
8764	0.16780				0.16163	
9393	0.18822				0.17350	
10063	0.22266				0.19341	
10188	0.22856				0.19919	
10288	0.23570				0.20057	

Continued Below

10454	**0.25099**				**0.20071**	
10594	**0.26558**				**0.21603**	
10698	**0.28472**				**0.21966**	
10800	**0.34846**				**0.23475**	
10821	**0.34846**				**0.23479**	
10862	**0.34846**		**0.08184**			**Through Thickness**
10884	**0.34846**		**0.11738**			
10905	**0.34846**		**0.23182**			
10927	**0.34846**		**0.34846**			
Ligament Failed						

OFF-PC-CX2024-4 Fatigue Crack Growth Data Sheet

Width: 4.0020 in. Thick: 0.2550 in. Area: 1.0205 in^2

Precrack Information

Precrack Date: 8-Aug-11 Loading Condition: Constant-amplitude R= 0.1
Frequency: 20 Hz Hole Diameter: 0.47575 in. Peak Stress: 20.0 ksi
Surface EDM Length: 0.01414 in.

Experiment Information

Experiment Date: 11-Aug-11 Loading Condition: Constant-amplitude R= 0.1
Frequency: 20 Hz Hole Diameter: 0.50192 in.
Peak Stress: 25.0 ksi Ligament Length: 0.34988 in.
Surface EDM Length: 0.00824 in.

Total Cycles	Crack Length (inches)					Comments
	Surface of Hole				Bore	
	EDM		NEDM			
	A	B	A	B		
0						Precrack
14095	0.04910				0.05074	
0	0.04380				0.04010	Testing
1253	0.05406				0.06116	
2242	0.05762				0.07254	
3202	0.06056				0.07835	
4189	0.06290				0.08392	
5237	0.06898				0.09198	
6263	0.07170				0.09348	
7919	0.08414				0.10541	
8918	0.09090				0.11968	
9933	0.09974				0.12639	
10952	0.10871				0.14133	
11992	0.11620				0.14137	
13008	0.12624				0.14409	
14022	0.13234				0.15160	
15041	0.14746				0.16132	

Continued Below

16218	**0.16350**				**0.16294**	
17216	**0.18328**				**0.18803**	
17927	**0.20066**				**0.19704**	
18599	**0.21672**				**0.22873**	
19217	**0.26278**				**0.24603**	
19686	**0.34988**		**0.34988**			
Ligament Failed						

OFF-PC-CX2024-5 Fatigue Crack Growth Data Sheet

Width: 4.0030 in. Thick: 0.2540 in. Area: 1.0168 in^2

Precrack Information

Precrack Date: 8-Aug-11 Loading Condition: Constant-amplitude R= 0.1
Frequency: 20 Hz Hole Diameter: 0.47582 in. Peak Stress: 10.0 ksi
Surface EDM Length: 0.01146 in.

Experiment Information

Experiment Date: 18-Aug-11 Loading Condition: Variable-amplitude
Loading Rate: 150000 lbs/s Hole Diameter: 0.50275 in.
Peak Stress: 32.5 ksi Ligament Length: 0.35182 in.
Surface EDM Length: 0.00758 in.

Total Flight Hours	Crack Length (inches)					Comments
	Surface of Hole				Bore	
	EDM		NEDM			
	A	B	A	B		
0						Precrack (cycles)
94911	0.04966				0.06406	
0	0.04834				0.09391	Testing (flight hours)
478	0.06918				0.09992	
1161	0.07746				0.12005	
1681	0.08578				0.13429	
2124	0.09132				0.14803	
2323	0.09470				0.14806	
2839	0.10560				0.17575	
3620	0.12400				0.20684	
3961	0.13884				0.22783	
4294	0.15530		0.01758			Through Thickness
4388	0.16156		0.03640			
4456	0.17868		0.05646			
4591	0.19714		0.08008			
4743	0.20574		0.10084			
4833	0.22620		0.12026			

Continued Below

4978	**0.24078**		**0.14446**			
5076	**0.25956**		**0.16930**			
5185	**0.29098**		**0.18998**			
5275	**0.30766**		**0.22482**			
5325	**0.35182**		**0.24526**			
5369	**0.35182**		**0.27542**			
5374	**0.35182**		**0.35182**			
Ligament Failed						

OFF-PC-CX2024-6 Fatigue Crack Growth Data Sheet

Width: 3.9920 in. Thick: 0.2540 in. Area: 1.0140 in^2

Precrack Information

Precrack Date: 8-Aug-11 Loading Condition: Constant-amplitude R= 0.1
Frequency: 20 Hz Hole Diameter: 0.47605 in. Peak Stress: 10.0 ksi
Surface EDM Length: 0.01462 in.

Experiment Information

Experiment Date: 19-Aug-11 Loading Condition: Variable-amplitude
Loading Rate: 150000 lbs/s Hole Diameter: 0.50217 in.
Peak Stress: 32.5 ksi Ligament Length: 0.35330 in.
Surface EDM Length: 0.01026 in.

Total Flight Hours	Crack Length (inches)					Comments
	Surface of Hole				Bore	
	EDM		NEDM			
	A	B	A	B		
0						Precrack (cycles)
101117	0.06230				0.07680	
0	0.05930				0.07205	Testing (flight hours)
129	0.06744				0.09820	
248	0.07042				0.10898	
745	0.08090				0.12939	
1803	0.09056				0.13878	
2398	0.10152				0.15836	
3118	0.10402				0.18167	
4318	0.12026				0.20380	
5038	0.13390				0.20459	
5278	0.14260				0.22538	Through Thickness
5758	0.16310				0.25205	
5998	0.17900		0.02858			
6238	0.19616		0.07568			
6478	0.22050		0.14312			
6718	0.25800		0.20850			

Continued Below

6912	**0.29376**		**0.22134**			
6957	**0.30368**		**0.23918**			
7001	**0.32328**		**0.25696**			
7029	**0.35330**		**0.27382**			
7039	**0.35330**		**0.31688**			
7047	**0.35330**		**0.35330**			
Ligament Failed						

OFF-PC-CX2024-7 Fatigue Crack Growth Data Sheet

Width: 3.9860 in. Thick: 0.2540 in. Area: 1.0124 in^2

Precrack Information

Precrack Date: 8-Aug-11 Loading Condition: Constant-amplitude R= 0.1
Frequency: 20 Hz Hole Diameter: 0.47620 in. Peak Stress: 10.0 ksi
Surface EDM Length: 0.01304 in.

Experiment Information

Experiment Date: 30-Aug-11
Loading Condition: Constant-amplitude - Marker Banding R= 0.1
Frequency: 20 Hz Hole Diameter: 0.50187 in.
Peak Stress: 25.0 ksi Ligament Length: 0.34866 in.
Surface EDM Length: 0.00718 in.

Specimen used for marker banding.

OFF-PC-CX2024-8 Fatigue Crack Growth Data Sheet

Width: 3.9910 in. Thick: 0.2540 in. Area: 1.0137 in^2

Precrack Information

Precrack Date: 8-Aug-11 Loading Condition: Constant-amplitude R= 0.1
Frequency: 20 Hz Hole Diameter: 0.47607 in. Peak Stress: 10.0 ksi
Surface EDM Length: 0.01114 in.

Experiment Information

Experiment Date: 20-Aug-11 Loading Condition: Variable-amplitude
Loading Rate: 180000 lbs/s Hole Diameter: 0.50170 in.
Peak Stress: 32.6 ksi Ligament Length: 0.34856 in.
Surface EDM Length: 0.00538 in.

Total Flight Hours	Crack Length (inches)					Comments
	Surface of Hole				Bore	
	EDM		NEDM			
	A	B	A	B		
0						Precrack (cycles)
80109	0.05758				0.07083	
0	0.05072				0.06923	Testing (flight hours)
254	0.06670				0.08867	
555	0.07426				0.10188	
1201	0.08652				0.12195	
2158	0.09996				0.14563	
2878	0.10966				0.16509	
3598	0.12426				0.17969	
4078	0.13992				0.20040	
4558	0.16372				0.22375	
4798	0.18040				0.24311	
5038	0.20330		0.04808			Through Thickness
5264	0.22872		0.10424			
5418	0.24882		0.14140			
5519	0.26846		0.17038			
5652	0.29890		0.22144			
5711	0.35394		0.27182			
5718	0.34856		0.34856			
Ligament Failed						

OFF-PC-CX2024-9 Fatigue Crack Growth Data Sheet

Width: 3.9850 in. Thick: 0.2540 in. Area: 1.0122 in^2

Precrack Information

Precrack Date: 8-Aug-11 Loading Condition: Constant-amplitude R= 0.1
Frequency: 20 Hz Hole Diameter: 0.47610 in. Peak Stress: 10.0 ksi
Surface EDM Length: 0.01628 in.

Experiment Information

Experiment Date: 1-Sep-11 Loading Condition: Variable-amplitude
Loading Rate: 380000 lbs/s Hole Diameter: 0.50192 in.
Peak Stress: 32.6 ksi Ligament Length: 0.34752 in.
Surface EDM Length: EDM removed during final reaming

Total Flight Hours	Crack Length (inches)					Comments
	Surface of Hole				Bore	
	EDM		NEDM			
	A	B	A	B		
0						Precrack (cycles)
119135	0.05840				0.07826	
0	0.04704				0.06931	Testing (flight hours)
379	0.06452				0.10831	
1918	0.09026				0.15911	
3358	0.11146				0.17649	
4078	0.13826				0.18501	
4566	0.16582				0.23136	
5038	0.20728		0.07814			Through Thickness
5278	0.24720		0.13514			
5518	0.28628		0.20066			
5591	0.31170		0.22176			
5611	0.34752		0.34752			
Ligament Failed						

OFF-PC-CX2024-10 Fatigue Crack Growth Data Sheet

Width: 3.9850 in. Thick: 0.2540 in. Area: 1.0122 in^2

Precrack Information

Precrack Date: 8-Aug-11 Loading Condition: Constant-amplitude R= 0.1
Frequency: 20 Hz Hole Diameter: 0.47625 in. Peak Stress: 10.0 ksi
Surface EDM Length: 0.01652 in.

Experiment Information

Experiment Date: 6-Sep-11 Loading Condition: Variable-amplitude
Loading Rate: 380000 lbs/s Hole Diameter: 0.50265 in.
Peak Stress: 32.6 ksi Ligament Length: 0.34502 in.
Surface EDM Length: Specimen removed during final reaming

Total Flight Hours	Crack Length (inches)					Comments
	Surface of Hole				Bore	
	EDM		NEDM			
	A	B	A	B		
0						Precrack (cycles)
118622	0.05840				0.07826	
0	0.04704				0.06931	Testing (flight hours)
379	0.06452				0.10831	
1918	0.09026				0.15911	
3358	0.11146				0.17649	
4078	0.13826				0.18501	
4566	0.16582				0.23136	
5038	0.20728		0.07814			Through Thickness
5278	0.24720		0.13514			
5518	0.28628		0.20066			
5591	0.31170		0.22176			
5611	0.34752		0.34752			
Ligament Failed						

OFF-CX2024-1 Fatigue Crack Growth Data Sheet

Width: 4.0080 in. Thick: 0.2555 in. Area: 1.0240 in^2

Precrack Information

Precrack Date: 25-Aug-11 Loading Condition: Constant-amplitude R= 0.1
Frequency: 20 Hz Hole Diameter: 0.48865 in. Peak Stress: 25.0 ksi
Surface EDM Length: 0.01976 in.

Experiment Information

Experiment Date: 23-Sep-11 Loading Condition: Variable-amplitude
Loading Rate: 520000 lbs/s Hole Diameter: 0.50135 in.
Peak Stress: 32.2 ksi Ligament Length: 0.35224 in.
Surface EDM Length: 0.01414 in.

Total Cycles	Crack Length (inches)					Comments
	Surface of Hole				Bore	
	EDM		NEDM			
	A	B	A	B		
0						Precrack
14250	0.04944				0.06461	
0	0.03642				0.05317	Testing
238	0.04988				0.07402	
478	0.05318				0.08236	
1678	0.06792				0.10245	
3837	0.08606				0.14030	
5758	0.11146				0.18114	
6718	0.13468				0.21009	
7198	0.15744				0.23334	
7438	0.17774		0.03996			Through Thickness
7678	0.19958		0.08450			
7918	0.22916		0.13438			
8050	0.24586		0.15286			
8126	0.26444		0.17456			
8223	0.28642		0.19850			
8297	0.30316		0.23378			
8329	0.34502		0.34502			
Ligament Failed						

OFF-CX2024-2 Fatigue Crack Growth Data Sheet

Width: 4.0090 in. Thick: 0.2535 in. Area: 1.0163 in^2

Precrack Information

Precrack Date: 25-Aug-11 Loading Condition: Constant-amplitude R= 0.1
Frequency: 20 Hz Hole Diameter: 0.48835 in. Peak Stress: 25.0 ksi
Surface EDM Length: 0.01614 in.

Experiment Information

Experiment Date: 23-Sep-11 Loading Condition: Variable-amplitude
Loading Rate: 600000 lbs/s Hole Diameter: 0.50087 in.
Peak Stress: 32.5 ksi Ligament Length: 0.34984 in.
Surface EDM Length: 0.01132 in.

Total Flight Hours	Crack Length (inches)					Comments
	Surface of Hole				Bore	
	EDM		NEDM			
	A	B	A	B		
0						Precrack (cycles)
14706	0.05158				0.05991	
0	0.04474				0.05749	Testing (flight hours)
1678	0.06400				0.08618	
4318	0.08370				0.13310	
5758	0.10428				0.16002	
6718	0.12752				0.18549	
7198	0.14724				0.20965	
7678	0.18444		0.01486			Through Thickness
7918	0.20726		0.07602			
8158	0.23998		0.13518			
8398	0.28092		0.20302			
8574	0.34984		0.34984			
Ligament Failed						

OFF-CX2024-3 Fatigue Crack Growth Data Sheet

Width: 4.0095 in. Thick: 0.2530 in. Area: 1.0144 in^2

Precrack Information

Precrack Date: 25-Aug-11 Loading Condition: Constant-amplitude R= 0.1
Frequency: 20 Hz Hole Diameter: 0.48907 in. Peak Stress: 25.0 ksi
Surface EDM Length: 0.01744 in.

Experiment Information

Experiment Date: 21-Sep-11 Loading Condition: Constant-amplitude R= 0.1
Frequency: 20 Hz Hole Diameter: 0.50165 in.
Peak Stress: 25.0 ksi Ligament Length: 0.34598 in.
Surface EDM Length: 0.00968 in.

Total Cycles	Crack Length (inches)					Comments
	Surface of Hole				Bore	
	EDM		NEDM			
	A	B	A	B		
0						Precrack
15728	0.05892				0.09300	
0	0.04930				0.06373	Testing
2000	0.07212				0.09407	
8907	0.09046				0.12899	
14657	0.10926				0.16025	
19658	0.13024				0.17858	
23277	0.15416				0.20305	
26231	0.19918				0.24830	
27107	0.22444		0.01778			Through Thickness
27713	0.25858		0.05394			
27907	0.28704		0.09444			
28045	0.34598		0.14678			
28077	0.34598		0.34598			
Ligament Failed						

OFF-CX2024-4 Fatigue Crack Growth Data Sheet

Width: 4.0065 in. Thick: 0.2545 in. Area: 1.0197 in^2

Precrack Information

Precrack Date: 26-Aug-11 Loading Condition: Constant-amplitude R= 0.1
Frequency: 20 Hz Hole Diameter: 0.48837 in. Peak Stress: 25.0 ksi
Surface EDM Length: 0.01834 in.

Experiment Information

Experiment Date: 8-Sep-11 Loading Condition: Constant-amplitude R= 0.1
Frequency: 20 Hz Hole Diameter: 0.50267 in.
Peak Stress: 25.0 ksi Ligament Length: 0.34906 in.
Surface EDM Length: 0.01064 in.

Total Cycles	Crack Length (inches)					Comments
	Surface of Hole				Bore	
	EDM		NEDM			
	A	B	A	B		
0						Precrack
305446	0.03398				0.03366	
0	0.03138				0.02996	Testing
2782	0.04522				0.0414	
5005	0.05614				0.05922	
5977	0.06678				0.06188	
7998	0.0768				0.07522	
9389	0.08535				0.0803	
10241	0.0934				0.08458	
11454	0.10718				0.09616	
12186	0.12186				0.10824	
14289	0.14532				0.11944	
15510	0.16602				0.1253	
16145	0.18514				0.13436	
16460	0.20562				0.14094	
16917	0.22036		0.05772			Thru Thickness
17240	0.23814		0.1014			
17527	0.34906		0.34906			
Ligament Failed						

OFF-CX2024-5 Fatigue Crack Growth Data Sheet

Width: 4.0085 in. Thick: 0.2545 in. Area: 1.0202 in^2

Precrack Information

Precrack Date: 26-Aug-11 Loading Condition: Constant-amplitude R= 0.1
Frequency: 20 Hz Hole Diameter: 0.48872 in. Peak Stress: 25.0 ksi
Surface EDM Length: 0.02080 in.

Experiment Information

Experiment Date: 8-Sep-11 Loading Condition: Variable-amplitude
Loading Rate: 380000 lbs/s Hole Diameter: 0.50362 in.
Peak Stress: 32.3 ksi Ligament Length: 0.35226 in.
Surface EDM Length: 0.01854 in.

Total Flight Hours	Crack Length (inches)					Comments
	Surface of Hole				Bore	
	EDM		NEDM			
	A	B	A	B		
0						Precrack (cycles)
14484	0.04982				0.05731	
0	0.04946				0.06131	Testing (flight hours)
3840	0.06716				0.09774	
5280	0.07418				0.11793	
5903	0.07706				0.12709	
7200	0.08638				0.13956	
8880	0.10216				0.17021	
9840	0.12230				0.18749	
10429	0.14110				0.20345	
10757	0.15848				0.22433	
11040	0.17796				0.24950	
11239	0.19394		0.05762			Through Thickness
11427	0.21222		0.09322			
11501	0.22398		0.11208			
11668	0.23652		0.14096			
11745	0.25416		0.16398			

Continued Below

11867	**0.26856**		**0.18308**			
11949	**0.29450**		**0.22462**			
11962	**0.30356**		**0.23044**			
12002	**0.31956**		**0.23978**			
12019	**0.34018**		**0.25506**			
12042	**0.35226**		**0.35226**			
Ligament Failed						

OFF-CX2024-6 Fatigue Crack Growth Data Sheet

Width: 4.0075 in. Thick: 0.2550 in. Area: 1.0219 in^2

Precrack Information

Precrack Date: 26-Aug-11 Loading Condition: Constant-amplitude R= 0.1
Frequency: 20 Hz Hole Diameter: 0.48862 in. Peak Stress: 25.0 ksi
Surface EDM Length: 0.01726 in.

Experiment Information

Experiment Date: 20-Sep-11 Loading Condition: Variable-amplitude
Loading Rate: 380000 lbs/s Hole Diameter: 0.50187 in.
Peak Stress: 32.3 ksi Ligament Length: 0.35200 in.
Surface EDM Length: 0.01182 in.

Total Flight Hours	Crack Length (inches)					Comments
	Surface of Hole				Bore	
	EDM		NEDM			
	A	B	A	B		
0						Precrack (cycles)
14774	0.04920				0.06713	
0	0.03856				0.05815	Testing (flight hours)
485						
2398	0.05762				0.08300	
6238	0.07304				0.11639	
9598	0.08916				0.13565	
11278	0.10768				0.18583	
11702	0.11162				0.19037	
12478	0.12834				0.20349	
13087	0.14748				0.24843	
13438	0.16682		0.02812			Through Thickness
13678	0.18534		0.05164			
14019	0.21286		0.10112			
14116	0.23068		0.12286			
14296	0.25212		0.16388			
14508	0.29302		0.21910			
14568	0.35200		0.35200			
Ligament Failed						

OFF-CX2024-7 Fatigue Crack Growth Data Sheet

Width: 4.0045 in. Thick: 0.2550 in. Area: 1.0212 in^2

Precrack Information

Precrack Date: 26-Aug-11 Loading Condition: Constant-amplitude R= 0.1
Frequency: 20 Hz Hole Diameter: 0.48857 in. Peak Stress: 25.0 ksi
Surface EDM Length: 0.02062 in.

Experiment Information

Experiment Date: 8-Sep-11 Loading Condition: Constant-amplitude R= 0.1
Frequency: 20 Hz Hole Diameter: 0.50287 in.
Peak Stress: 25.0 ksi Ligament Length: 0.35082 in.
Surface EDM Length: 0.01314 in.

Total Cycles	Crack Length (inches)					Comments
	Surface of Hole				Bore	
	EDM		NEDM			
	A	B	A	B		
0						Precrack
13978	0.05804				0.06527	
0	0.05058				0.06013	Testing
537	0.05348				0.06699	
2709	0.06816				0.08433	
5785	0.07604				0.09342	
7241	0.08394				0.11510	
9254	0.09312				0.12644	
11501	0.10744				0.13973	
13342	0.12730				0.15795	
15068	0.14648				0.17297	
16922	0.16752				0.20219	
17978	0.18606				0.20440	
18879	0.20112				0.21718	
19386	0.21824				0.22973	
19845	0.24762				0.23866	
20156	0.29570		0.05968			Through Thickness
20280	0.35082		0.13754			
20418	0.35082		0.35082			
Ligament Failed						

OFF-CX2024-8 Fatigue Crack Growth Data Sheet

Width: 4.0035 in. Thick: 0.2555 in. Area: 1.0229 in^2

Precrack Information

Precrack Date: 26-Aug-11 Loading Condition: Constant-amplitude R= 0.1
Frequency: 20 Hz Hole Diameter: 0.48960 in. Peak Stress: 25.0 ksi
Surface EDM Length: 0.02002 in.

Experiment Information

Experiment Date: 15-Sep-11 Loading Condition: Constant-amplitude R= 0.1
Frequency: 20 Hz Hole Diameter: 0.50242 in.
Peak Stress: 25.0 ksi Ligament Length: 0.35078 in.
Surface EDM Length: 0.01362 in.

Total Cycles	Crack Length (inches)					Comments
	Surface of Hole				Bore	
	EDM		NEDM			
	A	B	A	B		
0						Precrack
13957	0.04946				0.04742	
0	0.04226				0.04139	Testing
6234	0.06402				0.07239	
19094	0.08428				0.09601	
30142	0.10442				0.14609	
38665	0.12224				0.18342	
43063	0.14338		0.04352			
46329	0.17426		0.04710			
49062	0.22764		0.04812			
49507	0.25512		0.06312			
49720	0.29786		0.08552			
49889	0.35078		0.35078			
Ligament Failed						

APPENDIX D

SPECIMEN CRACK GROWTH CURVES

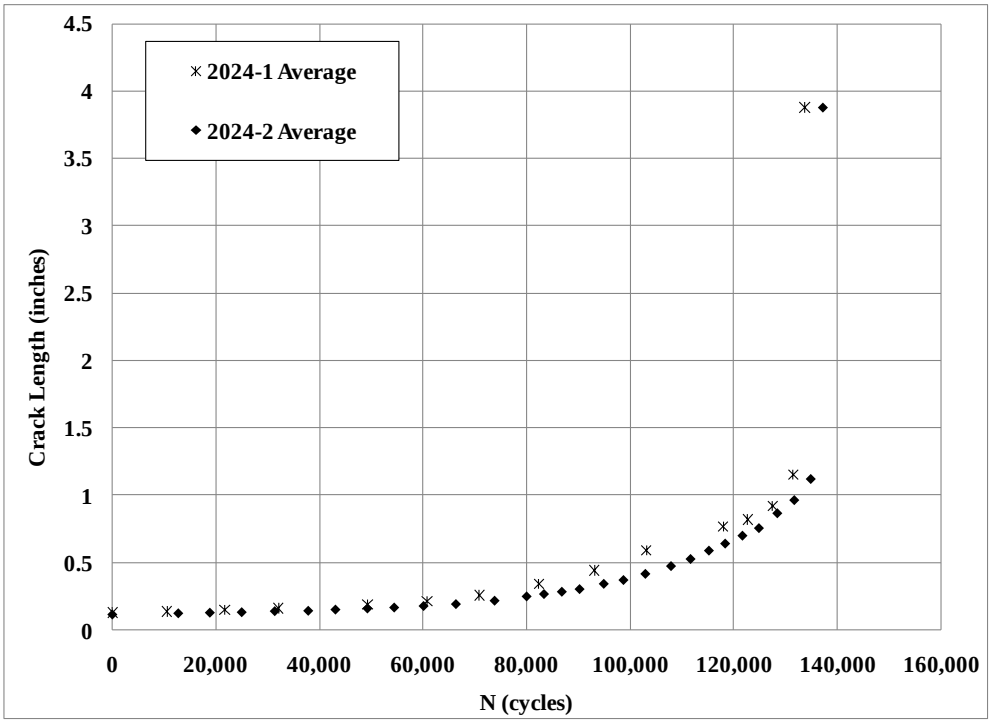

Fig. 75 ASTM E 647 M(T) specimens 2024-1 and 2024-2 crack growth curves; σ_{max} = 11.4 ksi, R=0.1, 20 Hz, Lab Air

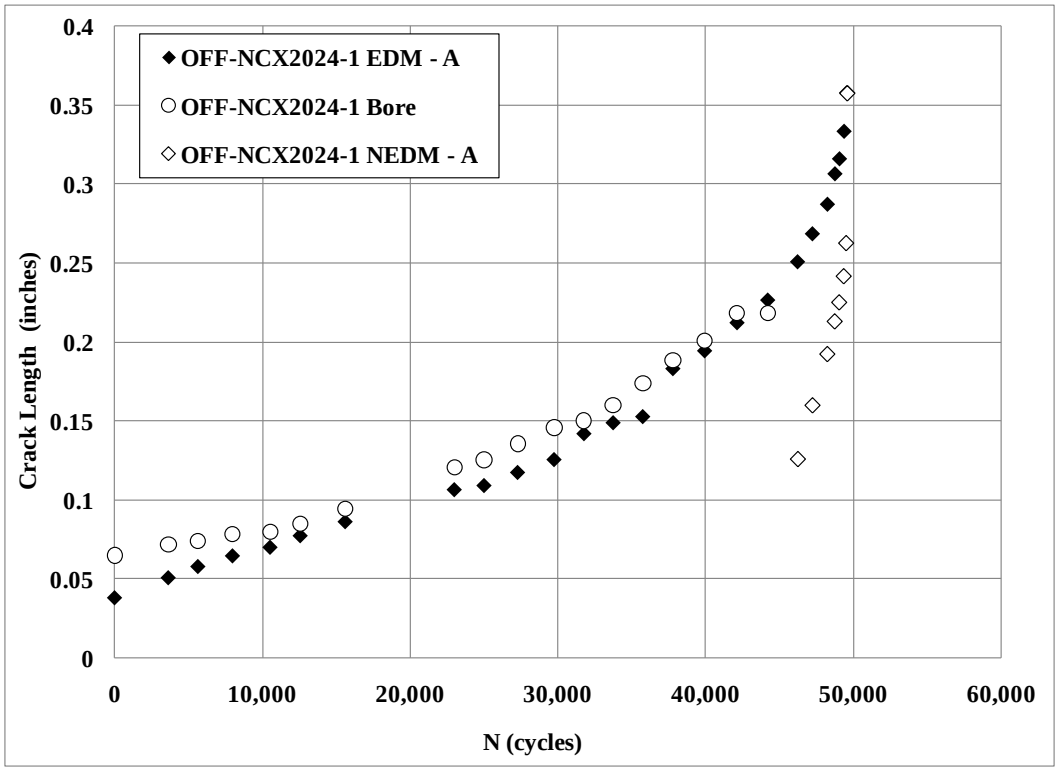

Fig. 76 Specimen OFF-NCX2024-1 crack growth curves; σ_{max} = 10 ksi, Constant-amplitude R=0.1, 20 Hz, Lab Air

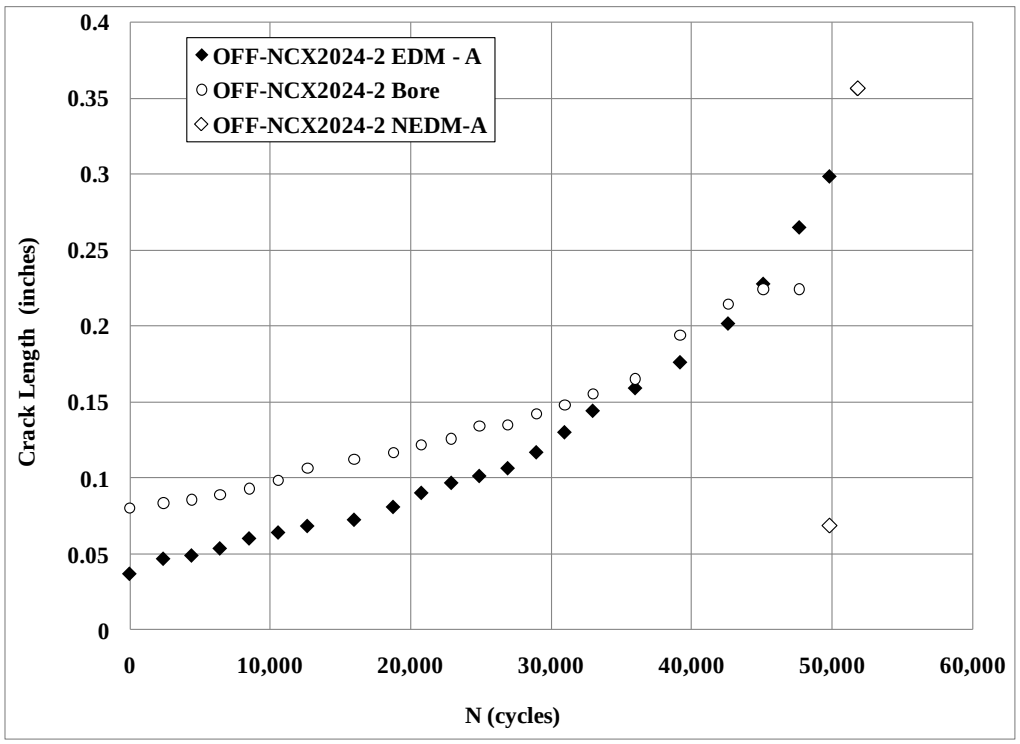

Fig. 77 Specimen OFF-NCX2024-2 crack growth curves; σ_{max} = 10 ksi, Constant-amplitude R=0.1, 20 Hz, Lab Air

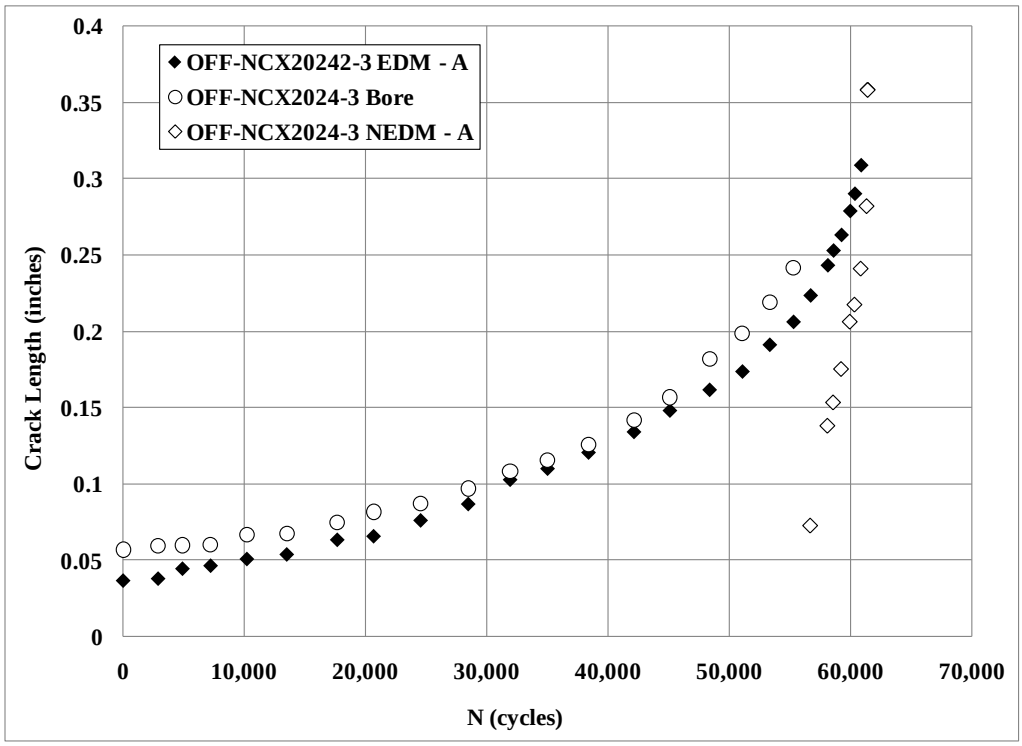

Fig. 78 Specimen OFF-NCX2024-3 crack growth curves; σ_{max} = 10 ksi, Constant-amplitude R=0.1, 20 Hz, Lab Air

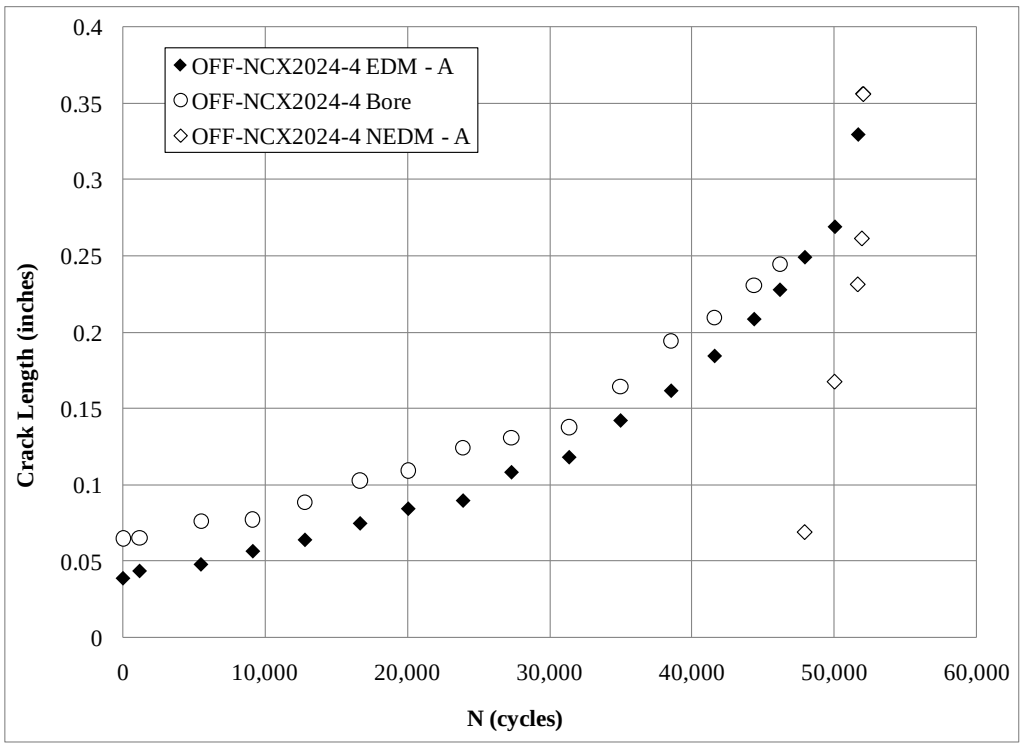

Fig. 79 Specimen OFF-NCX2024-4 crack growth curves; σ_{max} = 10 ksi, Constant-amplitude R=0.1, 20 Hz, Lab Air

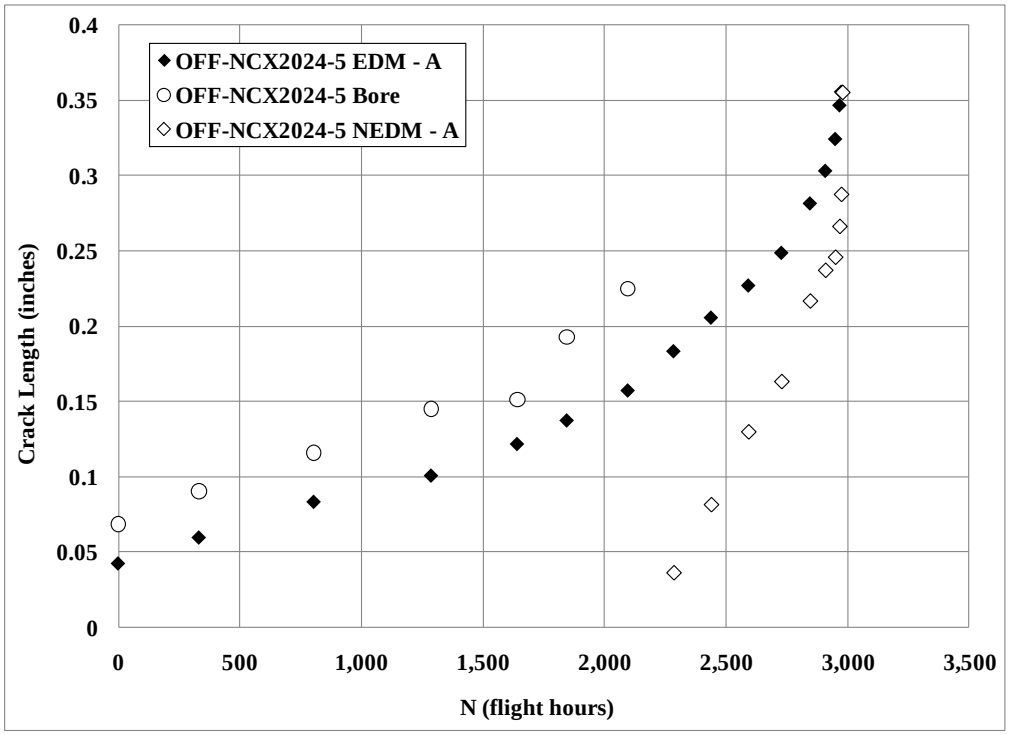

Fig. 80 Specimen OFF-NCX2024-5 crack growth curves; σ_{max} = 33 ksi, Variable-amplitude, A-10 wing spectrum, Lab Air

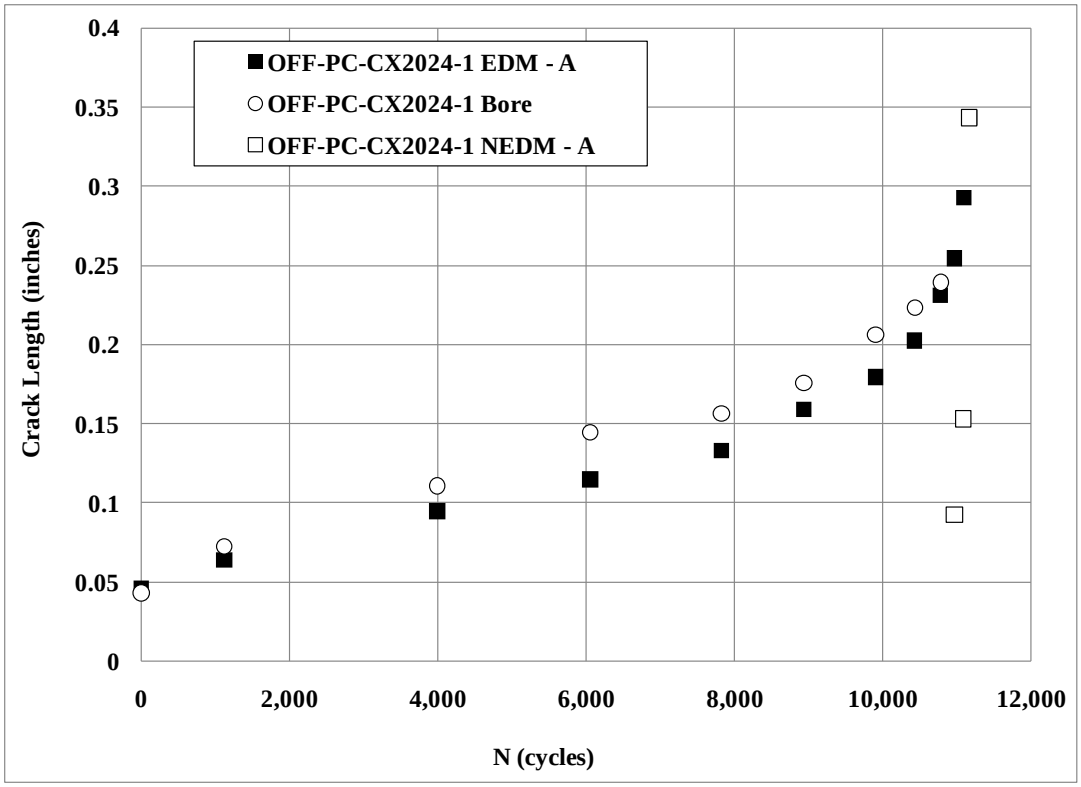

Fig. 81 Specimen OFF-PC-CX2024-1 crack growth curves; σ_{max} = 25 ksi, Constant-amplitude R=0.1, 20 Hz, Lab Air

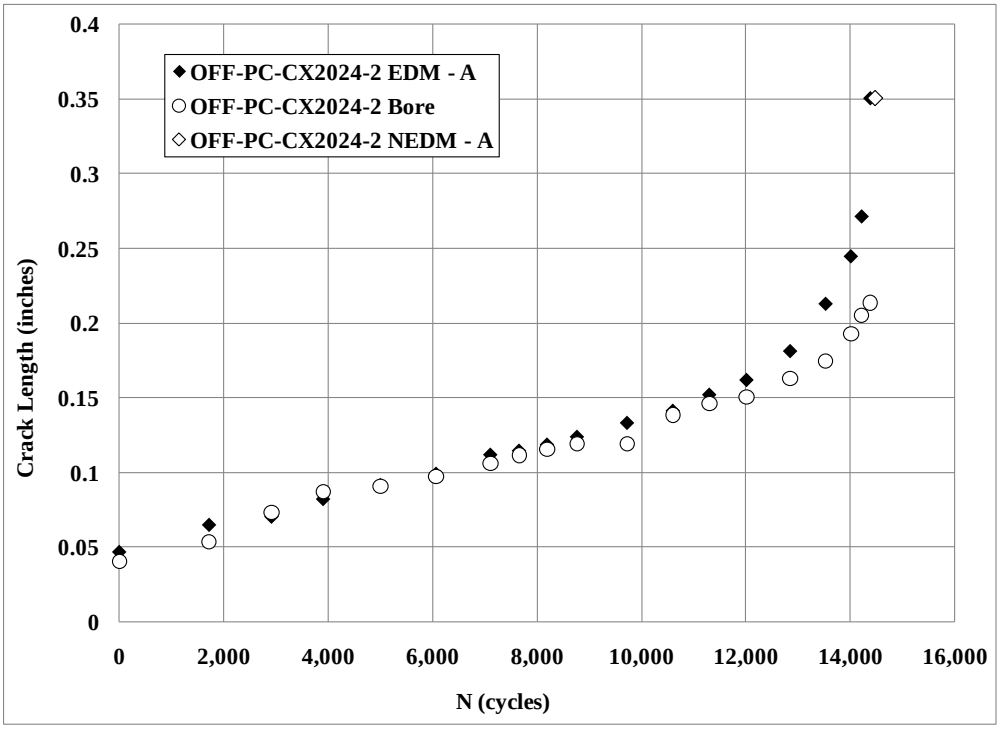

Fig. 82 Specimen OFF-PC-CX2024-2 crack growth curves; σ_{max} = 25 ksi, Constant-amplitude R=0.1, 20 Hz, Lab Air

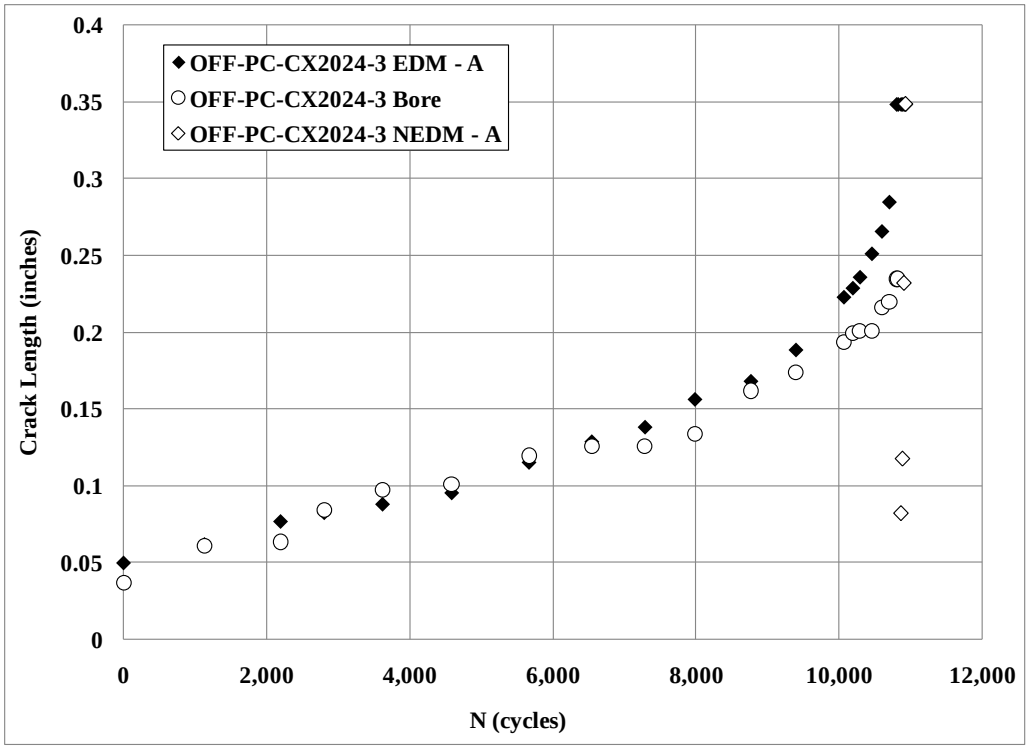

Fig. 83 Specimen OFF-PC-CX2024-3 crack growth curves; σ_{max} = 25 ksi, Constant-amplitude R=0.1, 20 Hz, Lab Air

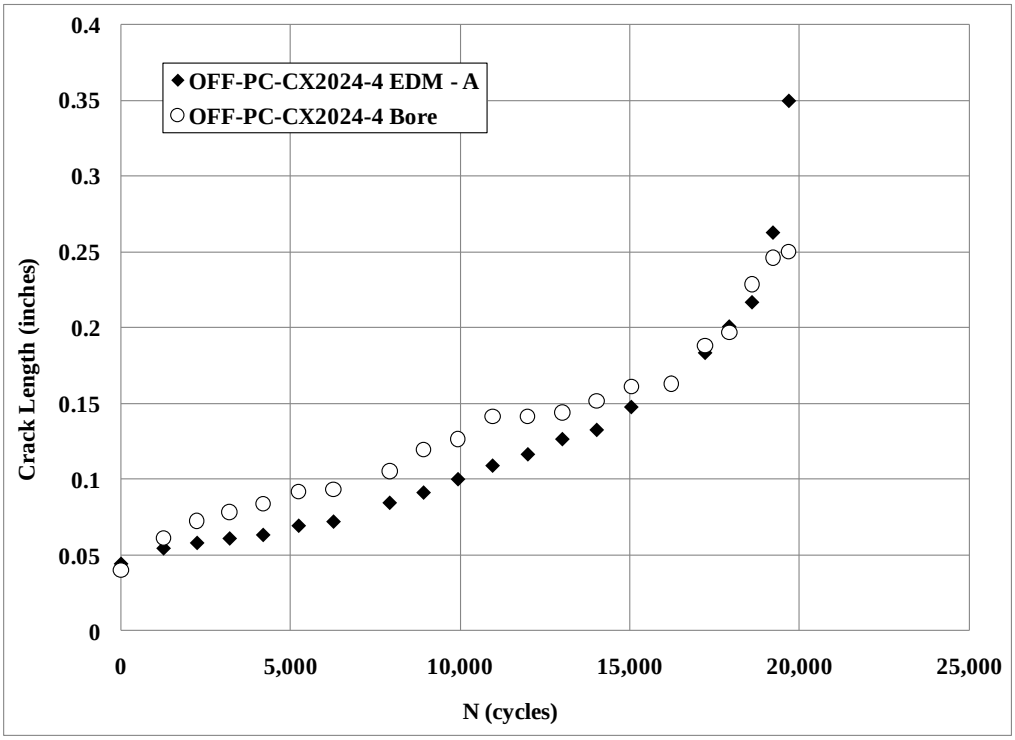

Fig. 84 Specimen OFF-PC-CX2024-4 crack growth curves; σ_{max} = 25 ksi, Constant-amplitude R=0.1, 20 Hz, Lab Air

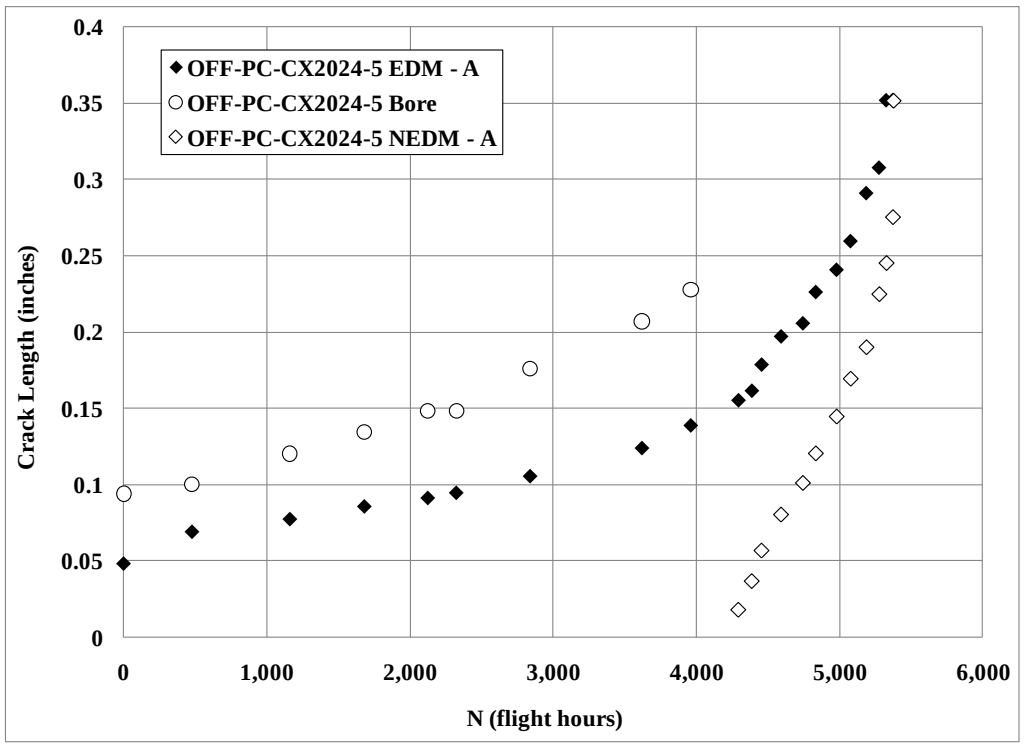

Fig. 85 Specimen OFF-PC-CX2024-5 crack growth curves; σ_{max} = 33 ksi, Variable-amplitude, A-10 wing spectrum, Lab Air

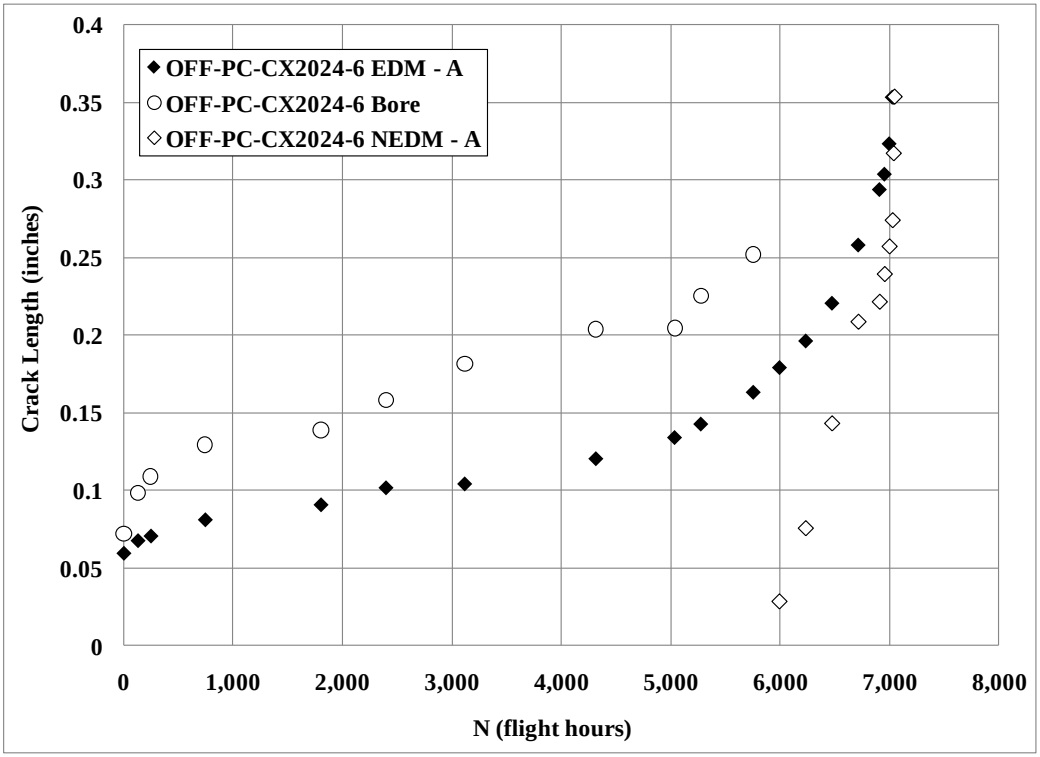

Fig. 86 Specimen OFF-PC-CX2024-6 crack growth curves; σ_{max} = 33 ksi, Variable-amplitude, A-10 wing spectrum, Lab Air

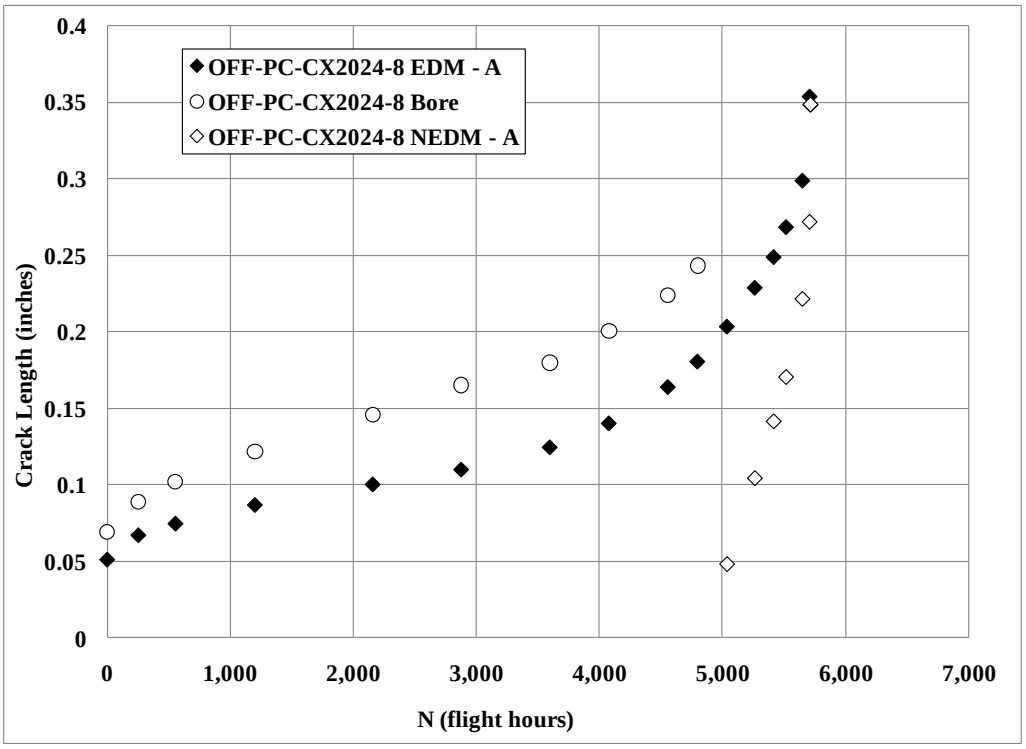

Fig. 87 Specimen OFF-PC-CX2024-8 crack growth curves; σ_{max} = 33 ksi, Variable-amplitude, A-10 wing spectrum, Lab Air

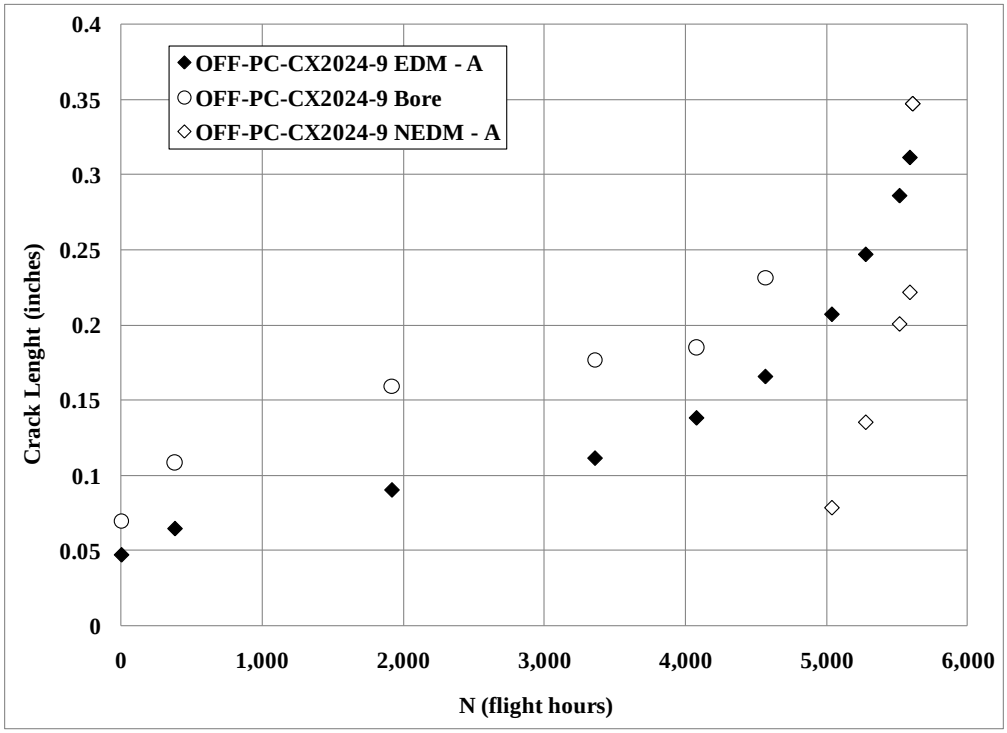

Fig. 88 Specimen OFF-PC-CX2024-9 crack growth curves; σ_{max} = 33 ksi, Variable-amplitude, A-10 wing spectrum, Lab Air

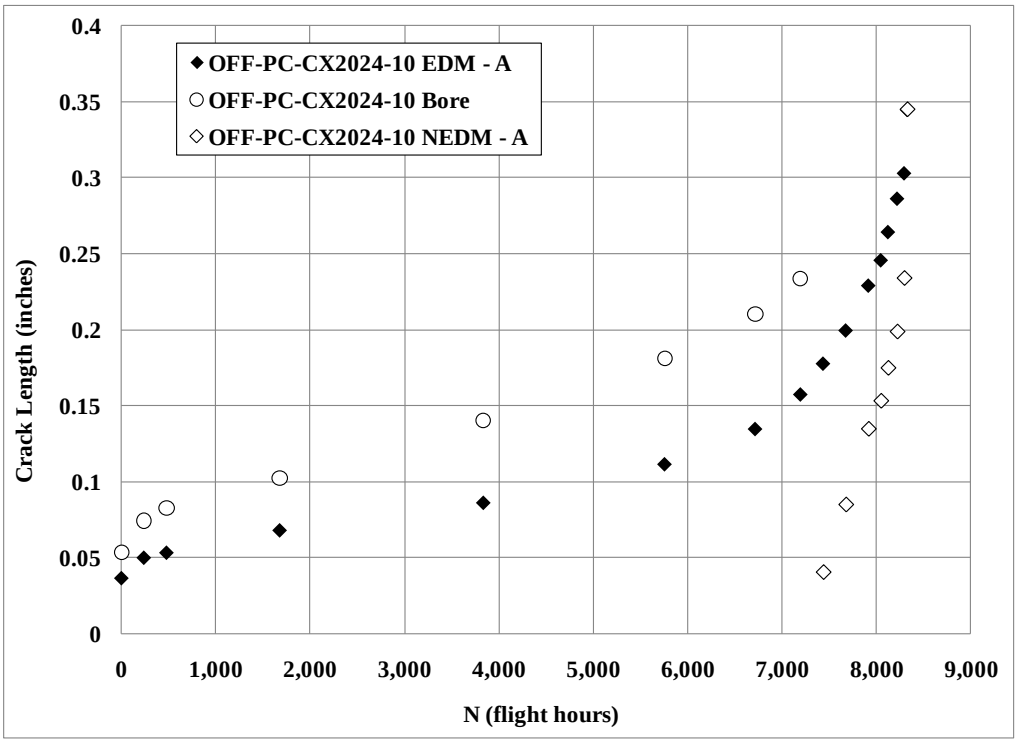

Fig. 89 Specimen OFF-PC-CX2024-10 crack growth curves; σ_{max} = 33 ksi, Variable-amplitude, A-10 wing spectrum, Lab Air

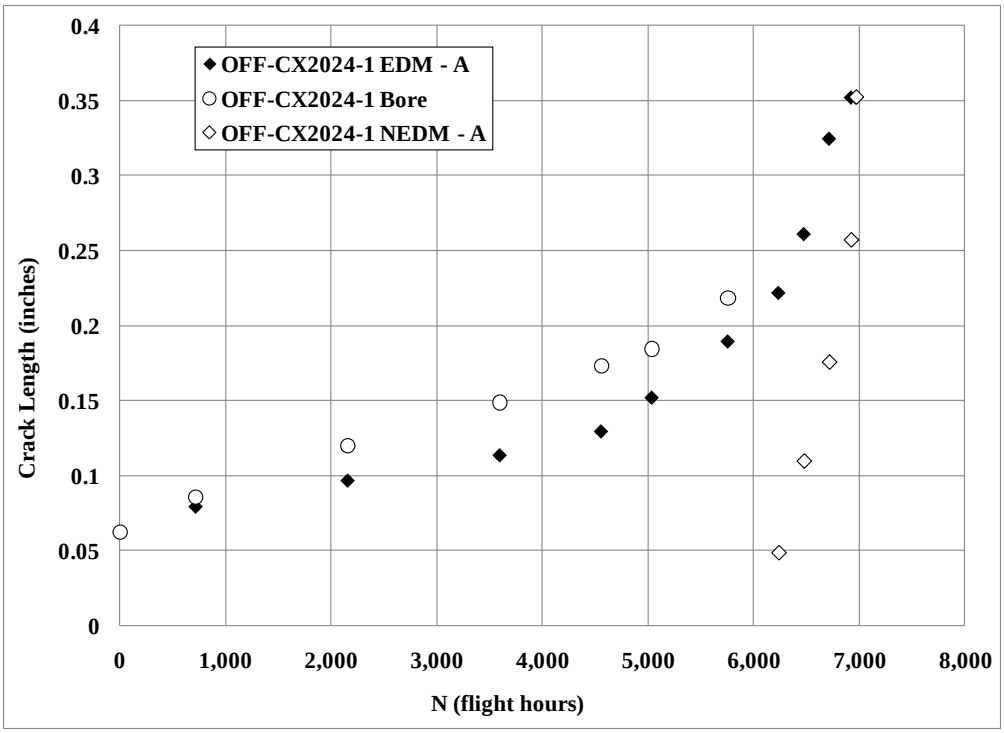

Fig. 90 Specimen OFF-CX2024-1 crack growth curves; σ_{max} = 33 ksi, Variable-amplitude, A-10 wing spectrum, Lab Air

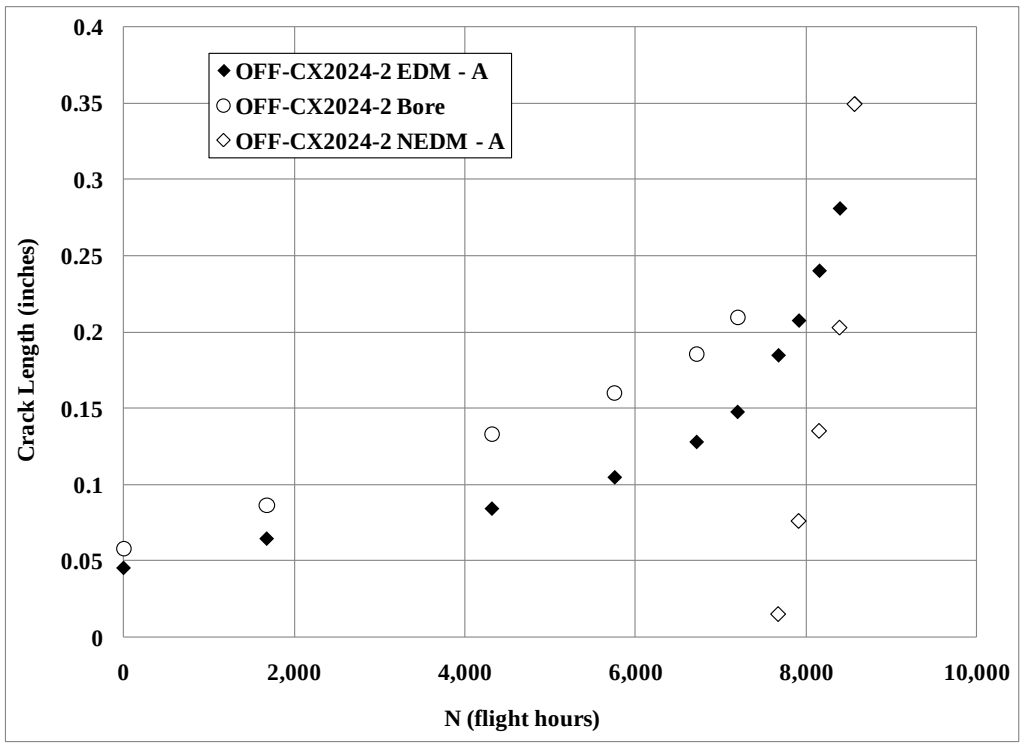

Fig. 91 Specimen OFF-CX2024-2 crack growth curves; σ_{max} = 33 ksi, Variable-amplitude, A-10 wing spectrum, Lab Air

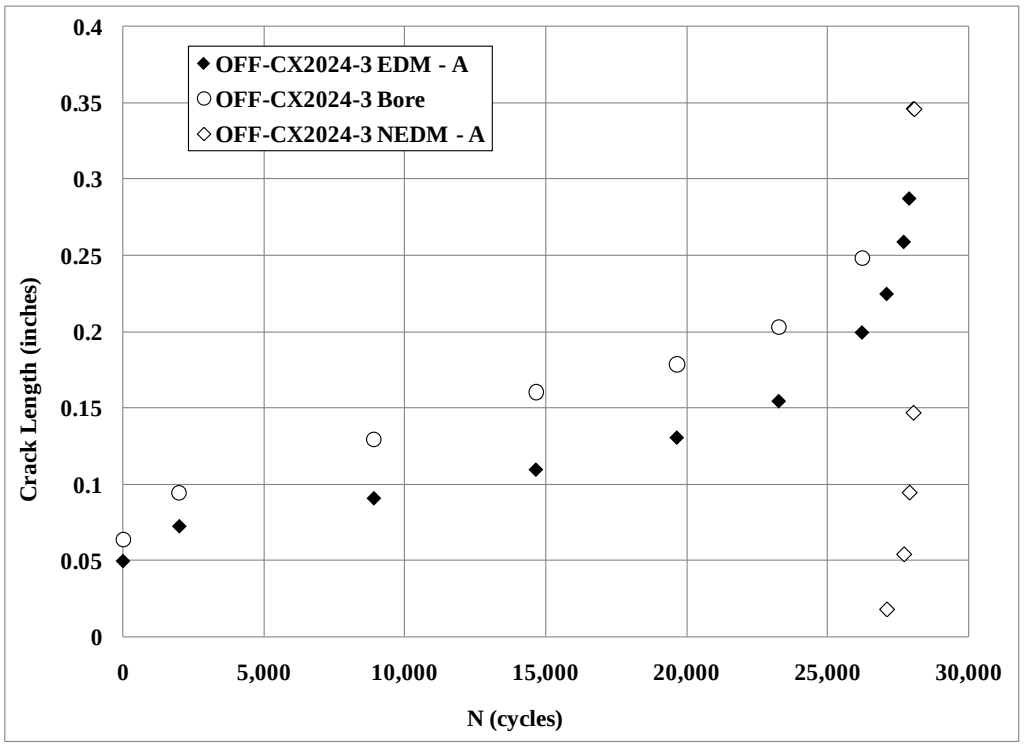

Fig. 92 Specimen OFF-CX2024-3 crack growth curves; σ_{max} = 25 ksi, Constant-amplitude R=0.1, 20 Hz, Lab Air

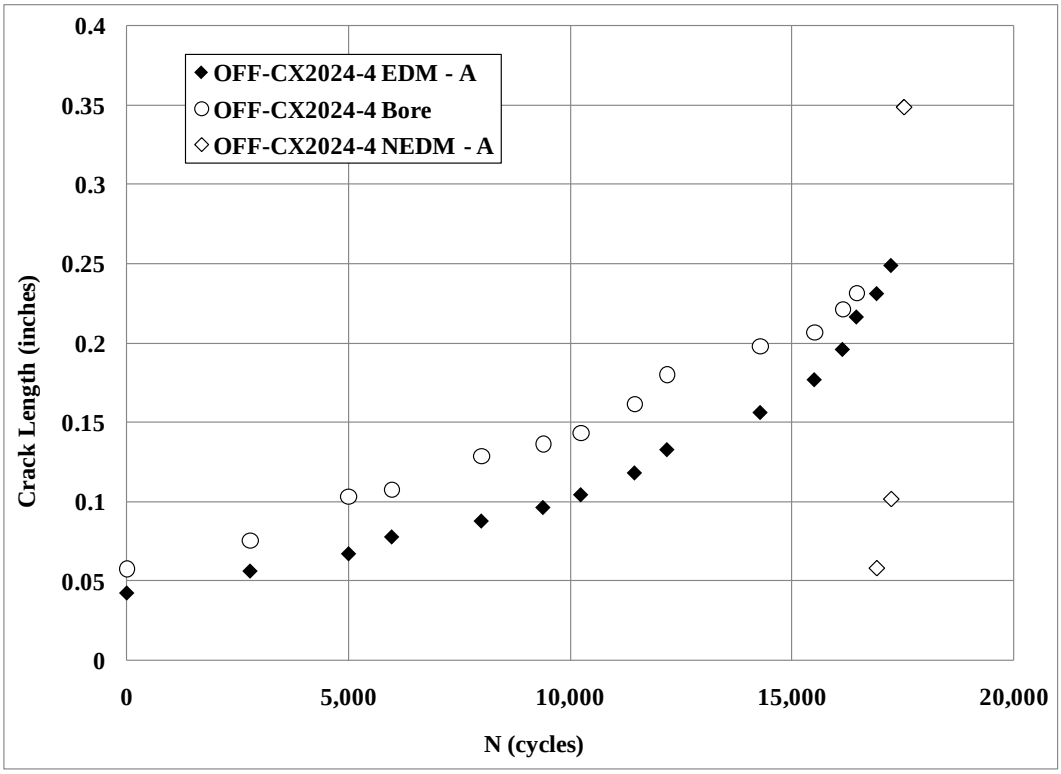

Fig. 93 Specimen OFF-CX2024-4 crack growth curves; σ_{max} = 25 ksi, Constant-amplitude R=0.1, 20 Hz, Lab Air

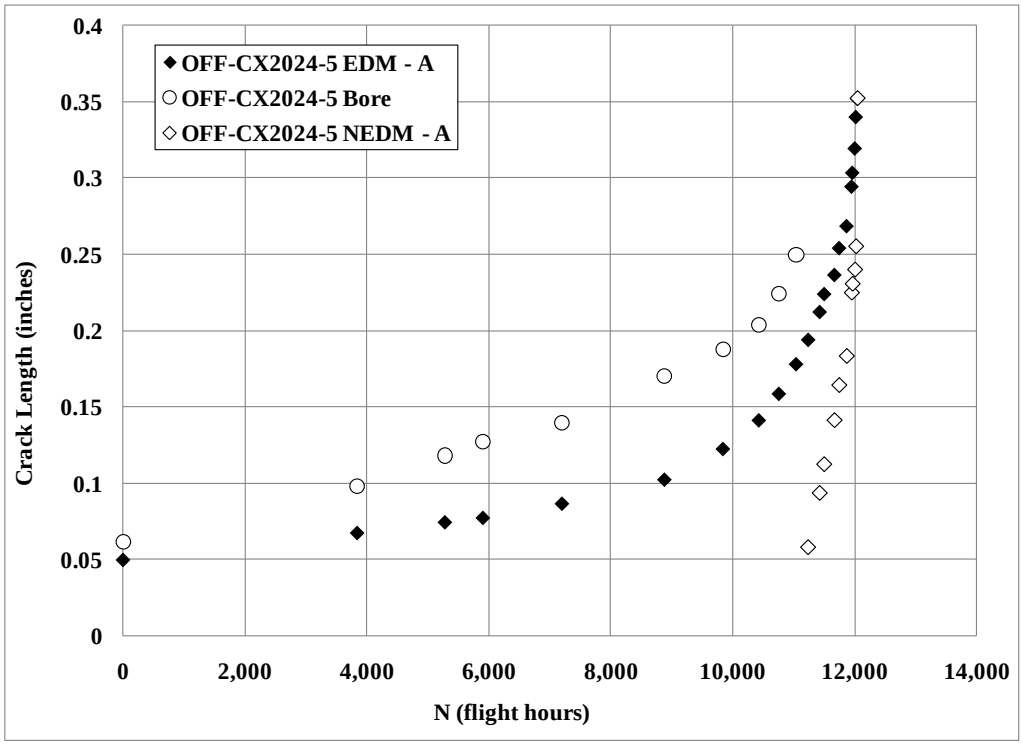

Fig. 94 Specimen OFF-CX2024-5 crack growth curves; σ_{max} = 33 ksi, Variable-amplitude, A-10 wing spectrum, Lab Air

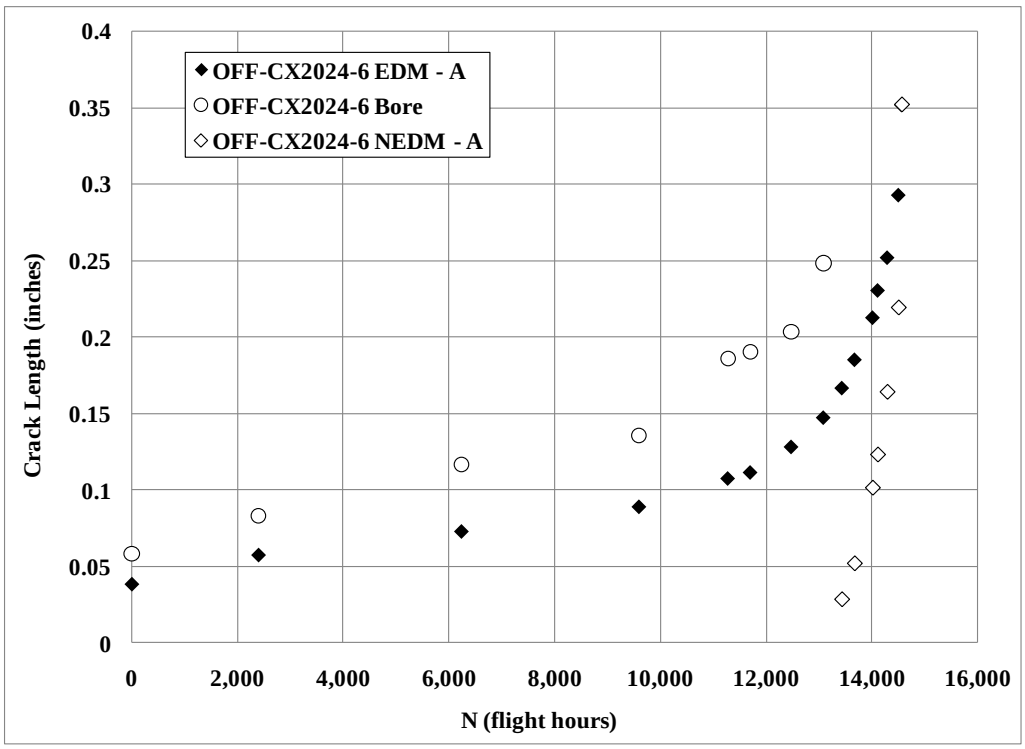

Fig. 95 Specimen OFF-CX2024-6 crack growth curves; σ_{max} = 33 ksi, Variable-amplitude, A-10 wing spectrum, Lab Air

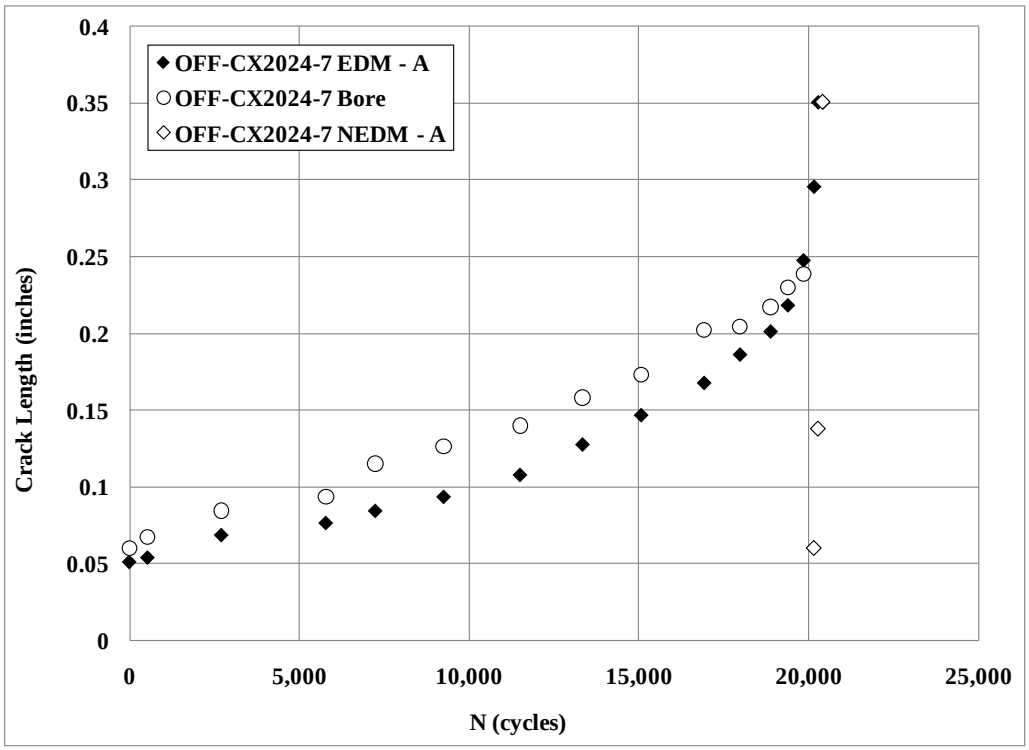

Fig. 96 Specimen OFF-CX2024-7 crack growth curves; σ_{max} = 25 ksi, Constant-amplitude R=0.1, 20 Hz, Lab Air

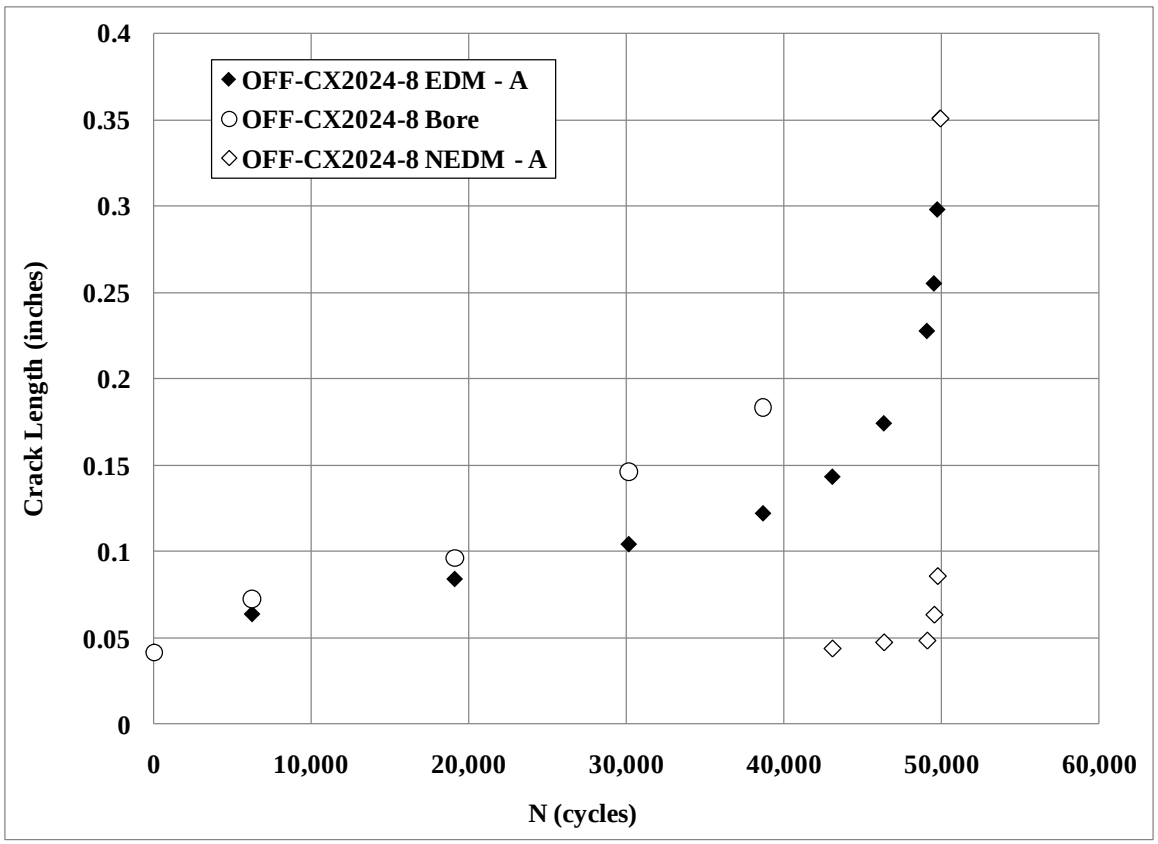

Fig. 97 Specimen OFF-CX2024-8 crack growth curves; σ_{max} = 25 ksi, Constant-amplitude R=0.1, 20 Hz, Lab Air

APPENDIX E

AFGROW CRACK GROWTH PREDICTIONS

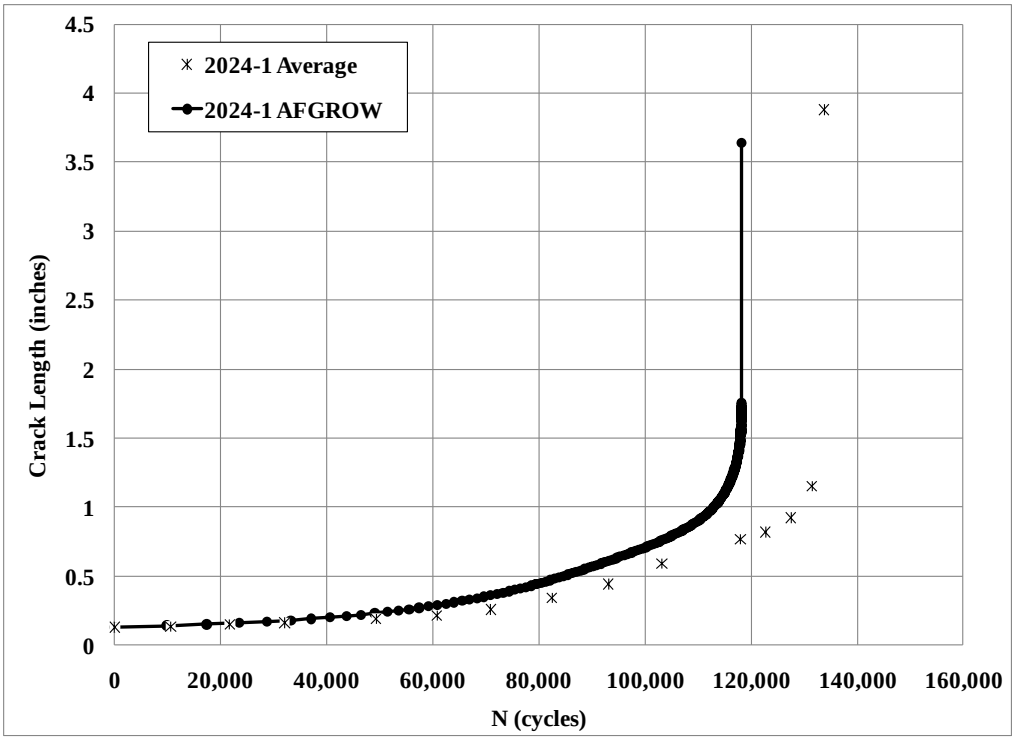

Fig. 98 ASTM E 647 M(T) specimens 2024-1 crack growth curve with AFGROW prediction; σ_{max} = 11.4 ksi, R=0.1, 20 Hz, Lab Air

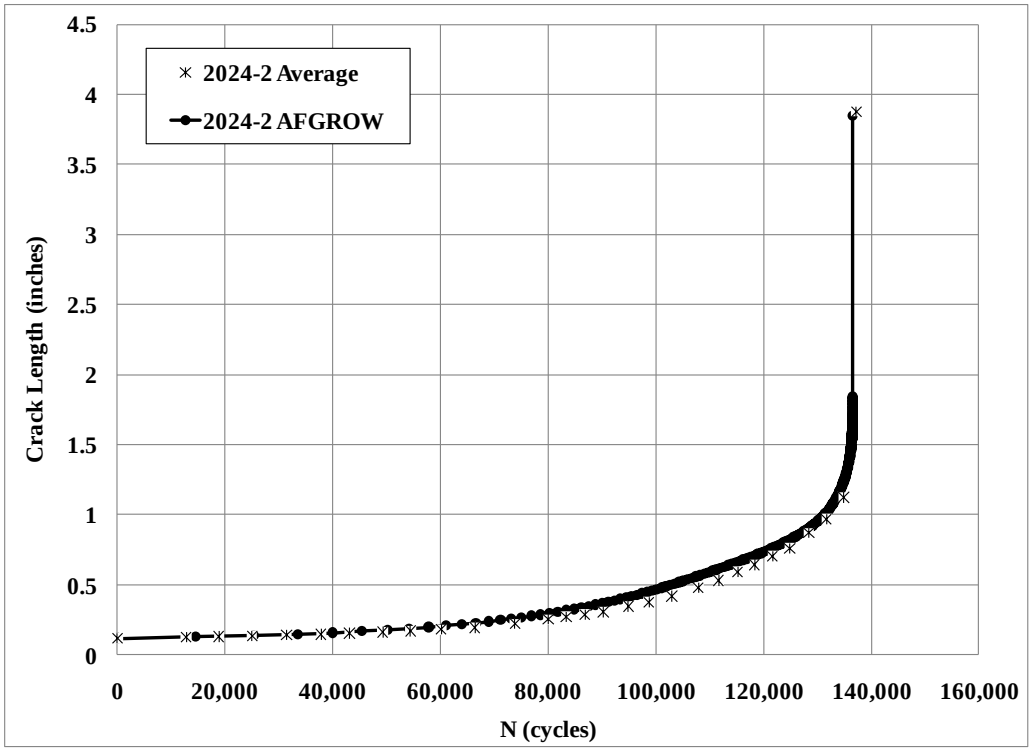

Fig. 99 ASTM E 647 M(T) specimens 22024-2 crack growth curve with AFGROW prediction; σ_{max} = 11.4 ksi, R=0.1, 20 Hz, Lab Air

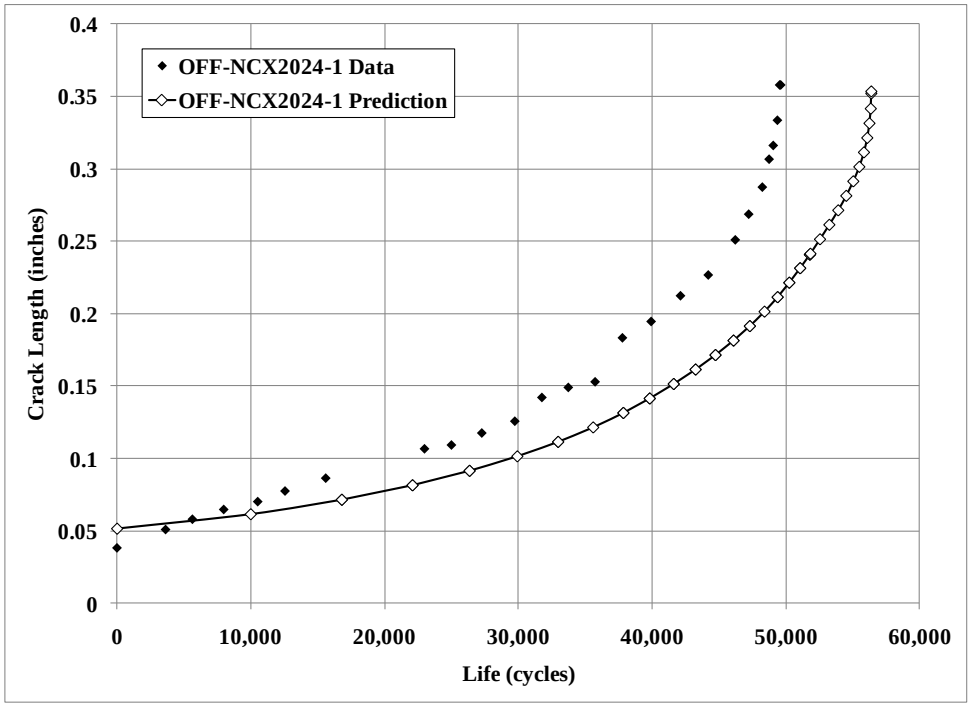

Fig. 100 Specimen OFF-NCX2024-1 EDM-A crack growth curve with AFGROW prediction; σ_{max} = 10 ksi, Constant-amplitude R=0.1, 20 Hz, Lab Air

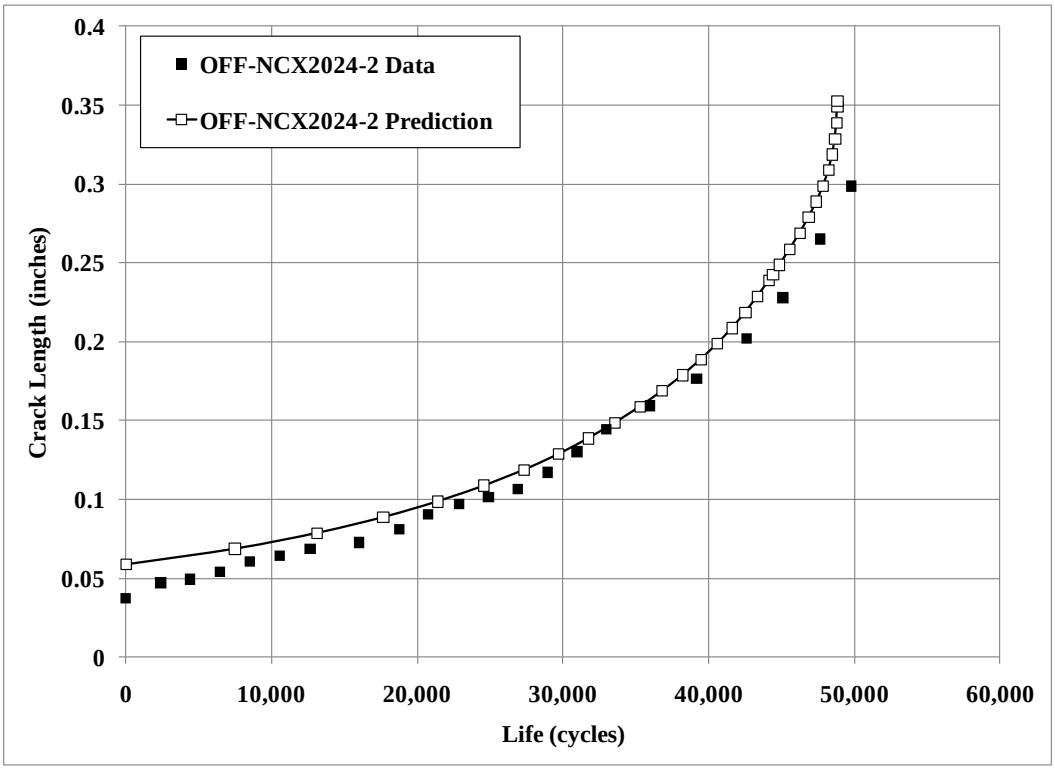

Fig. 101 Specimen OFF-NCX2024-2 EDM-A crack growth curve with AFGROW prediction; σ_{max} = 10 ksi, Constant-amplitude R=0.1, 20 Hz, Lab Air

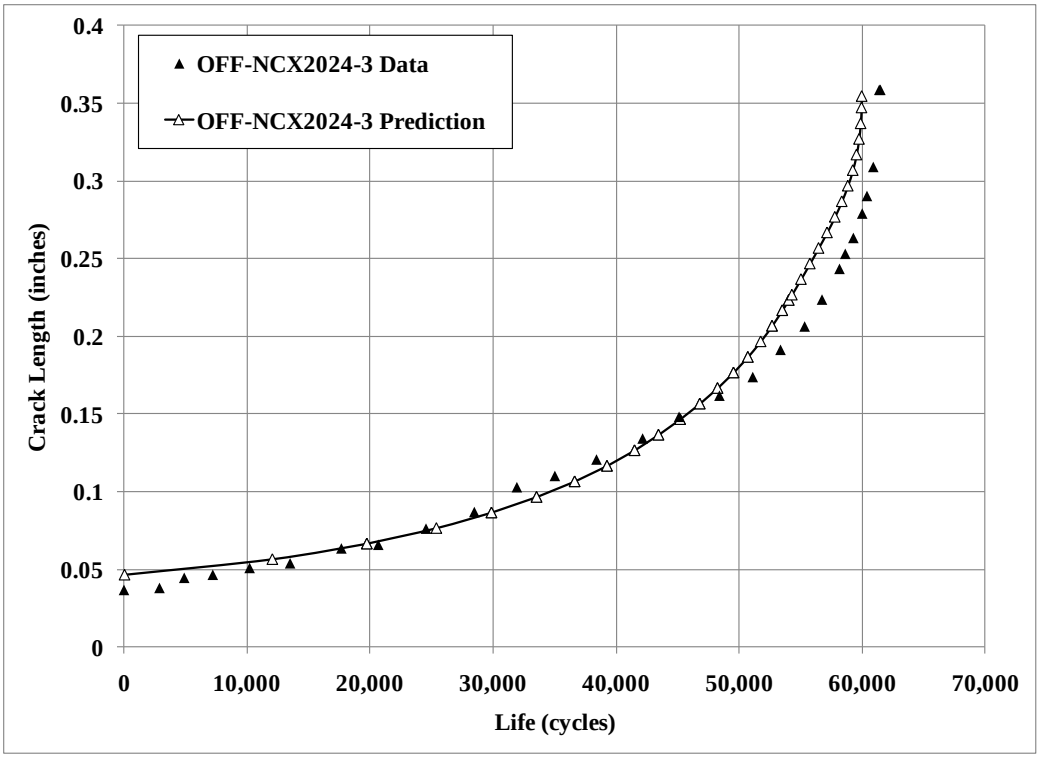

Fig. 102 Specimen OFF-NCX2024-3 EDM-A crack growth curve with AFGROW prediction; σ_{max} = 10 ksi, Constant-amplitude R=0.1, 20 Hz, Lab Air

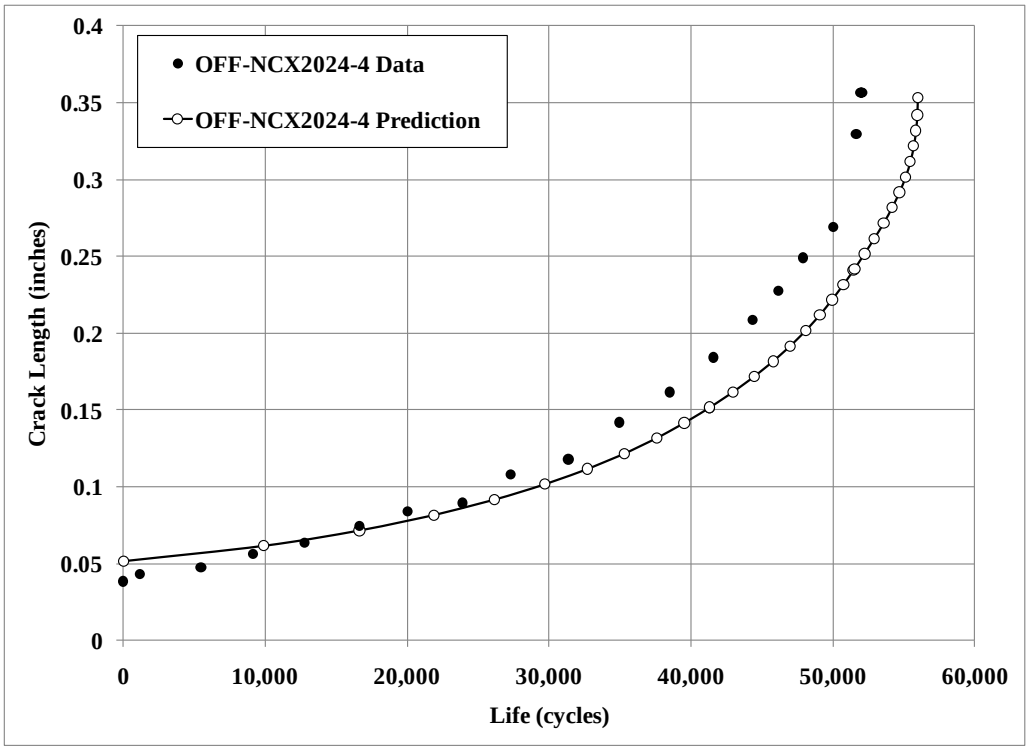

Fig. 103 Specimen OFF-NCX2024-4 EDM-A crack growth curve with AFGROW prediction; σ_{max} = 10 ksi, Constant-amplitude R=0.1, 20 Hz, Lab Air

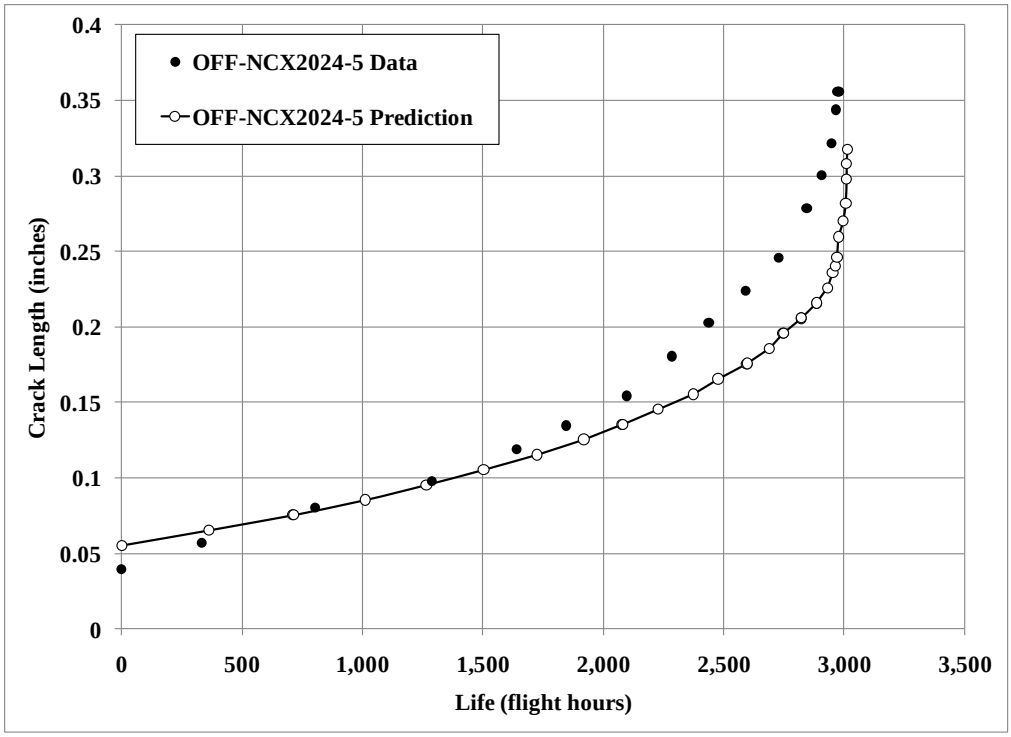

Fig. 104 Specimen OFF-NCX2024-5 EDM-A crack growth curve with AFGROW prediction; σ_{max} = 33 ksi, Variable-amplitude, A-10 wing spectrum, Lab Air

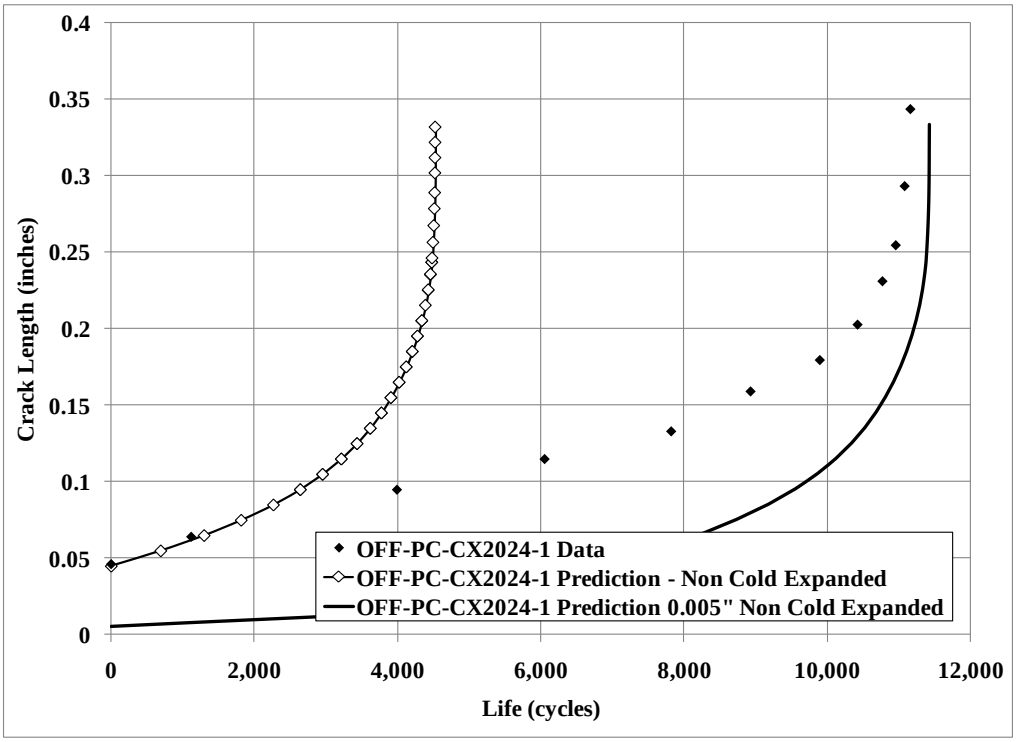

Fig. 105 Specimen OFF-PC-CX2024-1 EDM-A crack growth curve with AFGROW predictions; σ_{max} = 25 ksi, Constant-amplitude R=0.1, 20 Hz, Lab Air

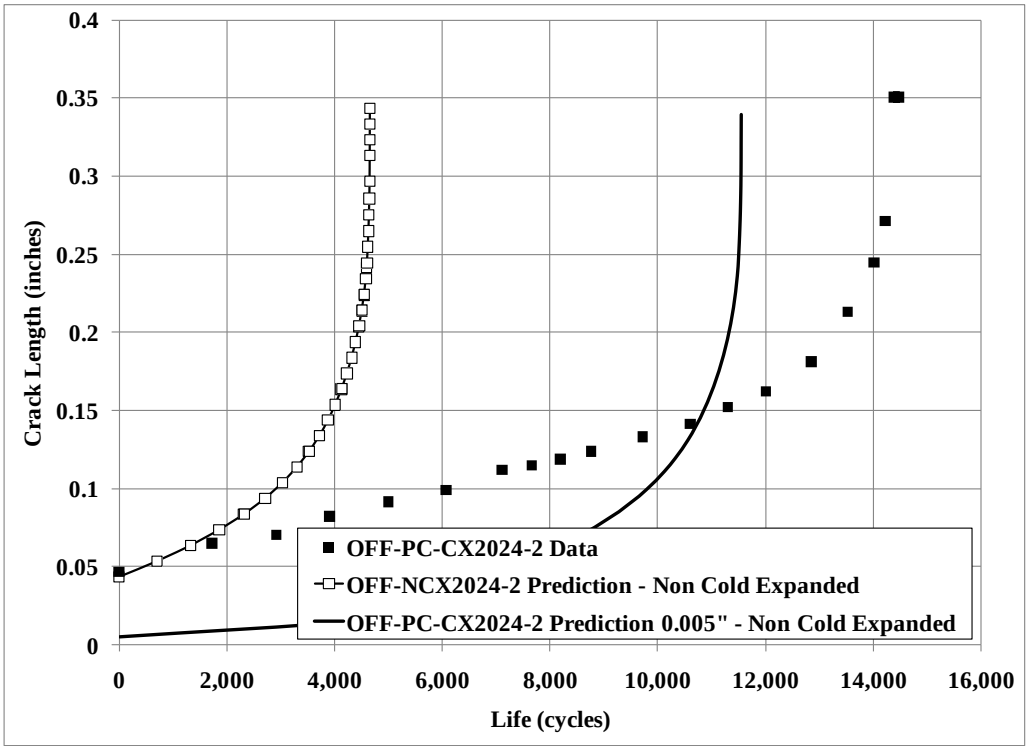

Fig. 106 Specimen OFF-PC-CX2024-2 EDM-A crack growth curve with AFGROW predictions; σ_{max} = 25 ksi, Constant-amplitude R=0.1, 20 Hz, Lab Air

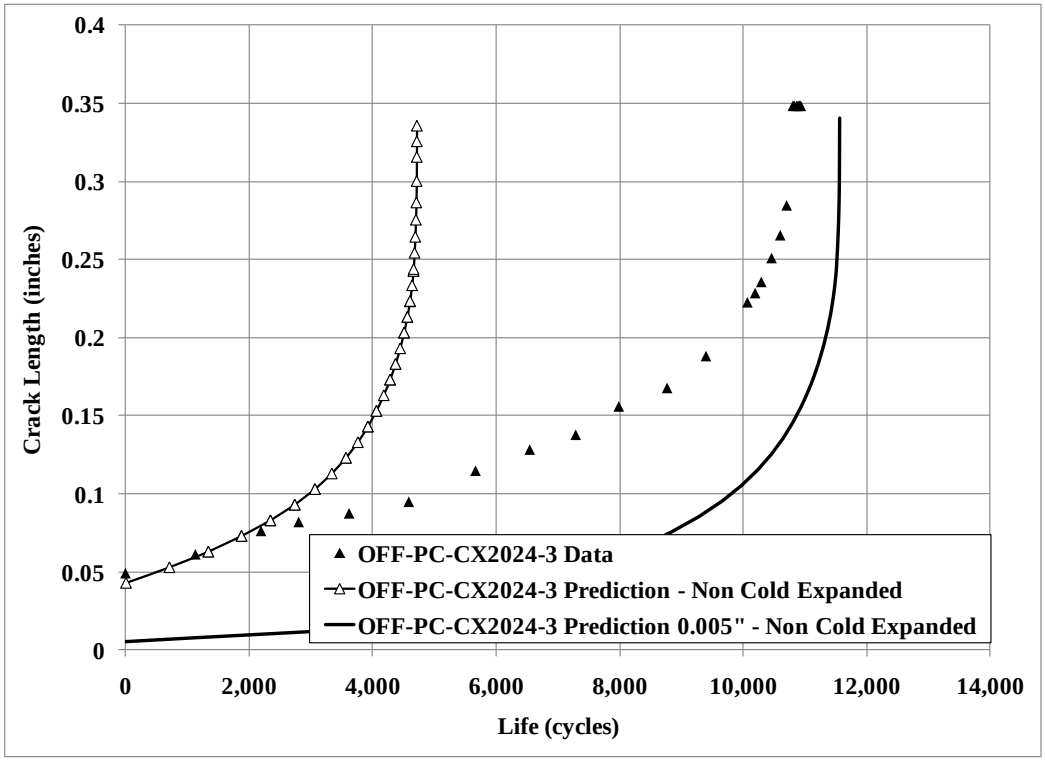

Fig. 107 Specimen OFF-PC-CX2024-3 EDM-A crack growth curve with AFGROW predictions; σ_{max} = 25 ksi, Constant-amplitude R=0.1, 20 Hz, Lab Air

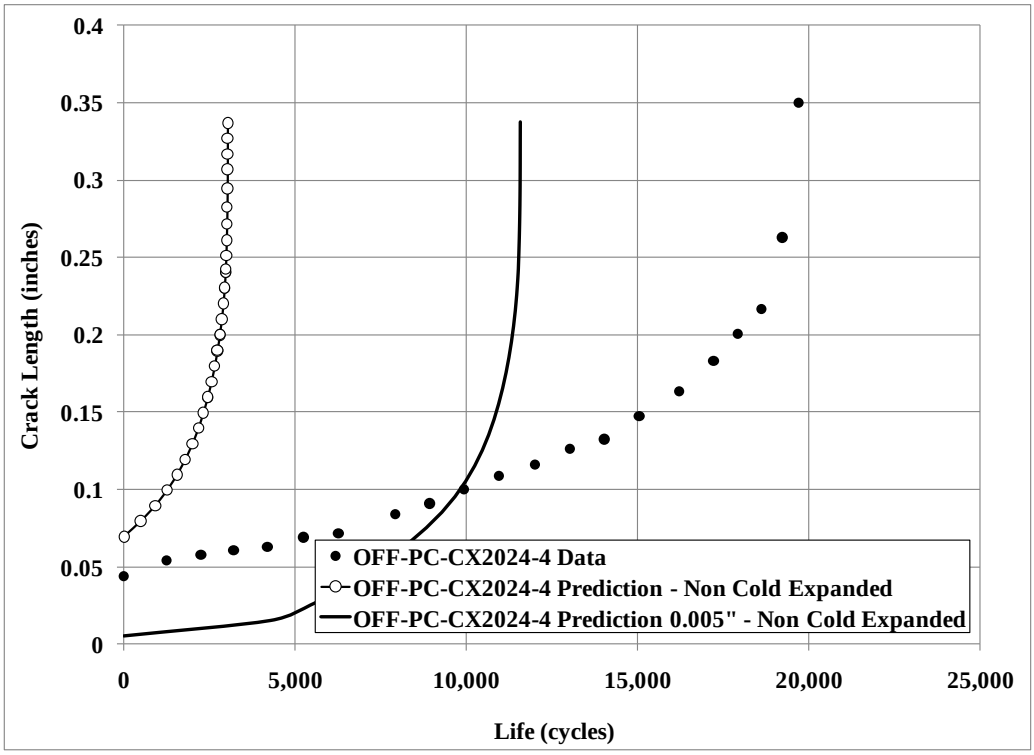

Fig. 108 Specimen OFF-PC-CX2024-4 EDM-A crack growth curve with AFGROW predictions; σ_{max} = 25 ksi, Constant-amplitude R=0.1, 20 Hz, Lab Air

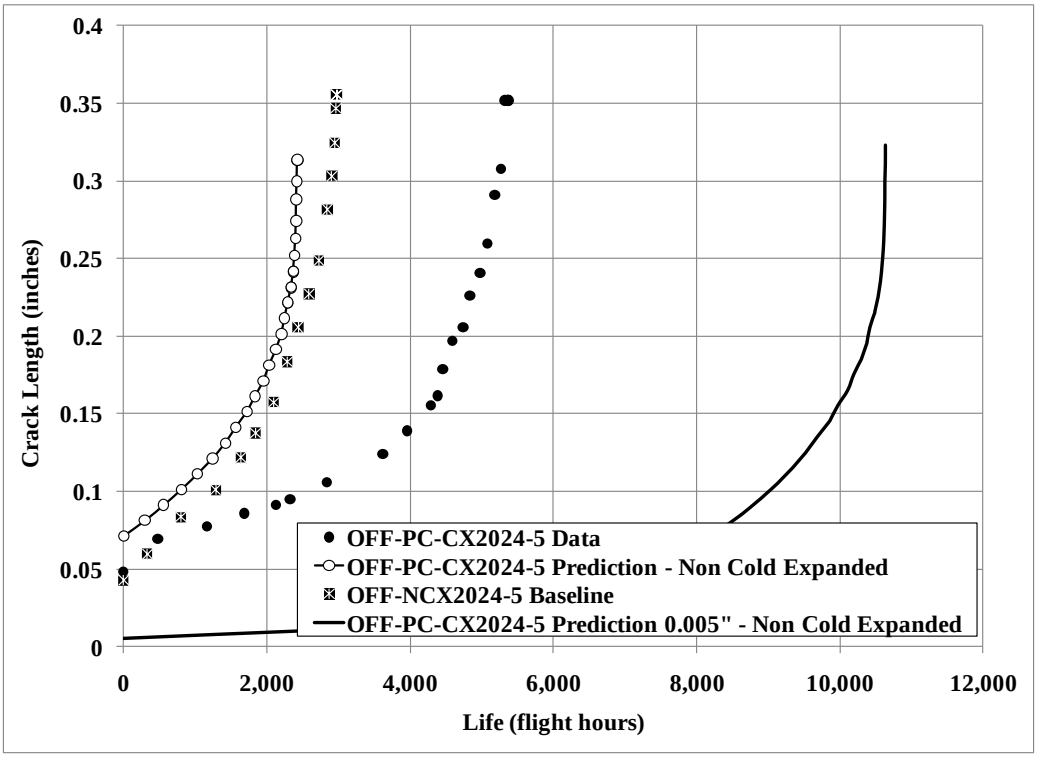

Fig. 109 Specimen OFF-PC-CX2024-5 EDM-A crack growth curve with AFGROW predictions; σ_{max} = 33 ksi, Variable-amplitude, A-10 wing spectrum, Lab Air

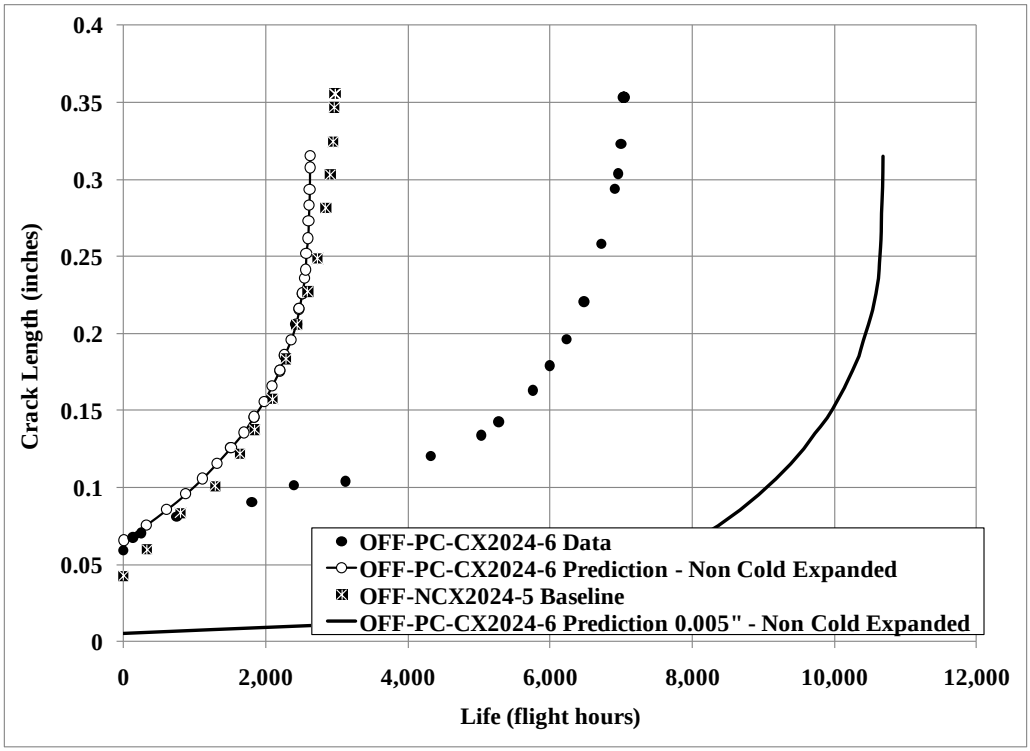

Fig. 110 Specimen OFF-PC-CX2024-6 EDM-A crack growth curve with AFGROW predictions; σ_{max} = 33 ksi, Variable-amplitude, A-10 wing spectrum, Lab Air

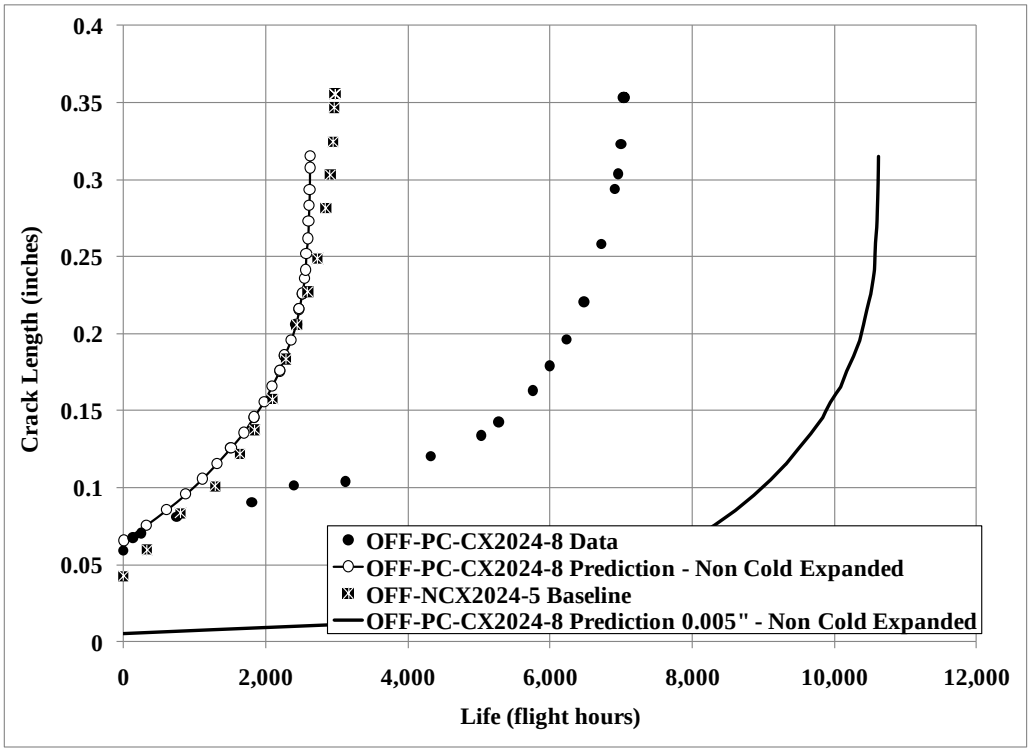

Fig. 111 Specimen OFF-PC-CX2024-8 EDM-A crack growth curve with AFGROW predictions; σ_{max} = 33 ksi, Variable-amplitude, A-10 wing spectrum, Lab Air

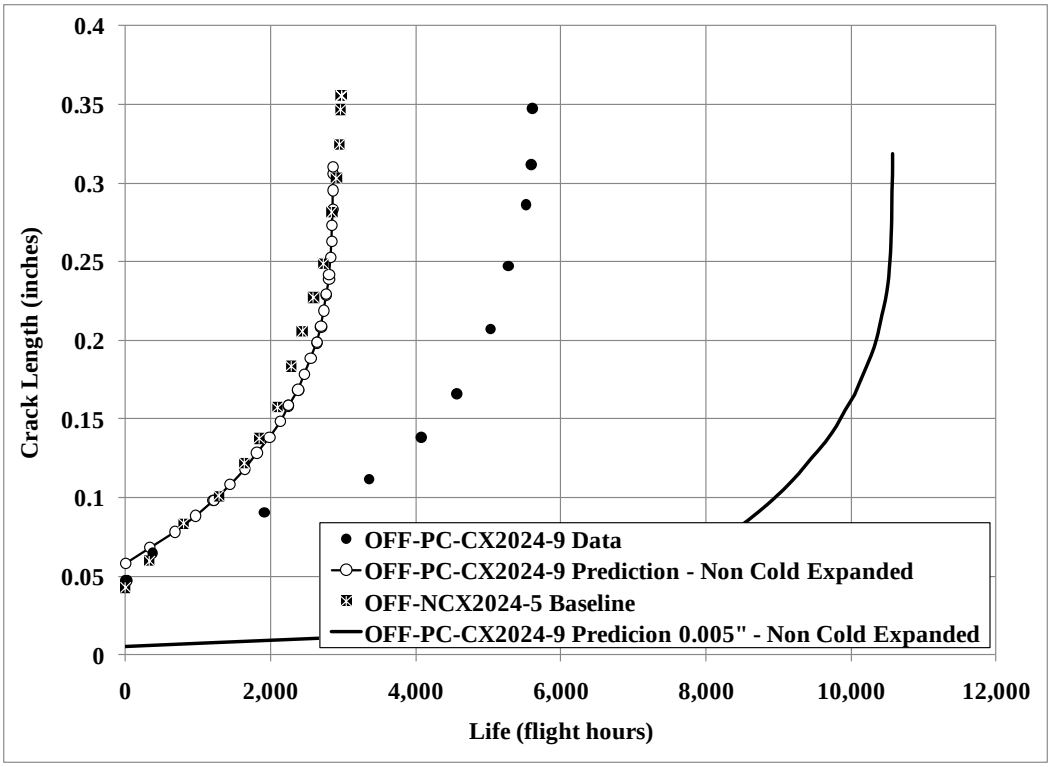

Fig. 112 Specimen OFF-PC-CX2024-9 EDM-A crack growth curve with AFGROW predictions; σ_{max} = 33 ksi, Variable-amplitude, A-10 wing spectrum, Lab Air

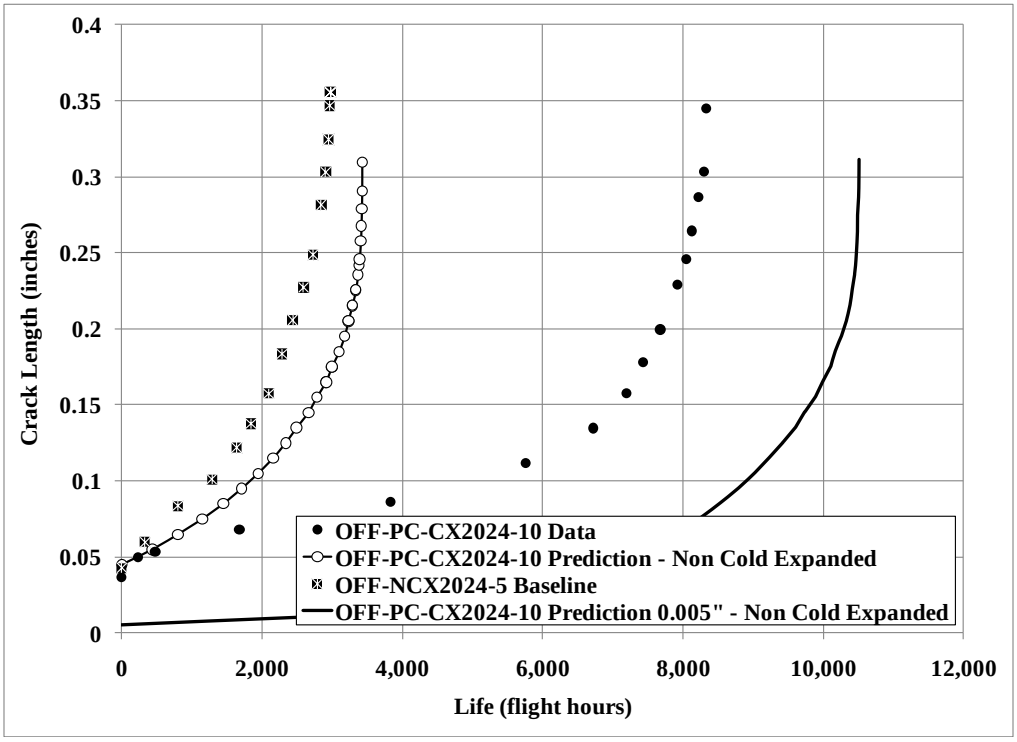

Fig. 113 Specimen OFF-PC-CX2024-10 EDM-A crack growth curve with AFGROW predictions; σ_{max} = 33 ksi, Variable-amplitude, A-10 wing spectrum, Lab Air

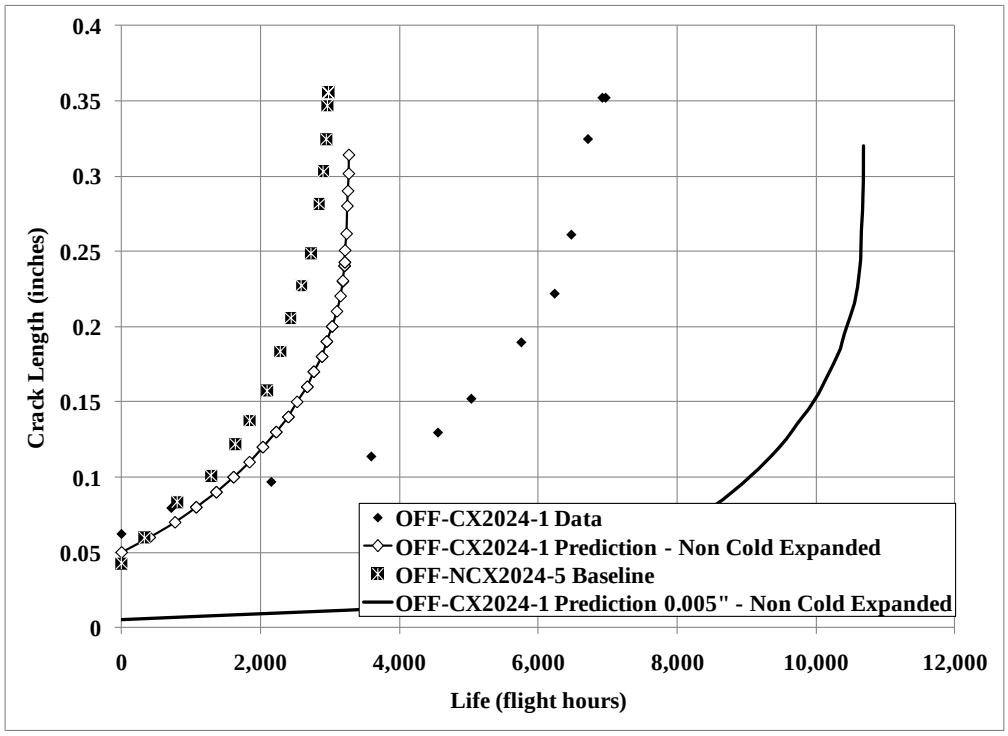

Fig. 114 Specimen OFF-CX2024-1 EDM-A crack growth curve with AFGROW predictions; σ_{max} = 33 ksi, Variable-amplitude, A-10 wing spectrum, Lab Air

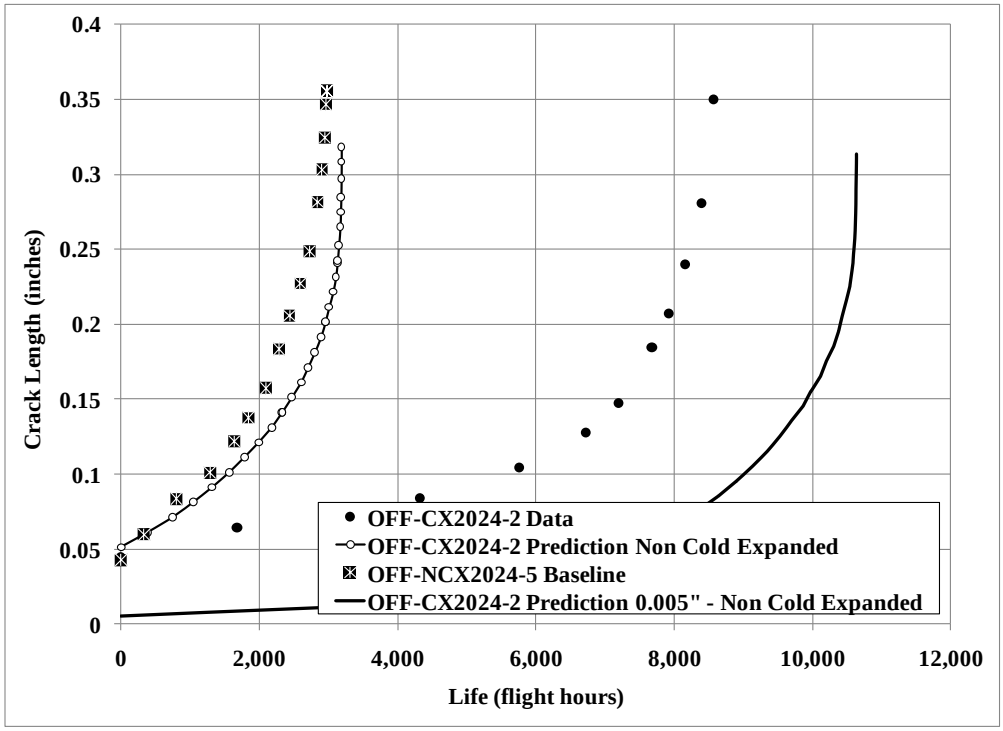

Fig. 115 Specimen OFF-CX2024-2 EDM-A crack growth curve with AFGROW predictions; σ_{max} = 33 ksi, Variable-amplitude, A-10 wing spectrum, Lab Air

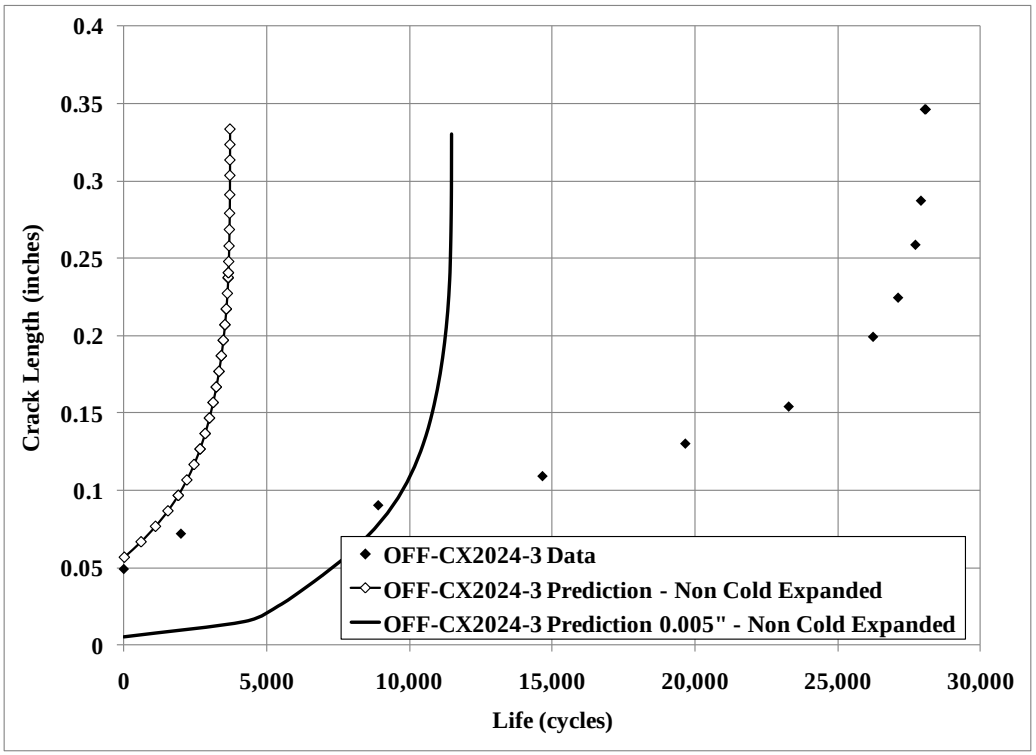

Fig. 116 Specimen OFF-CX2024-3 EDM-A crack growth curve with AFGROW predictions; σ_{max} = 25 ksi, Constant-amplitude R=0.1, 20 Hz, Lab Air

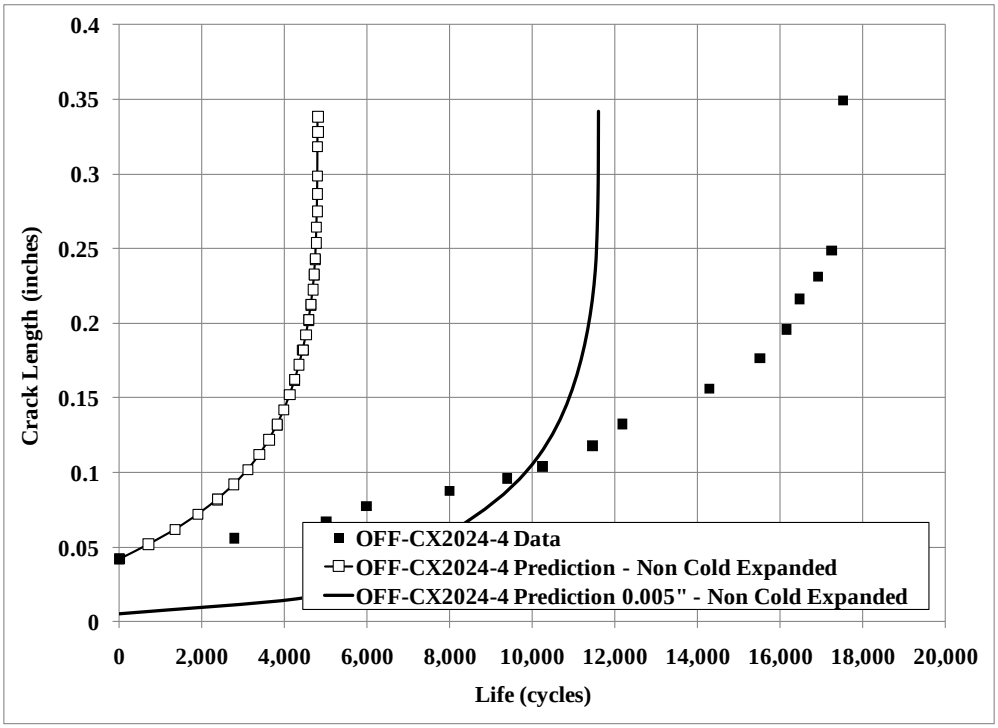

Fig. 117 Specimen OFF-CX2024-4 EDM-A crack growth curve with AFGROW predictions; σ_{max} = 25 ksi, Constant-amplitude R=0.1, 20 Hz, Lab Air

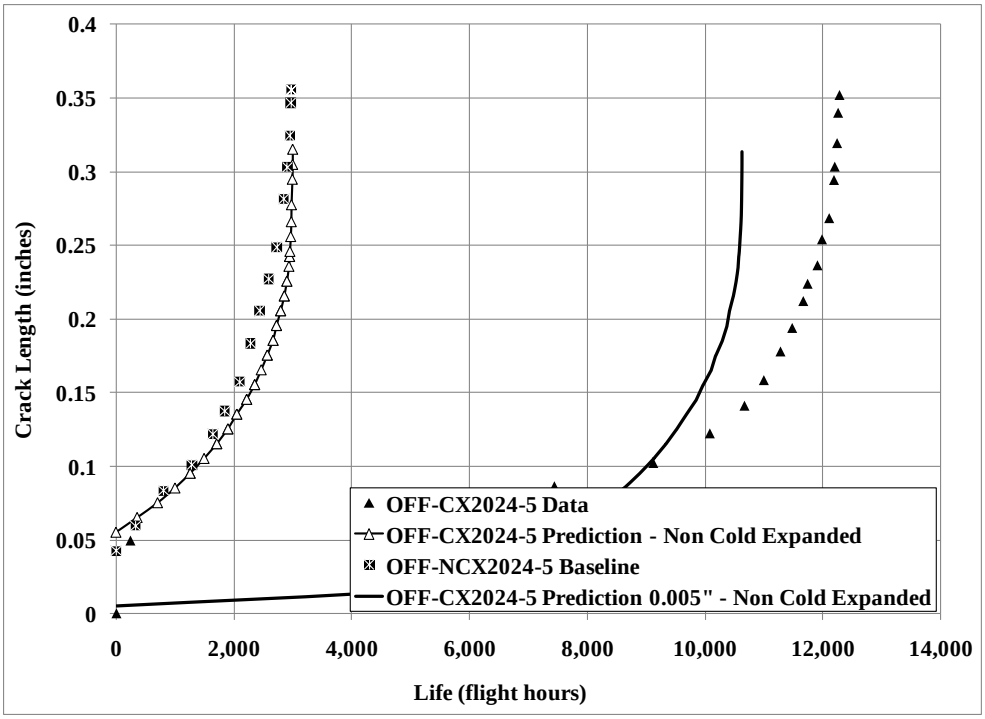

Fig. 118 Specimen OFF-CX2024-5 EDM-A crack growth curve with AFGROW predictions; σ_{max} = 33 ksi, Variable-amplitude, A-10 wing spectrum, Lab Air

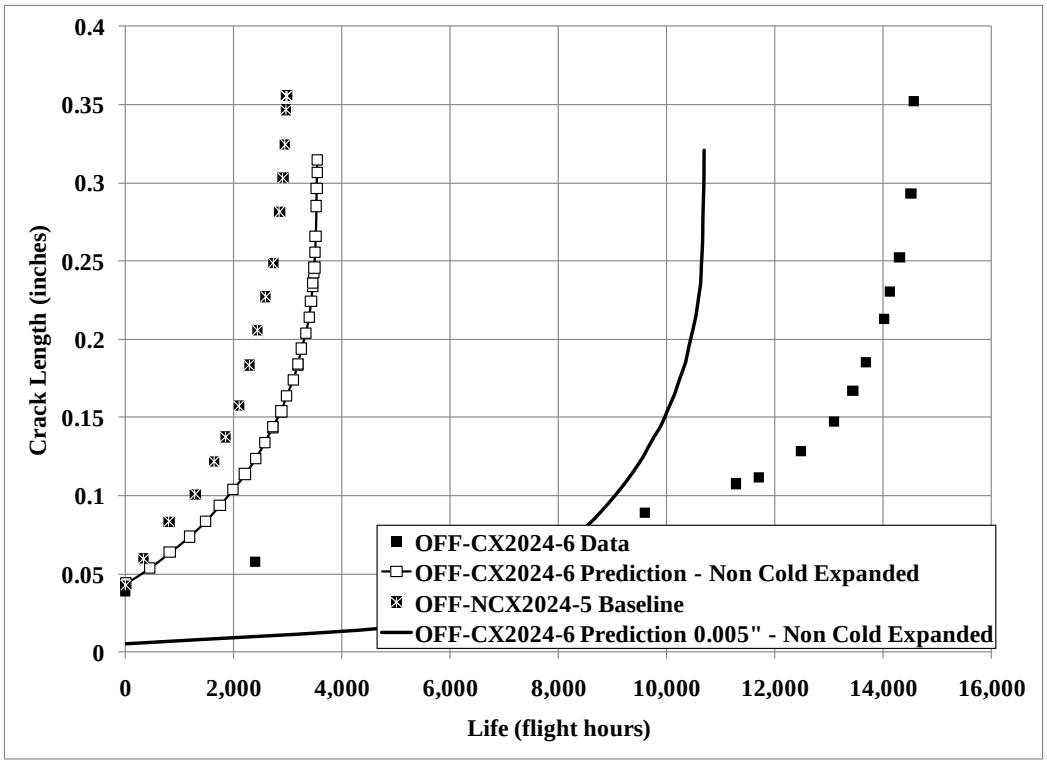

Fig. 119 Specimen OFF-CX2024-6 EDM-A crack growth curve with AFGROW predictions; σ_{max} = 33 ksi, Variable-amplitude, A-10 wing spectrum, Lab Air

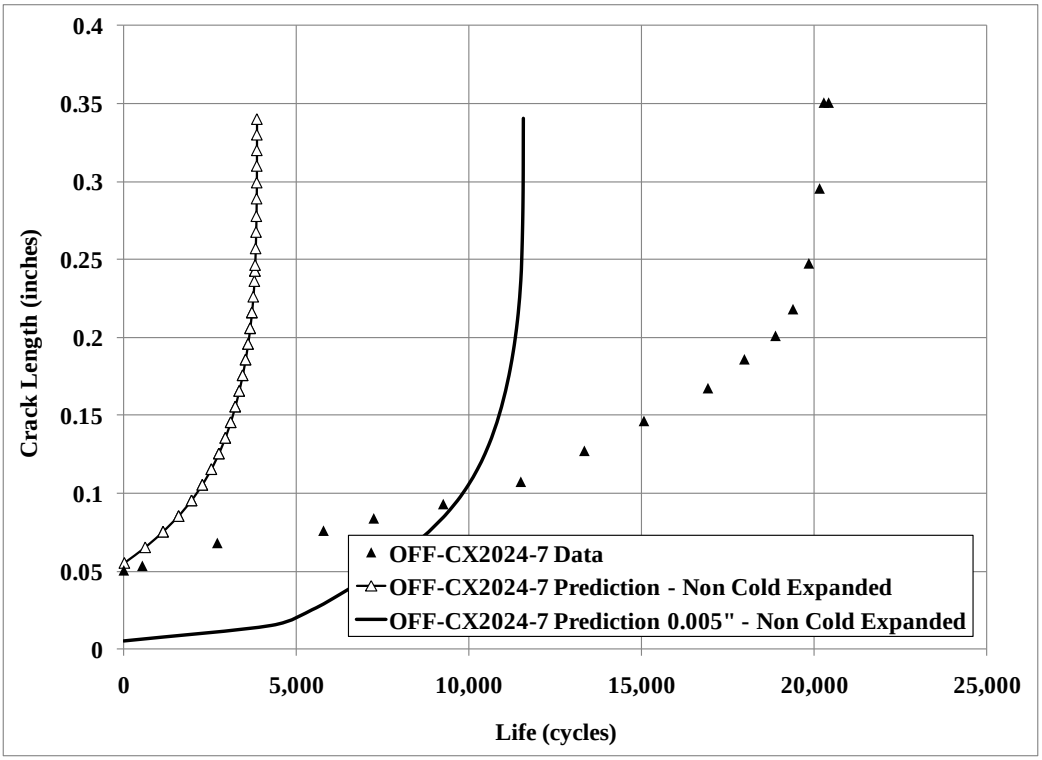

Fig. 120 Specimen OFF-CX2024-7 EDM-A crack growth curve with AFGROW predictions; σ_{max} = 25 ksi, Constant-amplitude R=0.1, 20 Hz, Lab Air

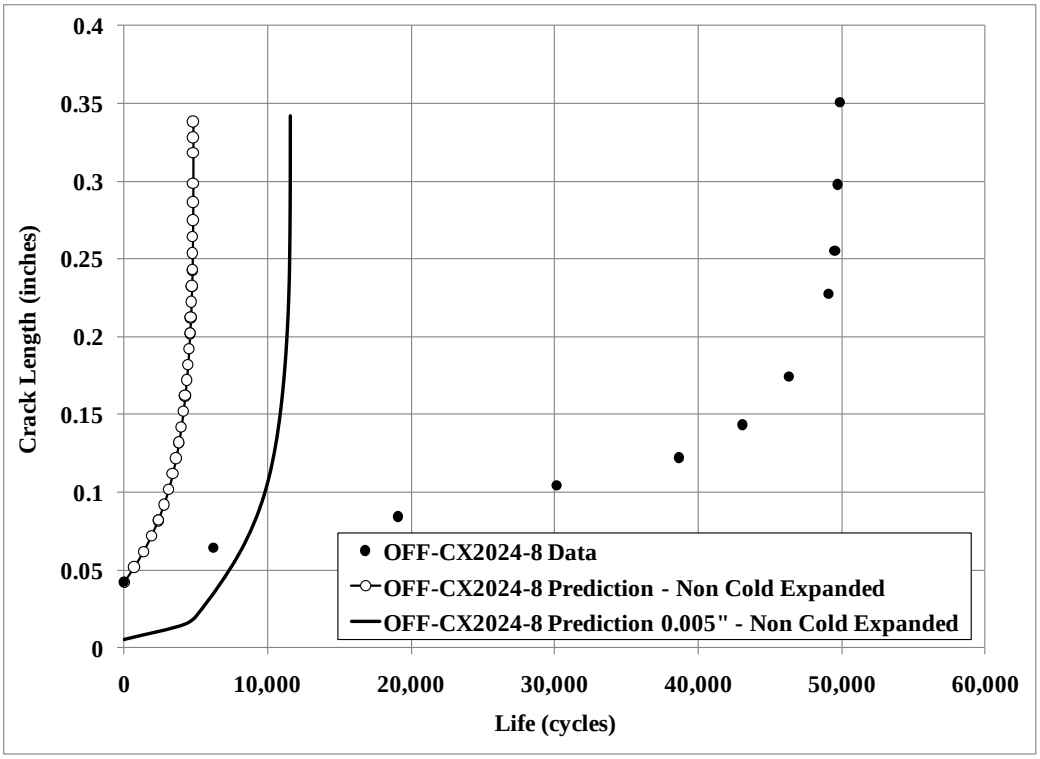

Fig. 121 Specimen OFF-CX2024-8 EDM-A crack growth curve with AFGROW predictions; σ_{max} = 25 ksi, Constant-amplitude R=0.1, 20 Hz, Lab Air

APPENDIX F

CRACK GROWTH RATE DATA

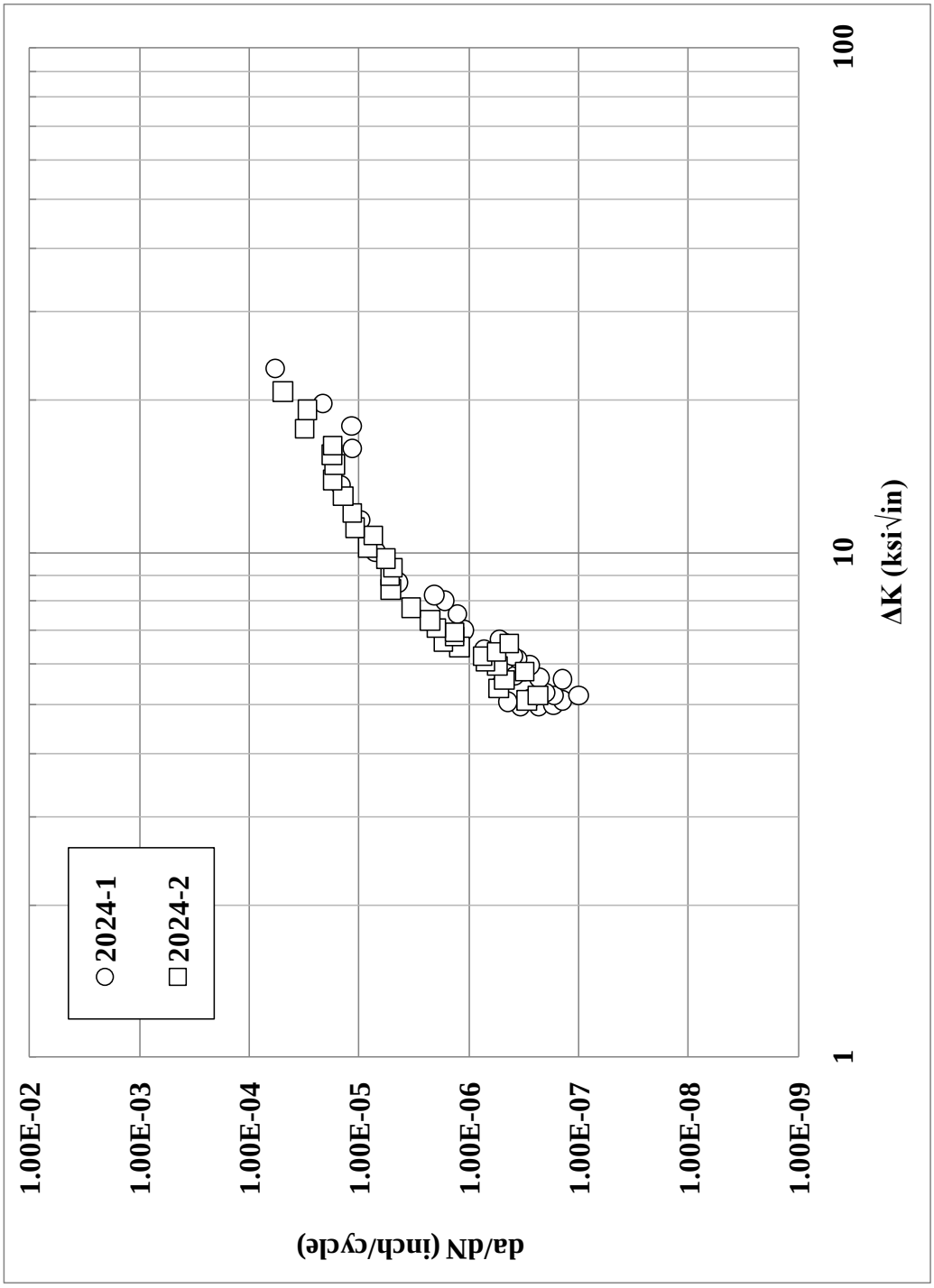

Fig. 122 Crack growth rate data for the two ASTM E 647 specimens

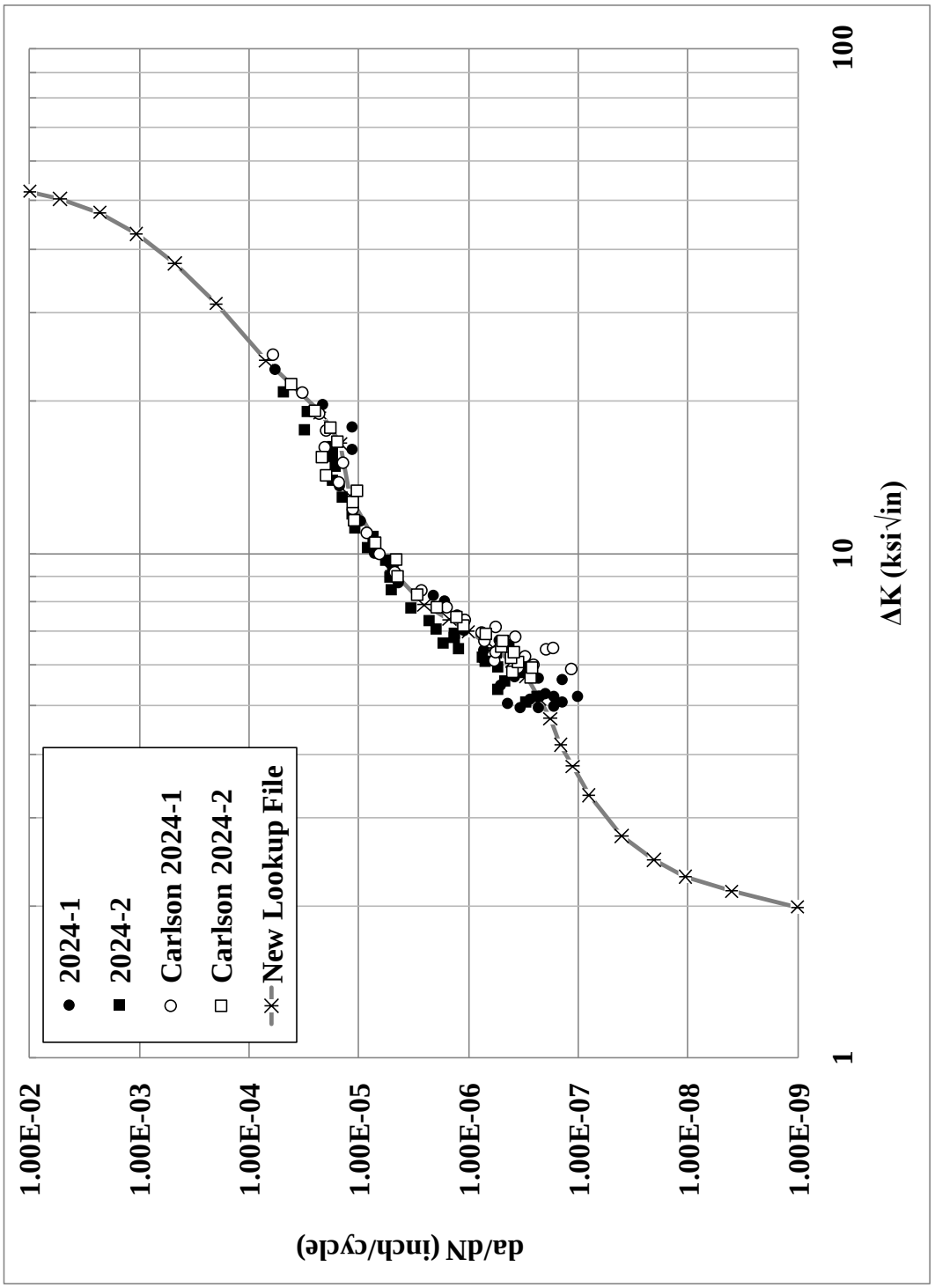

Fig. 123 Crack growth rate data for four ASTM E 647 specimens and correspoding curve fit

APPENDIX G

FRACTOGRAPHIC IMAGES

F.1 ASTM E 647 M(T) Specimens

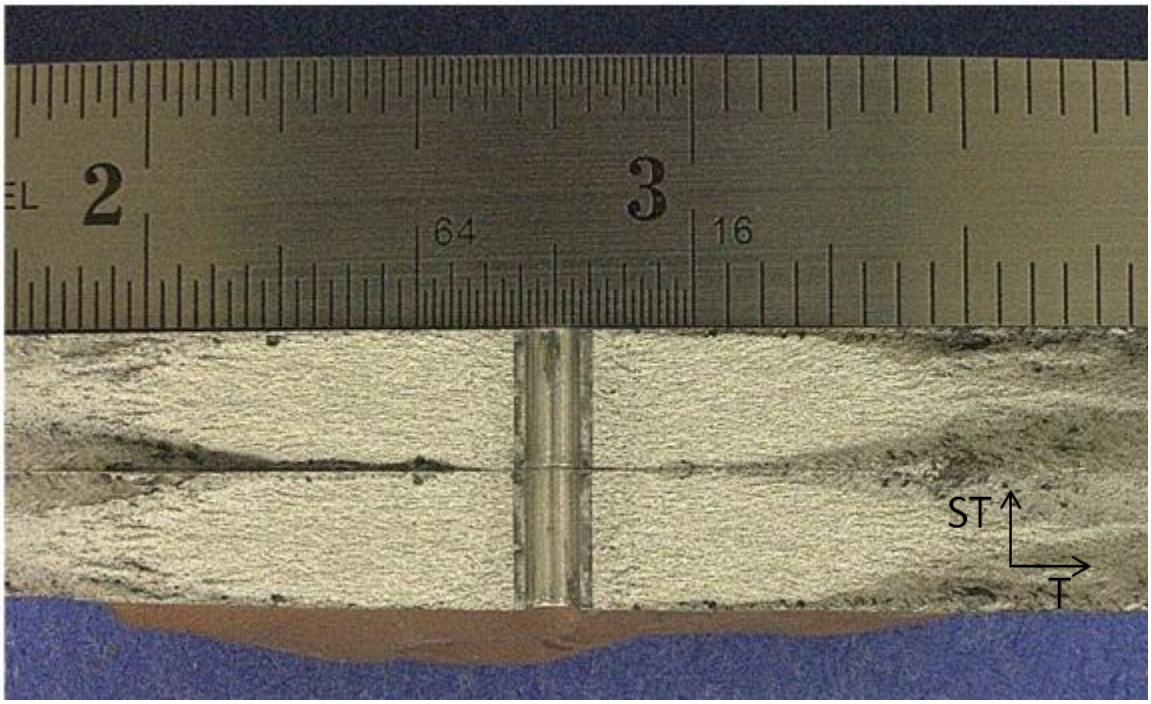

Fig. 124 Fracture surfaces for ASTM E 647 specimen (5X magnification); 2024-1, Constant-amplitude R=0.1, σ_{max} = 11.4 ksi, 20 Hz, Lab Air

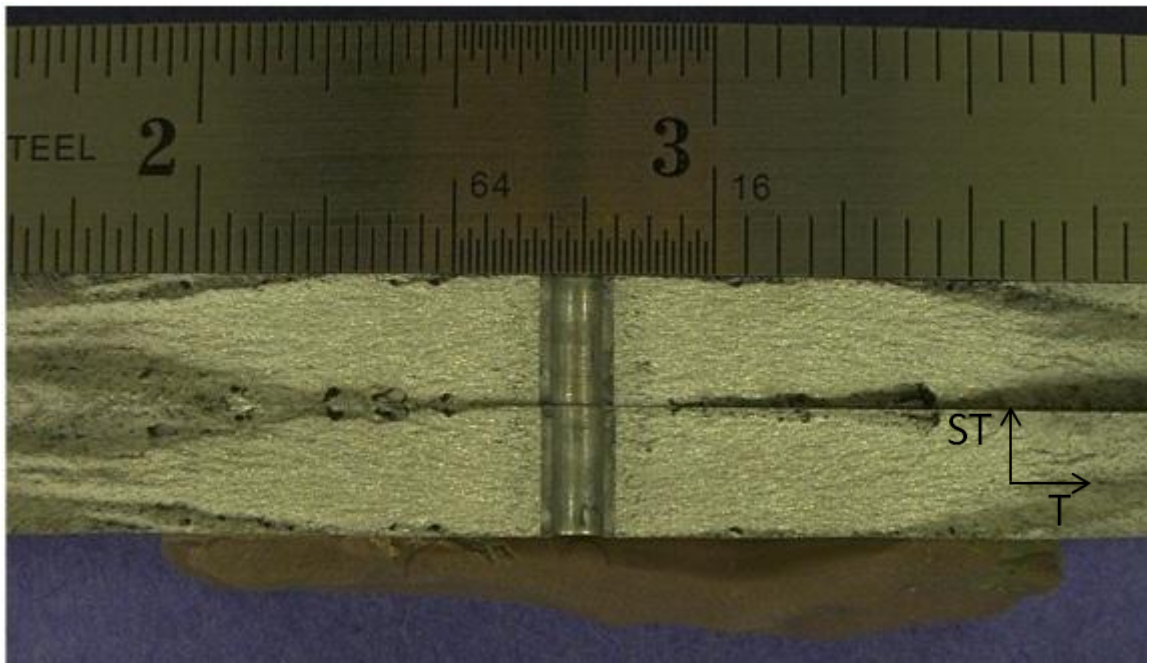

Fig. 125 Fracture surfaces for ASTM E 647 specimen (5X magnification); 2024-2, Constant-amplitude R=0.1, σ_{max} = 11.4 ksi, 20 Hz, Lab Air

F.1 Non-cold-expanded Specimens

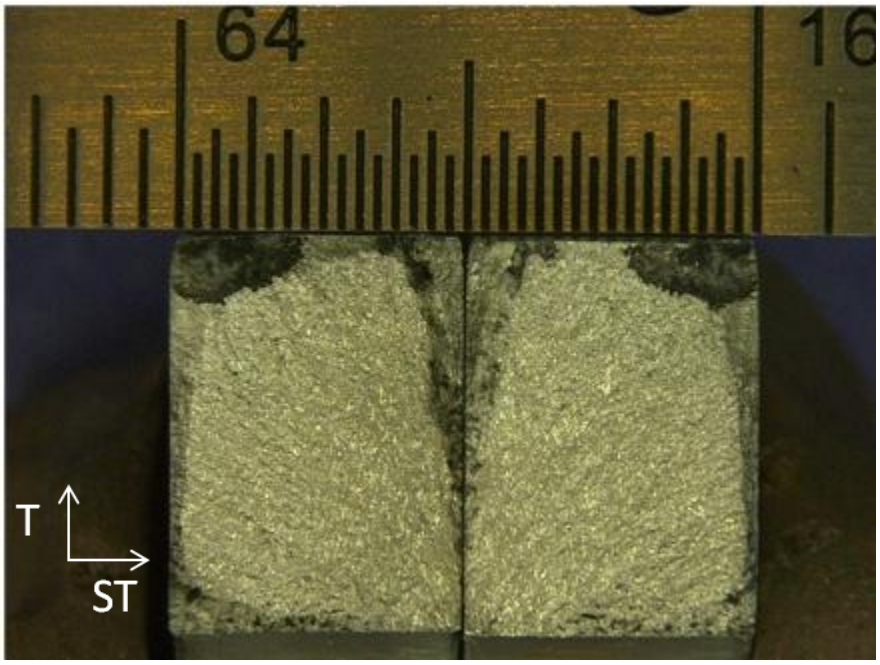

Fig. 126 Fracture surfaces for constant amplitdue non-cold-expanded specimen (19X magnification); OFF-NCX2024-1, Constant-amplitude R=0.1, σ_{max} = 25 ksi, 20 Hz, Lab Air

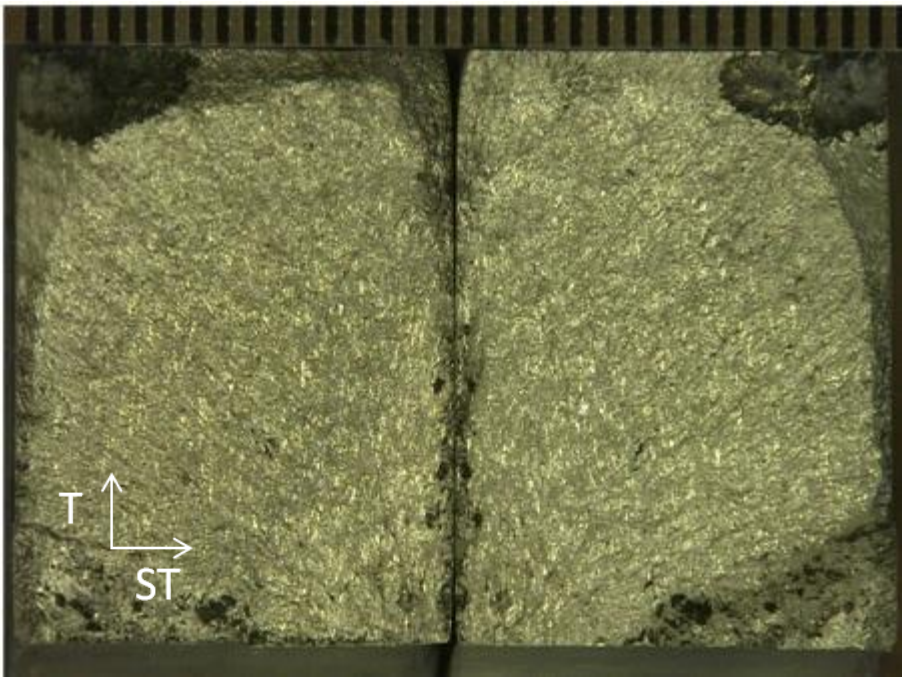

Fig. 127 Fracture surfaces for constant amplitdue non-cold-expanded specimen (28X magnification); OFF-NCX2024-2, Constant-amplitude R=0.1, σ_{max} = 25 ksi, 20 Hz, Lab Air

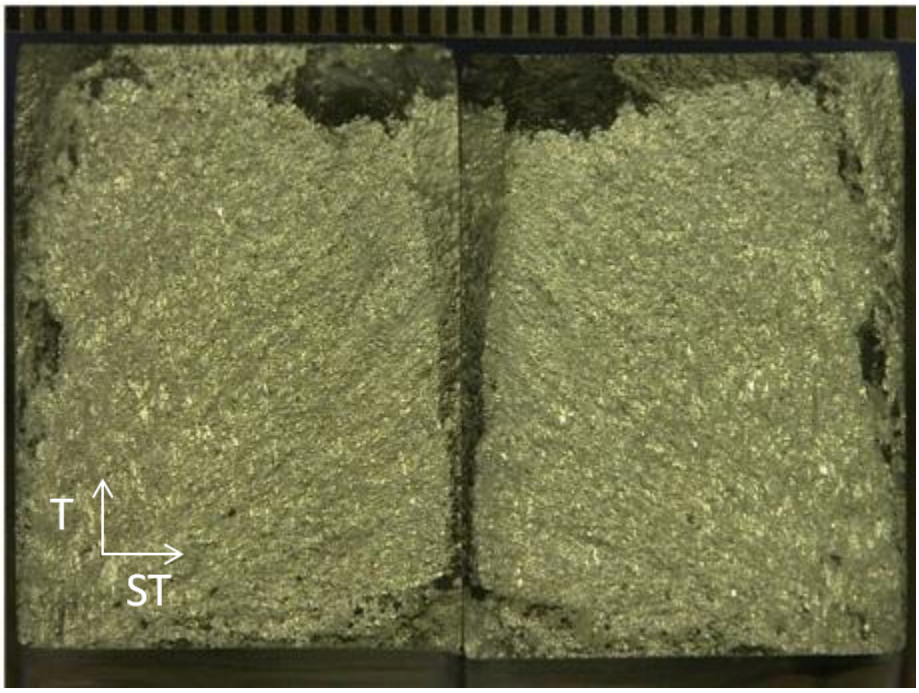

Fig. 128 Fracture surfaces for constant amplitdue non-cold-expanded specimen (28X magnification); OFF-NCX2024-3, Constant-amplitude R=0.1, σ_{max} = 25 ksi, 20 Hz, Lab Air

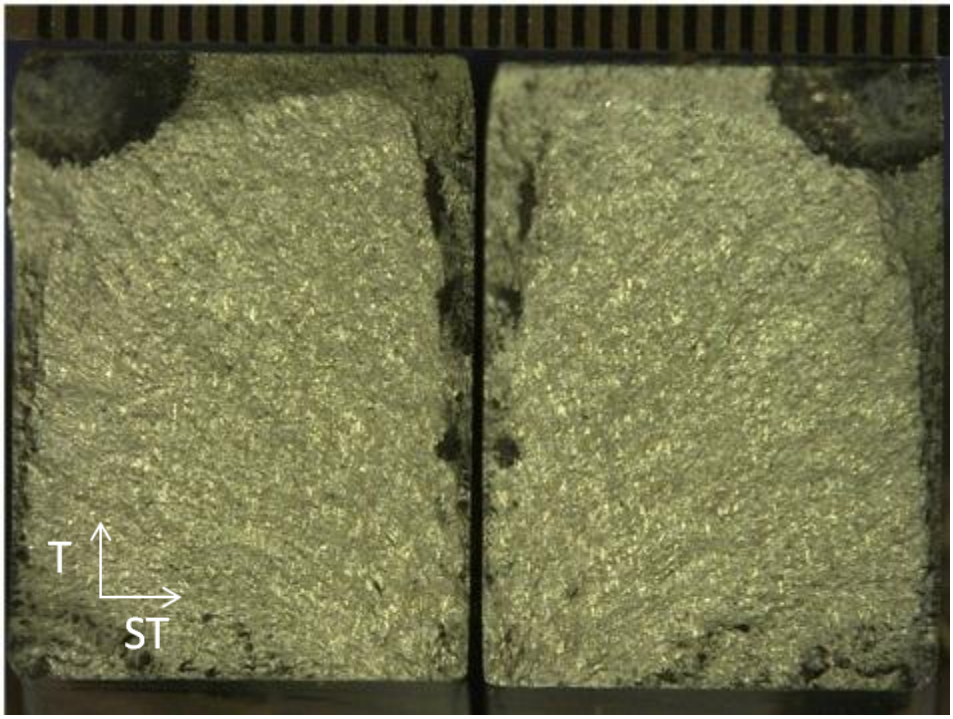

Fig. 129 Fracture surfaces for constant amplitdue non-cold-expanded specimen (28X magnification); OFF-NCX2024-4, Constant-amplitude R=0.1, σ_{max} = 25 ksi, 20 Hz, Lab Air

F.2 Precracked Cold-expanded Specimens

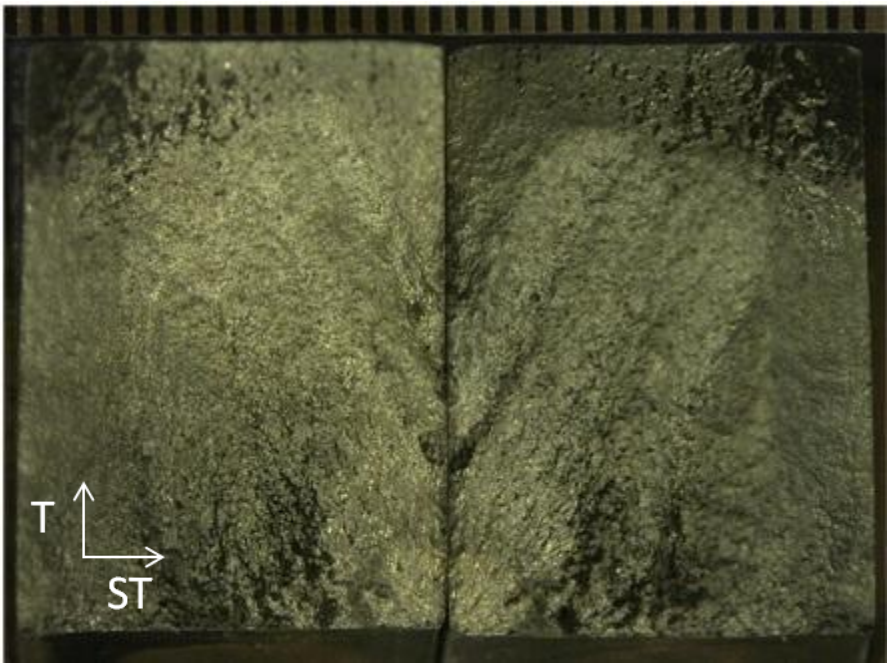

Fig. 130 Fracture surfaces for constant amplitdue precracked cold-expanded specimen (28X magnification); OFF-PC-CX2024-1, Constant-amplitude R=0.1, σ_{max} = 25 ksi, 20 Hz, Lab Air

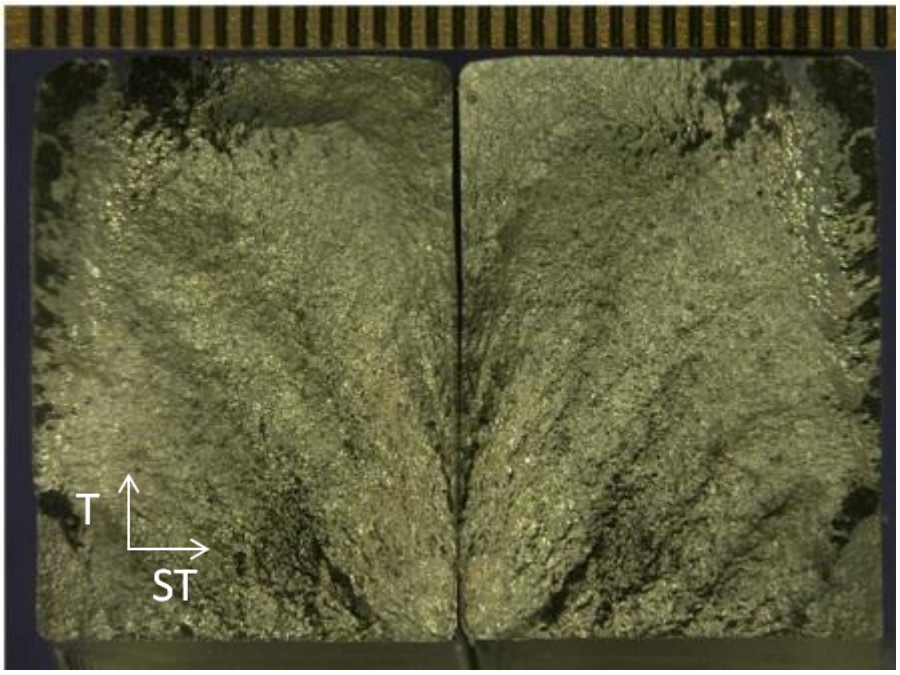

Fig. 131 Fracture surfaces for constant amplitdue precracked cold-expanded specimen (28X magnification); OFF-PC-CX2024-2, Constant-amplitude R=0.1, σ_{max} = 25 ksi, 20 Hz, Lab Air

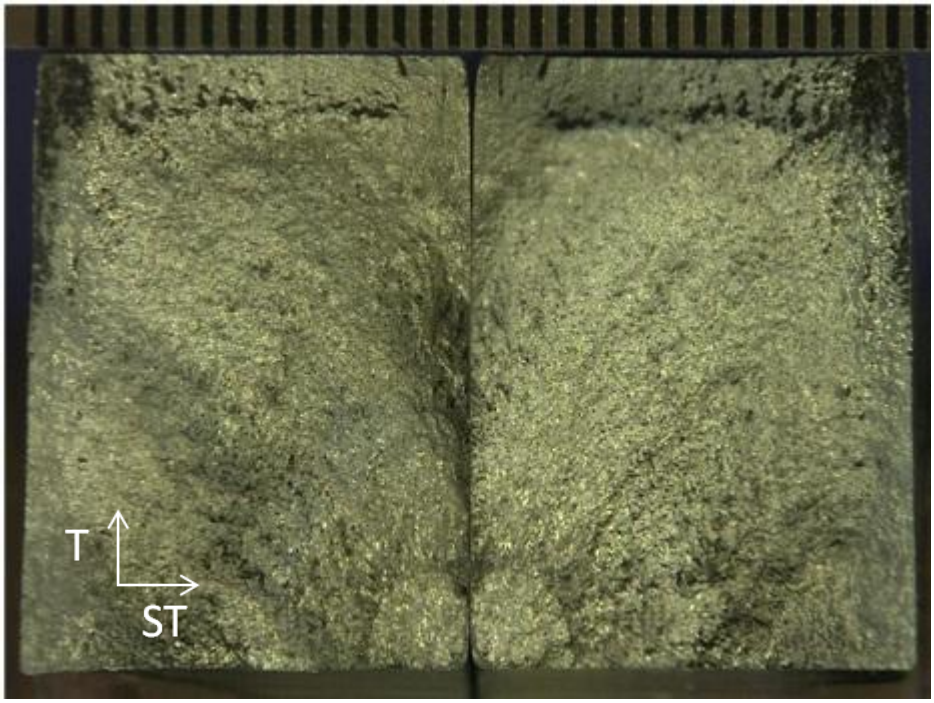

Fig. 132 Fracture surfaces for constant amplitdue precracked cold-expanded specimen (28X magnification); OFF-PC-CX2024-3, Constant-amplitude R=0.1, σ_{max} = 25 ksi, 20 Hz, Lab Air

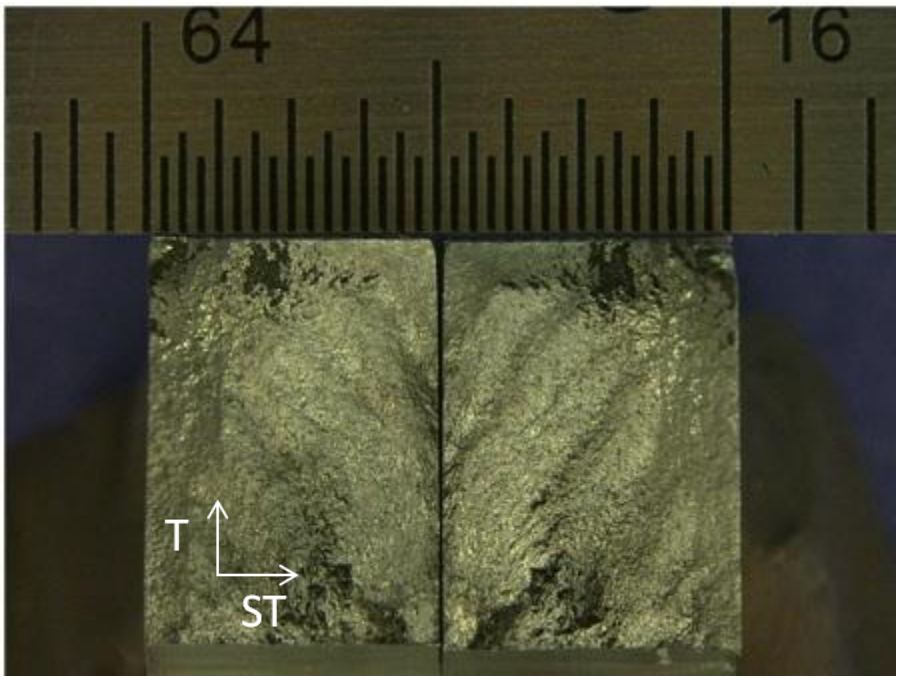

Fig. 133 Fracture surfaces for constant amplitdue precracked cold-expanded specimen (19X magnification); OFF-PC-CX2024-4, Constant-amplitude R=0.1, σ_{max} = 25 ksi, 20 Hz, Lab Air

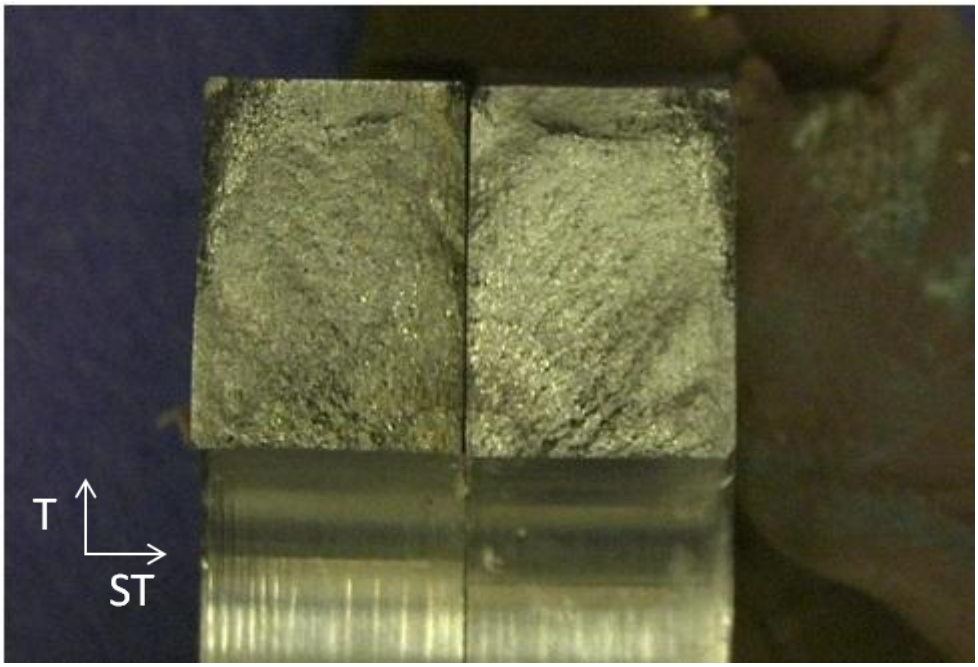

Fig. 134 Fracture surfaces for constant amplitdue precracked cold-expanded specimen used with marker band loading (10X magnification); OFF-PC-CX2024-7, Constant-amplitude R=0.1 and 0.9, σ_{max} = 25 ksi, 20 Hz and 40 Hz, Lab Air

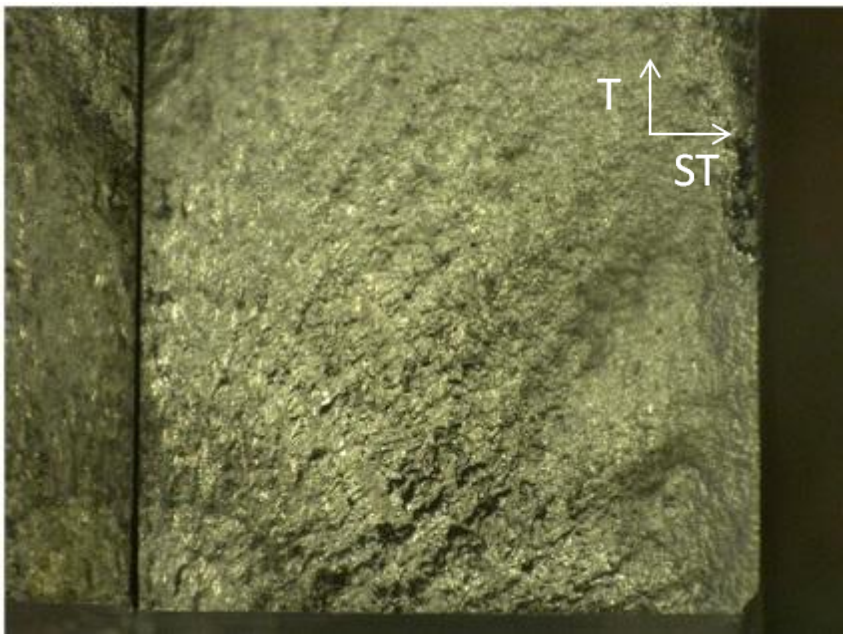

Fig. 135 Fracture surfaces for constant amplitdue precracked cold-expanded specimen used with marker band loading (40X magnification); OFF-PC-CX2024-7, Constant-amplitude R=0.1 and 0.9, σ_{max} = 25 ksi, 20 Hz and 40 Hz, Lab Air

APPENDIX H

DAMAGE TOLERANCE ANALYSIS GROUND RULES FOR A-10A RECONFIGURED POST DESERT STORM SPECTRUM

This document outlines the approach for conducting damage tolerance analyses to support the A-10 Damage Tolerance Re-Assessment and resultant Force Structural Maintenance Plan (FSMP) update as well as any field or depot repair actions. These ground rules apply to analyses using the USAF crack growth software AFGROW.

1. Version 4.12.15.0 of AFGROW released 08/11/2009, or version 5.1.3.16 released 06/13/2010.
    a. Prepare AFGROW Electronic Input file (.dax) as part of deliverable.
2. Title: Brief description of model.
3. Material: reference RPDS DTR Master Document for guidance related to material model (Forman Lookup or Tabular Lookup) as well as material properties for cp locations. Reference "A-10 Material Reference" document for new analysis not covered by the RPDS Master Document. This document is a general guide and some material properties may need to be adjusted based on manufacturing thicknesses or other factors. Reference the RPDS DTR Master Document and the "Metallic Materials Properties Development and Standardization" (formerly MIL HNDBK 5) document to verify correct material properties.
    a. Tabular Lookup File
        i. Select appropriate tabular lookup file from A-10 Materials Folder.
            1. **Verify** correct material properties *for each control point* as prescribed in RPDS DTR Master Document.

        NOTE: Ultimate strength and R_{LO} default to 66ksi and -1.0; these values will need to be modified in accordance with the RPDS DTR Master Document. Altering the ultimate strength does not seem to affect the result from AFGROW.
    b. Forman Lookup File
        i. Select appropriate Forman lookup file from A-10 Materials Folder.
            1. **Verify** correct material properties *for each control point* as prescribed in RPDS DTR Master Document
            2. Special note: <u>Fracture Toughness</u>
                a. "K_c" from RPDS DTR Master Document must be entered into AFGROW → Predict Function Preferences → Propagation Limits → User Defined 'K_{max}'

        NOTE: R_{LO} defaults to -1.0; this value will need to be modified in accordance with the RPDS DTR Master Document, typically -0.3
    c. Material Properties
        i. Select from RPDS DTR Master Document.
4. Model:
    a. Classic models
        i. Select appropriate geometric model
        ii. Enter problem geometric factors including: thickness, width, hole diameter, initial flaw size (IFS), offset, etc
            1. Keep A/C constant=YES (checked)
                a. Note: Keep A/C constant=NO [For surface flaws and in specific cases as noted in SA220R0207 (2nd 6000 Hour DTR)]

2. Oblique through crack=NO (unchecked)
3. Initial Flaw Size: Unless otherwise specified, the initial flaw size should be the same in both the "A" & "C" directions. See Section 10 for appropriate initial flaw sizes.
4. Countersunk Holes:
    a. A stress concentration (K_t), as calculated by Shavikumar and Newman (NASA TP-3192, 1992), is used to calculate beta corrections to be used for countersunk holes.
    b. The A-10 countersunk hole macro can be used to calculate beta corrections for a given model and countersink geometry.
    c. The shank diameter of the hole should be used in the analysis.
    d. A reduced model thickness should be used in the analysis (true thickness minus the depth of the countersink).
        i. For materials where SOLR changes with thickness, assume the full thickness in determining SOLR.
    e. For locations with load transfer, the shank diameter and full thickness of the component should be used to calculate the bearing stress fraction.
    f. Reference SA220R0207, Rev. C, Appendix J for fastener head size information.
    g. Knife edge fasteners ($t_{CS} \geq t$) are not allowed in airframe design because of fatigue requirements.

    The maximum countersink depth is $t_{cs} = \frac{2}{3}(t)$

iii. Load: Ratio of tension or bearing stress to reference stress must be input for each load case (tension stress fraction = 1.0, if bearing stress is zero).
iv. For pin loaded fastener holes, the tension stress fraction should reflect the reduced bypass stress fraction (i.e.: 20% load transfer equates to 80% tension stress fraction).
    1. Effective Widths: Refer to RPDS DTR Master Document for appropriate Effective Width for each CP.
        a. New analysis: For the purpose of determining the Bearing Stress Fraction (BrSF) in AFGROW the following approach should be used.
        b. For all capstrips, angles etc., the effective width as shown in the figure below: A) the length of the leg, B) the offset doubled, or C) one-half the leg length as in the case of a leg with a double row of fasteners. In cases where multiple cases could be applicable, use the smallest effective width.

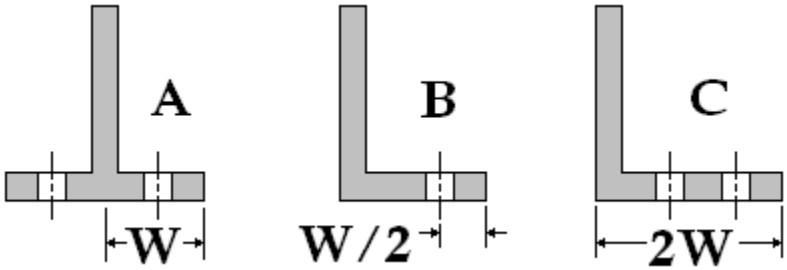

c. In situations where there is a line of fasteners the effective width can be taken as 1) offset plus half the distance to the neighboring hole, 2 & 3) the sum of half the distance to the neighboring holes, or 4) offset doubled, which ever is less.

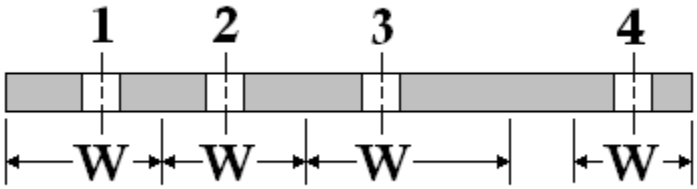

d. The final method of finding the BrSF is to determine it directly from the load reports. The far field stress is easily determined using the load and the cross-sectional area, the bearing stress is the load taken out by the fastener divided by (width * thickness). Typically, doing this method in lieu of the above technique should result in the same BrSF.

2. Further modeling may be necessary via, FEM, Stress-Check, etc.

v. The "Filled Unloaded Hole" option is not typically used unless engineering judgment overrides this approach. If used, justification must be provided in the analysis report.

b. Advanced Model
   i. Advanced models can be used for some situations, i.e. crack growth between adjacent holes. The analyst should ensure the model details are within the bounds of the solutions in AFGROW. The classic model inputs detailed in section 4.a are also applicable for advanced models.
   ii. Advanced continuing damage model (slot)
      1. The in-plane bending constraint option should typically be selected. Some situations, where in plane bending may occur in a continuing damage scenario, may warrant the use of the unconstrained in-plane bending option.

c. Lug Model
   i. Use AFGROW default preferences (see Predict Function Preferences in this document).

5. Spectrum:
    a. Stress Multiplication Factor (SMF)
        i. Enter maximum stress (normalized spectrum will be used for all analyses).
            1. Maximum stresses come from Northrop Grumman stress equations (reference SA220R0474), these values are also listed in the RPDS DTR Master Document.
            2. For non-CP locations engineering judgment with referenced justification should be used to select the appropriate SMF.
                a. For details similar and near a CP location, the SMF for that location may be used when appropriate.
                b. The ultimate stress reports may be used to scale a known CP location SMF to the location of interest.
    b. Residual Strength Requirement (P_{xx})
        i. Enter the higher of either the maximum spectrum stress or the limit stress if known.
    c. Open existing spectrum file
            1. Use only RPDS severe spectrum from approved spectrum folder.
                a. A common spectrum electronic folder will be utilized.
                b. Spectrum files are:
                    i. Flight-by-flight
                    ii. Base-peak-base converted
                    iii. Normalized
            2. In the event an AFGROW ready spectrum file (filename.sp3) is not in existence, use the spectrum converter file to be certain the spectrum file is in the proper format to be read by AFGROW.
6. Retardation:
    a. Generalized Willenborg Retardation
        i. Turn OFF the “Adjust Yield Zone Size for Compressive Cycles” toggle.
        ii. For all SOLR values, see the RPDS DTR Master Document and/or Appendix F.
7. Predict Function Preferences:
    a. Growth Increment
        i. Cycle by Cycle Beta and Spectrum calculation
            1. For advanced models use “Cycle by Cycle Spectrum calculation”.
                a. Use Max. Growth Increment of 0.25%.
    b. Output Intervals
        i. Specify Crack Growth Increments. Increment = 0.01”
        ii. Number of Hours per Pass.
            1. Spectra based on 240 hours for all except landing gear

2. Landing gear spectra based on 250 landings (assumes 1.5 hours per landing).

c. Output Options (AFGROW output files are part of deliverables).
   i. Output
      1. Data File
      2. Plot File
d. Propagation Limits
   i. K_{max} failure criteria (If using Forman: see 3.b.i.2.a of these ground rules)
   ii. Net section yield: to be evaluated on a case-by-case basis
e. Transition to Through Crack
   i. Default = 95% (Stick with default unless documented otherwise.)
f. Lug Boundary Conditions
   i. Use default of combined bearing and spring solution and default values:
      1. Bearing: 70%
      2. Spring 80%
   ii. Use Spring Boundary Condition for applications with an interference fit fastener or interference fit bushing where fastener/bushing is steel in aluminum lug.

8. Stress State
   a. Use Stress State to be determined automatically.
9. Betas
   a. Use AFGROW standard solution betas for standard geometries.
   b. Non-standard geometries shall be dealt with on a case-by-case basis (User Defined Betas: Legacy, StressCheck, etc.)
10. Inspection intervals
   a. Initial inspection intervals based upon the safety limit (Initial Flaw Size** to fracture) divided by 2.

**Ref: JSSG-2006 Table XXX, page 449.

      i. New Structure Initial Flaw Sizes (IFS)
         1. Non-Cold Worked Holes:
            a. Aluminum: IFS = 0.050”
            b. Steel: IFS = 0.050”
         2. Cold Worked Holes:
            a. Aluminum: IFS = 0.005”
            b. Steel: IFS = 0.005”
         3. Surface Flaws
            a. IFS = 0.100” = 2c (This is the total crack length)
   b. Recurring inspection intervals based upon the field safety limit (Detectable Flaw Size** to fracture) divided by 3.

**Ref: Structures Bulletin EN-SB-08-012, Revision A.

      i. Field safety limit detectable flaw sizes (DFS)
         1. For Bolt Hole Eddy-Current inspections
            a. Aluminum: DFS = 0.050”
            b. Stainless & Ni-Co Steels: DFS = 0.060”

c. 4000 Series Steel: DFS = 0.100”
d. Note: minimum part thickness of 0.040” is required
e. The DFS for a coldworked hole using Bolt-Hole Eddy Current inspections is the same as a non-coldworked hole, however, the recurring inspection intervals should be based upon the field safety limit divided by 2.

2. Eddy Current Surface Scan
    a. Flat Open Surface--Free Hand Scanning—Radius of Curvature > 1.0”
        i. Aluminum: DFS = 0.250” = 2c
    b. Radii
        i. Free Hand Scanning—Radius of Curvature < 1.0”
            1. Aluminum: DFS = 0.500” = 2c
        ii. Conformal Radius Probe (specialty probe)
            1. Aluminum: DFS = 0.150” = 2c
    c. Edges
        i. Free Hand Scanning
            1. Aluminum: DFS = 0.250”
        ii. Articulating Edge Probe (specialty probe)
            1. Aluminum: DFS = 0.150”
    d. Around Raised Fastener Heads (or Collars)
        i. Fastener Head as Guide
            1. Aluminum: DFS = 0.200” + fastener head (or collar) overlap
            2. Reference SA220R0207, Rev. C, Appendix J for fastener head size information.
        ii. Socket Scanner Probes (specialty probe)
            1. Aluminum: DFS = 0.150” + fastener head (or collar) overlap
            2. Reference SA220R0207, Rev. C, Appendix J for fastener head size information.
    e. Around Countersunk Fastener Heads
        i. Aluminum: DFS = 0.250” + fastener head overlap
        ii. Reference SA220R0207, Rev. C, Appendix J for fastener head size information.
    f. See EN-SB-08-012, Rev A for additional guidance on inspections using guides, fixtures, or specialty probes.
    g. For inspections of steel components the following DFS guidelines apply:

i. Stainless & Ni-Co Steels: DFS = 1.2 x DFS for Aluminum
ii. 4000 Series Steels: DFS = 2.0 x DFS for Aluminum
iii. Guidelines were provided by HAFB NDI Program Office.

h. Consult the A-10 ASIP group and the HAFB NDI Program Office for additional guidance for other inspection methods.

11. Continuing Damage Option: This section explains some of the common situations for employing continuing damage. Engineering judgment may overrule these guidelines as determined for each situation analyzed. *(e.g.: fleet history may dictate more conservative assumptions than those presented here)*
    a. Use standard Air Force practice when justified.
        i. JSSG 2006 Table XXXI, page 450
    b. For continuing damage on diametrically opposite side of hole
        i. Use advanced AFGROW model with hole and slot
        ii. Standard holes (Non-Cold Worked holes)
            1. IFS: 0.050”x0.050” (primary) and 0.005”x0.005” (secondary)
            2. Continuing damage: Ligament failed and (0.005”x0.005” + Δa*)
            3. Inspection Interval:
                a. Safety Limit: Total Life divided by two
                b. Field Safety Limit: Life from DFS divided by three
        iii. Cold Worked holes *(note: divided by two for FSL, see 11.b.iii.2)*
            1. Safety Limit
                a. IFS: 0.005”x0.005” (primary) and 0.005”x0.005” (secondary)
                b. Continuing damage: Ligament failed and (0.005”x0.005” + Δa*)
                c. Initial Inspection: Total Life divided by two
            2. Field Safety Limit
                a. IFS: 0.050”x0.050” (primary) and 0.005”x0.005” (secondary)
                b. Continuing damage: Ligament failed and (0.005:x0.005” + Δa*)
                c. Inspection Interval: Life from DFS ***divided by two***

    * Δa found with a separate model with one continuing damage flaw on the opposite side of the hole as the primary crack, ran the number of cycles it took the primary crack to grow from the initial flaw to failure. Note: The primary crack is not included in this model

    c. For continuing damage in adjacent structure.
        i. Continuing damage IFS = 0.005” + Δa

ii. Δa should be calculated based on the life in the primary component from IFS to failure.

d. Significant detail shall be documented in the write-up to fully explain all details of the analysis.

12. Document analysis using A-10 USAF-SwRI-NGC DTA template.

REFERENCES

[1]Burnside, H. (1993). Flying longer, with confidence. Southwest Research Institute, San Antonio, TX, USA.

[2]Century of Flight, Airlines and Airliners, De Havilland Comet, <http://www.century-of-flight.net/Aviation%20history/coming%20of%20age/De%20Havilland%20Comet.htm>.

[3]Hoeppner, D.W. (2011). ME EN 7060 – Lecture 1. University of Utah, Salt Lake City, UT, USA.

[4]Buntin, W.D. (1971). Concept and conduct of proof test of F-111 production aircraft. Paper presented to the Royal Aeronautical Society, London, England.

[5]Department of Defense (2005). *Aircraft Structural Integrity Program (MIL STD 1530C)*, Department of Defense Standard Practice, United States Air Force.

[6]Wood, H.A., Engle, R.M. (1979). *USAF damage tolerance design handbook: Guidelines for the analysis and design of damage tolerant aircraft*. USAF Systems Command, Wright-Patterson Air Force Base, OH, USA.

[7]American Society for Testing and Materials (ASTM). (2010). Standard terminology relating to fatigue and fracture testing (E 1823), *Am. Soc. For Testing and Materials*, West Conshohocken, PA, USA.

[8]Hoeppner, D.W. (2011). The formation/nucleation of fatigue cracks in aircraft structural materials. In: *26th ICAF Symposium*, Montreal, Canada.

[9]Griffith, A. A. (1920) "The phenomena of rupture and flow in solids." *Philosophical Transaction of the Royal Society*, London, Series A, **221**, Delft, Netherlands.

[10]Pilarczyk, R. (2008). Experimentally derived beta corrections to predict fatigue crack growth at cold-expanded holes in 7075-T651 aluminum alloy. *Mechanical Engineering*. University of Utah, Salt Lake City, UT, USA.

[11]Broek, D. (1986). *Elementary Engineering Fracture Mechanics*. Martinus Nijhoff Publ., Dordrecht, pp. 374–380.

[12]Fatigue Technologies Inc. (2002). *FTI process specification 8101D cold expansion of holes using the standard split sleeve system and countersink cold expansion (CsCx™)*, Seattle, WA, USA.

[13]Carlson, S. (2008). Experimentally derived beta (β) corrections to accurately model the fatigue crack growth behavior at cold-expanded holes in 2024-T351 aluminum alloys. Mechanical Engineering. University of Utah, Salt Lake City, UT, USA.

[14]Horsley, J.J., Wylie, C.B. (1973) Fatigue testing of pre-cracked cold-worked fastener holes in 7178-T6 aluminum alloy load transfer joints. The Boeing Company, Wichita.

[15]Petrak, G.J., Stewart, R.P. (1974) Retardation of cracks emanating from fastener holes. *Eng. Fract. Mech.* **6**, 275-282.

[16]Toor, P.M. (1976) Cracks emanating from precracked coldworked holes. *Eng. Fract. Mech.* **8**, 391-395.

[17]Brot, A., Nathan, A. (1985) Increasing fatigue and crack growth lives of short edge margin holes. In: *13th Symposium of the International Committee on Aeronautical Fatigue*, 22 May 1985, Pisa, Italy.

[18]Buxbaum, O., Huth, H. (1987) Expansion of cracked fastener holes as a measure for extension of lifetime to repair. *Eng. Fract. Mech.* **28**, 689-698.

[19]Ayatollahi, M.R., Nik, M.A. (2009) Edge distance effects on residual stress distribution around a cold-expanded hole in Al 2024 alloy. *Comput. Mater. Sci.* **45**, 1134-1141.

[20]Ball, D.L., Lowry, D.R., (1998). Experimental investigation on the effects of cold expansion of fastener holes. *Fatigue Fract. Engng. Mater. Struct.* **21**, 17-34.

[21]Cathey, W.H., Grandt, A.F. Jr. (1980) Fracture mechanics consideration of residual stresses introduced by coldworking fastener holes. *J. Eng. Mater. Technol.* **102**, 85-91.

[22]Heller, M., Jones, R., Williams, J.F. (1991) Analysis of cold-expansion for cracked and uncracked fastener holes. *Eng. Fract. Mech.* **39**, 195-212.

[23]Kang, J., Johnson, W.S. (2005) Analysis of the cold working process on holes containing preexisting cracks. *J. Aircraft* **42**, 1281-1287.

[24]Lam, Y.C. (1993) A comparative study on the effects of interference fit and cold expansion on the fatigue life of cracked holes. *Scr. Metall. Mater.* **27**, 191-195.

[25]Lowry, D.R. (1991) D6ac steel bolt life improvement – F-111 coldwork modification development program (Phase II). FZS-12-588, General Dynamics/Fort Worth Division.

[26]Moreira, P.M.G.P., De Matos, P.F.P., Pinho, S.T., Pastrama, S.D., Camanho, P.P., De Castro, P.M.S.T., (2004). The residual stress intensity factors for coldworked cracked holes a technical note. *Fatigue Fract. Engng. Mater. Struct.* **27**, 879-886.

[27]Pell, R.A., Beaver, P.W., Mann, J.Y., Sparrow, J.G. (1989) Fatigue of thick-section cold-expanded holes with and without cracks. *Fatigue Fract. Engng. Mater. Struct.* **12**, 553-567.

[28]Ponzoha, W., Hammond, M., Greer, J., Shah, S., Royall, B. (2010) Effects of cold expansion on T-38 steel dorsal longeron near fatigue critical location B-12 [Draft]. United States Air Force Academy, Colorado Springs, CO, USA.

[29]Stefanescu, D., Santisteban, J.R. (2004) Residual stress measurement and fatigue crack growth prediction after cold expansion of cracked fastener holes. *J. Aerosp. Eng.* **17**, 91-97.

[30]Alloy 2024 Sheet and Plate (2011). ALCOA Mill Products, Inc. Bettendorf, IA,USA.

[31]American Society for Testing and Materials (ASTM). (2000). Standard test method for measurement of fatigue crack growth rates (E 647), *Am. Soc. For Testing and Materials*, West Conshohocken, PA. USA.

[32]Hoeppner, D.W. (1981). Estimation of component life by application of fatigue crack growth threshold knowledge. In: *Fatigue, creep, and pressure vessels for elevated temperature service.* Presented at: *The winter annual meeting of the American Society of Mechanical Engineers*, 15-21 Nov. 1981, Washington D.C.

[33]Thomsen, M. (2011). USAF A-10 ASIP Manager, Personal Communication.

[34]Rose, J.B. (1922). Machining and lapping very deep holes. *Mech. Eng.*,**44**, ASME, Easton, PA, USA.

[35]American Society for Testing and Materials (ASTM). (2010). Standard practices for force verificaiton of testing machines (E 4), *Am. Soc. For Testing and Materials*, West Conshohocken, PA. USA.

[36]Department of Defense (2006). *DoD Joint Service Specification Guide, Aircraft Structures,* USA.

[37]Schijve, J. and Broek, D. (1962). Crack propagation based on a gust spectrum with variable-amplitude loading. *Aircraft Eng*, **34**, pp. 314-316.

[38]Air Force Structures (2011). *Structures Bulletin EN-SB-08-012, Revision B – Nondestructive inspection capability guidelines for United States Air Force aircraft structure*s, Wright-Patterson AFB, OH, USA.

[39]Air Force Structures (2011*). EN-SB-08-002 Revision A – revised damage tolerance requirements and determination of operational life limits for slow crack growth metallic structures,* Wright-Patterson AFB, OH, USA.

[40]United States Air Force (2008). Damage tolerance re-assessment: Reconfigured post desert storm severe spectrum, Hill Air Force Base, UT, USA.

[41]LexTech Inc. (2010) *AFGROW (fracture mechanics and fatigue crack growth analysis software)*, version 5.1.5.16.